THE UNIVERSITY OF CHICAGO

SYNTHESIS AND REACTIVITY OF PSEUDO-TETRAHEDRAL COBALT AND NICKEL COMPLEXES

A DISSERTATION SUBMITTED TO

THE FACULTY OF THE DIVISION OF THE PHYSICAL SCIENCES

IN CANDIDACY FOR THE DEGREE OF

DOCTOR OF PHILOSOPHY

DEPARTMENT OF CHEMISTRY

BY

NORMAN ZHAO

CHICAGO, ILLINOIS

DECEMBER 2022

Table of Contents

List of Figures

Chapter 1

Chapter 2

Chapter 3

Chapter 4

Appendix 1

Appendix 2

Appendix 3

Appendix 4

List of Schemes

Chapter 1

Chapter 2

Chapter 3

Chapter 4

Appendix 4

List of Tables

Chapter 4

Appendix 1

Appendix 2

Appendix 3

List of Equations

Chapter 2

Chapter 4

List of Abbreviations

$\{^1H\}$	proton decoupled
°	degree
°C	degree Celsius
^{11}B	Boron-11
^{13}C	Carbon-13
^{19}F	Fluorine-19
^1H	Hydrogen-1
^{31}P	Phosphorus-31
A	absorbance
Å	Angstrom
Ad	adamantyl
AdIm	1-adamantyl imidazol-2-ylidene
Avg	average
B.M.	Bohr magnetons
BAr^F_4	tetrakis(3,5-bis(trifluoromethyl)phenyl)borate
BD(F)E	bond dissociation (free) energy
Bu	butyl

C	Standard reduction potential of $H^+/H\cdot$ in a given solvent
cm	centimeter
cm^{-1}	wavenumber
CPET	concerted proton-electron transfer
CV	cyclic voltammetry or cyclic voltammogram
δ	chemical shift
d	deuterium or doublet
DCM	dichloromethane
DFT	density functional theory
DHA	9,10-dihydroanthracene
DMSO	dimethylsulfoxide
ε	molar extinction coefficient
e^-	electron
E^0	standard reduction potential
EPR	electron paramagnetic resonance
Equiv.	equivalents
ET	electron transfer
Et	ethyl

EXAFS	Extended X-ray absorption fine structure
Fc	ferrocene
Fl	fluorene
G	Gibbs free energy or Gauss
g	gram
g	g-factor
GC	gas chromatography
η	asynchronicity
H	enthalpy
HMDS	hexamethyldisilazide
Hz	Hertz
Im	imdazol-2-ylidene
^{i}Pr	isopropyl
IR	infrared
J	coupling constant
K	Kelvin
k	rate constant
kcal	kilocalorie

KIE	kinetic isotope effect
LDA	lithium diisopropylamide
λ	wavelength
M	molarity
m	medium
Me	methyl
μ	bridging
μ_{eff}	effective magnetic moment
mg	milligram
MHz	megahertz
mL	milliliter
μL	microliter
mM	millimolar
mm	millimeter
mmol	millimole
MS	mass spectrometry
mV	millivolt
ν	frequency

n.b.	nonbonding
^{n}Bu	n-butyl
NHC	N-heterocyclic carbene
nm	nanometer
NMR	nuclear magnetic resonance
OTf	triflate
PCET	proton coupled electron transfer
Ph	phenyl
pK_a	–log(K_a)
PT	proton transfer
PTFE	polytetrafluoroethylene
R	organic group or R-factor
r	radius
RT	room temperature
s	singlet or strong
S	spin
S	entropy
Std. dev.	standard deviation

t	triplet or time
T	temperature
TBA	tetra-butylammonium
^{t}Bu	tert-butyl
^{t}BuIm	1-tert-butyl-imidazol-2-ylidene
^{t}BuImH	1-tert-butylimidazolium
T_c	coalescence temperature
TD	time dependent
THF	tetrahydrofuran
TMS	trimethylsilyl
UV	ultraviolet
w	weak
V	volt
vis	visible
wR	weighted R-factor
XANES	X-ray absorption near edge structure
XAS	X-ray absorption spectroscopy
XRD	X-ray diffraction

Acknowledgements

First and foremost, I would like to thank my PhD advisor, Professor John Anderson, for the opportunity to conduct research in his laboratory. His genuine enthusiasm for both science and teaching fostered an environment that pushed me to grow as a scientist. I would also like to thank my committee members, Professors Mark Levin and Guangbin Dong, for their time and feedback on my dissertation.

I would like to thank the Anderson laboratory for their support throughout my time there. In particular, I would like to thank my mentors, Prof. Ethan Hill, Dr. McKenna Smith and Dr. Margaret Kelty for their support throughout my graduate career. Being able to share a glovebox with the three of you was truly a highlight. I appreciated feeling that I could turn to any of you to give chemistry help and advice. Drs. Jorge Martinez and Patrick Crossland have been great lab mates and invaluable sources of support throughout the later stages of my PhD. I would also like to thank Joseph Schneider for helpful scientific discussion on theory and computations.

The managers of the XRD and NMR facilities, Dr. Alex Filatov and Dr. Josh Kurutz, do an excellent job in keeping the department running smoothly, and have been incredibly helpful for scientific advice. Additionally, I would like to thank Dr. Andrew McNeece, Dr. Kate Jesse and Sophie Anferov for helping me with my SXRD samples, many of which were challenging to work with. I would also like to thank Prof. Anna Wuttig for her support, and for an excellent CHEM 301 teaching experience, as well as Prof. Daniel Weix and Dr. Jill Caputo to introducing me to chemistry research as an undergraduate.

I am fortunate to have an amazing group of friends and family who gave me the support to persevere through graduate school. I would like to thank my mother and grandmother for their

love and encouragement over the years. I am grateful to have met Brad Studnitzer, Adam Weiss and Dr. James Callahan so early on in my graduate career. Thank you for the fun breaks from research and humoring me with Uncle Joe's. Last but not least, I would like to thank Dr. Kevin Au, Corinna Wong, Chieri Ono, Elliott Yim and Denise Aung, for their unwavering love and support from the west coast.

Abstract

High-valent oxygenated transition metal complexes are implicated in a variety of synthetic and biological transformations, including O–O bond-formation and C–H functionalization. These intermediates span a range of transition metals, supporting ligands, and oxygen binding modes. As such, there has been a wide body of research dedicated to exploring the relationship between their structure and reactivity. Insights from isolated well-defined oxygenated transition metal complexes have allowed for the rational design of catalysts for the above-mentioned important transformations. However, the reactivity of these compounds can make their isolation and detailed study challenging. This thesis focuses on the synthesis and reactivity of compounds supported by strongly-donating tris(imidazol-2-ylidene)phenylborate ligands to stabilize unusual high-valent oxygenated transition metal species.

Previous works have demonstrated that tris(imidazol-2-ylidene)phenylborate ligand scaffolds stabilize unusual high-valent Fe and Co complexes, such as transition metal-oxo and -imido species. However, analogous chemistry with Ni has yet to be explored, and the chemistry of Co systems is only nascent. Chapter 2 of this thesis focuses on the isolation and characterization of several Ni complexes that feature these tris(imidazol-2-ylidene)phenylborate ligands. These complexes serve as a platform to explore further oxidative reactivity. Additionally, the donor strength of this ligand scaffold is exemplified by the terminal Ni-methyl complexes PhB(RIm)NiMe, which are distorted from pseudo-tetrahedral to seesaw geometries.

Chapter 3 of this thesis explores the oxidative reactivity of these precursor complexes, where dioxygen activation by a Ni^{II}-chloride precursor yields an unprecedented binuclear Ni^{III}_2-(μ-1,2-peroxo) complex. The isolation of this complex confirms the viability of such a species as an intermediate in water oxidation by Ni(oxy)hydroxide materials. While this complex is thermally

unstable, we demonstrate its reactivity with both nucleophiles and electrophiles at low temperatures which suggest possible mechanistic paradigms in nickel-based water oxidation materials.

Chapter 4 of this thesis explores the X–H bond activation reactivity of a terminal Co^{III}-oxo complex supported by tris(imidazol-2-ylidene)phenylborate ligands. Previous work has demonstrated that the rate of C–H bond activation by the terminal Co^{III}-oxo complex $PhB(^{t}BuIm)_3CoO$ correlates with substrate acidity, rather than substrate bond dissociation energy. Mechanistic studies have demonstrated that this selectivity is imparted by the bacisity of the $Co^{III}O$ complex, giving rise to a basic asynchronous concerted proton electron transfer mechanism, wherein the transition state adopts more proton transfer character. In this chapter, the C–H bond activation reactivity of the adamantyl congener $PhB(AdIm)_3CoO$ is demonstrated to be even more sensitive to substrate acidity, ultimately resulting in mechanistic crossover from a concerted mechanism to a stepwise proton transfer-electron transfer mechanism in a series of substituted phenol substrates. This observation underscores that a multitude of factors, other than reactant-product bond dissociation energies, play a role in the selectivity, mechanism, and rate of X–H bond activation.

Preface

All compounds share a numbering scheme throughout this thesis. Characterization spectra are provided in the corresponding appendix for each chapter.

Chapter 1: Introduction to Oxygenated Late Transition Metal Complexes

1.1 Importance and Diversity of Oxygenated Transition Metal Complexes

Oxygenated transition metal complexes are ubiquitous intermediates in biological and synthetic oxidative transformations, such as C–H activation/functionalization, alkene epoxidation and O–O bond formation.[1–7] Transition metal (di)oxygen complexes span a variety of different metal centers, metal oxidation states, and ligand coordination sphere, dictating the binding mode, redox state and reactivity of the (di)oxygen ligand (**Figure 1.1**).[8] While numerous efforts have attempted to elucidate the mechanistic details of these processes, many consist of short-lived, highly reactive intermediates that are difficult to isolate and characterize. Understanding the structure-reactivity relationships of these complexes is key to rational design of higher yielding and more selective oxidative processes.

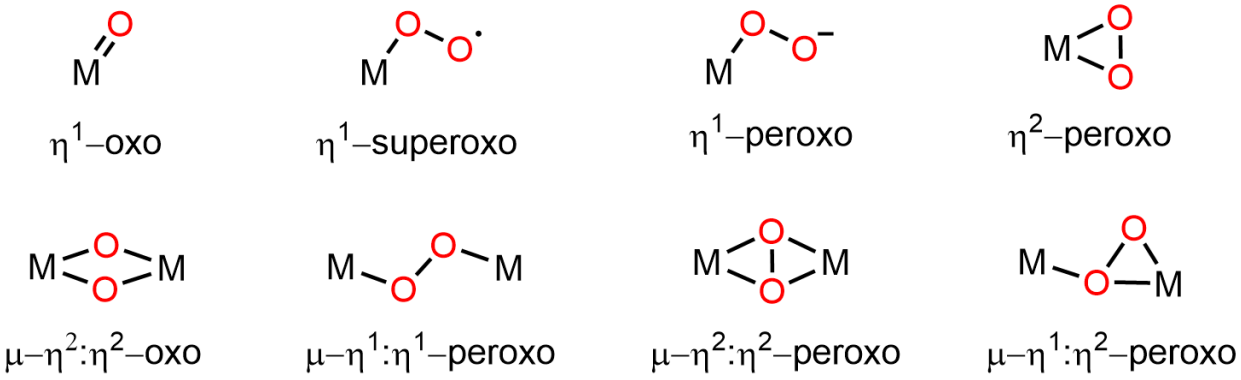

Figure 1.1. Sample of (di)oxygen binding modes.

Indeed, small changes in the coordination sphere of metal-oxo complexes can lead to significant changes in reactivity. This, and the diversity of oxygenated metal complexes, is exemplified in hemeproteins which have evolved to carry out a number of different functions, despite containing similar Fe-porphyrin active sites (**Figure 1.2**).[9–11] For example, cytochromes P450 are a family of cysteine-ligated hemeproteins responsible for the pharmacological clearance

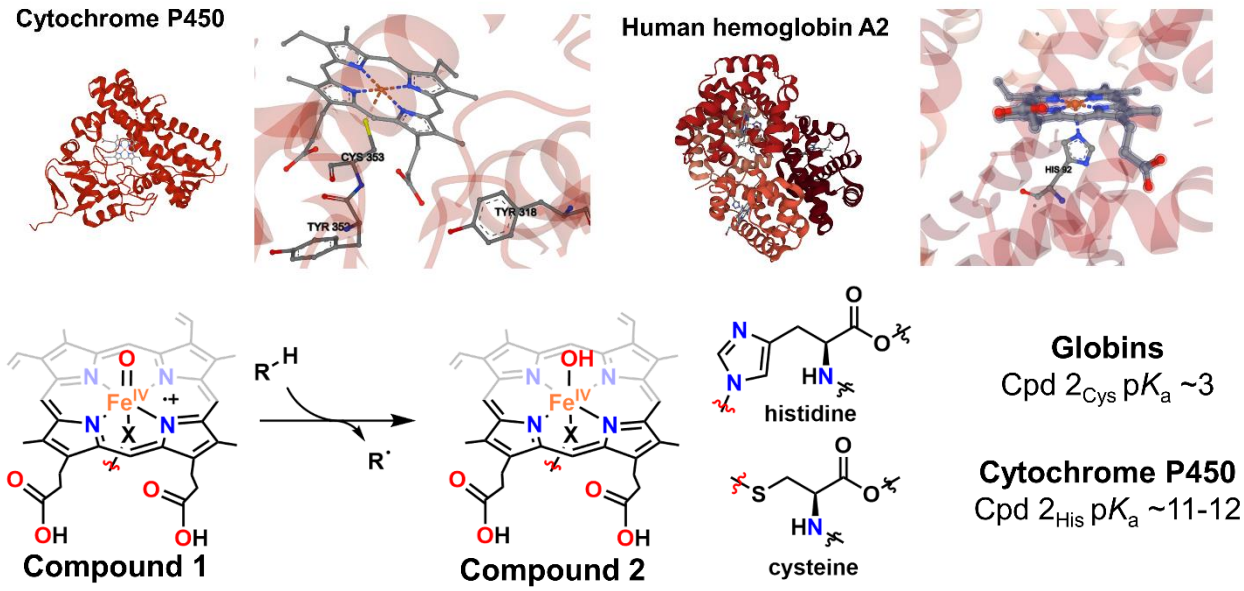

Figure 1.2. Change in pKa of Compound 2 ligated by histidine (globins, PDB 1SE6) and cysteines (cyotochrome 450, PDB 1S5L).

of metabolites *via* C–H activation/functionalization. In this system, Fe-aquo, -superoxo and -peroxo species are proposed *en route* to Compound I, an Fe^{IV}-oxo complex with a delocalized cationic radical that mediates the rapid C–H bond activation of substrates. In this process, a substrate C–H bond is homolytically cleaved to yield Compound II, an Fe^{IV}-hydroxo complex.

This functionality can be contrasted with that of hemoglobin, a hemeprotein that features a conserved histidine-ligated heme motif. In biology, hemoglobin is responsible for oxygen transport in the blood, but not C–H functionalization. Protein mutagenesis and stopped flow studies suggested that a cysteine-ligated heme motif is necessary for the basicity needed for C–H functionalization and to avoid non-productive protein auto-oxidation pathways. Notably, the corresponding Fe^{IV}-hydroxo complex (Compound II) is ~10 pKa units more basic in cysteine-ligated systems than histidine-ligated systems.[12] This underscores that small changes to the structure of these complexes can drastically affect their thermodynamic properties and thus reactivity. Studying well-defined model complexes allows for further insight into these structure-

reactivity relationships, spectroscopic signatures, and synthetic viability of these proposed intermediates.

1.2 Electronic Structure of Transition Metal-oxo Complexes

Late (M = Fe, Co, Ni, Cu) transition metal-oxo complexes have been implicated in the functionalization of unactivated C–H bonds. Despite their importance, few examples of isolated late metal-oxo complexes exist in the chemical literature. Both the reactive nature of these species and their relative scarcity can be rationalized by a d-orbital splitting diagram, first derived for the vanadyl ion (**Figure 1.3**).[13,14] In an octahedral ligand field, the d_{xz} and d_{yz} interact with the lone pair electrons on the terminal oxo ligand in a π-antibonding fashion. Thus, in a metal-oxo complex with 4 d-electrons, both $\pi^*_{M\text{-}O}$ orbitals are population, causing both π-bonding interactions to be broken and rendering the compound unstable. This concept, combined with oxidation state considerations, gives rise to the "oxo wall", which predicts that terminal oxo complexes past group 8 are not isolable. Consequently, most terminal metal-oxo complexes reported in the literature are those of high-valent, early metals.

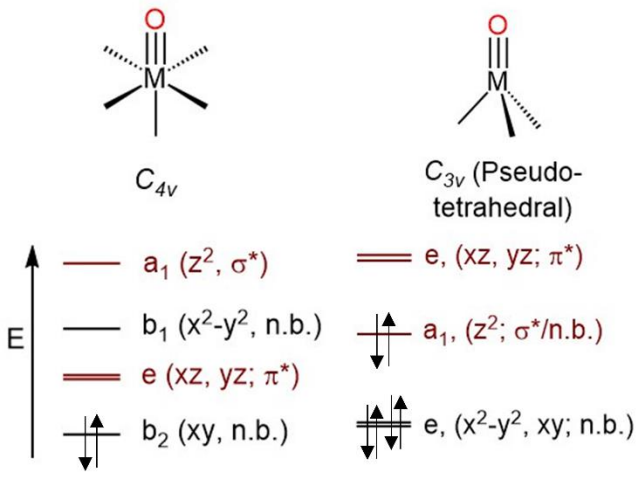

Figure 1.3. Molecular orbital diagram of terminal metal-oxo complexes.

Nevertheless, descent in symmetry of the ligand field by decreasing coordination number can allow for higher d-counts without population of the $\pi^*_{M\text{-}O}$ orbitals. This strategy has enabled the isolation of metal-oxo complexes with more than 4 d-electrons. For example, in a pseudo-tetrahedral C_{3v} symmetry, the d-orbital manifold can accommodate up to 6 d-electrons before populating the $\pi^*_{M\text{-}O}$ orbitals.[15] Our group has employed a tris(imidazole-2-ylidene) phenylborate scaffold to stabilize a terminal d^6 Co^{III}-oxo complex (**Figure 1.4**).[16] This complex was characterized by single crystal X-ray diffraction, representing the first example of an isolated first-row metal oxo complex past group 8.

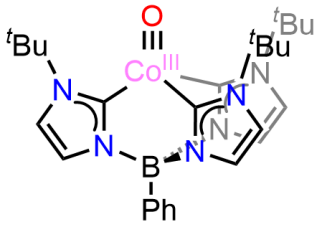

Figure 1.4. Terminal Co^{III} complex supported by a tris(imidazol-2-ylidene) scaffold.

1.3 Transition State Asynchronicity in X–H Bond Activation by Transition Metal-oxo Complexes

One longstanding challenge in organic synthesis is the selective activation and functionalization of unactivated C–H bonds.[17,18] Transition metal-oxo complexes typically activate C–H bonds with the lowest bond dissociation free energy (BDFE), as predicted by the Bell-Evans-Polyani principle (**Figure 1.5**).[19–21] To circumvent this, Nature primarily achieves chemo- and

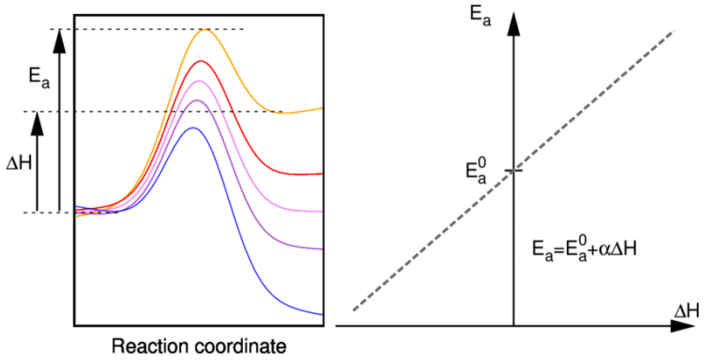

Figure 1.5. Reaction coordinate diagram showing Bell-Evans-Polyani principle. From ref 21.

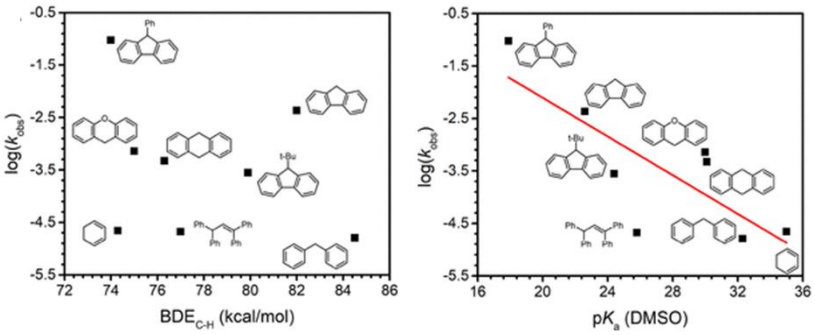

Figure 1.6. Plots of log(kobs) versus BDE and pKa of C-H substrates in reactions with PhB(^{t}BuIm)Co^{III}O.

regioselective C–H bond activation by positioning substrates using active site hydrogen-bonding networks. While synthetic chemists have harnessed artificial metalloenzymes for a variety of reactions, engineering these complex supramolecular frameworks for different substrates and transformations can be challenging.[22] Understanding the intricacies of how the chemical properties of an oxidant dictate its reactivity is important in developing strategies for selective and predictable C–H bond activation.

In transition metal-oxo complexes, the initial step in this process is the transfer of a hydrogen atom (a proton and an electron) from the substrate to the oxo moiety, termed PCET (proton coupled

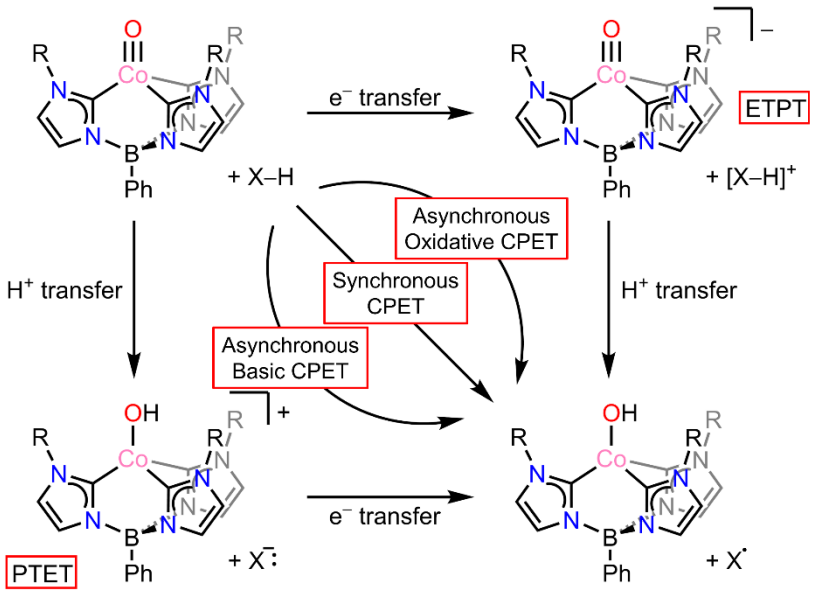

Scheme 1.1. Mechanisms for PCET.

electron transfer). PCET can occur through multiple different mechanisms: a concerted fashion, termed CPET (concerted proton-electron transfer), or in a stepwise fashion wherein the proton and electron are transferred sequentially (PTET, proton transfer-electron transfer, or ETPT, electron transfer-proton transfer) (**Scheme 1.1**). In general, the concerted transfer of a proton and electron has been thought to be a lower energy process than the corresponding stepwise process as coupling of proton and electron movement allows for a charge-neutral process.[23] However, recent studies into the mechanisms of PCET have challenged this notion, and have demonstrated that CPET is not always favorable pathway for the kinetics or selectivity of a reaction. As such, a deep understanding of how the chemical properties of the oxidant and substrate affect the operative mechanism is key to controlling the chemoselectivity of this C–H functionalization.

More recently, our group has isolated terminal Co^{III}-oxo complex PhB(^{t}BuIm)CoO. We sought to establish a lower bound for the O–H BDFE of the corresponding Co^{II}-hydroxo complex, by screening a variety of different C–H substrates.[24] Interestingly, a plot of the observed pseudo-first order rate constant (k_{obs}) versus the BDFE of various C–H substrates showed no correlation. Rather, plotting k_{obs} versus substrate pK_a revealed a negative correlation (Figure 1.6). Mechanistic studies were inconsistent with concerted and stepwise PCET mechanisms. Around that time, computational studies proposed intermediate PCET mechanisms between CPET and stepwise PTET/ETPT mechanisms.[25] In these proposed mechanisms, proton and electron transfer is concerted, but the proton or electron lags behind the other in the transition state (Figure 1.7). These mechanisms have been termed asynchronous basic PCET or asynchronous oxidative PCET, respectively. Both computational and kinetic data supported an asynchronous basic mechanism in this system. Since this study, other systems have invoked asynchronous PCET pathways in C–H activation.[26–33]

The concept of asynchronous or imbalanced transition states has been proposed in several different organic reactions including hydrogen atom transfer between organic molecules and pericyclic reactions.[34,35] However, asynchronicity in PCET involving metal-oxo complexes has only recently been considered. As such, the feasibility and implications of imbalanced transition states in PCET has been debated.[23,36,37]

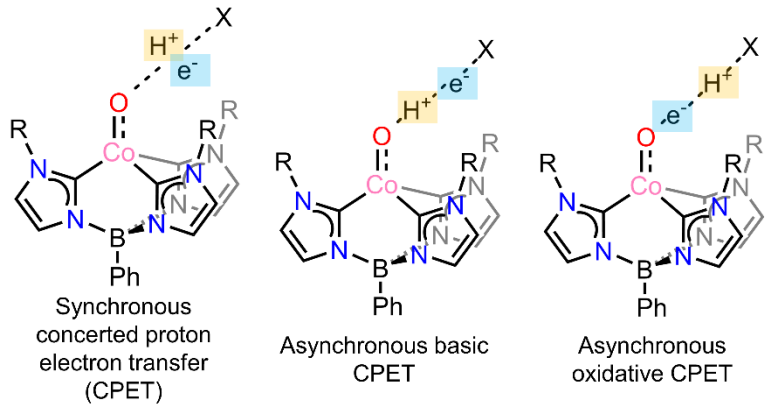

Figure 1.7. Synchronous versus asynchronous PCET pathways.

A better understanding pKa-driven asynchronicity is key to designing a new class of catalysts that activate the most acidic proton, instead of the homolytically-weakest C–H bond, expanding the synthetic chemist's toolkit.[17] However, how the electronic structure of the oxidant affects its PCET reactivity is poorly understood. Additionally, the tools to predict whether an oxidant-substrate pair will react in a concerted synchronous, concerted asynchronous or stepwise mechanism have not yet been developed. One goal of this thesis is to develop structure-reactivity relationships for such oxidant-substrate pairs, which will allow for further exploration of this reaction space.

1.4 Oxygenated Transition Metal Complexes in the Oxygen Evolving Reaction

The scalable and sustainable method of renewable energy storage is a barrier to the widespread adoption of solar energy.[38] In photosynthesis, the oxygen evolving complex (OEC) of photosystem II stores energy in the form of chemical bonds by splitting water into oxygen, protons and electrons (Figure 1.8).[39] Synthetic analogs of this process have been developed.[40] However, the best performing water oxidation catalysts employ precious metals, such as platinum and iridium.[41,42] Materials with first-row transition metals have been shown to catalyze water oxidation.[43,44] In particular, nickel materials have shown promise for their cost, low overpotentials and robustness under reaction conditions.[45]

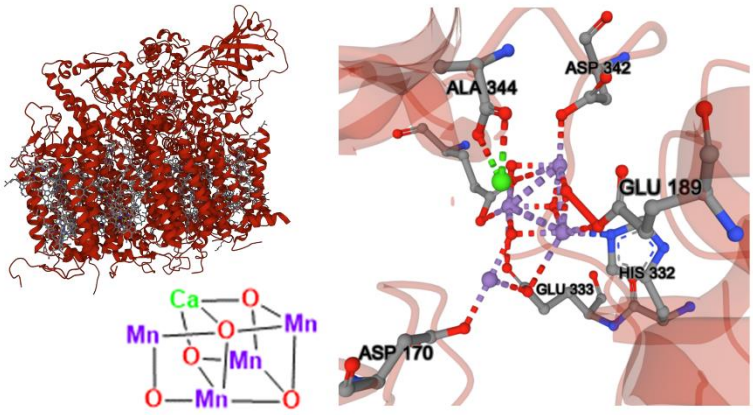

Figure 1.8. The oxygen evolving complex in photosystem II.

Nickel-based oxygen evolution electrocatalysts have been known since the 1980s.[46] While the first examples of Ni materials were proposed to consist of pure Ni-oxides, later studies suggested that Fe impurities were responsible for the high activity of these catalysts.[47] The intentional doping of Ni materials with Fe has given rise to a new class of candidates for oxygen evolution. However, little is known about what makes these materials effective catalysts. As such, these materials have been studied spectroscopically to better understand the mechanisms by which they operate.[48–52] High-valent metal-oxo complexes have been proposed to be involved in the key O–O bond

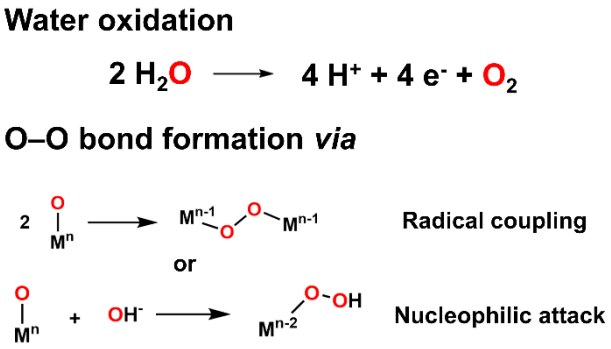

Scheme 1.2. Water oxidation and O–O bond formation mechanisms.

forming step before release of O_2. Two mechanisms have been proposed for this step. In the first mechanism, two terminal-oxo complexes couple in a radical fashion to furnish a binuclear μ-1,2-peroxo complex, termed the radical coupling mechanism (Scheme 1.2). Alternatively, a metal-oxo complex can undergo nucleophilic attack by a hydroxide ion to furnish a mononuclear hydroperoxo complex.

To better understand the intermediates and mechanistic intricacies of the OEC, Mn-oxo complexes have been isolated and studied as model complexes for the OEC.[53,54] However, oxygenated Ni complexes are significantly less commonly encountered in the literature, relative to their Mn, Fe, Co and Cu counterparts, due in part to the relative scarcity of proposed oxygenated Ni-complexes in biological and synthetic systems that mediate oxidative reactivity.[55] Thus, the synthetic viability of such complexes is poorly understood. Oxygenated Ni complexes were only first isolated and studied in the late 1990's, when Mora-oka isolated a binuclear bridging Ni-O complex.[56] Mononuclear terminal nuclear-oxo complexes have been proposed, but poorly characterized.[57] For example, Company and co-workers have proposed the capture of a Ni^{III}-oxo complex, but were only able to characterize this species through CSI-MS and unlabelled vibrational spectroscopy.[58]

Low-valent mononuclear and binuclear Ni-peroxo and -superoxo complexes have been isolated and characterized.[59–64] While high-valent Ni complexes are uncommon, as well as high-valent mononuclear Ni-peroxo and superoxo complexes have been reported.[65–67] However, high-valent binuclear Ni-peroxo complexes have not been observed or characterized. Such a compound would be a key intermediate in the radical coupling of two Ni^{IV}-oxo complexes in oxygen evolution systems. Chapter 3 of this thesis explores the synthesis and reactivity of a Ni_2-(μ-1,2-peroxo) complex supported by a tris(imidazol-2-ylidene) phenylborate scaffold.

1.5 References

(1) Nam, W. *Acc. Chem. Res.* **2015**, *48*, 2415–2423.

(2) Yee, G. M.; Tolman, W. B. Transition Metal Complexes and the Activation of Dioxygen BT - Sustaining Life on Planet Earth: Metalloenzymes Mastering Dioxygen and Other Chewy Gases; Kroneck, P. M. H., Sosa Torres, M. E., Eds.; Springer International Publishing: Cham, 2015; pp 131–204.

(3) Quist, D. A.; Diaz, D. E.; Liu, J. J.; Karlin, K. D. *J. Biol. Inorg. Chem.* **2017**, *22*, 253–288.

(4) McDonald, A. R.; Que, L. *Coord. Chem. Rev.* **2013**, *257*, 414–428.

(5) Fiedler, A. T.; Fischer, A. A. *J. Biol. Inorg. Chem.* **2017**, *22*, 407–424.

(6) Petsi, M.; Zografos, A. L. *Synth.* **2018**, *50*, 4715–4745.

(7) Ray, K.; Lee, Y. M.; Nam, W. *Coord. Chem. Rev.* **2017**, *334*, 25–42.

(8) Holland, P. L. *Dalton Trans.* **2010**, *39*, 5415–5425.

(9) Huang, X.; Groves, J. T. *JBIC J. Biol. Inorg. Chem.* **2017**, *22*, 185–207.

(10) Zhao, B.; Guengerich, F. P.; Bellamine, A.; Lamb, D. C.; Izumikawa, M.; Lei, L.; Podust, L. M.; Sundaramoorthy, M.; Kalaitzis, J. A.; Reddy, L. M.; Kelly, S. L.; Moore, B. S.; Stec, D.; Voehler, M.; Falck, J. R.; Shimada, T.; Waterman, M. R. *J. Biol. Chem.* **2005**, *280*, 11599–11607.

(11) Sen, U.; Dasgupta, J.; Choudhury, D.; Datta, P.; Chakrabarti, A.; Chakrabarty, S. B.; Chakrabarty, A.; Dattagupta, J. K. *Biochemistry* **2004**, *43*, 12477–12488.

(12) Yosca, T. H.; Rittle, J.; Krest, C. M.; Onderko, E. L.; Silakov, A.; Calixto, J. C.; Behan, R. K.; Green, M. T. *Science* **2013**, *342*, 825–829.

(13) Ballhausen, C. J.; Gray, H. B. *Inorg. Chem.* **1962**, *1*, 111–122.

(14) Winkler, J. R.; Gray, H. B. Electronic Structures of Oxo-Metal Ions. In *Molecular Electronic Structures of Transition Metal Complexes I*; Mingos, D. M. P., Day, P., Dahl, J. P., Eds.; Springer Berlin Heidelberg: Berlin, Heidelberg, 2012; pp 17–28.

(15) Saouma, C. T.; Peters, J. C. *Coord. Chem. Rev.* **2011**, *255*, 920–937.

(16) Goetz, M. K.; Hill, E. A.; Filatov, A. S.; Anderson, J. S. *J. Am. Chem. Soc.* **2018**, *140*, 13176–13180.

(17) Gentry, E. C.; Knowles, R. R. *Acc. Chem. Res.* **2016**, *49*, 1546–1556.

(18) Agarwal, R. G.; Coste, S. C.; Groff, B. D.; Heuer, A. M.; Noh, H.; Parada, G. A.; Wise, C.

F.; Nichols, E. M.; Warren, J. J.; Mayer, J. M. *Chem. Rev.* **2022**, *122*, 1–49.

(19) Bell, R. P.; Hinshelwood, C. N. *Proc. R. Soc. London. Ser. A - Math. Phys. Sci.* **1936**, *154*, 414–429.

(20) Evans, M. G.; Polanyi, M. *Trans. Faraday Soc.* **1938**, *34*, 11–24.

(21) Hermet, J. Theoretical Study of Protonic Conduction in Gd-Doped BaCeO3 : An Electrolyte for Fuel Cell. **2013**.

(22) Davis, H. J.; Ward, T. R. *ACS Cent. Sci.* **2019**, *5*, 1120–1136.

(23) Tyburski, R.; Liu, T.; Glover, S. D.; Hammarström, L.. *J. Am. Chem. Soc.* **2021**, *143*, 560–576.

(24) Goetz, M. K.; Anderson, J. S.. *J. Am. Chem. Soc.* **2019**, *141*, 4051–4062.

(25) Bím, D.; Maldonado-Domínguez, M.; Rulíšek, L.; Srnec, M. *Proc. Natl. Acad. Sci. U.S.A.* **2018**, *115*, E10287–E10294.

(26) Usharani, D.; Lacy, D. C.; Borovik, A. S.; Shaik, S. *J. Am. Chem. Soc.* **2013**, *135*, 17090–17104.

(27) Darcy, J. W.; Kolmar, S. S.; Mayer, J. M. *J. Am. Chem. Soc.* **2019**, *141*, 10777–10787.

(28) Mandal, M.; Elwell, C. E.; Bouchey, C. J.; Zerk, T. J.; Tolman, W. B.; Cramer, C. J. *J. Am. Chem. Soc.* **2019**, *141*, 17236–17244.

(29) Zhang, J.; Lee, Y.-M.; Seo, M. S.; Kim, Y.; Lee, E.; Fukuzumi, S.; Nam, W. *Inorg. Chem. Front.* **2022**, *9*, 3233–3243.

(30) Barman, S. K.; Yang, M.-Y.; Parsell, T. H.; Green, M. T.; Borovik, A. S. *Proc. Natl. Acad. Sci. U.S.A.* **2021**, *118*, e2108648118.

(31) Warm, K.; Paskin, A.; Kuhlmann, U.; Bill, E.; Swart, M.; Haumann, M.; Dau, H.; Hildebrandt, P.; Ray, K. *Angew. Chem. Int. Ed.* **2021**, *60*, 6752–6756.

(32) Mayfield, J. R.; Grotemeyer, E. N.; Jackson, T. A. *Chem. Commun.* **2020**, *56*, 9238–9255.

(33) Kotani, H.; Shimomura, H.; Ikeda, K.; Ishizuka, T.; Shiota, Y.; Yoshizawa, K.; Kojima, T. *J. Am. Chem. Soc.* **2020**, *142*, 16982–16989.

(34) Buckle, R. N.; Liu, P.-Y.; Roberts, E. W. D.; Burnell, D. J. *Tetrahedron* **1999**, *55*, 11455–11464.

(35) Liu, T.; Tyburski, R.; Wang, S.; Fernández-Terán, R.; Ott, S.; Hammarström, L. *J. Am. Chem. Soc.* **2019**, *141*, 17245–17259.

(36) Costentin, C.; Savéant, J.-M. *Chem. Sci.* **2020**, *11*, 1006–1010.

(37) Coste, S. C.; Brezny, A. C.; Koronkiewicz, B.; Mayer, J. M. *Chem. Sci.* **2021**, *12*, 13127–13136.

(38) Gray, H. B.; Winkler, J. R. *Acc. Chem. Res.* **2018**, DOI: 10.1021/acs.accounts.8b00245.

(39) Ferreira, K. N.; Iverson, T. M.; Maghlaoui, K.; Barber, J.; Iwata, S. *Science* **2004**, *303*, 1831–1838.

(40) Nocera, D. G. *Acc. Chem. Res.* **2012**, *45*, 767–776.

(41) Zhao, Y.; Hernandez-Pagan, E. A.; Vargas-Barbosa, N. M.; Dysart, J. L.; Mallouk, T. E. *J. Phys. Chem. Lett.* **2011**, *2*, 402–406.

(42) Gasteiger, H. A.; Kocha, S. S.; Sompalli, B.; Wagner, F. T. *Appl. Catal. B Environ.* **2005**, *56*, 9–35.

(43) McCrory, C. C. L.; Jung, S.; Peters, J. C.; Jaramillo, T. F. *J. Am. Chem. Soc.* **2013**, *135*, 16977–16987.

(44) Singh, A.; Spiccia, L. *Coord. Chem. Rev.* **2013**, *257*, 2607–2622.

(45) Chen, Y.; Rui, K.; Zhu, J.; Dou, S. X.; Sun, W. *Chem. – A Eur. J.* **2019**, *25*, 703–713.

(46) Hall, D. S.; Lockwood, D. J.; Bock, C.; Macdougall, B. R.; Lockwood, D. J. *Proc. R. Soc. A* **2014**, *471*, 1–65.

(47) Enman, L. J.; Burke, M. S.; Batchellor, A. S.; Boettcher, S. W. *ACS Catal.* **2016**, *6*, 2416–2423.

(48) Li, N.; Bediako, D. K.; Hadt, R. G.; Hayes, D.; Kempa, T. J.; von Cube, F.; Bell, D. C.; Chen, L. X.; Nocera, D. G. *Proc. Natl. Acad. Sci. U.S.A.* **2017**, *114*, 1486–1491.

(49) Lee, S.; Bai, L.; Hu, X. *Angew. Chem. Int. Ed.* **2020**, DOI: 10.1002/anie.201915803.

(50) Lee, S.; Banjac, K.; Lingenfelder, M.; Hu, X. *Angew. Chem. Int. Ed.* **2019**, *58*, 10295–10299.

(51) Stevens, M. B.; Trang, C. D. M.; Enman, L. J.; Deng, J.; Boettcher, S. W. *J. Am. Chem. Soc.* **2017**, *139*, 11361–11364.

(52) Burke, M. S.; Enman, L. J.; Batchellor, A. S.; Zou, S.; Boettcher, S. W. *Chem. Mater.* **2015**, *27*, 7549–7558.

(53) Neu, H. M.; Baglia, R. A.; Goldberg, D. P. *Acc. Chem. Res.* **2015**, *48*, 2754–2764.

(54) Larson, V. A.; Battistella, B.; Ray, K.; Lehnert, N.; Nam, W. *Nat. Rev. Chem.* **2020**, *4*, 404–419.

(55) Maroney, M. J.; Ciurli, S. *Chem. Rev.* **2014**, *114*, 4206–4228.

(56) Hikichi, S.; Yoshizawa, M.; Sasakura, Y.; Akita, M.; Moro-Oka, Y. *J. Am. Chem. Soc.* **1998**, *120*, 10567–10568.

(57) Corona, T.; Company, A. *Chem. – A Eur. J.* **2016**, *22*, 13422–13429.

(58) Corona, T.; Pfaff, F. F.; Acuña-Parés, F.; Draksharapu, A.; Whiteoak, C. J.; Martin-Diaconescu, V.; Lloret-Fillol, J.; Browne, W. R.; Ray, K.; Company, A. *Chem. Eur. J.* **2015**, *21*, 15029–15038.

(59) Kieber-Emmons, M. T.; Riordan, C. G. *Acc. Chem. Res.* **2007**, *40*, 618–625.

(60) Duan, P.-C.; Manz, D.-H.; Dechert, S.; Demeshko, S.; Meyer, F. *J. Am. Chem. Soc.* **2018**, *140*, 4929–4939.

(61) Kim, J.; Shin, B.; Kim, H.; Lee, J.; Kang, J.; Yanagisawa, S.; Ogura, T.; Masuda, H.; Ozawa, T.; Cho, J. *Inorg. Chem.* **2015**, *54*, 6176–6183.

(62) Yao, S.; Driess, M. Lessons from Isolable Nickel(I) Precursor Complexes for Small Molecule Activation. **2018**, *7*, 34.

(63) Rettenmeier, C. A.; Wadepohl, H.; Gade, L. H. *Angew. Chem. Int. Ed.* **2015**, *54*, 4880–4884.

(64) Rettenmeier, C. A.; Wadepohl, H.; Gade, L. H. *Chem. Sci.* **2016**, *7*, 3533–3542.

(65) Mirica, L. M.; Smith, S. M.; Griego, L. *Nickel Catalysis in Organic Synthesis*. January 28, 2020, pp 223–248.

(66) Cho, J.; Kang, H. Y.; Liu, L. V.; Sarangi, R.; Solomon Cd, E. I.; Nam, W.; Solomon, E. I.; Nam, W. *Chem. Sci.* **2013**, *4*, 1502–1508.

(67) Cho, J.; Sarangi, R.; Annaraj, J.; Kim, S. Y.; Kubo, M.; Ogura, T.; Solomon, E. I.; Nam, W. *Nat. Chem.* **2009**, *1*, 568–572.

(68) Fan, Y.; Cheng, J.; Gao, Y.; Shi, M.; Deng, L. *Acta Chim. Sin.* **2018**, *76*, 445–452.

Chapter 2: Ni^{II}-Methyl Complexes Adopting Unusual Seesaw Geometries

This chapter has been adapted from the following source with permission: Hill, E. A*., Zhao, N.*, Filatov, A.S., Anderson, J. S. *Chem. Commun.*, **2020**, *56*, 7861-7864. *indicates equal contribution

2.1 Introduction

Nickel-alkyl complexes have been invoked as important intermediates in a host of chemical transformations including the production of acetic acid and cross-coupling reactions.[1–6] In all reported examples of crystallographically characterized Ni^{II}-methyl complexes, a diamagnetic, square planar geometry is observed and many attempts to synthesize such species in other, four-coordinate geometries have proven unsuccessful frequently leading to reduction or other degradation.[7–11] Despite this, catalytically active Ni^{II}-alkyl species may likely exhibit or transition through different coordination geometries.[12–14] For example, other synthetic Ni^{II} complexes can be found in tetrahedral geometries in addition to the more common square planar geometries. While a square planar geometry is favored due to electronic stabilization of the d^8 Ni^{II} ion, a tetrahedral geometry may be favored with suitably bulky or chelating ligands.[15]

An alternative geometry for four-coordinate metal centers that has rarely been observed is a seesaw geometry. In fact, only a handful of examples of Ni^{II} complexes in this geometry have been reported.[13,16–18] In these cases, steric bulk is used to enforce the desired geometry. For example, the first of these reported by Bröring and co-workers utilized a tripyrranato ligand which positions methyl substituents within the square plane, forcing halide ligands above this plane.[19–21] Other examples include those by Gossage and Baruah where homoleptic complexes of Ni^{II} were synthesized with bulky propan-2-ylidene and oxazoline substituents that prevent planarization of

the Ni^{II} coordination environment.[14,22] Another recent example of a seesaw geometry at a Ni^{II} center involves a diisopropylpyrazole-substituted carbazole ligand to enforce steric crowding of the square plane.[13] Finally, an example of a ligand-constrained geometry around a Ni^{II} center can be seen in a complex bound to a triphosphacyclododecane ligand.[23] This ligand binds in a facial manner with strongly donating trialkylphosphines which are proposed to enforce a low-spin state at nickel. Due to the constrained ligand environment, the coordination geometry distorts to accommodate the low-spin state but cannot fully isomerize to a square planar geometry. These examples demonstrate the lengths required to enforce this geometry at a d^8 Ni^{II} center.

2.2 Results and Discussion

2.2.1 Synthesis and characterization of novel four-coordinate Ni-chloride and methyl complexes

We have been interested in exploring the chemistry of late transition metals supported by chelating and strongly donating tris-N-heterocyclic carbene (NHC) borate scaffolds.[24,25] These ligand scaffolds typically enforce a pseudo-tetrahedral geometry, but also favor low-spin states due to the strong donor properties of the carbene ligands. These factors suggest that Ni^{II} complexes supported by this ligand would have geometric frustration between an electronically preferred square planar geometry and a chelate-enforced pseudo-tetrahedral geometry. We therefore rationalized that Ni^{II} complexes of this ligand with suitably strong ligand fields might display unusual geometries and electronic structures.[26–28] Here we report the isolation and characterization

of two Ni^{II}-methyl complexes supported by a strongly donating tris-carbene borate ligand which display unusual seesaw geometries.

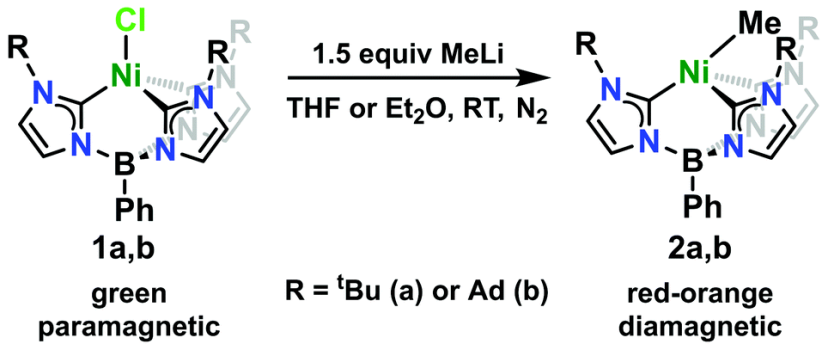

Scheme 2.1. Synthesis of complexes 2a and 2b.

The Ni^{II}-chloride complexes were first synthesized by initial deprotonation of the proligand, $[PhB(RImH)_3][OTf]_2$ (where R = ^{t}Bu or Ad), with in situ generated lithium diisopropylamide (LDA) followed by metalation with tetraethylammonium tetrachloronickelate ($[Et_4N]_2[NiCl_4]$) to yield $PhB(^tBuIm)_3NiCl$ and $PhB(AdIm)_3NiCl$ (**1a** and **1b**) in low but synthetically viable yields. The title complexes, $PhB(^tBuIm)_3NiMe$ and $PhB(AdIm)_3NiMe$ (**2a** and **2b**), were synthesized by treatment of the Ni^{II}-chloride complexes **1a** and **1b** with a solution of methyllithium following a similar reported procedure for related complexes of cobalt (Scheme 2.1).[29] Complexes **2a** and **2b** can be isolated as red, microcrystalline solids in good yield. These complexes are thermally unstable at room temperature, but pure solids can be stored at –35 °C for weeks to months without noticeable decomposition. Despite their intense, red-orange color in solution, complexes **2a** and **2b** display no distinct absorption features by UV-vis spectroscopy with only trailing absorbances from the UV region of the spectra into the visible region (**Figure A1.12Figure A1.13**). Contrary to the parent Ni^{II}-chloride complexes **1a** and **1b**, both complexes **2a** and **2b** are diamagnetic (see Appendix 1. However, ^{1}H NMR spectra of both the Cl and Me complexes in C_6D_6 indicate C_3-

symmetric geometries in solution at room temperature. We then turned to single-crystal X-ray diffraction (SXRD) measurements to probe the structures of these Ni complexes in the solid-state. As expected from their threefold symmetric NMR spectra, complexes **1a** and **1b** are pseudo-tetrahedral in the solid-state and have a C_3-axis with a B–Ni–Cl angle of 177.92(6)° and 178.8(2)°, respectively. In contrast, while the room temperature ^{1}H NMR spectra of the methyl complexes **2a** and **2b** are consistent with a C_3-symmetric structure, an unusual seesaw coordination geometry at the Ni^{II} centers is observed in their solid-state structures (Figure 2.1). The metrical parameters of the Ni centers in complexes **2a** and **2b** are consistent with a seesaw geometry around the Ni^{II} center composed of three carbon donors from the tris-carbene borate ligand and a fourth from the bound methyl group. The Ni-methyl carbon atom distances are nearly identical between the two complexes at 1.965(2) and 1.959(2) Å, respectively. Additionally, there is no evidence of agostic interactions between the Me hydrogen atoms and the Ni^{II} center. The two widest C–Ni–C angles which describe the seesaw geometry are 177.19(8)° and 121.49(8)° for **2a** and 177.80(7)° and 121.25(7)° for **2b**. Using both of these angles, a geometry index parameter τ_4 can be calculated to describe the coordination environment of the Ni^{II} center between square planar ($\tau_4 = 0$) or tetrahedral ($\tau_4 = 1$).[30,31] For both **2a** and **2b**, the τ_4 parameter is calculated to be 0.43, indicating a nearly perfect mono-vacant, trigonal bipyramidal or seesaw geometry around the Ni^{II} center. These are the first such cases to be crystallographically characterized.[§] With the disparity between solid-state and solution structural data, we sought to better understand the dynamics of complexes **2a** and **2b** in solution. Variable temperature ^{1}H NMR experiments were conducted in d_8-toluene to determine an isomerization barrier, $\Delta G^{\ddagger}$ (Figure 2.1).[32,33]

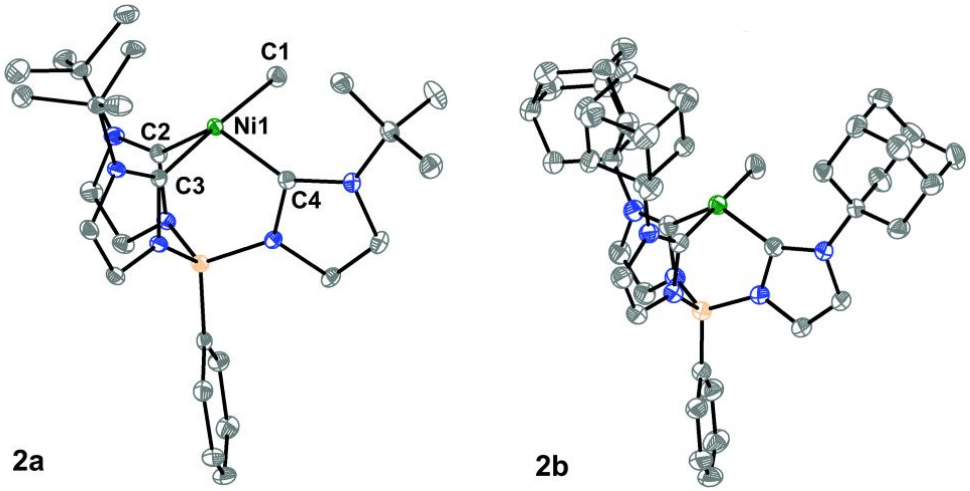

Figure 2.1. SXRD structures of 2a and 2b.

Ellipsoids are shown at 50% and H atoms are omitted for clarity. Ni is shown in green, N in blue, B in tan, and C in gray. Atom labels for 2b are the same as those depicted for 2a. Selected bond lengths (Å) and angles (°) and geometric parameters for **2a**: Ni1–C1 = 1.965(2), Ni1–C2 = 1.895(2), Ni1–C3 = 1.922(2), Ni1–C4 = 1.887(2), C1–Ni1–C3 = 177.19(8), C2–Ni1–C4 = 121.49(8), τ_4 = 0.43. For **2b**: Ni1–C1 = 1.959(2), Ni1–C2 = 1.886(2), Ni1–C3 = 1.912(2), Ni1–C4 = 1.884(2), C1–Ni1–C3 = 177.79(7), C2–Ni1–C4 = 121.25(7), τ_4 = 0.43.

In these complexes, the barrier being measured represents the energy to reorient the methyl substituent from between one pair of NHC groups to between a different pair through either an effective lever mechanism or via B–Ni–Me linearization to a C_3-symmetric isomer (*vide infra*).[34] For an NHC resonance of **2a**, a coalescence temperature of 215 K was determined and from the value of $\Delta\nu$, the peak-to-peak splitting in Hz of the fully resolved asymmetric structure, a barrier to isomerization was calculated to be 10.4 ± 0.5 kcal mol^{-1}. In the case of **2b** with the larger adamantyl groups, we anticipated a higher calculated barrier. However, the calculated value for the analogous imidazol-2-ylidene proton resonance is the same within an estimate of the error. From the coalescence temperature of 225 K and the measured $\Delta\nu$ values, a barrier of 10.9 ± 0.5

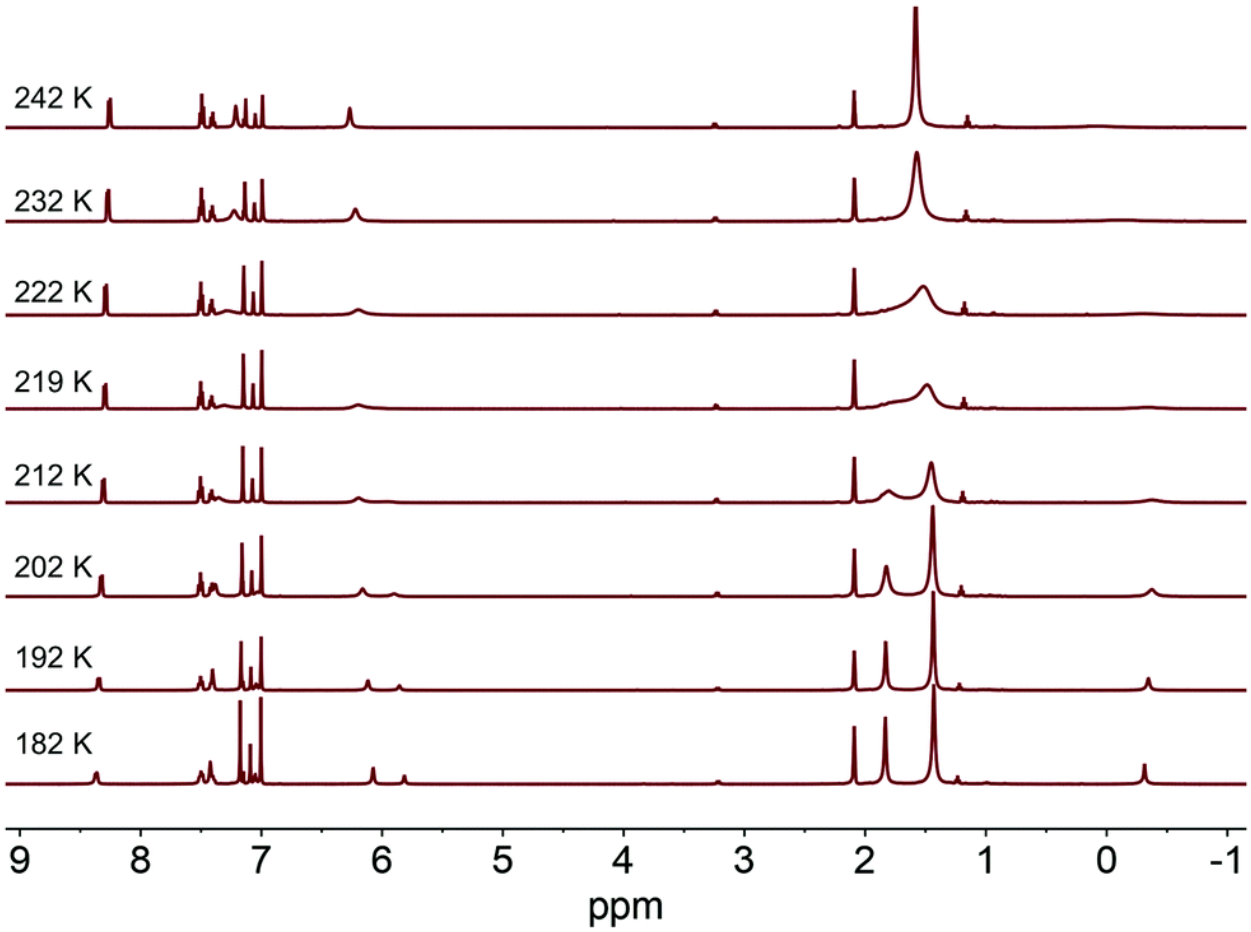

Figure 2.2. Variable temperature ^{1}H NMR spectra for complex 2a in d_8-toluene.

kcal mol^{-1} was calculated. This suggests that while the adamantyl groups are bulkier, extending further away from the Ni center, this does not appreciably alter the barrier to isomerization in this complex.

A point of interest upon studying complexes **2a** and **2b** was to rationalize the observed seesaw structures in the solid-state. A crude examination of the geometries a four-coordinate Ni^{II} complex may adopt indicates three possible isomers as discussed above: tetrahedral, square planar, and seesaw. The parent chloride complexes **1a** and **1b** are characterized as high-spin S = 1 complexes in a pseudo-tetrahedral geometry. Given the additional strong field methyl ligand in complexes **2a**

and **2b**, it is likely that diamagnetic, low-spin Ni^{II} species would be most stable.[35] While low-spin Ni^{II} complexes are typically found in square planar geometries, the chelate ring of the tris(carbene)borate scaffold precludes the complex from distortion to a square planar geometry that would be otherwise electronically favored. Additionally, this stronger ligand field disfavors pseudo-tetrahedral geometries, as this would qualitatively result in occupation of a high energy,

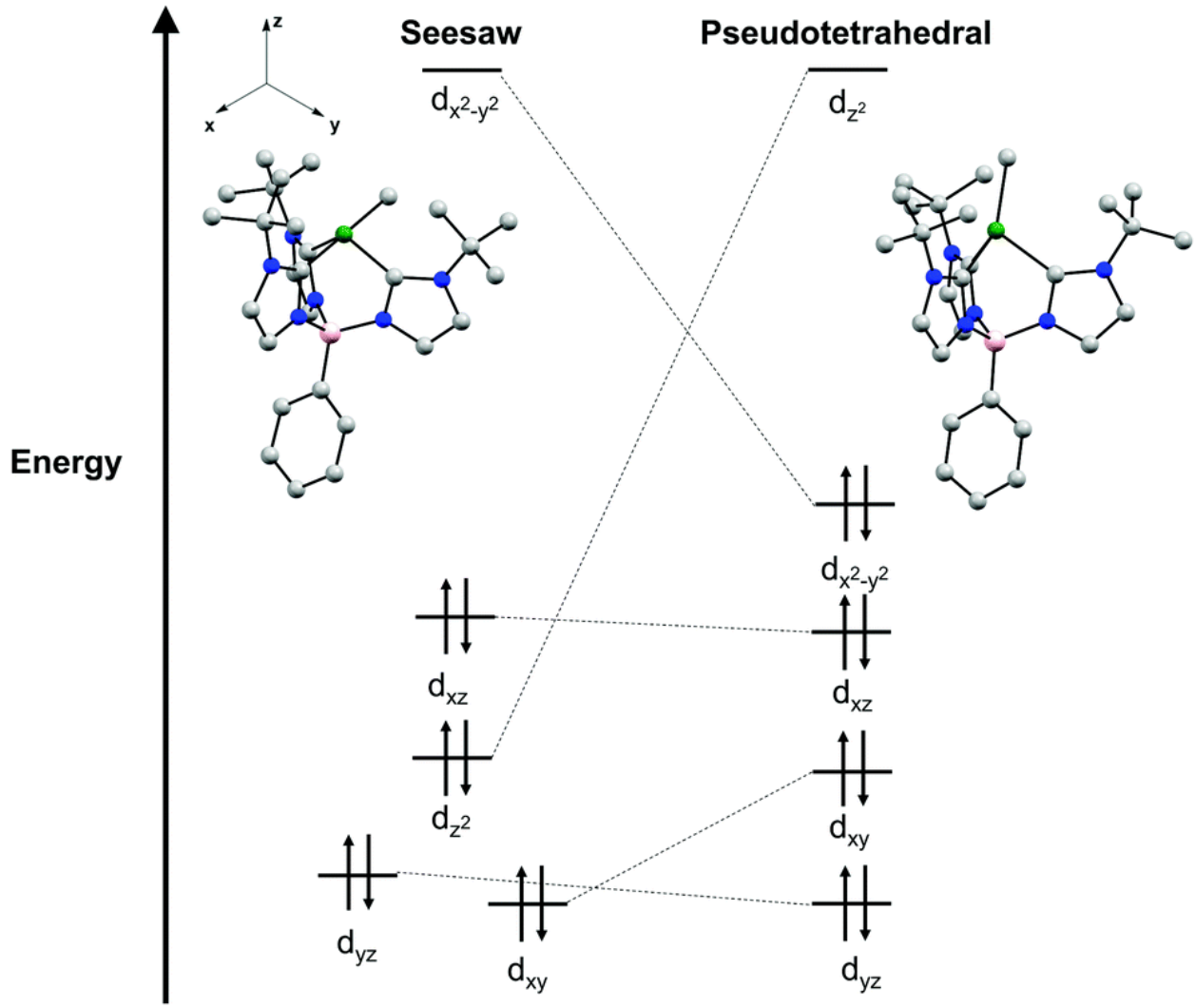

Figure 2.3. Qualitative Walsh diagram depicting the relative energies of the d-orbitals for the seesaw and pseudo-tetrahedral geometries.

Determined from DFT calculations of the geometry optimized singlet of **2a**. Basis set/functional used: def2-TZVPP on Ni, N, and C bound to Ni, def2-SVP on all other atoms/O3LYP.

antibonding orbital (Figure 2.3). As a result, the intermediate seesaw geometry is most stable, distorted away from pseudo-tetrahedral but restricted from planarization.

This qualitative description of the preference for seesaw geometries observed in complexes **2a** and **2b** is also supported by density functional theory (DFT) calculations. The geometry optimization of **2a** in a singlet electronic configuration yields a structure that is in agreement with its solid-state structure. Geometry optimization of **2a** in a triplet state shows instead a pseudo-tetrahedral geometry, similar to the geometry seen in **1a** and **1b**. The DFT calculations predict the $S = 0$ seesaw geometry to be 31 kcal mol^{-1} lower in energy than the corresponding $S = 0$ pseudo-tetrahedral isomer but only 11 kcal mol^{-1} lower than the $S = 1$ threefold symmetric species. Qualitative comparison of the frontier molecular orbitals of singlet **2a** reveals that deviation from a pseudotetrahedral to seesaw geometry stabilizes the d_{z^2} orbital (Figure 2.3). This results in a single, high-lying $d_{x^2-y^2}$ orbital that remains unoccupied with a clustering of occupied orbitals at overall lower energy than those in the pseudo-tetrahedral geometry. This qualitative orbital depiction for the seesaw geometry is similar to the classical depiction of square planar d-orbital splitting, further suggesting such a geometry would be preferred in this system if not for the chelate ring constraint imposed by the tris-carbene borate ligand.

The DFT calculations above suggest that an isomerization mechanism involving a linear $S = 1$ transition state is energetically reasonable, but we also wanted to probe the feasibility of a lever type mechanism for this isomerization computationally. In this mechanism the Me group migrates between NHC groups without linearizing to a pseudo-tetrahedral symmetry (Figure A1.18).[34] The C_{Me}–Ni–$C_{carbene}$–$N_{carbene}$ dihedral angle was held fixed at 0° and the Ni–Me group allowed to move between a pseudo-tetrahedral orientation and close proximity to the R-group of the NHC in order to find a low energy intermediate which would model the transition state for this isomerization. In

doing so, a conformer higher in energy by 20 kcal mol^{-1} relative to the seesaw geometry was found. This energy is high enough to rule out this pathway as operative given the ~10 kcal mol^{-1} energy barrier calculated from the variable temperature ^1H NMR experiments (Figure A1.19). Given the computed relative energies of the S = 0 (+31 kcal mol^{-1}) and S = 1 (+11 kcal mol^{-1}) pseudo-tetrahedral isomers, it is likely that the isomerization proceeds through the S = 1 C_3-symmetric isomer. This conclusion is also supported by the relatively broad Ni–CH_3 proton resonance at room temperature that shifts with temperature displaying Curie behavior. This effect is likely the result of perturbation from a minor amount of the paramagnetic, pseudo-tetrahedral isomer at room temperature as has been previously observed.[36] Interestingly, this observation suggests that paramagnetic Ni-methyl intermediates are accessible at room temperature in the current system, and that similarly high-spin Ni^{II}-alkyl complexes may be reasonable intermediates in catalysis.

2.3 Conclusion

The Ni^{II}-methyl complexes **2a** and **2b** are the first examples of such species to be found in a seesaw coordination geometry as revealed by their solid-state structures. Variable temperature ^1H NMR spectroscopy demonstrates that this distortion also occurs in the solution state and has an electronic origin as opposed to arising from any solid-state crystal packing. Using DFT calculations, the observed structures are rationalized by an overall lowering of filled orbitals by distortion from pseudotetrahedral to a seesaw geometry. This geometry is proposed to be favored over square planar geometry due to the chelate constraint of the tris(carbene)borate ligand. This work shows that Ni-alkyl species with chelating ligands can adopt this geometry and draws attention to the potential effects of this distortion and electronic structure on the reactivity of Ni intermediates in catalytic transformations.

2.4 Experimental

2.4.1 Materials and Instrumentation

All manipulations were performed under a dry nitrogen atmosphere using either standard Schlenk techniques or in an mBraun Unilab Pro glove box unless otherwise stated. All chemicals were obtained from commercial sources and used as received unless otherwise stated. Solvents were dried on a solvent purification system from Pure Process Technologies and passed through a column of activated alumina before storing over 4 Å molecular sieves under N_2. Diethyl ether and tetrahydrofuran (THF) were stirred over NaK alloy and passed through a column of activated alumina prior to storing over 4 Å sieves under N_2. Tetraethylammonium tetrachloronickelate ($[Et_4N]_2[NiCl_4]$), $[PhB(^tBuIm)_3][OTf]_2$, 1-adamantylimidazole, and $[PhB(AdIm)_3][OTf]_2$ were prepared according to literature procedures.[37-40]

UV-vis spectra were recorded on a Thermo Scientific Evolution 300 spectrometer with the VISIONpro software suite. IR spectra were recorded on a Bruker Tensor II spectrometer with the OPUS software suite. NMR spectra for ^1H, $^{13}C\{^1H\}$, and $^{11}B\{^1H\}$ were recorded on either Bruker DRX-400 or AVANCE-500 spectrometers. ^1H and $^{13}C\{^1H\}$ spectra were referenced to residual solvent peaks. Combustion analysis was performed by Midwest Microlab. Magnetic moments were determined using the Evans method.[41]

2.4.2 Complex Synthesis and Characterization

*$PhB(^tBuIm)_3Ni^{II}Cl$ (**1a**):* To a Schlenk flask was added proligand $[PhB(^tBuIm)_3][OTf]_2$ (5.00 g, 6.59 mmol) and THF (100 mL). In a separate Schlenk flask, $^iPr_2NH$ (2.6 mL, 20.1 mmol) was added to THF (30 mL). Both Schlenk flasks were sealed with rubber septa, brought out of the glovebox, attached to a Schlenk line, and cooled to –78 ºC using a dry ice/isopropanol bath. A solution of ^{n}BuLi (8.1 mL, 20.1 mmol, 2.5 M in hexanes) was then added to the solution of iPr_2NH

to generate lithium diisopropylamide (LDA) *in situ*. The solution of LDA in THF was then transferred via cannula to a cold suspension of the proligand. The reaction mixture was stirred at –78 ºC for approximately 45 minutes, and then solid $[Et_4N]_2[NiCl_4]$ (2.87 g, 6.92 mmol) was added under positive nitrogen pressure. After stirring at room temperature overnight, the brown reaction mixture was concentrated under vacuum to yield a green/brown residue. The flask was returned to a glovebox and triturated with hexanes (30 mL) and dried once more under vacuum. The residue was extracted into toluene (100 mL) and filtered through a pad of Celite. The resulting green solution was concentrated and redissolved in a minimal amount of toluene before layering under pentane at –35 ºC. Green crystals form after several days which are separated from a flocculent yellow/brown powder by washing with cold pentane. Crystals were dried under vacuum and lyophilized from benzene to yield pure **1a** (1.05 g, 1.90 mmol 29% yield). After separating and drying the mother liquor under vacuum, several successive crystallizations are required to achieve yields varying from 10-29%. Single crystals suitable for X-ray diffraction were grown from liquid diffusion of pentane into a concentrated solution of toluene solution of the complex at –35 ºC over several days. ^{1}H NMR (400 MHz, C_6D_6) δ 106.31, 15.27, 7.43, 7.26, 6.34. ^{11}B NMR (128 MHz, C_6D_6) δ −9.7. μ_{eff} (C_6D_6): 2.9 μ_B (for S = 1, μ_{SO} = 2.83 μ_B) UV-vis, nm in dichloromethane (ε, M^{-1} cm^{-1}): 446 (166), 718 (228). IR (KBr): 3142 (w), 3076 (w), 3051 (w), 3018 (w), 2978 (s), 2934 (m), 2876 (w), 1478 (w), 1432 (w), 1369 (m), 1333 (m), 1278 (s), 1232 (w), 1207 (s), 1193 (s), 1151 (s), 1123 (m), 1027 (m), 1021 (s), 931 (w), 898 (w), 880 (s), 824 (w), 806 (w), 792 (m), 722 (s), 710 (s), 700 (m), 669 (w). Anal.; Calc. for $C_{27}H_{38}N_6BNiCl$: C 58.79, H 6.94, N 15.24.; C 59.02, H 6.80, N 14.92.

*$PhB(AdIm)_3Ni^{II}Cl$ (**1b**)*: The proligand, $[PhB(AdIm)_3][OTf]_2$, was synthesized in an analogous manner to $[PhB(^tBuIm)_3][OTf]_2$ and its spectroscopic data matched previous literature.[68] To a 250

mL Schlenk flask was added $[PhB(AdIm)_3][OTf]_2$ (4.52 g, 4.55 mmol) and THF (60 mL). In a separate 50 mL Schlenk flask was added ^{i}PrNH (1.43 g, 14.0 mmol) and THF (20 mL). Both flasks were sealed with rubber septa, removed from the glovebox, and attached to a Schlenk line before cooling to −78 °C using a dry ice/isopropanol bath. After cooling, a solution of nBuLi (5.6 mL, 2.5 M in hexanes) was added via syringe to the cold ^{i}PrNH solution to generate LDA *in situ*. After briefly stirring (~5 min) the solution of LDA was transferred via cannula to a the cooled solution of $[PhB(AdIm)_3][OTf]_2$ and the mixture stirred for 1 h at −78 °C whereupon a turbid, peach-colored solution results. Under a positive flow of N_2, the septum was quickly removed and solid $[Et_4N]_2[NiCl_4]$ (2.10 g, 4.55 mmol) was added in one portion before replacing the septum. The mixture was stirred overnight and allowed to slowly warm to room temperature. The resulting brown solution was dried under vacuum at 50 °C for 1 h before returning to a glovebox. The brown residue was triturated once with hexanes (50 mL) before drying once more under vacuum. A brown, chalky residue results which is washed with several portions of room temperature toluene (typically ~50 mL in total) until a green solid remains. The green solid is transferred to a 125 mL Erlenmeyer flask and treated with hot toluene (100 °C, ~50-100 mL in total) until a green solution separates from a gray, oily solid (sometimes pale blue due to unreacted $[Et_4N]_2[NiCl_4]$). The mixture is filtered hot through a pad of Celite before drying to a green residue under vacuum. The resulting residue is dissolved in a minimum of dichloromethane (DCM) before layering under pentanes and storing at −35 °C for several days to yield dark green crystalline blocks (833 mg, 1.06 mmol, 23% yield). After separating and drying the mother liquor under vacuum, several successive crystallizations are required to achieve yields varying from 15-23%. ^{1}H NMR (400 MHz, CD_2Cl_2) δ 103.84, 13.85, 7.55-7.52, 3.79, 1.54. ^{11}B NMR (128 MHz, C_6D_6) δ −11.3. μ_{eff} (CD_2Cl_2): 3.0 μ_B (for $S = 1$, $\mu_{SO} = 2.83\ \mu_B$) UV-vis, nm in THF (ε, $M^{-1}\ cm^{-1}$): 360 (532) 450 (171),

720 (312) 835 (sh, 80). IR (KBr): 3153 (w), 3041 (w), 2903 (s), 2847 (s), 2667 (w), 1654 (w), 1544 (w), 1454 (m), 1404 (m), 1390 (m), 1326 (m), 1277 (m), 1239 (m), 1183 (s), 1163 (s), 1125 (m), 1103 (m), 1073 (w), 1019 (s), 880 (s), 835 (m), 790 (m), 735 (m), 713 (s), 695 (m), 645 (w), 625 (w). Anal.; Calc. for $C_{45}H_{56}N_6BNiCl$: C 68.77, H 7.18, N 10.69; C 68.92, H 7.40, N 10.20.

*PhB(^{t}BuIm)$_3$Ni^{II}Me (**2a**):* A solution of methyllithium (1.6 M in diethyl ether, 250 μL, 0.40 mmol) was added to a suspension of **1** (200 mg, 0.36 mmol) in diethyl ether (10 mL) at room temperature. After stirring for 30 minutes, the dark red mixture was filtered through a pad of Celite and concentrated under reduced pressure. The residue was washed with hexanes (3 x 5 mL) and dried once more under vacuum to yield a red-orange powder (71 mg, 0.13 mmol, 37% yield). Crystals suitable for X-ray diffraction were grown in a concentrated solution of diethyl ether at –35 ºC. ^{1}H NMR (400 MHz, C_6D_6) δ 8.30 (d, Ph, 2H), 7.48 (t, Ph, 2H), 7.39 (t, Ph, 1H), 7.28 (s, Im, 3H), 6.52 (s, Im, 3H), 1.60 (s, ^{t}Bu, 27H), 1.25 (br s, Me, 3H). Note that the Ni-CH_3 resonance displays solvent dependence, shifting from 1.25 ppm in C_6D_6, to 0.89 ppm in d_8-toluene, and 0.29 ppm in d_8-THF. ^{11}B NMR (128 MHz, C_6D_6) δ 1.4. ^{13}C NMR (126 MHz, C_6D_6) δ 144.2, 135.4, 127.4, 124.9, 116.6, 55.9, 31.5. UV-vis in THF: trailing UV absorbances (see below). IR (KBr): 3139 (w), 3049 (w), 2975 (s), 2925 (m), 2873 (w), 1650 (m), 1636 (m), 1475 (w), 1433 (m), 1398 (m), 1370 (m), 1337 (m), 1267 (m), 1194 (s), 1150 (m), 1110 (m), 1109 (m), 1030 (m), 931 (w), 876 (m), 826 (s), 792 (s), 737 (s), 707 (s), 638 (w). Several attempts at obtaining suitable elemental analysis data were unsuccessful. This is attributed to either incomplete drying or decay during shipping and handling, both as a result of the thermal instability of the complex.

*PhB(AdIm)$_3$Ni^{II}Me (**2b**)*: In a 20 mL scintillation vial, **1b** (200 mg, 0.25 mmol) was dissolved in THF (10 mL). To this solution was added MeLi (225 μL, 0.36 mmol, 1.6 M solution in diethyl ether) via microsyringe. The solution was stirred for 2 h, during which time a color change from

green to red occurs. The solution was dried to a red-brown residue under vacuum and extracted into toluene (15 mL) before filtering through a pad of Celite. The resulting dark red solution was layered under hexamethyldisiloxane and stored at −35 °C to yield a dark red, microcrystalline solid (99 mg, 0.13 mmol, 51% yield). Single crystals suitable for XRD were grown from toluene layered under pentane at −35 °C. ^{1}H NMR (400 MHz, C_6D_6) δ 8.34 (d, Ph, 2H), 7.50 (t, Ph, 2H), 7.41 (m, Ph, 1H), 7.30 (d, Im, 3H), 6.58 (s, Im, 3H), 2.42 (s, Ad, 18H), 2.09 (s, Ad, 9H), 1.65 (m, Ad, 18H), 1.05 (br s, Me, 3H). ^{11}B NMR (128 MHz, C_6D_6) δ 1.2. ^{13}C NMR (126 MHz, C_6D_6) δ 135.4, 128.2, 127.4, 124.4, 115.2, 56.2, 44.4, 36.7, 30.5. UV-vis in THF: broad shoulders and trailing UV absorbances (see below). IR (KBr): 3136 (w), 3060 (w), 2908 (s), 2852 (s), 2680 (w), 1644 (s), 1478 (w), 1451 (m), 1431 (w), 1398 (m), 1376 (w), 1357 (w), 1331 (m), 1307 (m), 1283 (m), 1240 (m), 1186 (m), 1169 (m), 1129 (w), 1104 (w), 1052 (w), 1026 (w), 876 (m), 835 (s), 792 (s), 736 (m), 703 (m), 680 (m). Several attempts at obtaining suitable elemental analysis data were unsuccessful. This is attributed to either incomplete drying or decay during shipping and handling, both as a result of the thermal instability of the complex.

2.4.3 Other Experimental Procedures

Crystallographic Details: The diffraction data for **2b** were measured at 110 K on a Bruker D8 fixed-chi with PILATUS1M (CdTe) pixel array detector (synchrotron radiation, λ = 0.41328 Å (30 KeV)) at the Chem-MatCARS 15-ID-B beamline at the Advanced Photon Source (Argonne National Laboratory). The diffraction data for **1a, 1b,** and **2a** were measured at 100 K on a Bruker D8 VENTURE diffractometer equipped with a microfocus Mo-target X-ray tube (λ = 0.71073 Å) and PHOTON 100 CMOS detector. Data reduction and integration were performed with the Bruker APEX3 software package (Bruker AXS, version 2017.3-0, 2018). Data were scaled and corrected for absorption effects using the multi-scan procedure as implemented in SADABS

(Bruker AXS, version 2014/5).[42] The structures were solved by SHELXT (Version 2014/5) and refined by a full-matrix least-squares procedure using OLEX2 (XL refinement program version 2018/1).[43-45]

Computational Methods: Geometry optimizations were performed using the ORCA program suite.[46] The O3LYP hybrid functional was used for all calculations, unless otherwise specified. The basis sets for each atom were as follows: def2-TZVPP for Ni, N, and carbene C; def2-SVP for B, H, and remaining C.[47-49] A full frequency calculation was performed on the optimized seesaw geometry of **2a** to ensure that there were no imaginary frequencies and ensure true minima in the energies. This geometry was then optimized as a triplet to obtain the linearized geometry, which was used to generate the molecular orbitals and geometry scan for the lever mechanism. The initial geometries were generated using crystallographic data. The geometry plots were created from the optimized xyz cartesian coordinates in Diamond 3.2.[50] The free energies of the respective species are shown in Table A1.2. The Kohn-Sham molecular orbitals were plotted in Avogadro with ISO values for the surface set at 0.09.[51]

Calculation of $\Delta G^{\ddagger}$ from variable temperature ^1H NMR spectroscopy: A method for determining activation barriers to exchange processes between two inequivalent species has previously been described.[52] Using this method, two different activation barriers are calculated for the two inequivalent species in solution. In this case these two species are in fact topomers, distinguished only by arbitrarily assigning the three NHC groups and changing the orientation of the methyl ligand from between one pair to a neighboring pair. For simplicity, only one set of the coalescence temperatures and $\Delta G^{\ddagger}$ values were reported in the text where the $\Delta G^{\ddagger}$ value was calculated as the average of the A and B components with the standard deviation used as an estimate of the error.

$$\boldsymbol{\Delta G^{\ddagger} = 4.575 * 10^{-3} * Tc * \left(10.62 + \log\left(\frac{X}{2\pi(1 \pm \Delta P)}\right) + \log\left(\frac{Tc}{\Delta \nu}\right)\right)} \qquad \textbf{(Equation 2.1)}$$

Below are the data for a total of three different resonances of each species reported here for completeness. The equation shown was used to calculate the $\Delta G^{\ddagger}$ values where T_c = coalescence temperature, X and ΔP (0.67) are related to the difference in population of the doublet,[53] and $\Delta\nu$ = difference in Hz of the fully resolved doublet of the exchanging species.

2.5 References

§ Determined by searching the Cambridge Crystallographic Database using Conquest by limiting a 4-coordinate Ni center with two pairs of ligand bond angles restricted between 150–180° and 110–130°.

(1) P. A. Lindahl, J. Biol. *Inorg. Chem.*, **2004**, *9*, 516–524.

(2) X. Zhao, H.-Y. Tu, L. Guo, S. Zhu, F.-L. Qing and L. Chu, *Nat. Commun.*, **2018**, *9*, 3488.

(3) 3. L. Guo and M. Rueping, *Acc. Chem. Res.*, **2018**, *51*, 1185–1195.

(4) J. Hu, Y. Zhao, J. Liu, Y. Zhang and Z. Shi, *Angew. Chem., Int. Ed.*, **2016**, *55*, 8718–8722.

(5) D. Nianios, S. Thierbach, L. Steimer, P. Lulchev, D. Klostermeier and S. Fetzner, *BMC Biochem.*, **2015**, *16*, 10.

(6) M. Can, F. A. Armstrong and S. W. Ragsdale, *Chem. Rev.*, **2014**, *114*, 4149–4174.

(7) E. Carmona, F. Gonza´lez, M. L. Poveda, J. L. Atwood and R. D. Rogers, *J. Chem. Soc., Dalton Trans.*, **1980**, 2108–2116.

(8) P. Stoppioni, P. Dapporto and L. Sacconi, *Inorg. Chem.*, **1978**, *17*, 718–725.

(9) C. E. MacBeth, J. C. Thomas, T. A. Betley and J. C. Peters, *Inorg. Chem.*, **2004**, *43*, 4645–4662.

(10) P. J. Schebler, B. S. Mandimutsira, C. G. Riordan, L. M. Liable-Sands, C. D. Incarvito and A. L. Rheingold, *J. Am. Chem. Soc.*, **2001**, *123*, 331–332.

(11) N. Shirasawa, T. T. Nguyet, S. Hikichi, Y. Moro-oka and M. Akita, *Organometallics*, **2001**, *20*, 3582–3598.

(12) S. A. Macgregor, Z. Lu, O. Eisenstein and R. H. Crabtree, *Inorg. Chem.*, **1994**, *33*, 3616–3618.

(13) J. Ghannam, T. Al Assil, T. C. Pankratz, R. L. Lord, M. Zeller and W.-T. Lee, *Inorg. Chem.*, **2018**, *57*, 8307–8316.

(14) A. Tarai and J. B. Baruah, *Dalton Trans.*, **2018**, *47*, 4921–4930.

(15) T. A. Albright, J. K. Burdett and M.-H. Whangbo, Orbital Interactions in Chemistry, John Wiley & Sons, Inc., Hoboken, NJ, USA, 2nd edn, 2013.

(16) C. A. Grapperhaus, J. A. Bellefeuille, J. H. Reibenspies and M. Y. Darensbourg, *Inorg. Chem.*, **1999**, *38*, 3698–3703.

(17) R. Graziani, M. Vidali, U. Casellato and P. A. Vigato, *Transition Met. Chem.*, **1978**, *3*, 99–103.

(18) J. Li, D. Tian, H. Song, C. Wang, X. Zhu, C. Cui and J. P. Cheng, *Organometallics*, **2008**, *27*, 1605–1611.

(19) M. Bröring, S. Prikhodovski and C. D. Brandt, J. Chem. Soc., *Dalton Trans*., **2002**, 4213–4218.

(20) M. Bröring, S. Prikhodovski and C. D. Brandt, *Inorg. Chim. Acta*, **2004**, *357*, 1733–1738.

(21) M. Bröring, S. Prikhodovski, C. D. Brandt and E. C. Tejero, *Chem. – Eur. J.*, **2007**, *13*, 396–406.

(22) J. A. Adjei, A. J. Lough and R. A. Gossage, *RSC Adv.*, **2019**, *9*, 3956–3964.

(23) P. G. Edwards, F. Ingold and M. B. Hursthouse, *Chem. Commun*., **1998**, 545–546.

(24) M. K. Goetz, E. A. Hill, A. S. Filatov and J. S. Anderson, *J. Am. Chem. Soc.*, **2018**, *140*, 13176–13180.

(25) M. K. Goetz and J. S. Anderson, *J. Am. Chem. Soc.*, **2019**, *141*, 4051–4062.

(26) R. A. Juarez, W.-T. Lee, J. M. Smith and H. Wang, *Dalton Trans*., **2014**, *43*, 14689–14695.

(27) I. Nieto, R. P. Bontchev and J. M. Smith, Eur. J. *Inorg. Chem*., **2008**, 2476–2480.

(28) S. B. Mun˜oz, W. K. Foster, H.-J. Lin, C. G. Margarit, D. A. Dickie and J. M. Smith, *Inorg. Chem.*, **2012**, *51*, 12660–12668.

(29) R. E. Cowley, R. P. Bontchev, E. N. Duesler and J. M. Smith, *Inorg. Chem.*, **2006**, *45*, 9771–9779.

(30) L. Yang, D. R. Powell and R. P. Houser, *Dalton Trans.*, **2007**, 955–964.

(31) D. Rosiak, A. Okuniewski and J. Chojnacki, *Polyhedron*, **2018**, *146*, 35–41.

(32) H. Shanan-Atidi and K. H. Bar-Eli, *J. Phys. Chem*., **1970**, *74*, 961–963.

(33) J. Sandström, Dynamic NMR Spectroscopy, Academic Press, London, 1982.

(34) M. Mauksch and P. v. R. Schleyer, *Inorg. Chem*., **2001**, *40*, 1756–1769.

(35) J. Cirera, E. Ruiz and S. Alvarez, *Inorg. Chem*., **2008**, *47*, 2871–2889.

(36) B. Le Guennic, T. Floyd, B. R. Galan, J. Autschbach and J. B. Keister, *Inorg. Chem*., **2009**, *48*, 5504–5511.

(37) N. S. Gill and R. S. Nyholm, *J. Chem. Soc.*, **1959**, *0*, 3997.

(38) R. E. Cowley, R. P. Bontchev, E. N. Duesler and J. M. Smith, *Inorg. Chem.*, **2006**, *45*, 9771–9779.

(39) Y. Xiong, S. Yao, T. Szilvási, E. Ballestero-Martínez, H. Grützmacher and M. Driess, *Angew. Chem., Int. Ed*., **2017**, *56*, 4333–4336.

(40) Y. Fan, J. Cheng, Y. Gao, M. Shi and L. Deng, *Acta Chim. Sin*., **2018**, *76*, 445–452.

(41) D. F. Evans, *J. Chem. Soc*., **1959**, 2003–2005.

(42) G. M. Sheldrick, SHELXTL, 2014.

(43) G. M. Sheldrick, *Acta Crystallogr*., **2015**, *A71*, 3–8.

(44) G. M. Sheldrick, *Acta Crystallogr*., **2015**, *C71*, 3–8.

(45) L. Krause, R. Herbst-Irmer, G. M. Sheldrick and D. Stalke, *J. Appl. Crystallogr*., **2015**, *48*, 3–10.

(46) F. Neese, Wiley *Interdiscip. Rev. Comput. Mol. Sci.*, **2012**, *2*, 73–78.

(47) F. Weigend and R. Ahlrichs, *Phys. Chem. Chem. Phys*., **2005**, *7*, 3297–3305.

(48) A. Schäfer, C. Huber and R. Ahlrichs, *J. Chem. Phys*., **1994**, *100*, 5829–5835.

(49) A. Schäfer, H. Horn and R. Ahlrichs, *J. Chem. Phys*., **1992**, *97*, 2571–2577.

(50) D. H. Putz and D. K. Brandenburg, Diamond - Crystal and Molecular Structure Visualization, Crystal Impact, GbR, Kreuzherrenstr. 102, 53227 Bonn, Germany.

(51) M. D. Hanwell, D. E. Curtis, D. C. Lonie, T. Vandermeersch, E. Zurek and G. R. Hutchison, *J. Cheminform*., **2012**, *4*, 17.

(52) H. Shanan-Atidi and K. H. Bar-Eli, *J. Phys. Chem*., **1970**, *74*, 961–963.

(53) J. Sandström, Dynamic NMR Spectroscopy, Academic Press, London, 1982

Chapter 3: Synthesis and Reactivity of a Ni^{III}_2-(μ-1,2-peroxo) Complex

This chapter has been adapted from the following source with permission: Zhao, N., Filatov, A. S., Xie, J., Hill, E. A., Rogachev, A.Yu., Anderson, J. S. *J. Am. Chem. Soc.*, **2020**, *142*, 21634-21639.

3.1 Introduction

High-valent oxygenated transition metal species, such as oxo, peroxo, and superoxo complexes, are ubiquitous intermediates in oxidative reactivity. In particular, oxygenated first-row transition metal complexes are prominent in both biological and synthetic systems for the oxidation of organic substrates,[1,2] water oxidation,[3,4] and oxygen reduction.[5,6] Despite the generality of these proposed intermediates, the high reactivity of oxygenated transition metal complexes can make isolation and characterization challenging. Nevertheless, understanding their structure, properties, and viability is essential to elucidating or improving many processes.[7]

While numerous examples of high-valent oxygenated complexes of Mn,[8–14] Fe,[11,12,14–18] Co,[13,19–24] and Cu[25–33] have been isolated and studied, significantly fewer oxygenated Ni complexes have been reported,[13,34–49] despite the fact that high-valent Ni-oxo, -peroxo, and -superoxo complexes have been invoked in water oxidation,[50,51] biological superoxide dismutation,[52] oxygen reduction,[53] and organic oxidation catalysis.[35,40,54] No well-defined terminal Ni-oxo complexes are known, and Ni-superoxo species are still rare.[40,41,55,56] In the case of Ni-peroxo complexes, several examples of mononuclear Ni^{III} species have been reported,[57–60] and some dinuclear complexes have been transiently observed.[61,62] One Ni^{II}_2-(μ-1,2-peroxo) complex has recently been structurally characterized,[63] but no high-valent bridging Ni–peroxo complexes

are known, despite the potential importance of these species in, for example, oxo coupling mechanisms for water oxidation by Ni-based layered double hydroxides.[50,51,64]

Previously, tris(NHC)phenylborate (NHC = N-heterocyclic carbene) ligands have been used to stabilize unusual Co^{III}-oxo and Fe^{III}-oxo complexes.[19,65] We rationalized that this system might also aid in the stabilization of high-valent Ni complexes with oxygen-based ligands. Herein we report the use of $PhB(^tBuIm)_3^-$ to isolate the first example of a Ni^{III}_2-(μ-1,2-peroxo) complex, $\{[PhB(^tBuIm)_3]Ni{-}O{-}O{-}Ni\text{-}[(^tBuIm)_3BPh]\}\{BAr^F{}_4\}_2$ (**3**) ($BAr^F{}_4$ = tetrakis(3,5-bis-(trifluoromethyl)phenyl)borate). Complex **3** has been structurally characterized, and its properties have been examined using a variety of spectroscopic techniques. Reactivity studies show that **3** is comparatively stable toward oxygen dissociation, C−H activation, and O atom transfer but reacts rapidly with both nucleophiles and electrophiles at low temperature. These results demonstrate that high-valent bridging Ni-peroxo intermediates are viable and provide insight into their properties and reactivity.

3.2 Synthesis and Characterization of a Ni^{III}_2-(μ-1,2- peroxo) Complex

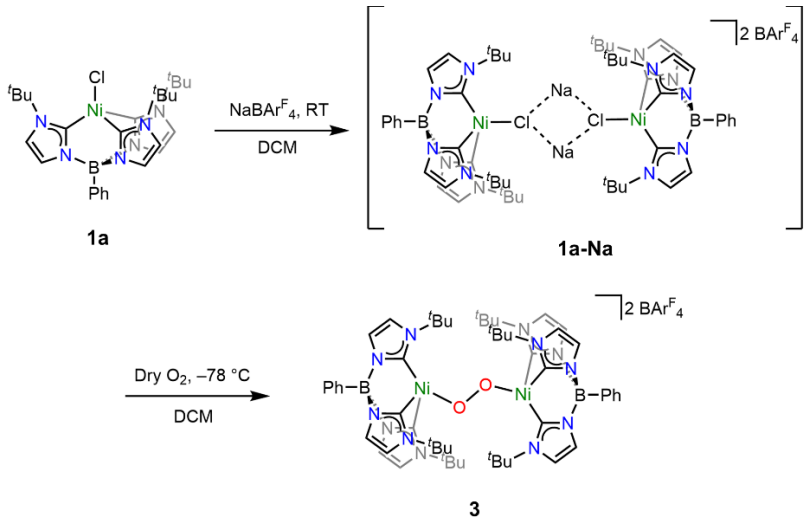

Scheme 3.1. Synthesis of 1a-Na and 3.

The synthesis of the Ni−chloride precursor [PhB(^{t}BuIm)$_3$]NiCl (**1a**) was recently reported by our group.[66] As **1a** shows no reactivity under an atmosphere of oxygen for several days, we screened common halide abstractors such as Na^+, Ag^+, and Tl^+ salts to encourage reactivity. While addition of AgOTf or TlOTf led to intractable mixtures of diamagnetic products, treatment of 1 with $NaBAr^F_4$ in dichloromethane (DCM) caused the solution to change from dull chartreuse green to dark emerald green, indicative of the formation of a new species, **1a-Na** (Scheme 3.1 and Figure 3.1). A similar color change was observed in other noncoordinating solvents such as 1,3-difluorobenzene. However, **1a-Na** is extremely sensitive to even small amounts of coordinating impurities such as ethers or variations in preparation conditions, precluding detailed characterization of this species (Figure A2.1). While we do not have concrete characterization data on this complex, we tentatively propose an intermediate structurally similar to **1a-Na** with a weak interaction between Na^+ ions and the chloride ligand. This proposed structure is also supported by a comparison of the paramagnetic ^{1}H NMR spectra of **1a** and **1a-Na**, which show shifted but similar overall patterns of resonances. Furthermore, treatment of **1a-Na** with 12-crown-4 ether to sequester Na^+ ions regenerates **1a** as determined by ^{1}H NMR spectroscopy (Figure A2.2). On the basis of these data and similar species previously reported, we tentatively propose that **1a-Na** is a dimer as depicted in Scheme 1.[67]

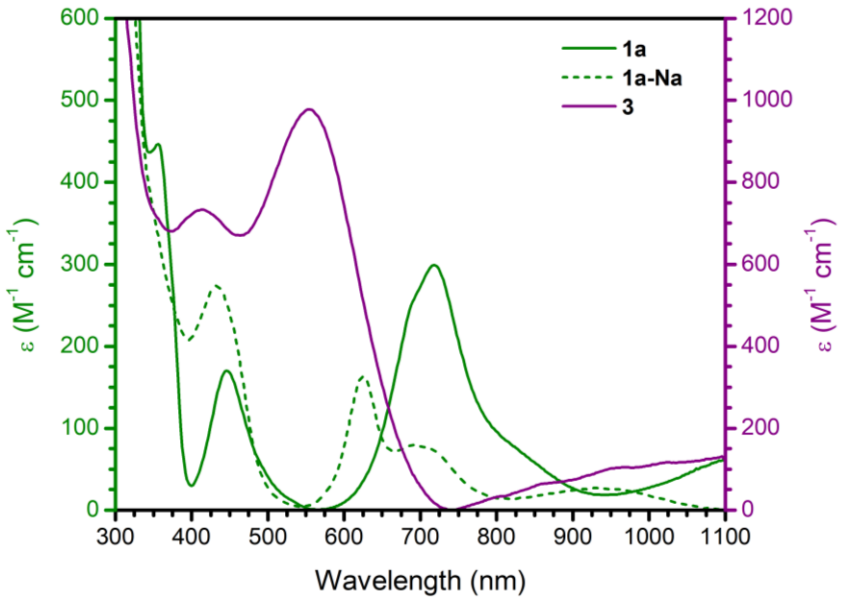

Figure 3.1. UV–vis spectra of 1a, 1a-Na (RT), and 3 (−78 °C) in DCM.

Treatment of **1a-Na** in DCM with dry oxygen at room temperature results in an intractable brown mixture of diamagnetic products as ascertained by ^{1}H NMR spectroscopy. However, at −78 °C addition of either stoichiometric or excess oxygen to **1a-Na** in DCM results in a nearly instantaneous color change from emerald green to dark purple (Figures S3 and S4). We assign this new purple species as the dimeric Ni^{III}_2-(μ-1,2-peroxo) complex {[PhB(^{t}BuIm)$_3$]-Ni−O−O−Ni-[(^{t}BuIm)$_3$BPh]}{BAr$^{F}_4$}$_2$ (**3**) (**Scheme 3.1**). The distinct color change is reflected in the UV−vis spectrum of **3** (Figure 3.1), which displays features at 410 nm (740 M^{-1} cm^{-1}) and 550 nm (970 M^{-1} cm^{-1}) that are dramatically different from those in the spectrum of **1a** or **1a-Na**. Time-dependent density functional theory (TD-DFT) calculations provide a reasonable reproduction of the electronic absorption spectrum, assigning the main feature at 550 nm to a mixed ligand-to-metal charge transfer transition.

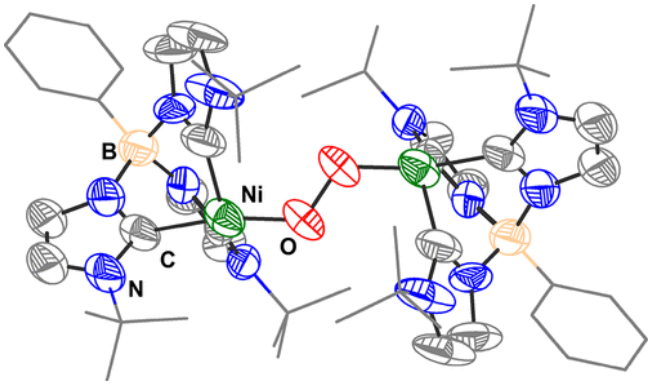

Figure 3.2. SXRD structure of 3.

Ni atoms are shown in green, O atoms in red, C atoms in gray, N atoms in blue, and B atoms in tan. Ellipsoids are shown at 50% probability. For clarity, solvent molecules, counterions, and H atoms have been omitted, and parts of the ligand scaffold are shown as wireframe.

Fortunately, dark-purple crystals of **3** could be grown over several days at −78 °C. Single-crystal X-ray diffraction (SXRD) confirmed the formation of a Ni^{III}_2-(μ-1,2-peroxo) complex (**Figure 3.2**). While the quality and resolution of the data set is limited because the crystal contained large numbers of solvent molecules and severe disorder of BAr^F_4−counterions, the structure of **3** nevertheless provides important information. The O−O bond length is 1.42(2) Å, which falls between the O−O bond lengths observed in Meyer's β-diketiminato Ni^{II}_2-(μ-1,2-peroxo) complex (1.465(2) Å) and Nam's mononuclear η^2 12-TMC and 13-TMC Ni^{III}-peroxo complexes (12-TMC = 1,4,7,10-tetramethyl-1,4,7,10-tetraazacyclododecane, 13-TMC = 1,4,7,10-tetramethyl-1,4,7,10-tetraazacyclotridecane) (1.386(4) and 1.383(4) Å, respectively).[57,63] For comparison, the O−O bond lengths in two previously isolated Ni_2-(μ-1,2-superoxo) complexes are 1.33 and 1.35 Å.[34,63] The spin density of **3** calculated by DFT is primarily localized on Ni, which further supports the formulation of this complex as a Ni^{III}_2-(μ-1,2-peroxo) complex (Figure S5). The solid-state structure of **3** shows that the Ni^{III} centers adopt a seesaw geometry, with a Ni−O bond length of 1.796(9) Å and a Ni−O−O−Ni dihedral angle of 161.8(5)°. The Ni−O bond lengths are shorter than those in Meyer's Ni^{II}_2-(μ-1,2-peroxo) complex, which has Ni−O bond lengths of

1.834(2) Å and a dihedral angle of 89.9(2)°.[63] The shorter Ni−O distances are consistent with the higher oxidation state of Ni^{III} in **3**.

Similar solution and solid-state structures of **3** are supported by NMR spectroscopic data. The ^{1}H NMR spectrum of **3** collected at −78 °C has broadened and shifted resonances, consistent with a paramagnetic species (Figure A2.4). In compound **1a**, the ^{1}H NMR resonances (CD_2Cl_2) at 106 and 16 ppm have been assigned to the hydrogens of the imidazol-2-ylidene backbone. A similar pattern is seen in **3**, but with a doubling of these signals (118, 106, −13, −17 ppm), suggestive of an asymmetric dimer at −78 °C. Additionally, two large resonances corresponding to the tert-butyl groups are visible at 15 and 17 ppm. We propose that this pattern arises from a combination of the seesaw geometry about the nickel centers and slow isomerization about the B−Ni−O vector at −78 °C, as observed in a Ni-methyl complex supported by this ligand scaffold.[66] The same ^{1}H NMR spectra are observed for samples of crystalline **3** dissolved in CD_2Cl_2 and samples of **3** generated in situ by addition of O_2 to **1a-Na**, confirming that complex **3** is formed in situ in a relatively clean manner.

The effective magnetic moment of **3** was measured by Evans' method at −78 °C to be μ_{eff} = 3.2(1) μ_B. This value is higher than would be expected for two weakly coupled S = 1/2. centers ($\mu_{S.O.}$ = 2.45 μ_B) and is more consistent with ferromagnetic coupling to give an S = 1 ground state ($\mu_{S.O.}$ = 2.82 μ_B). DFT calculations support this assignment, predicting a ferromagnetically coupled system (J = 36 cm^{-1}) and showing spin density consistent with ferromagnetic exchange. Additionally, the X-band electron paramagnetic resonance spectrum of a solution of **3** in DCM at 15 K is nearly silent, with only a weak signal centered around g = 2 that accounts for <10% of the Ni in the sample by spin integration. While metal complexes bridged by dioxygen ligands are commonly antiferromagnetically coupled, there is a recent example of a ferromagnetically coupled

copper system.[68] While we were unable to perform solid-state magnetometry on **3** because of its thermal instability, we did perform variable-temperature Evans' method measurements. An accurate determination of the J coupling constant is not possible because of the limited temperature range from the solvent freezing point and compound stability, but a persistent moment of ~3 μ_B further supports the assigned $S = 1$ ground state (Figure S7).

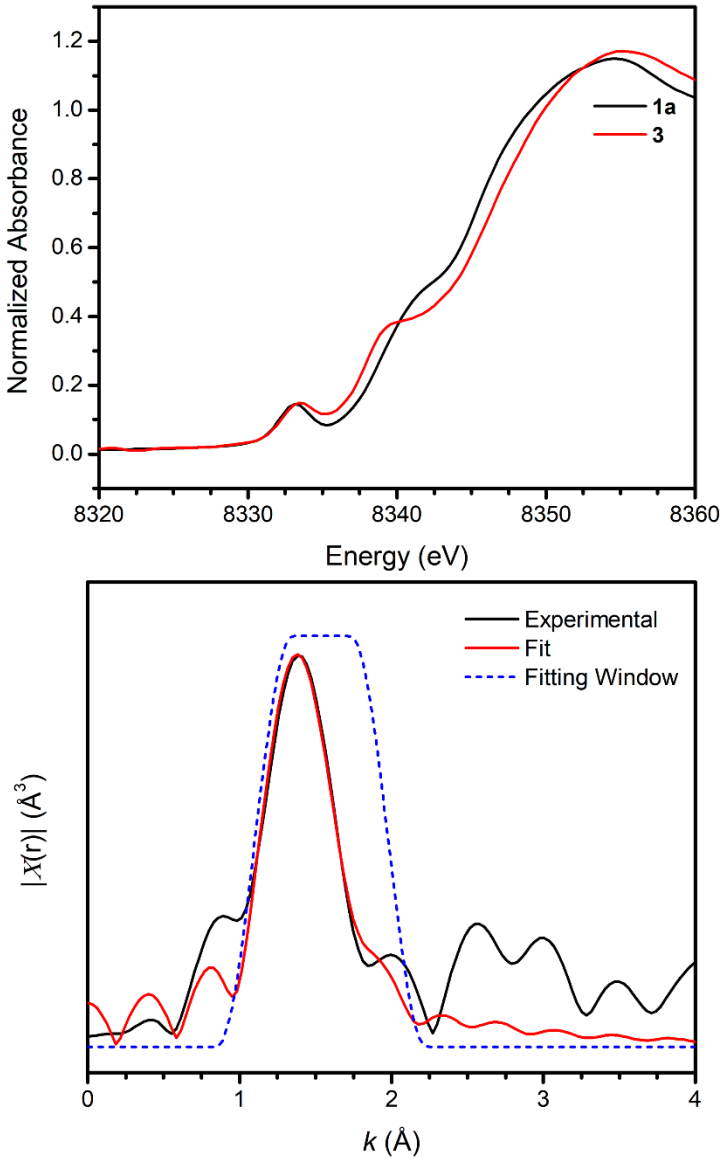

Figure 3.3. Ni K-edge X-ray absorption spectra of 1a and 3, (top) XANES region and (bottom) EXAFS (black) and fit (red) in R space of 3.

To further interrogate the solution-state structure of **3** and probe the assigned oxidation states of Ni, we turned to Ni K-edge X-ray absorption spectroscopy (XAS). The Ni K-edge of **3** (8346.1 eV, THF frozen solution, −135 °C) occurs at higher energy than that of **1a** (8345.4 eV, powder, room temperature) (Figure 3.3, Figure A2.6, Figure A2.7, Figure A2.8 and Table A2.2Table A2.3). The difference in the Ni K-edge between **1a** and **3** is outside of error (±0.4 eV), but it should be noted that one-electron oxidation from Ni^{II} to Ni^{III} in synthetic complexes produces shifts ranging from 0 to 1.8 eV and care must therefore be taken in interpreting this shift as an indicator of a change in oxidation state.[35,57,69,70] Analysis of the extended X-ray absorption fine structure (EXAFS) region of **3** suggests a reasonable fit with a simple model containing one oxygen and three carbon atoms in the first shell, consistent with the structure obtained by SXRD. Taken together, the observed bond lengths, magnetic properties, and shift in the Ni K-edge of **3** support the assignment of a Ni^{III}-peroxo complex.

We synthesized the $^{18}O_2$ isotopologue of **3** to further characterize the O−O bond through vibrational spectroscopy. However, we were unable to assign a vibrational band to the O−O stretch by either infrared or Raman spectroscopy of **3** at low temperatures, likely because of either Raman laser photodegradation of **3** or weak resonance enhancement of the peroxo vibration (Figure A2.9).[37]

3.3 Reactivity of Compound **3**

With complex **3** in hand, we sought to examine its reactivity, particularly the possible reversibility of dioxygen binding, as this process has relevance to oxygen evolution. Subjecting **3** to several freeze-pump-thaw cycles in DCM resulted in no change in the UV-vis spectrum of the solution. This observation excludes an equilibrium process for O_2 binding. Additionally, 3 does not react with dihydroanthracene or phosphines at low temperature. However, addition of 10 equiv

of tetrabutylammonium chloride (TBACl) to **3** in DCM at −78 °C produced a color change from dark purple to green upon warming to −50 °C, and 87% recovery of **1a** was observed by ^{1}H NMR spectroscopy (**Figure A2.10, Figure** A2.11). The balanced reaction requires the formal release of O_2, but we were not able to observe dioxygen release into the headspace by GC analysis under the reaction conditions. We hypothesize that a shortlived reactive oxygen species (ROS) or Ni complex must be generated that reacts further in solution. However, we were unable to definitively intercept any such species using a variety of reagents, including the singlet oxygen trap 9,10-dimethylanthracene or the ROS trap 1,3-diphenylisobenzofuran.[71]

To investigate alternative reactivity, we next treated **3** with trimethylsilyl chloride (TMSCl), hypothesizing that oxygen could be released in the form of bis(trimethylsilyl) peroxide (TMS_2O_2). Instead, addition of 10 equiv of TMSCl to **3** at −78 °C yielded bis(trimethylsilyl) ether (TMS_2O) in good yield as determined by ^{1}H NMR and GC-MS analysis. Complex **1a** was not observed in this reaction mixture. Addition of TMSCl to ^{18}O-labeled **3** followed by GC−MS analysis confirmed that the oxygen in the resultant TMS_2O arose from **3**. We propose that any TMS_2O_2 formed in the reaction is decomposed by reactive Ni-containing products. Indeed, TMS_2O_2 that was added concomitantly with TMSCl to **3** under the same reaction conditions decomposed. Despite these complicated product distributions, the observed reactivity suggests that this Ni^{III}_2-(μ-1,2-peroxo) complex does not release oxygen dissociatively and instead reacts with other species such as nucleophiles or electrophiles.

3.4 Conclusion

In summary, we have generated and characterized an unusual Ni^{III}_2-(μ-1,2-peroxo) complex, **3**. The SXRD structure and X-ray absorption, ^{1}H NMR, and UV-vis spectra of **3** confirm the assignment of a Ni^{III}_2-(μ-1,2-peroxo) moiety. Furthermore, this complex is reactive toward both

nucleophiles, such as Cl−, and electrophiles, such as TMSCl. Taken together, these data demonstrate that Ni^{III}_2-(μ-1,2-peroxo) species are synthetically accessible and provide insights into their reactivity.

3.5 Experimental

3.5.1 Materials and Instrumentation

All manipulations were performed under a dry nitrogen atmosphere using either standard Schlenk techniques or in an mBraun Unilab Pro glove box unless otherwise stated. All chemicals were obtained from commercial sources and used as received unless otherwise stated. Solvents were dried on a solvent purification system from Pure Process Technologies and passed through a column of activated alumina before storing over 4 Å molecular sieves under N_2. Diethyl ether and tetrahydrofuran (THF) were stirred over NaK alloy and passed through a column of activated alumina prior to storing over 4 Å sieves under N_2. Natural abundance oxygen (98%) was passed through a column of Drierite prior to use, and ^{18}O-enriched ^{18}O2 (99.9% O_2, 1.5 atom% ^{16}O, 0.5 atom% ^{17}O) was used as received from ICON isotopes. PhB(^{t}BuIm)$_3$NiCl and sodium tetrakis(3,5-bis(trifluoromethyl)phenyl)borate) ($NaBAr^F_4$) were prepared according to literature procedures.[72] Genuine samples of 9,10-dimethylanthracene endoperoxide and 1,2-dibenzoylbenzene were synthesized using previously reported literature procedures.[73] UV-vis spectra were recorded on a Thermo Scientific Evolution 300 spectrometer with the VISIONpro software suite. A standard 1 cm quartz cuvette with an air-tight screw cap was used for all measurements. A Unisoku CoolSpek cryostat was used for low temperature measurements. EPR spectra were recorded on a Bruker Elexsys E500 spectrometer with an Oxford ESR 900 X-band cryostat and a Bruker Cold-Edge Stinger. ^{1}H NMR spectra were recorded using either Bruker DRX-400 or AVANCE-500 spectrometers and referenced to residual solvent peaks. Magnetic moments were determined using the Evans' method.[74] Gas chromatograms (GC) and electron ionization-mass spectra (EI-MS) were recorded on an Agilent 6890/5973 GC/MS (low resolution) instrument. X-ray Absorption Measurements Samples of PhB(^{t}BuIm)$_3$NiCl (1) were prepared by packing finely ground powder

into a PTFE washer (5.3 mm internal diameter) sealed on one side with Kapton tape. The powder was compacted with a PTFE rod and one face of the washer sealed with Kapton tape. All sample preparation was performed under an inert atmosphere. Data were acquired at the Advanced Photon Source at Argonne National Laboratory with a bending magnet source with ring energy at 7.00 GeV. Ni K-edge (8332.8 eV) data were acquired at the MRCAT 10-BM beam line in transmission. The incident, transmitted and reference X-ray intensities were monitored using gas ionization chambers. A metallic nickel foil standard was used as a reference for energy calibration and was measured simultaneously with experimental samples. X-ray absorption spectra of 1 were collected at room temperature. Samples of **3** were prepared by precipitating **3** with cold hexanes from dichloromethane (DCM) solution. The purple powder was then quickly weighed and dissolved in cold tetrahydrofuran (THF) to make 2 mL of a ca. 30 mM solution. A rectangular window (0.5 cm x 1.5 cm) was cut into a strip of PTFE (5 x 1 x 0.2 cm) and Kapton tape was used to seal one side of the window with the other side partially covered with Kapton to leave a gap on top for sample addition. The PTFE sample window was partially immersed in liquid nitrogen and the THF solution of **3** was carefully pipetted into the top of the window. The frozen solution was kept at −135 °C during data collection using a Unisoku CoolSpek cryostat fitted with Kapton windows. Data collected was processed using the Demeter software suite by extracting the EXAFS oscillations $\chi(k)$ as a function of photoelectron wavenumber k. The theoretical paths were generated using FEFF6 and the models were determined using the fitting program Artemis.[75] For analysis of the EXAFS region, the K-edge position was chosen using the maximum of the first derivative of the Ni XANES spectrum. Two possible models were considered, one with 3 C atoms at ~1.9 Å and one O at ~1.8 Å, and one fit with 2 C atoms at ~1.9 Å and 1 C/1 O (2 O's for fitting

purposes) at ~1.8 Å. Both models give similar quality fits. The model with 3 C's at 1.9 Å is preferred due to slightly better fit statistics and is shown in main chapter.

Raman Spectroscopy Solid-state Raman spectra were recorded on a Horiba LabRAM HR evolution confocal Raman microscope, using a 50x objective lens, using a variety of laser wavelengths (473, 532, 633, 785 nm) with a 600 or 1800/mm grating and a Synapse CCD detector system. Of these conditions, the sharpest spectra resulted from excitation wavelengths of 532 nm (10 mW), with 1800/mm grating. Solid samples of **3** were cooled in a Linkam stage to 100 K under positive nitrogen pressure. The Raman spectrum of $NaBAr^{F}{}_{4}$ was recorded on a microscope slide at room temperature. Frozen solution Raman spectra were collected on samples contained in NMR tubes that were submersed in liquid nitrogen and upon excitation with a Coherent I-305 Ar^{+} ion laser (514 nm) with 20 mW laser power at the sample. The ~135° backscattered light was dispersed by an Acton Research triple monochromator equipped with 1200 and 2400 groves/mm gratings and analyzed with a Princeton Instruments Spec X:100BR deep depletion, back-thinned CCD camera.

Density functional theory (DFT) calculations

Geometry optimizations were performed with help of BP86 density functional using relativistically re-contracted basis sets of triple-ζ quality for all atoms (ZORA-def2-TZVP). No symmetry restrictions were applied. Scalar relativistic effects were taken into account by applying ZORA approximation.[76]

The optimized geometry for the triplet state was then used for broken-symmetry DFT calculations (in BS(1,1) variant) using hybrid exchange-correlation functional PBE0 (ultra-high integration grid Grid6 and GridX8).[77,78] The J-coupling constant was calculated using Yamaguchi formula.[79]

Throughout all calculations the accelerating technique RIJCOSX was applied.[80] All computations were carried out with help of ORCA program package (version 4.2.0).[81] TDDFT calculations were calculated using the def2/SVP basis set on all atoms except for Ni, O, N and carbene C's where def2/TZVVP was used. The RIJCOSX approximation and the PBE0 functional were also used. The UV-vis spectra were generated using the orca_plot module using a broadening of 3000. Spin densities and electron densities were visualized using Avogadro software.[82]

3.5.2 Complex Synthesis and Characterization

{[PhB(^{t}BuIm)$_3$]NiCl–Na$_2$–ClNi[(^{t}BuIm)$_3$BPh]}{BAr$^F{}_4$}$_2$ (1a-Na): In a nitrogen-filled glovebox, a vial was charged with equimolar chartreuse green PhB(^{t}BuIm)$_3$NiCl (10 mg, 0.018 mmol) and NaBAr$^F{}_4$ (16 mg, 0.018 mmol). The solids were dissolved in DCM, such that the concentration of Ni was greater than 1.75 mM, whereupon standing for five minutes, the solution changed from dull chartreuse green to an intense emerald green. ^{1}H NMR (d$_2$-DCM, 500 MHz, 298 K): δ 120.71 (Im), 19.07 (^{t}Bu), 11.75 (Im), 8.20 (Ph), 8.02 (Ph), 7.73 (BAr$^F{}_4^-$), 7.57 (BAr$^F{}_4^-$). UV-vis, nm in DCM (ε, M^{-1} cm^{-1}): 434 (270), 624 (160), 696 (80), 938 (30). The sensitivity of the complex to conditions such as solvent, concentration, air and moisture precluded isolation or analysis by other methods.

{[PhB(^{t}BuIm)$_3$]NiO$_2$Ni[(^{t}BuIm)$_3$BPh]}{BAr$^F{}_4$}$_2$ (3): In a nitrogen-filled glovebox, a filter flask was charged with PhB(^{t}BuIm)$_3$NiCl (55 mg, 0.10 mmol) and NaBAr$^F{}_4$ (89 mg, 0.10 mmol). The solids were then dissolved in DCM (5 mL) and allowed to stand for 5 minutes to form a solution of 1-Na in DCM. The top and sidearm of the filter flask were then sealed with rubber septa, and brought out of the glovebox. The flask was swiftly placed under positive nitrogen pressure and cooled to –78 °C in an acetone/dry ice bath. Addition of excess dry oxygen (20 mL, 160 equiv) to the emerald green solution resulted in an immediate color change to dark purple. Crystals suitable

for X-ray diffraction were obtained by storing this solution at –78 °C. Alternatively, hexanes (–78 °C) can be added to the reaction mixture resulting in the bulk precipitation of **3**. After decanting the supernatant, the dark purple solid was then washed with cold pentane (3 x 10 mL) and dried briefly at reduced temperatures under vacuum to obtain a free-flowing purple powder (84 mg, 60% yield). ^{1}H NMR (d_2-DCM, 500 MHz, 195 K): δ 109.43 (Im), 100.11 (Im), 21.67 (Ph), 17.14 (^{t}Bu), 14.84 (^{t}Bu), 7.71 ($BAr^{F}_{4}^{-}$), 7.50 ($BAr^{F}_{4}^{-}$), –13.02 (Im), –15.04 (Im). Evans' method (average of 3 trials): μ_{eff} = 3.35(7) μ_B. UV-vis, nm in DCM (ε, M^{-1} cm^{-1}): 410 (740) and 550 (970). Due to thermal instability, elemental analysis and IR spectra were unable to be collected for this complex.

^{18}O-labeled isotopologue: ^{18}O-labeled **3** was prepared as described above, using $^{18}O_2$ in the place of natural abundance O_2.

3.5.3 Other Experimental Procedures

UV-vis Spectroscopy of 1a. A solution of **1a** (2 mM) was transferred to a quartz cuvette and sealed in the glovebox before collecting a spectrum at room temperature.

UV-vis Spectroscopy of 1a-Na. A scintillation vial was charged with equimolar **1a** and $NaBAr^{F}_{4}$. Solids were dissolved in DCM to make a 4 mM solution, allowed to stand for 5 minutes and transferred to a quartz cuvette and sealed with a screwtop septum cap in the glovebox before collecting a spectrum at room temperature.

UV-vis Spectroscopy of 3. A scintillation vial was charged with equimolar **1a** and $NaBAr^{F}_{4}$. Solids were dissolved in DCM to make a 2 mM solution of **1a-Na** and allowed to stand for 5 minutes. Next, 0.25 mL of the solution was transferred to a quartz cuvette and sealed with a screwtop cap in the glovebox. The solution was then cooled to –78 °C in the cryostat set up in the UV-vis spectrometer. Separately, sparged 10 mL DCM with oxygen for 30 minutes at –78 °C.

Then, 2.25 mL of the oxygenated DCM was swiftly injected into the precooled cuvette. To monitor the formation of **3**, spectra were collected every 100 ms at 550 nm (under superstoichiometric O_2 conditions).

Oxygen uptake of 1a-Na to form 3. A scintillation vial was charged with equimolar **1a** and $NaBAr^F{}_4$. Solids were dissolved in DCM to make a 2 mM solution of **1a-Na** and allowed to stand for 5 minutes. Next, 0.25 mL of the solution was transferred to a quartz cuvette and sealed with a screwtop cap in the glovebox. The solution was then cooled to –78 °C in the cryostat set up in the UV-vis spectrometer. Then, 7 μL (1.25 equiv) dry O_2 was injected into the reaction mixture with a 10 μL gas-tight syringe, followed by 2.25 mL of dry, deoxygenated DCM, cold. Evans' method of **3**. A scintillation vial was charged with **1a** (15 mg) and $NaBAr^F{}_4$ (24 mg) and 400 μL of d_2-DCM was added to dissolve the solids, forming **1a-Na**. Then, filtered through a thin pad of celite, and flushed pad of celite with 300 μL of d_2-DCM. The solution was transferred to a J. Young tube and sealed before being brought out the glovebox and immediately frozen in liquid nitrogen. The tube was warmed to –78 °C while oxygen was bubbled through solution. A capillary containing 2% DCM in d_2-DCM was added to the J. Young tube before being stored at –78 °C prior to data collection. A ^{1}H NMR spectrum was collected at –78 °C and the shift of the residual solvent signal was used to calculate the magnetic moment. This procedure was done six times, with an average μ_{eff} of 3.2(2) μ_B. For variable temperature experiments, spectra were recorded at points ranging from –91 °C and –60 °C. Solvent densities at each temperature were corrected according to previously reported values for DCM.[83]

Reactivity of 3 with tetrabutylammonium chloride (TBACl). A scintillation vial was charged with 1 (15 mg) and $NaBAr^F{}_4$ (24 mg) and 2 mL of DCM was added to dissolve the solids, forming **1a-Na**. The solution of **1a-Na** was transferred to a flame-dried 10 mL Schlenk flask, sealed,

brought out of the glovebox and then cooled to –78 °C under positive nitrogen pressure. To the solution was then bubbled excess (10 mL) dry oxygen. After five minutes, the solution of 3 was freeze-pump-thawed three times before the flask was backfilled with nitrogen. To this was added 10 equiv. TBACl (per Ni center) dissolved in DCM, and the reaction mixture was then slowly warmed to room temperature over an hour. The reaction mixture was observed to turn from purple to green at ca. –50 °C. Volatiles were removed from the green reaction mixture and residue was redissolved in C_6D_6 before collecting a ^{1}H NMR spectrum at room temperature. This was done in triplicate to give an 87% yield of **1a** by ^{1}H NMR integration. The yield of **1a** was determined by comparing the integration of the peak at 15 ppm with a calibration curve generated using pure **1a** in d_2-DCM integrated versus a mesitylene standard (0.01 mmol) to ensure the fidelity of integrated paramagnetically broadened peaks.

Reactivity of 3 with singlet oxygen acceptors 9,10-dimethylanthracene and 1,3-diphenylisobenzofuran. A scintillation vial was charged with **1a** (15 mg) and $NaBAr^F{}_4$ (24 mg) and 2 mL of DCM was added to dissolve the solids, forming **1a-Na**. The solution of **1a-Na** was transferred to a flame-dried 10 mL Schlenk flask, sealed, brought out of the glovebox and then immediately frozen in liquid nitrogen under positive nitrogen pressure. After warming the reaction mixture to –78 °C, bubbled excess (4 mL) $^{18}O_2$. After five minutes, the solution of **3** was freeze-pump-thawed three times before the flask was backfilled with nitrogen. A solution of either 9,10-dimethylanthracene or 1,3-diphenylisobenzofuran in DCM (10 equiv. per peroxo complex, in 1 mL) was added to a frozen solution of **3** (^{18}O-enriched in the case of 9,10-dimethylanthracene). The reaction mixture was vigorously stirred and warmed to room temperature over one hour, concentrated and brought into the glovebox. The residue was resuspended in 2 mL DCM and filtered through a thin pad of silica. The contents were analyzed with GC-MS, with 1 μL dodecane

added as an internal standard. Neither $^{18}O_2$-entriched 9,10-dimethylanthracene endoperoxide nor 1,2-dibenzoylbenzene were observed in their respective reactions, but can be observed by GC-MS when independently synthesized and subjected to the workup conditions.

Reactivity of 3 with trimethylsilyl chloride A scintillation vial was charged with **1a** (15 mg) and $NaBAr^F{}_4$ (24 mg) and 2 mL of DCM was added to dissolve the solids, forming **1a-Na**. The solution of **1a-Na** was transferred to a flame-dried 10 mL Schlenk flask, sealed, brought out of the glovebox and then immediately frozen in liquid nitrogen under positive nitrogen pressure. After warming the reaction mixture to –78 °C, bubbled excess (4 mL) natural abundance O_2 or $^{18}O_2$. After five minutes, the solution of **3** was freeze-pump-thawed three times before the flask was backfilled with nitrogen. A solution of trimethylsilyl chloride (TMSCl) (10 equiv., 1 mL solvent) was added to the frozen solution of **3**. The reaction mixture was vigorously stirred and warmed to room temperature over one hour, concentrated and brought into the glovebox. The residue was resuspended in 2 mL DCM and filtered through a thin pad of silica. The contents were analyzed with GC-MS, with 1 μL dodecane added as an internal standard. Reactions were run in triplicate for natural abundance O_2 and $^{18}O_2$. Yield for adding TMSCl to natural abundance O_2-**3**: 127±10%. Yield for adding TMSCl to $18O_2$-**3**: 117±3%; 27±9% enrichment of ^{18}O in TMS_2O. Yields calculated assuming a 1:1 stoichiometry of 3 and TMSCl.

Reactivity of 3 with trimethylsilyl chloride, spiked with bis(trimethylsilyl) peroxide: A scintillation vial was charged with **1a** (15 mg) and $NaBAr^F{}_4$ (24 mg) and 2 mL of DCM was added to dissolve the solids, forming **1a-Na**. The solution of **1a-Na** was transferred to a flame-dried 10 mL Schlenk flask, sealed, brought out of the glovebox and then immediately frozen in liquid nitrogen under positive nitrogen pressure. After warming the reaction mixture to –78 °C, bubbled excess (10 equiv) $^{18}O_2$. After five minutes, the solution of 3 was freeze-pump-thawed three times

before the flask was backfilled with nitrogen. A solution of TMSCl and bis(trimethylsilyl) peroxide (TMS_2O_2) (5 equiv. and 0.5 equiv. per Ni center respectively, in 1 mL solvent) was added to the frozen solution of **3**. The reaction mixture was vigorously stirred and warmed to room temperature over one hour, concentrated and brought into the glovebox. The residue was resuspended in 2 mL DCM and filtered through a thin pad of silica. The contents were analyzed with GCMS, with 1 μL dodecane added as an internal standard. No TMS_2O_2 was observed by GCMS, can be observed by GC-MS when independently subjected to the workup conditions and run.

Crystallographic Details The diffraction data were measured at 100 K on a Bruker D8 VENTURE diffractometer equipped with a microfocus Mo-target X-ray tube ($\lambda = 0.71073$ Å) and PHOTON 100 CMOS detector. Data were collected using ϕ and ω scans to survey a hemisphere of reciprocal space. Data reduction and integration were performed with the Bruker APEX3 software package (Bruker AXS, version 2017.3-0, 2018). Data were scaled and corrected for absorption effects using the multi-scan procedure as implemented in SADABS.[84] The structure was solved by SHELXT and refined by a full-matrix least-squares procedure using OLEX2.[85,86] Crystallographic data and details of the data collection and structure refinement are listed in Table A2.4.

3.6 References

(1) Yee, G. M.; Tolman, W. B. Kroneck, P. M. H., Sosa Torres, M. E., Eds.; Springer: Cham, Switzerland, 2015; pp 131−204

(2) Engelmann, X.; Monte-Perez, I.; Ray, K. *Angew. Chem., Int. Ed.* **2016**, *55*, 7632−7649.

(3) Askerka, M.; Brudvig, G. W.; Batista, V. S. *Acc. Chem. Res.* **2017**, *50*, 41−48.

(4) Hunter, B. M.; Gray, H. B.; Müller, A. M. *Chem. Rev.* **2016**, *116*, 14120−14136.

(5) Pegis, M. L.; Wise, C. F.; Martin, D. J.; Mayer, J. M. *Chem. Rev.* 2018, 118, 2340−2391.

(6) Gewirth, A. A.; Varnell, J. A.; DiAscro, A. M. *Chem. Rev.* **2018**, *118*, 2313−2339.

(7) Vicens, L.; Olivo, G.; Costas, M. *ACS Catal.* **2020**, *10*, 8611−8631.

(8) Kovacs, J. A. *Acc. Chem. Res.* **2015**, 48, 2744−2753.

(9) Neu, H. M.; Baglia, R. A.; Goldberg, D. P. *Acc. Chem. Res.* **2015**, *48*, 2754−2764.

(10) Kanady, J. S.; Mendoza-Cortes, J. L.; Goddard, W. A., III;́ Agapie, T. Oxygen-Evolving Complex of Photosystem II: Insights from Computation and Synthetic Models; CRC Press: Boca Raton, FL, 2015.

(11) Baglia, R. A.; Zaragoza, J. P. T.; Goldberg, D. P. *Chem. Rev.* **2017**, *117*, 13320−13352.

(12) Larson, V. A.; Battistella, B.; Ray, K.; Lehnert, N.; Nam, W. *Nat. Rev. Chem.* **2020**, 4, 404−419.

(13) Fiedler, A. T.; Fischer, A. A. *JBIC, J. Biol. Inorg. Chem.* **2017**, *22*, 407−424.

(14) Battistella, B.; Ray, K. *Coord. Chem. Rev.* **2020**, *408*, 213176.

(15) Nam, W. *Acc. Chem. Res.* **2015**, *48*, 2415−2423.

(16) Lu, X.; Li, X.-X.; Lee, Y.-M.; Jang, Y.; Seo, M. S.; Hong, S.; Cho, K.-B.; Fukuzumi, S.; Nam, W. *J. Am. Chem. Soc.* **2020**, *142*, 3891−3904.

(17) Oswald, V. F.; Lee, J. L.; Biswas, S.; Weitz, A. C.; Mittra, K.; Fan, R.; Li, J.; Zhao, J.; Hu, M. Y.; Alp, E. E.; Bominaar, E. L.; Guo, Y.; Green, M. T.; Hendrich, M. P.; Borovik, A. S. *J. Am. Chem. Soc.* **2020**, *142*, 11804−11817.

(18) Drummond, M. J.; Ford, C. L.; Gray, D. L.; Popescu, C. V.; Fout, A. R. J. Am. Chem. Soc. 2019, 141, 6639−6650. *J. Am. Chem. Soc.* **2020**, *142*, 21634−21639.

(19) Goetz, M. K.; Hill, E. A.; Filatov, A. S.; Anderson, J. S. *J. Am. Chem. Soc.* **2018**, *140*, 13176−13180.

(20) Kumar, P.; Lindeman, S. V.; Fiedler, A. T. *J. Am. Chem. Soc.* **2019**, *141*, 10984− 10987.

(21) Corona, T.; Padamati, S. K.; Acuña-Pares, F.; Duboc, C.;´ Browne, W. R.; Company, A. *Chem. Commun.* **2017**, *53*, 11782−11785.

(22) Tcho, W.-Y.; Wang, B.; Lee, Y.-M.; Cho, K.-B.; Shearer, J.; Nam, W. *Dalton Trans.* **2016**, *45*, 14511− 14515.

(23) Kim, D.; Cho, J.; Lee, Y.-M.; Sarangi, R.; Nam, W. *Chem. - Eur. J.* **2013**, *19*, 14112−14118.

(24) Jo, Y.; Annaraj, J.; Seo, M. S.; Lee, Y.-M.; Kim, S. Y.; Cho, J.; Nam, W. *J. Inorg. Biochem.* **2008**, *102*, 2155−2159.

(25) Elwell, C. E.; Gagnon, N. L.; Neisen, B. D.; Dhar, D.; Spaeth, A. D.; Yee, G. M.; Tolman, W. B. *Chem. Rev.* **2017**, *117*, 2059−2107.

(26) Fukuzumi, S.; Karlin, K. D. *Coord. Chem. Rev.* **2013**, *257*, 187−195.

(27) Gagnon, N.; Tolman, W. B. *Acc. Chem. Res.* **2015**, *48*, 2126−2131.

(28) Dahl, E. W.; Dong, H. T.; Szymczak, N. K. *Chem. Commun.* **2018**, *54*, 892−895.

(29) Kim, B.; Jeong, D.; Cho, J. *Chem. Commun.* **2017**, *53*, 9328−9331.

(30) Iovan, D. A.; Wrobel, A. T.; McClelland, A. A.; Scharf, A. B.; Edouard, G. A.; Betley, T. A. *Chem. Commun.* **2017**, *53*, 10306−10309.

(31) Kindermann, N.; Günes, C.-J.; Dechert, S.; Meyer, F. *J. Am. Chem. Soc.* **2017**, *139*, 9831−9834.

(32) Isaac, J. A.; Thibon-Pourret, A.; Durand, A.; Philouze, C.; Le Poul, N.; Belle, C. *Chem. Commun.* **2019**, *55*, 12711−12714.

(33) Large, T. A. G.; Mahadevan, V.; Keown, W.; Stack, T. D. P. *Inorg. Chim. Acta*. **2019**, *486*, 782−792.

(34) Shiren, K.; Ogo, S.; Fujinami, S.; Hayashi, H.; Suzuki, M.; Uehara, A.; Watanabe, Y.; Moro-Oka, Y. *J. Am. Chem. Soc.* **2000**, *122*, 254−262.

(35) Corona, T.; Draksharapu, A.; Padamati, S. K.; Gamba, I.; Martin-Diaconescu, V.; Acuña-Pares, F.; Browne, W. R.; Company, A.´ *J. Am. Chem. Soc.* **2016**, *138*, 12987−12996.

(36) Corona, T.; Company, A. *Chem. - Eur. J.* **2016**, *22*, 13422−13429.

(37) Fujita, K.; Schenker, R.; Gu, W.; Brunold, T. C.; Cramer, S. P.; Riordan, C. G. *Inorg. Chem*. **2004**, *43*, 3324−3326.

(38) Noh, H.; Cho, J. *Coord. Chem. Rev.* **2019**, *382*, 126−144.

(39) Hikichi, S.; Yoshizawa, M.; Sasakura, Y.; Akita, M.; Moro-Oka, Y. *J. Am. Chem. Soc.* **1998**, *120*, 10567−10568.

(40) Padamati, S. K.; Angelone, D.; Draksharapu, A.; Primi, G.; Martin, D. J.; Tromp, M.; Swart, M.; Browne, W. R. *J. Am. Chem. Soc.* **2017**, *139*, 8718−8724.

(41) McNeece, A. J.; Jesse, K. A.; Xie, J.; Filatov, A. S.; Anderson, J. S. *J. Am. Chem. Soc.* **2020**, *142*, 10824−10832.

(42) Morimoto, Y.; Takagi, Y.; Saito, T.; Ohta, T.; Ogura, T.; Tohnai, N.; Nakano, M.; Itoh, S. *Angew. Chem., Int. Ed.* **2018**, *57*, 7640−7643.

(43) Cho, J.; Furutachi, H.; Fujinami, S.; Tosha, T.; Ohtsu, H.; Ikeda, O.; Suzuki, A.; Nomura, M.; Uruga, T.; Tanida, H.; Kawai, T.; Tanaka, K.; Kitagawa, T.; Suzuki, M. *Inorg. Chem.* **2006**, *45*, 2873− 2885.

(44) Mandimutsira, B. S.; Yamarik, J. L.; Brunold, T. C.; Gu, W.; Cramer, S. P.; Riordan, C. G. *J. Am. Chem. Soc.* **2001**, *123*, 9194−9195.

(45) Itoh, S.; Bandoh, H.; Nagatomo, S.; Kitagawa, T.; Fukuzumi, S. *J. Am. Chem. Soc.* **1999**, *121*, 8945−8946.

(46) Honda, K.; Cho, J.; Matsumoto, T.; Roh, J.; Furutachi, H.; Tosha, T.; Kubo, M.; Fujinami, S.; Ogura, T.; Kitagawa, T.; Suzuki, M. *Angew. Chem., Int. Ed.* **2009**, *48*, 3304−3307.

(47) Kieber-Emmons, M. T.; Annaraj, J.; Seo, M. S.; Van Heuvelen, K. M.; Tosha, T.; Kitagawa, T.; Brunold, T. C.; Nam, W.; Riordan, C. G. *J. Am. Chem. Soc.* **2006**, *128*, 14230−14231.

(48) Nagataki, T.; Tachi, Y.; Itoh, S. *Chem. Commun.* **2006**, 4016−4018.

(49) Yao, S.; Bill, E.; Milsmann, C.; Wieghardt, K.; Driess, M. *Angew. Chem., Int. Ed.* **2008**, *47*, 7110−7113.

(50) Li, N.; Bediako, D. K.; Hadt, R. G.; Hayes, D.; Kempa, T. J.; von Cube, F.; Bell, D. C.; Chen, L. X.; Nocera, D. G. *Proc. Natl. Acad. Sci. U. S. A.* **2017**, *114*, 1486−1491.

(51) Lee, S.; Banjac, K.; Lingenfelder, M.; Hu, X. *Angew. Chem., Int. Ed.* 2019, *58*, 10295−10299.

(52) Barondeau, D. P.; Kassmann, C. J.; Bruns, C. K.; Tainer, J. A.; Getzoff, E. D. *Biochemistry* **2004**, *43*, 8038−8047.

(53) Vij, V.; Sultan, S.; Harzandi, A. M.; Meena, A.; Tiwari, J. N.; Lee, W.-G. G.; Yoon, T.; Kim, K. S. *ACS Catal.* **2017**, *7*, 7196−7225.

(54) Morimoto, Y.; Bunno, S.; Fujieda, N.; Sugimoto, H.; Itoh, S. *J. Am. Chem. Soc.* **2015**, *137*, 5867−5870.

(55) Fukuzumi, S.; Lee, Y.-M.; Nam, W. *Dalton Trans.* **2019**, *48*, 9469−9489.

(56) Corona, T.; Pfaff, F. F.; Acuña-Pares, F.; Draksharapu, A.;́ Whiteoak, C. J.; Martin-Diaconescu, V.; Lloret-Fillol, J.; Browne, W. R.; Ray, K.; Company, A. *Chem. - Eur. J.* **2015**, *21*, 15029−15038.

(57) Cho, J.; Sarangi, R.; Annaraj, J.; Kim, S. Y.; Kubo, M.; Ogura, T.; Solomon, E. I.; Nam, W. *Nat. Chem.* **2009**, *1*, 568−572.

(58) Cho, J.; Kang, H. Y.; Liu, L. V.; Sarangi, R.; Solomon, E. I.; Nam, W. *Chem. Sci.* **2013**, *4*, 1502−1508.

(59) Yao, S.; Xiong, Y.; Vogt, M.; Grützmacher, H.; Herwig, C.; Limberg, C.; Driess, M. Angew. *Chem., Int. Ed.* **2009**, *48*, 8107−8110.

(60) Matsumoto, M.; Nakatsu, K. *Acta Crystallogr., Sect. B: Struct. Crystallogr. Cryst. Chem.* **1975**, *31*, 2711−2713.

(61) Kieber-Emmons, M. T.; Schenker, R.; Yap, G. P. A.; Brunold, T. C.; Riordan, C. G. *Angew. Chem., Int. Ed.* **2004**, *43*, 6716−6718.

(62) Rettenmeier, C. A.; Wadepohl, H.; Gade, L. H. *Angew. Chem., Int. Ed.* **2015**, *54*, 4880−4884.

(63) Duan, P.-C.; Manz, D.-H.; Dechert, S.; Demeshko, S.; Meyer, F. *J. Am. Chem. Soc.* **2018**, *140*, 4929−4939.

(64) Martirez, J. M. P.; Carter, E. A. *J. Am. Chem. Soc.* **2019**, *141*, 693−705.

(65) Smith, J. M.; Mayberry, D. E.; Margarit, C. G.; Sutter, J.; Wang, H.; Meyer, K.; Bontchev, R. P. *J. Am. Chem. Soc.* **2012**, *134*, 6516−6519.

(66) Hill, E. A.; Zhao, N.; Filatov, A. S.; Anderson, J. S. *Chem. Commun.* **2020**, *56*, 7861−7864.

(67) Holze, P.; Corona, T.; Frank, N.; Braun-Cula, B.; Herwig, C.; Company, A.; Limberg, C. *Angew. Chem., Int. Ed.* **2017**, *56*, 2307−2311.

(68) Kindermann, N.; Bill, E.; Dechert, S.; Demeshko, S.; Reijerse, E. J.; Meyer, F. A Angew. Chem., Int. Ed. **2015**, 54, 1738−1743.

(69) Colpas, G. J.; Maroney, M. J.; Bagyinka, C.; Kumar, M.; Willis, W. S.; Suib, S. L.; Mascharak, P. K.; Baidya, N. *Inorg. Chem.* **1991**, *30*, 920−928.

(70) Mondal, P.; Pirovano, P.; Das, A.; Farquhar, E. R.; McDonald, A. R. *J. Am. Chem. Soc.* 2018, *140*, 1834−1841.

(71) Greer, A. *Acc. Chem. Res.* **2006**, *39*, 797−804.

(72) Lesley, M. J. G.; Norman, N. C.; Rice, C. R.; Reger, D. L.; Little, C. A.; Lamba, J. J. S.; Brown, K. J.; Peters, J. C.; Thomas, J. C.; Sahasrabudhe, S.; Yearwood, B. C.; Atwood, D. A.; Hill, R. F.; Wood, G. L.; Danzer, R.; Paine, R. T.; Wagner, N. L.; Murphy, K. L.; Haworth, D. T.; Bennett, D. W.; Byers, P. K.; Canty, A. J.; Honeyman, R. T.; Arnáiz, F. J.; Miranda, M. J.; Bohle, D. S.; Sagan, E. S.; Chivers, T.; Sandblom, N.; Schatte, G. Main Group Compounds. In Inorganic Syntheses; *Inorganic Syntheses*; 2004; pp 1–48.

(73) Carney, J. M.; Hammer, R. J.; Hulce, M.; Lomas, C. M.; Miyashiro, D. *Synthesis*. 2012, *44*, 2560–2566.

(74) Schubert, E. M. *J. Chem. Educ.* **1992**, *69*, 62.

(75) Ravel, B.; Newville, M. *J. Synchrotron Radiat.* **2005**, *12*, 537–541.

(76) van Wüllen, C. *J. Chem. Phys.* **1998**, *109*, 392‑399.

(77) Perdew, J. P.; Burke, K.; Ernzerhof, M. *Phys. Rev. Lett.* **1996**, *77*, 3865‑3868.

(78) Perdew, J. P.; Burke, K.; Ernzerhof, M. *Phys. Rev. Lett.* **1997**, *78*, 1396.

(79) Yamaguchi, K.; Takahara, Y.; Fueno, T. Ab-Initio Molecular Orbital Studies of Structure and Reactivity of Transition Metal-Oxo Compounds BT - Applied Quantum Chemistry; Smith, V. H., Schaefer, H. F., Morokuma, K., Eds.; Springer Netherlands: Dordrecht, 1986; pp 155‑184.

(80) Neese, F.; Wennmohs, F.; Hansen, A.; Becker, U. *Chem. Phys.* **2009**, *356*, 98-109.

(81) Neese, F. *Wiley Interdiscip. Rev. Comput. Mol. Sci.* **2012**, *2*, 73‑78.

(82) Hanwell, M. D.; Curtis, D. E.; Lonie, D. C.; Vandermeersch, T.; Zurek, E.; Hutchison, G. *1.* R. *J. Cheminform.* **2012**, *4*, 17.

(83) Morgan, S. O.; Lowry, H. H. *J. Phys. Chem.* 1930, *34*, 2385–2432.

(84) Krause, L.; Herbst-Irmer, R.; Sheldrick, G. M.; Stalke, D. *J. Appl. Crystallogr.* 2015, *48*, 3–10.

(85) Dolomanov, O. V; Bourhis, L. J.; Gildea, R. J.; Howard, J. A. K.; Puschmann, H. *J. Appl. Crystallogr.* 2009, *42*, 339–341.

(86) Sheldrick, G. *Acta Crystallogr. Sect. A* 2015, *71*, 3–8.

Chapter 4: Testing the Limits of Imbalanced PCET Reactivity: Mechanistic Crossover in H-atom Abstraction by Co^{III}-oxo Complexes

Manuscript in preparation: Zhao, N., Goetz, M. K., Schneider, J. E., Anderson, J. S.

4.1 Introduction

Proton-coupled electron transfer (PCET), the transfer of a proton and an electron (equivalently a net hydrogen atom), and more specifically *coupled* proton-electron transfer (CPET) are fundamental elementary steps in synthetic and biological chemical reactions such as the activation and subsequent functionalization of kinetically inert C–H bonds by transition metal-oxo, imido, or nitrido complexes.[1–14] One prominent example in biology is Compound I, a terminal Fe^{IV}-oxo complex formed in cytochrome P450 that is responsible for the degradation of pharmaceuticals via hydroxylation of unactivated aliphatic C–H groups.[15–18] A number of synthetic transition-metal model oxo complexes have been isolated and studied in the context of C–H bond activation, yet harnessing these potent oxidants for controlled, selective reactivity remains a key challenge.[7,11,19–31]

The selectivity of transition metal-oxo complexes in CPET reactivity has traditionally been understood by the BDFEs (bond dissociation free energies) of the substrate C–H bond being broken and the transition metal O–H bond being formed. The BDFE of a given bond is given by the equation:

$$\text{BDFE} = 23.06\,(E^0) + 1.37\,(pK_a) + C_G, \quad \textbf{(Equation 4.1)}$$

where E^0 is the substrate oxidation potential and C_G is the standard reduction potential of $H^+/H^\cdot$ in a given solvent.[32,33] While this relationship compares purely thermodynamic parameters, rates for H-atom abstraction are typically linked to the thermodynamics of net H-atom transfer, ΔG_{CPET}, by

the Bell-Evans-Polyani principle which holds that as a reaction becomes more exergonic the activation barrier should become smaller leading to faster reactivity.[34–37] Indeed, several decades of study have demonstrated a predominant trend of for H-atom abstraction by oxo and related complexes with BDFE's.

While concerted reactivity dominates, particularly with C–H substrates, stepwise processes with initial proton transfer (PT) or electron transfer (ET) must also be considered (**Scheme 4.1**, corners). In fact, mechanistic crossover between concerted and stepwise reactivity has been observed in some cases.[33,38–41] Even in well-defined examples of concerted CPET, the energies of stepwise PT or ET manifest through their net contribution to BDFE's and ΔG_{CPET}, through Equation 1.[23,33,38,42–46]

While the above picture has been the dominant mechanistic paradigm, recent theoretical and computational results have suggested that the energetics of stepwise, or off-diagonal, intermediates can influence the rates of concerted reactions beyond their contributions to ΔG_{CPET}.

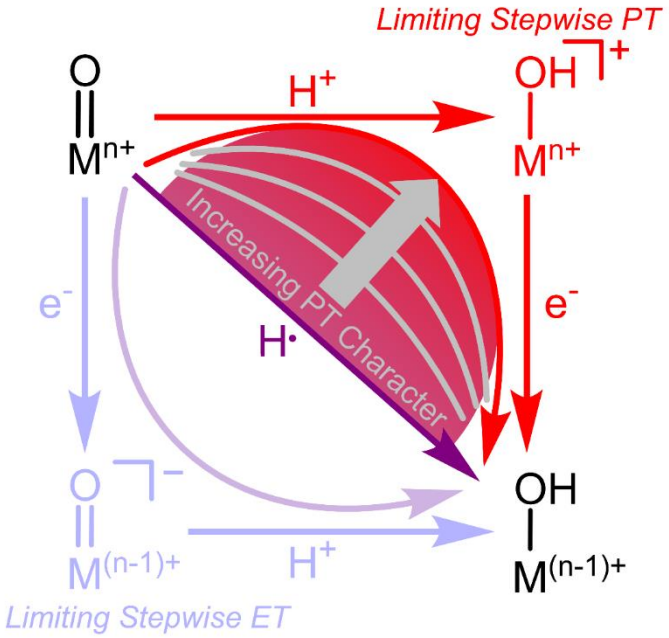

Scheme 4.1. Square scheme depicting CPET mechanisms.

Srnec and coworkers introduced the concept of imbalanced, or asynchronous, CPET wherein the difference between driving forces for stepwise PT or ET (the asynchronicity parameter, η) correlates with accelerated reactivity.[42,47] A positive value of η corresponds to a PCET process with dominant PT character, while a negative value of η corresponds to a PCET process with dominant ET. A greater magnitude ($|\eta|$) corresponds to a more imbalanced transition state and a faster reaction. While such asynchronous transition states have been proposed in other reactions such as organic hydrogen atom transfer,[48] hydride transfer[49] and pericyclic reactions,[50,51] there is significantly less support for such a phenomenon in CPET reactions. Nevertheless, several groups, including our own, have recently observed reactivity which displays a distinct dependence on the acidity and/or oxidation potential of substrates despite having apparent concerted mechanisms.[38,42,52,53] These combined theoretical and experimental observations suggest that, in addition to limiting concerted or stepwise mechanisms, asynchronous or imbalanced pathways are viable (**Scheme 4.1**, curved arrows), and perhaps common, in CPET reactivity. Indeed, there has been a vigorous debate in the literature around this possibility, particularly about how such trends would manifest in nonadiabatic systems with extensive proton tunneling.[42,45,54–60]

Our previous investigations of a terminal Co^{III}-oxo complex $PhB(^{t\text{Bu}}Im)_3Co^{III}O$ revealed rates of C–H activation that more strongly correlated with substrate pK_a rather than BDFE, consistent with an imbalanced CPET reaction in favor of basic (PT) reactivity.[38,43,45,52,61–63] Based on these results, we have been interested in synthesizing even more basic oxo complexes to explore the frontier between imbalanced CPET reactivity and stepwise reactivity. We recently reported an adamantyl (Ad) substituted oxo complex, $PhB(^{Ad}Im)_3Co^{III}O$, which, based on the greater electron donor properties of the Ad groups, should be even more basic than our previous oxo complex.[64] Here we demonstrate that this enhanced basicity of leads to even more highly imbalanced CPET

reactivity with C–H substrates. Moving to more acidic phenol substrates engenders a switch from asynchronous CPET to stepwise reactivity featuring initial PT. Computational analysis of the thermodynamics of phenol substrates suggests that stepwise reactivity dominates when the energy to form stepwise intermediates becomes thermodynamically favorable. Interestingly, we observe that net PCET through stepwise PT/ET is significantly slower than CPET in substrates with BDFEs that differ by only ~1 kcal/mol. These results suggest that optimal rates for H-atom abstraction can be realized with energetically accessible stepwise intermediates, but only up to the point where stepwise reactivity becomes favorable.

4.2 Results and Discussion

4.2.1 C–H Activation

The synthesis and characterization of PhB(^{t}BuIm)Co^{III}O (**4a**) and PhB(AdIm)Co^{III}O (**4b**) have previously been reported by our group (**Scheme 4.2**). A detailed mechanistic study on C–H activation reactivity was conducted for **4a**, but a similar systematic study for **4b** has not been performed. We have previously demonstrated that **4b** is more basic and more reducing than **4a**, as

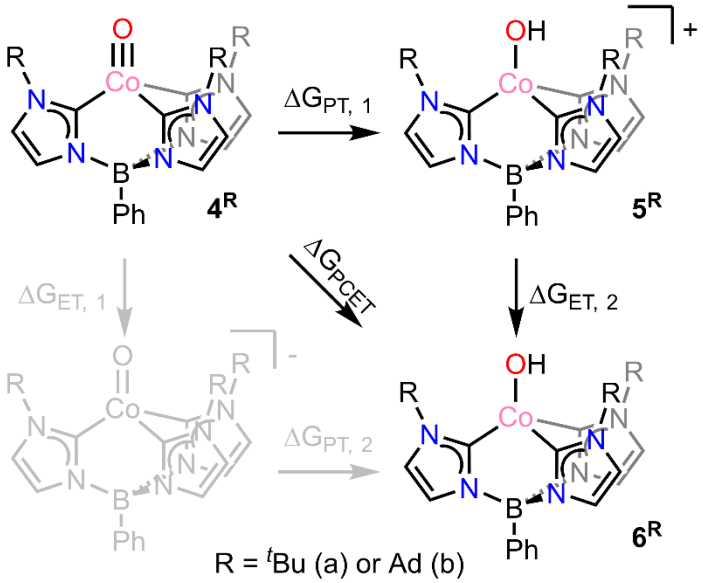

Scheme 4.2. Co complexes and elementary steps.

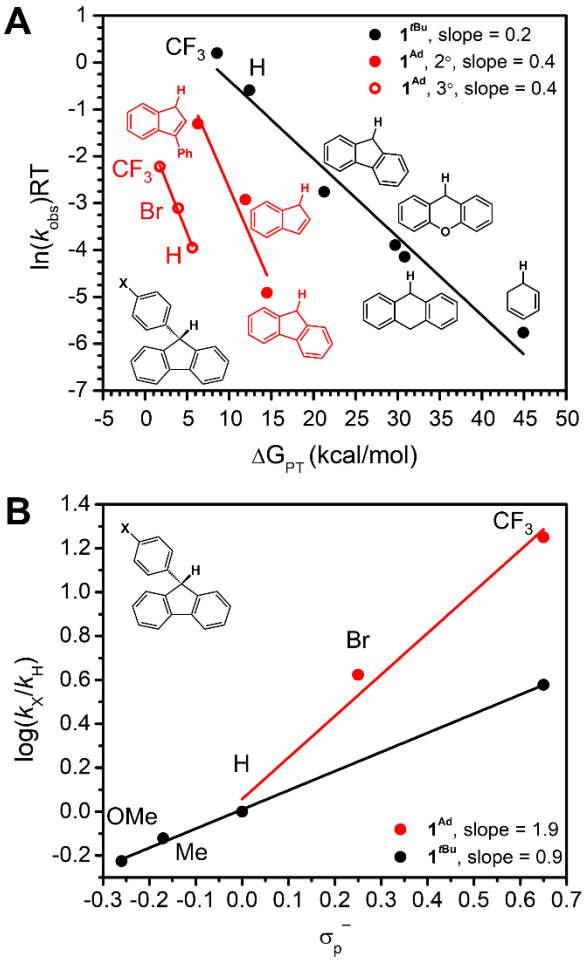

Figure 4.1. A) Trend between log(k_{obs}) and ΔG_{PT} for 4a and 4b. (B) Hammett analyses of 4a and 4b with substituted phenyl fluorenes. Solid lines indicate linear fits to the data.

expected based on the more electron-donating Ad substituents on the imidazol-2-ylidene ligand scaffold.[64] Additionally, the BDFE of **4b** is higher than that measured for **4a**. As **4a** displayed C–H activation reactivity that predominantly trended with substrate pK_a, we hypothesized that the enhanced basicity of **4b** would lead to even more pronounced imbalanced CPET reactivity.

Initially we sought to reproduce the series of substrates screened by **4a**. While **4a** reacts with 9,10-dihydroanthracene (DHA, p$K_{a,\,DMSO}$ = 30) to form **6a** and anthracene in an isosbestic fashion, we were surprised to see that **4b** did not perform the same reaction over several days. We initially hypothesized that the increased steric bulk of the Ad substituents renders **4b** less reactive toward C–H bonds than **4a** and thus investigated more acidic substrates that displayed faster

reactivity with **4a**. Indeed, **4b** reacts cleanly with fluorene (p$K_{a,DMSO}$ = 18) to generate **6b**, albeit at a rate slower than **4a**. We screened a variety of substrates with secondary or tertiary C–H's to account for sterically different substrates (**Figure 4.1A**, see Appendix 3). Not all of the relative thermodynamic parameters of interest (BDFE's, oxidation potentials, and pK_a's) have reliable literature values for all of the tested substrates, so we instead used DFT calculations to estimate the free energies of PCET, PT, and ET reactivity. We used a O3LYP/def2-SVP functional and basis set combination for these calculations, and while it is likely that there are some systematic errors in the absolute values of these free energies, comparison between computed and experimental values shows a good correlation (see **Figure A3.1**).[65–68] Furthermore, we note that the data for **4a**, which was previously shown to correlate with substrate pK_a, also shows a very good correlation with ΔG_{PT} (**Figure 4.1A**, R^2 = 0.96).

Screening a series of sterically similar C–H substrates reveals a linear dependence between log(k_{obs}) and ΔG_{PT} (**Figure 4.1A**). Interestingly, we note that the trendlines for the 2° and 3° C–H's substrates are parallel to each other, with effectively identical slopes of 0.4. This suggests that steric effects do impact the reactivity of **4b**, with slower overall reactivity for the 3° substrates. This steric influence is not observed for **4a**, albeit for a more limited dataset excluding some particularly large 3° substrates. Despite this convolution, the same slope of 0.4 is observed for all substrate sets for **4b**, providing us to compare its dependence on ΔG_{PT} with **4a**.

A comparison of the trendline between log(k_{obs}) and ΔG_{PT} in **4a** and **4b** is consistent with more basic **4b** exhibiting a larger rate dependence on ΔG_{PT} than **4a**. Indeed, comparison reveals that the slope for **4b** is roughly double that of **4a** (0.4 vs. 0.2). The observed slope of 0.4 for **4b** is quite large, supporting a large degree of PT transition state character. For contextualization, a value of 0.5 might be expected for a pure PT event.[42] As a last note on this data, extrapolation of the

trendline for **4b** suggests that the expected rate of reactivity with DHA is slower than the self-decay of **4b** (10^{-5}–10^{-6} $M^{-1}s^{-1}$). This suggests that in addition to steric hindrance, the large ΔG_{PT} dependency of **4b** makes reactivity with weakly acidic C–H bonds sluggish.

We also performed a Hammett analysis to further understand the effects of the more donating Ad substituent on the character of the C–H activation transition state. In analogy with our previous study, we used a series of substituted 9-((4-X-phenyl)fluorenes. We note that the substrate scope of **4b** is limited relative to **4a** due to side reactions observed with some substrates. Nevertheless, the Hammett slope determined for **4b** is positive and again roughly twice as steep as that of **4a** (**Figure 4.1B**). This observation is consistent with a greater buildup of negative charge at the carbon atom of the C–H bond as would be expected for greater PT character in the transition state.[69,70]

These trends indicate that for a given substrate, **4b** lies further than **4a** from a perfectly synchronous or balanced CPET diagonal in a thermodynamic square scheme, and closer to a stepwise PTET pathway. However, the enhanced steric profile of the Ad substituents generally mutes reactivity, and also mandates a narrower substrate scope for **4b**. Given this, we then turned to phenol substrates to provide a greater series of constant steric bulk, as well as a set of more acidic H-atom donors to test the limits of imbalanced reactivity.

4.2.2 H-atom Abstraction from Phenols: Mechanistic Crossover to Stepwise Reactivity

We then screened PCET reactivity with a series of 4-X, 2,6-di-tert-butylphenols. While O–H bonds differ from C–H bonds due to their polarity, we reasoned that this isosteric series of phenols would allow us to a greater number of viable substrates with a pK_a range spanning 7

units.[71,72] Furthermore, we were interested in seeing if the enhanced acidity of phenol substrates led to even more imbalanced reactivity or other emergent trends.

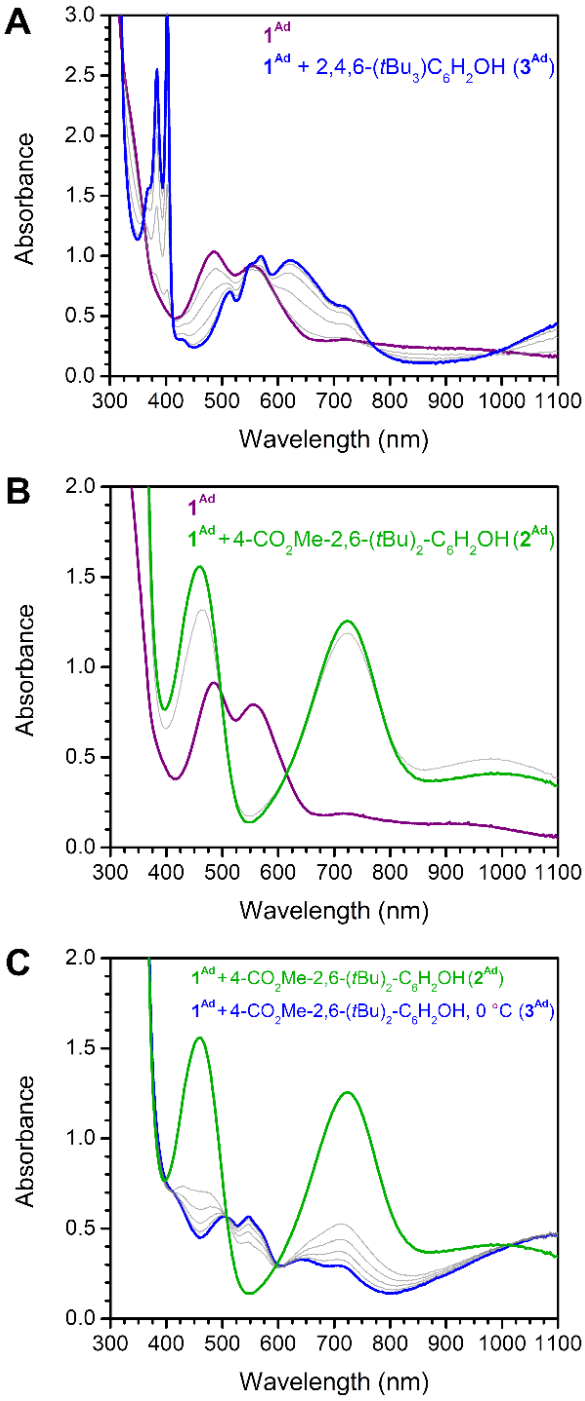

Figure 4.2. UV-vis traces of phenol substrates with 4b in THF.
A) 2,4,6-(^{t}Bu)$_3$C$_6$H$_2$OH at –100 °C showing a concerted mechanism. B) 4-CO$_2$Me-2,6-(^{t}Bu)$_2$C$_6$H$_2$OH at –100°C showing only PT. C) Warming of B) to 0 °C showing ET. Gray traces show intermediate time point spectra.

Complex **4b** exhibits clean reactivity with 10 equivalents of several 4-X, 2,6-di-tert-butylphenols (pKa 17.3-18.2) at –100 °C in an isosbestic fashion to form **6b** over ~5 minutes. A representative reaction with 2,4,6-(^{t}Bu)$_3$-C$_6$H$_2$OH in THF is shown in **Figure 4.2A**. During these studies, however, we noted distinct reactivity with some substrates, particularly those with enhanced acidity. For instance, **4b** reacts with 10 equivalents of 4-MeCO$_2$-2,6-(^{t}Bu)$_2$-C$_6$H$_2$OH (pK_a 11.9) at –100° to form a new green intermediate which can be assigned as [PhB(^{t}BuIm)Co^{III}OH]$^+$ (**5b**) based on comparison to independently prepared samples (**Figure 4.2B**). This suggests that, unlike C–H substrates and less-acidic phenols, **4b** reacts in a stepwise PT fashion with this substrate at low-temperature. The subsequent electron transfer is observed only upon warming to 0 °C, resulting in the formation of **6b** (**Figure 4.2C**). We note that we are not able to observe the final organic phenoxy radical formed upon PCET, although this is perhaps unsurprising as similar phenoxy radicals have been reported to undergo dimerization in solution.[40]

The stepwise nature of this reaction provides the ability to investigate the rates of the fundamental PT, ET, and unified CPET steps in more detail. Specifically, we were interested in comparing rate-limiting k_{ET} of this process to k_{CPET} of the concerted phenol substrates. This comparison has utility in testing mechanisms wherein a rapid pre-equilibrium PT step is followed by rate determining ET, where no PT intermediate would be expected to accumulate. We measured the rate of reaction between independently prepared **5b** and 10 equivalents of [TBA][4-MeCO$_2$-2,6-(^{t}Bu)$_3$-C$_6$H$_2$O] (TBA = tetrabutylammonium) at varying temperatures (see **Figure A3.13-A3.14**). An Eyring analysis suggests that k_{ET} at –100° is very slow, ~10^{-10} $M^{-1}s^{-1}$. Importantly, this rate is many orders of magnitude slower than any of the concerted phenol substrates (see below, **Table 4.1**). We have also analyzed the reaction of **5b** with 10 equivalents of [TBA][4-Br-2,6-(^{t}Bu)$_3$-C$_6$H$_2$O] (**Figure A3.17,** Figure A3.18). While this data quality is somewhat poorer, we can

estimate a rate of ~10^{-3} for this ET reaction at –100 °C, which is also slower than any of the concerted substrates.

4.2.3 Trends with Thermodynamic Parameters

This unusual mechanistic switch prompted us to evaluate trends between the rates of phenol activation and various thermodynamic parameters, akin to our analysis with C–H substrates above (**Table 4.1**). As with the C–H substrates above, not all of the relative parameters of interest (oxidation potentials and pK_a's) have reliable literature values for all of the tested substrates and thus we again used DFT calculations to estimate the free energies of CPET, PT, and ET reactivity. Similar to above, comparison between computed and experimental values shows a good correlation (see **Figure A3.23Figure A3.25**).

Table 4.1. Thermodynamic and rate data for substituted phenols.

X	ΔG_{PCET}	ΔG_{PT}	η	$\ln(k_{obs})RT$[a]
H	−4.27	4.58	−64.1	−1.60(5)
^{t}Bu	−6.06	5.44	−60.1	−1.82(5)
Me	−6.92	5.21	−59.2	−1.52(4)
OMe	−10.4	8.20	−52.3	−1.40(2)
Br	−4.96	1.30	−65.4	−1.44(2) (PT) −2 (ET)
$MeCO_2$	−2.03	−3.87	−74.8	−1.4(1) (PT) −8 (ET)
NO_2	0.52	−11.1	−85.1	−1.3(1) (PT) n.d.

[a] CPET reaction between **4b** with 10 equivalents of phenol at –100 °C unless noted. Stepwise substrates (Br, CO_2Me, and NO_2) have both the initial PT rates (with the same conditions as the concerted substrates) as well as their ET rates (reaction between **5b** and 10 equivalents of phenolate, extrapolated to −100 °C with an Eyring analysis) reported. Note that the ET rate for the NO_2 substituted phenol was not determined.

Initial comparison between the rates of reactivity (adjusted for the temperature of reaction) and the free energies of net PCET reactivity, ΔG_{PCET}, shows no clear correlation (**Figure 4.3A**). While a general trend of slower reactivity with less exergonic reactions is observed for the concerted substrates, as is typical for phenol substrates, a linear fit is poor with an extremely shallow slope (R^2 = 0.13, slope = 0.04(4), see **Figure A3.27**). Similarly convoluted trends are observed with η (see **Figure A3.31**). The substrates that follow a stepwise pathway also do not display any easily interpretable correlation with ΔG_{PCET} or η, however they do form a better linear

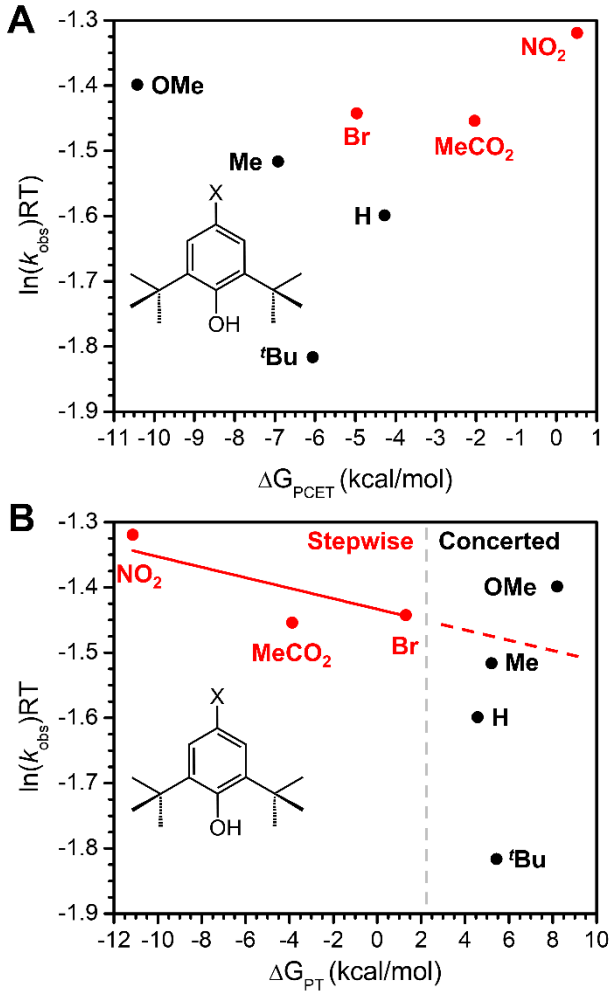

Figure 4.3. Rates of reaction between 4b **and substituted phenols plotted vs. A) the free energies of PCET, and B) the free energies of PT.**

The gray dashed line delineates a crossover between stepwise and concerted reactivity, and the red dashed line is an extrapolation of the rates of PT reaction, illustrating the maximum expected rate for stepwise PT mechanisms. Note that the rates for the stepwise (red) substrates are only for PT reactivity to generate *5b*.

correlation with the free energy of PT, ΔG_{PT}, as expected (**Figure 4.3B**). Still, we note an anomalously small slope of 0.01 even with this expected trend. In contrast, the concerted CPET substrates do not display any reasonable correlation with ΔG_{PT}. The origin of the convoluted correlations in these data is not immediately apparent. It is possible that cross-correlations between the energetics of PCET and PT, significant tunneling effects as we have observed with C–H substrates, hydrogen bonding effects, or some combination of these factors convolute reactivity trends. Despite the complicated trends between rates and thermodynamic parameters, there are several key conclusions that can be drawn from this data.

Firstly, the trend between rate and ΔG_{PT} can be used to rigorously assess the possible agency of stepwise PTET mechanisms for the apparently concerted substrates. Extrapolation of this trend to the ΔG_{PT} values for the concerted substrates provides a "ceiling" for the maximum expected rates for such a process. While some substrates lie below this line, the OMe substituted phenol is clearly above this line, demonstrating that for this substrate, and likely all the concerted substrates, a stepwise mechanism is not viable. This provides a clear way to assess how truly "concerted" these reactions are.

The second conclusion is the clear thermodynamic "crossover" point between stepwise and concerted substrates. While plots of rate vs. ΔG_{CPET} and η do not have a clear delineation between these mechanistic regimes, the plot of rate vs. ΔG_{PT} shows a clear break at ~2 kcal/mol. As mentioned above, while the relative trends in ΔG_{PT} are reliable, it is likely that there is some systematic error in the DFT-computed values of ΔG_{PT}. Thus, this break point can be crudely approximated as thermoneutral. This observation is somewhat intuitive, as reagents that adopt a stepwise mechanism are those for which a PT intermediate is thermodynamically favorable. This

also serves as a simple metric for determining whether a given PCET reaction should proceed through a stepwise or concerted mechanism.

The last conclusion also relies on the measured rates of ET for the stepwise substrates. These are significantly slower than k_{CPET} for the concerted substrates. An illustrative comparison can be made between 4-Br-2,6-(^{t}Bu)$_2$-C$_6$H$_2$OH and 2,6-(^{t}Bu)$_2$-C$_6$H$_2$OH. These two substrates have very similar (within ~1 kcal/mol) driving forces for PCET as well as asynchronicity values (**Table 4.1**). Despite this similarity, the rates for net H-atom transfer are very different between the two substrates, roughly an order of magnitude slower for the Br-substituted phenol. This observation is noteworthy as, for a similar driving force, the concerted substrate is significantly faster. Thus, in thinking of design parameters for rapid H-atom abstraction, concerted reactivity seems to be favored.[73] Furthermore, systems with imbalanced thermodynamic driving forces should realize their fastest rates up until the point where stepwise PT or ET reactivity becomes thermodynamically favorable. At this point, a crossover to stepwise reactivity may be expected to slow rates.

This conclusion is somewhat different than some observations for other PCET systems with concerted or stepwise reactivity. Stepwise reactivity is frequently faster than concerted reactivity, particularly in multi-site electrochemical or photochemically driven systems. One key difference to note is that in synthetic complexes, such as **4b**, variations in PT energetics are typically compensated by similar and counteracting changes in ET energetics. This leads to the overall driving forces for net PCET being relatively constant. In contrast, multi-site PCET systems with electrochemical, and in some cases photochemical, driving forces will frequently fix one of the PT or ET energetics, allowing the overall PCET driving force to float. Thus, these different approaches probe the effect of thermodynamic parameters in different contexts. Regardless, all of

these systems provide useful information on how different thermodynamic parameters can influence PCET reactivity, and further studies will be required for a holistic model for this evolving area.

4.3 Conclusion

We have investigated the PCET reactivity of a new, highly basic Co-oxo complex. Reactivity with C–H substrates is consistent with prior findings of imbalanced or asynchronous CPET reactivity, with an even more pronounced effect from the enhanced basicity of the oxo complex. Investigating more acidic phenol substrates reveals a mechanistic crossover from CPET to stepwise PTET reactivity. Such mechanistic crossover is rare in PCET reactions and provides the opportunity to investigate how the individual PT, ET, and PCET thermodynamics govern reaction pathways.

An analysis of these thermodynamics, obtained from DFT analysis, reveals that the determining factor governing mechanistic crossover is when PT becomes thermodynamically favorable. Furthermore, kinetic analysis of the individual PT and ET steps verifies a concerted mechanism for apparently concerted substrates and goes further to suggest that concerted mechanisms have faster overall rates than stepwise mechanisms for similar driving forces. These findings suggest an optimal thermodynamic paradigm for fast PCET reactivity, at least for imbalanced or asynchronous systems. Imbalanced reactions will be accelerated as the thermodynamics of stepwise intermediates become increasingly favorable. However, this gain in rates only occurs up to the point where the formation of stepwise intermediates becomes exergonic. At this point, stepwise mechanisms will occur, which slows down net PCET reactivity. This emergent mechanistic picture has implications for the design of more rapid and selective PCET

reactions, namely suggesting that the fastest rates will be realized with low-lying stepwise intermediates, as long as those stepwise intermediates do not become free energy minima.

4.4 Experimental

4.4.1 Materials and Instrumentation

All manipulations were performed under a dry nitrogen atmosphere using either standard Schlenk techniques or in an mBraun Unilab Pro glove box unless otherwise stated. All chemicals were obtained from commercial sources and used as received unless otherwise stated. Solvents were dried on a solvent purification system from Pure Process Technologies and passed through a column of activated alumina before storing over 4 Å molecular sieves under N_2. Diethyl ether and tetrahydrofuran (THF) were stirred over NaK alloy and passed through a column of activated alumina prior to storing over 4 Å sieves under N_2. The substituted phenylfluorenes, and 3-phenylindene as well as compounds **4**-**6** were prepared according to literature procedures.[43,74] $HNEt_3BF_4$ was synthesized by adding equimolar HBF_4 etherate to NEt_3. Tetra-butylammonium phenolate salts were generated by adding tetrabutylammonium hydroxide (in methanol) to a solution of the substituted phenol in benzene. UV-vis spectra were recorded on a Thermo Scientific Evolution 300 spectrometer with the VISIONpro software suite. A standard 1 cm quartz cuvette with an air-tight screw cap was used for all measurements. A Unisoku CoolSpek cryostat was used for low temperature measurements. All kinetic traces were fit to the following form: $A_t = A_{inf} + (A_0 - A_{inf})*\exp(-kt)$, where A_t is absorbance at time *t*, A_{inf} is the absorbance of the products at infinite time, A_0 is the initial absorbance of the reactants, *k* is the rate constant and t is time in seconds. ^{1}H NMR spectra were recorded using either Bruker DRX-400 or AVANCE-500 spectrometers and referenced to residual solvent peaks.

4.4.2 Other Experimental Procedures

Density Functional Theory (DFT) Calculations

DFT calculations for C–H and O–H substrates were performed using the def2/SVP basis set on all atoms, along with the. For calculations of compounds 1-3, the def2/SVP basis set was used except for Co, O, N and carbene C's where def2/TZVVP was used. All computations were carried out with the RIJCOSX approximation and with the help of ORCA program package (version 4.2.0).[75,76] Numerical frequency calculations were also performed verify optimized geometries and to obtain the free energies of all compounds.

Kinetic Data Measurement Procedures

General Experimental Procedure for C–H Substrate Kinetics

To a screw-top cuvette equipped with a stirbar was added 2 mL of a 1.25 mM solution of 4b in THF. The cuvette was sealed and brought out of the glovebox. The cuvette was then transferred to a Unisoku cryostat, with positive Ar gas flow. At room temperature, 50 equiv. substrate was injected through the septum, and the reaction was monitored by UV-vis spectroscopy (with stirring).

General Experimental Procedure for O–H Substrate PT Kinetics

To a screw-top cuvette equipped with a stirbar was added 2 mL of a 1.25 mM solution of 4b in THF. The cuvette was sealed and brought out of the glovebox. The cuvette was then transferred to a Unisoku cryostat, with positive Ar gas flow. The cryostat was cooled to –100 °C, and 10 equiv. substrate was injected through the septum, and the reaction was monitored by UV-vis spectroscopy (with stirring).

General Experimental Procedure for O–H Substrate ET Kinetics

To a screw-top cuvette equipped with a stirbar was added 2 mL of a 1.25 mM solution of 4b in THF. The cuvette was sealed and brought out of the glovebox. The cuvette was then transferred to a Unisoku cryostat, with positive Ar gas flow. The cryostat was cooled to –100 °C, then 1.5 eq. $HNEt_3BF_4$ as a solution in MeCN was was injected through the septum, and the reaction to form 5b was monitored by UV-vis spectroscopy. After 5 minutes, the cryostat was set to the temperature of interest and allowed to equilibrate 15 minutes before 10 equiv. of TBA 4-X-2,6-di-tert-butylphenolate was added as a solution in THF.

4.5 References

(1) Larson, V. A.; Battistella, B.; Ray, K.; Lehnert, N.; Nam, W. *Nat. Rev. Chem.* **2020**, *4*, 404–419.

(2) Borovik, A. S. *Chem. Soc. Rev.* **2011**, *40*, 1870–1874.

(3) Pannwitz, A.; Wenger, O. S. *Dalton Trans.* **2019**, *48*, 5861–5868.

(4) Milan, M.; Salamone, M.; Costas, M.; Bietti, M. *Acc. Chem. Res.* **2018**, *51*, 1984–1995.

(5) Davies, H. M. L.; Manning, J. R. *Nature* **2008**, *451*, 417–424.

(6) Costas, M. Remote Oxidation of Aliphatic C–H Bonds with Biologically Inspired Catalysts. In *Remote C–H Bond Functionalizations*; 2021; pp 383–421.

(7) Murray, P. R. D.; Cox, J. H.; Chiappini, N. D.; Roos, C. B.; McLoughlin, E. A.; Hejna, B. G.; Nguyen, S. T.; Ripberger, H. H.; Ganley, J. M.; Tsui, E.; Shin, N. Y.; Koronkiewicz, B.; Qiu, G.; Knowles, R. R. *Chem. Rev.* **2022**, *122*, 2017–2291.

(8) Fukuzumi, S.; Cho, K.-B.; Lee, Y.-M.; Hong, S.; Nam, W. *Chem. Soc. Rev.* **2020**, *49*, 8988–9027.

(9) Bullock, R. M.; Chen, J. G.; Gagliardi, L.; Chirik, P. J.; Farha, O. K.; Hendon, C. H.; Jones, C. W.; Keith, J. A.; Klosin, J.; Minteer, S. D.; Morris, R. H.; Radosevich, A. T.; Rauchfuss, T. B.; Strotman, N. A.; Vojvodic, A.; Ward, T. R.; Yang, J. Y.; Surendranath, Y. *Science* **2020**, *369*, eabc3183.

(10) Wang, F.; Stahl, S. S. *Acc. Chem. Res.* **2020**, *53*, 561–574.

(11) Gentry, E. C.; Knowles, R. R. *Acc. Chem. Res.* **2016**, *49*, 1546–1556.

(12) Kojima, T. *Dalton Trans.* **2020**, *49*, 7284–7293.

(13) Nocera, D. G. *J. Am. Chem. Soc.* **2022**, *144*, 1069–1081.

(14) Lee, J. L.; Ross, D. L.; Barman, S. K.; Ziller, J. W.; Borovik, A. S. *Inorg. Chem.* **2021**, *60*, 13759–13783.

(15) Rittle, J.; Green, M. T. *Science* **2010**, *330*, 933–937.

(16) Mittra, K.; Green, M. T. *J. Am. Chem. Soc.* **2019**, *141*, 5504–5510.

(17) Yosca, T. H.; Rittle, J.; Krest, C. M.; Onderko, E. L.; Silakov, A.; Calixto, J. C.; Behan, R. K.; Green, M. T. *Science* **2013**, *342*, 825–829.

(18) Shaik, S.; Kumar, D.; de Visser, S. P.; Altun, A.; Thiel, W. *Chem. Rev.* **2005**, *105*, 2279–2328.

(19) Kaizer, J.; Klinker, E. J.; Oh, N. Y.; Rohde, J.-U.; Song, W. J.; Stubna, A.; Kim, J.; Münck, E.; Nam, W.; Que, L. *J. Am. Chem. Soc.* **2004**, *126*, 472–473.

(20) England, J.; Guo, Y.; Farquhar, E. R.; Young Jr., V. G.; Münck, E.; Que Jr., L. *J. Am. Chem. Soc.* **2010**, *132*, 8635–8644.

(21) Valdez-Moreira, J. A.; Beagan, D. M.; Yang, H.; Telser, J.; Hoffman, B. M.; Pink, M.; Carta, V.; Smith, J. M. *ACS Cent. Sci.* **2021**, *7*, 1751–1755.

(22) Panda, C.; Doyle, L. M.; Gericke, R.; McDonald, A. R. *Angew. Chem. Int. Ed.* **2021**, *60*, 26281–26286.

(23) Mandal, M.; Elwell, C. E.; Bouchey, C. J.; Zerk, T. J.; Tolman, W. B.; Cramer, C. J. *J. Am. Chem. Soc.* **2019**, *141*, 17236–17244.

(24) Chen, M. S.; White, M. C. *Science* **2007**, *318*, 783–787.

(25) Schwarz, H.; Shaik, S.; Li, J. *J. Am. Chem. Soc.* **2017**, *139*, 17201–17212.

(26) Baglia, R. A.; Prokop-Prigge, K. A.; Neu, H. M.; Siegler, M. A.; Goldberg, D. P. *J. Am. Chem. Soc.* **2015**, *137*, 10874–10877.

(27) Groves, J. T.; Takahashi, T. *J. Am. Chem. Soc.* **1983**, *105*, 2073–2074.

(28) Groves, J. T.; Stern, M. K. *J. Am. Chem. Soc.* **1988**, *110*, 8628–8638.

(29) Groves, J. T.; Kruper, W. J.; Haushalter, R. C. *J. Am. Chem. Soc.* **1980**, *102*, 6375–6377.

(30) Groves, J. T.; Nemo, T. E. *J. Am. Chem. Soc.* **1983**, *105*, 6243–6248.

(31) Groves, J. T.; Nemo, T. E.; Myers, R. S. *J. Am. Chem. Soc.* **1979**, *101*, 1032–1033.

(32) Agarwal, R. G.; Coste, S. C.; Groff, B. D.; Heuer, A. M.; Noh, H.; Parada, G. A.; Wise, C. F.; Nichols, E. M.; Warren, J. J.; Mayer, J. M. *Chem. Rev.* **2022**, *122*, 1–49.

(33) Barman, S. K.; Jones, J. R.; Sun, C.; Hill, E. A.; Ziller, J. W.; Borovik, A. S. *J. Am. Chem. Soc.* **2019**, *141*, 11142–11150.

(34) Bell, R. P.; Hinshelwood, C. N. *Proc. R. Soc. London. Ser. A - Math. Phys. Sci.* **1936**, *154*, 414–429.

(35) Evans, M. G.; Polanyi, M. *Trans. Faraday Soc.* **1938**, *34*, 11–24.

(36) Migliore, A.; Polizzi, N. F.; Therien, M. J.; Beratan, D. N. *Chem. Rev.* **2014**, *114*, 3381–3465.

(37) Mayer, J. M. *Acc. Chem. Res.* **2011**, *44*, 36–46.

(38) Usharani, D.; Lacy, D. C.; Borovik, A. S.; Shaik, S. *J. Am. Chem. Soc.* **2013**, *135*, 17090–17104.

(39) Bailey, W. D.; Dhar, D.; Cramblitt, A. C.; Tolman, W. B. *J. Am. Chem. Soc.* **2019**, *141*, 5470–5480.

(40) Dhar, D.; Yee, G. M.; Markle, T. F.; Mayer, J. M.; Tolman, W. B. *Chem. Sci.* **2017**, *8*, 1075–1085.

(41) Zdilla, M. J.; Dexheimer, J. L.; Abu-Omar, M. M. *J. Am. Chem. Soc.* **2007**, *129*, 11505–11511.

(42) Darcy, J. W.; Kolmar, S. S.; Mayer, J. M. *J. Am. Chem. Soc.* **2019**, *141*, 10777–10787.

(43) Goetz, M. K.; Anderson, J. S. *J. Am. Chem. Soc.* **2019**, *141*, 4051–4062.

(44) Elwell, C. E.; Mandal, M.; Bouchey, C. J.; Que, L.; Cramer, C. J.; Tolman, W. B. *Inorg. Chem.* **2019**, *58*, 15872–15879.

(45) Barman, S. K.; Yang, M.-Y.; Parsell, T. H.; Green, M. T.; Borovik, A. S. *Proc. Natl. Acad. Sci. U.S.A.* **2021**, *118*, e2108648118.

(46) Schneider, J. E.; Goetz, M. K.; Anderson, J. S. *Chem. Sci.* **2021**, *12*, 4173–4183.

(47) Bím, D.; Maldonado-Domínguez, M.; Rulíšek, L.; Srnec, M. *Proc. Natl. Acad. Sci. U.S.A.* **2018**, *115*, E10287–E10294.

(48) Tedder, J. M. *Angew. Chem. Int. Ed.* **1982**, *21*, 401–410.

(49) Liu, T.; Tyburski, R.; Wang, S.; Fernández-Terán, R.; Ott, S.; Hammarström, L. *J. Am. Chem. Soc.* **2019**, *141*, 17245–17259.

(50) Buckle, R. N.; Liu, P.-Y.; Roberts, E. W. D.; Burnell, D. J. *Tetrahedron* **1999**, *55*, 11455–11464.

(51) Beno, B. R.; Houk, K. N.; Singleton, D. A. *J. Am. Chem. Soc.* **1996**, *118*, 9984–9985.

(52) Kotani, H.; Shimomura, H.; Ikeda, K.; Ishizuka, T.; Shiota, Y.; Yoshizawa, K.; Kojima, T. *J. Am. Chem. Soc.* **2020**, *142*, 16982–16989.

(53) Huang, T.; Rountree, E. S.; Traywick, A. P.; Bayoumi, M.; Dempsey, J. L. *J. Am. Chem. Soc.* **2018**, *140*, 14655–14669.

(54) Tyburski, R.; Liu, T.; Glover, S. D.; Hammarström, L. *J. Am. Chem. Soc.* **2021**, *143*, 560–576.

(55) Costentin, C.; Savéant, J.-M. *Chem. Sci.* **2020**, *11*, 1006–1010.

(56) Sayfutyarova, E. R.; Lam, Y.-C.; Hammes-Schiffer, S. *J. Am. Chem. Soc.* **2019**, *141*, 15183–15189.

(57) Maldonado-Domínguez, M.; Bím, D.; Fučík, R.; Čurík, R.; Srnec, M. *Phys. Chem. Chem. Phys.* **2019**, *21*, 24912–24918.

(58) Tyburski, R.; Hammarström, L. *Chem. Sci.* **2022**, *13*, 290–301.

(59) Coste, S. C.; Brezny, A. C.; Koronkiewicz, B.; Mayer, J. M. *Chem. Sci.* **2021**, *12*, 13127–13136.

(60) Sayfutyarova, E. R.; Goldsmith, Z. K.; Hammes-Schiffer, S. *J. Am. Chem. Soc.* **2018**, *140*, 15641–15645.

(61) Warm, K.; Paskin, A.; Kuhlmann, U.; Bill, E.; Swart, M.; Haumann, M.; Dau, H.; Hildebrandt, P.; Ray, K. *Angew. Chem. Int. Ed.* **2021**, *60*, 6752–6756.

(62) Zhang, J.; Lee, Y.-M.; Seo, M. S.; Kim, Y.; Lee, E.; Fukuzumi, S.; Nam, W. *Inorg. Chem. Front.* **2022**, *9*, 3233–3243.

(63) Goetz, M. K.; Hill, E. A.; Filatov, A. S.; Anderson, J. S. *J. Am. Chem. Soc.* **2018**, *140*, 13176–13180.

(64) Goetz, M. K.; Schneider, J. E.; Filatov, A. S.; Jesse, K. A.; Anderson, J. S. *J. Am. Chem. Soc.* **2021**, *143*, 20849–20862.

(65) Schäfer, A.; Horn, H.; Ahlrichs, R. *J. Chem. Phys.* **1992**, *97*, 2571–2577.

(66) Schäfer, A.; Huber, C.; Ahlrichs, R. *J. Chem. Phys.* **1994**, *100*, 5829–5835.

(67) Weigend, F.; Ahlrichs, R. *Phys. Chem. Chem. Phys.* **2005**, *7*, 3297–3305.

(68) Yu-Ran. Luo. *Handbook of Bond Dissociation Energies in Organic Compounds*; CRC Press, 2003.

(69) Hansch, C.; Leo, A.; Taft, R. W. *Chem. Rev.* **1991**, *91*, 165–195.

(70) Lansky, D. E.; Goldberg, D. P. *Inorg. Chem.* **2006**, *45*, 5119–5125.

(71) Rochester, C. H.; Rossall, B. *Trans. Faraday Soc.* **1969**, *65*, 1004–1013.

(72) Bordwell, F. G.; Zhang, X.-M. *J. Phys. Org. Chem.* **1995**, *8*, 529–535.

(73) Irebo, T.; Zhang, M.-T.; Markle, T. F.; Scott, A. M.; Hammarström, L. *J. Am. Chem. Soc.* **2012**, *134*, 16247–16254.

(74) Zheng, H.-X.; Xiao, Z.-F.; Yao, C.-Z.; Li, Q.-Q.; Ning, X.-S.; Kang, Y.-B.; Tang, Y. *Org. Lett.* **2015**, *17*, 6102–6105.

(75) Neese, F. The ORCA Program System. *Wiley Interdiscip. Rev. Comput. Mol. Sci.* **2012**, *2*, 73–78.

(76) Neese, F.; Wennmohs, F.; Hansen, A.; Becker, U. *Chem. Phys.* **2009**, *356*, 98–109.

Appendix 1: Supporting Data for Chapter 2

2a	Im (high ppm)		Im (low ppm)		^{t}Bu	
	A	B	A	B	A	B
ν (ppm)	7.05	7.42	5.82	6.07	1.83	1.43
ν (Hz)	3526	3711	2908	3037	916	716
Δν (Hz)	186		130		201	
Tc (K)	212		215		219	
$\Delta G^{\ddagger}_A$ (kcal/mol)	9.8		10.1		10.1	
$\Delta G^{\ddagger}_B$ (kcal/mol)	10.5		10.8		10.8	
Average	10.1		10.4		10.4	
Std Dev	0.5		0.5		0.5	

2b	Im (high ppm)		Im (low ppm)		Ad	
	A	B	A	B	A	B
ppm	7.20	7.38	5.98	6.20	2.64	2.19
Hz	3598	3690	2991	3099	1318	1094
ΔHz	92		108		224	
Tc (K)	219		225		231	
$\Delta G^{\ddagger}_A$ (kcal/mol)	10.4		10.6		10.6	
$\Delta G^{\ddagger}_B$ (kcal/mol)	11.1		11.4		11.3	
Average	10.7		11.0		11.0	
Std Dev	0.5		0.5		0.5	

Table A1.1. Values extracted from the variable temperature ^{1}H NMR spectra.used for calculating the ΔG‡ values for complexes 2a and 2b.

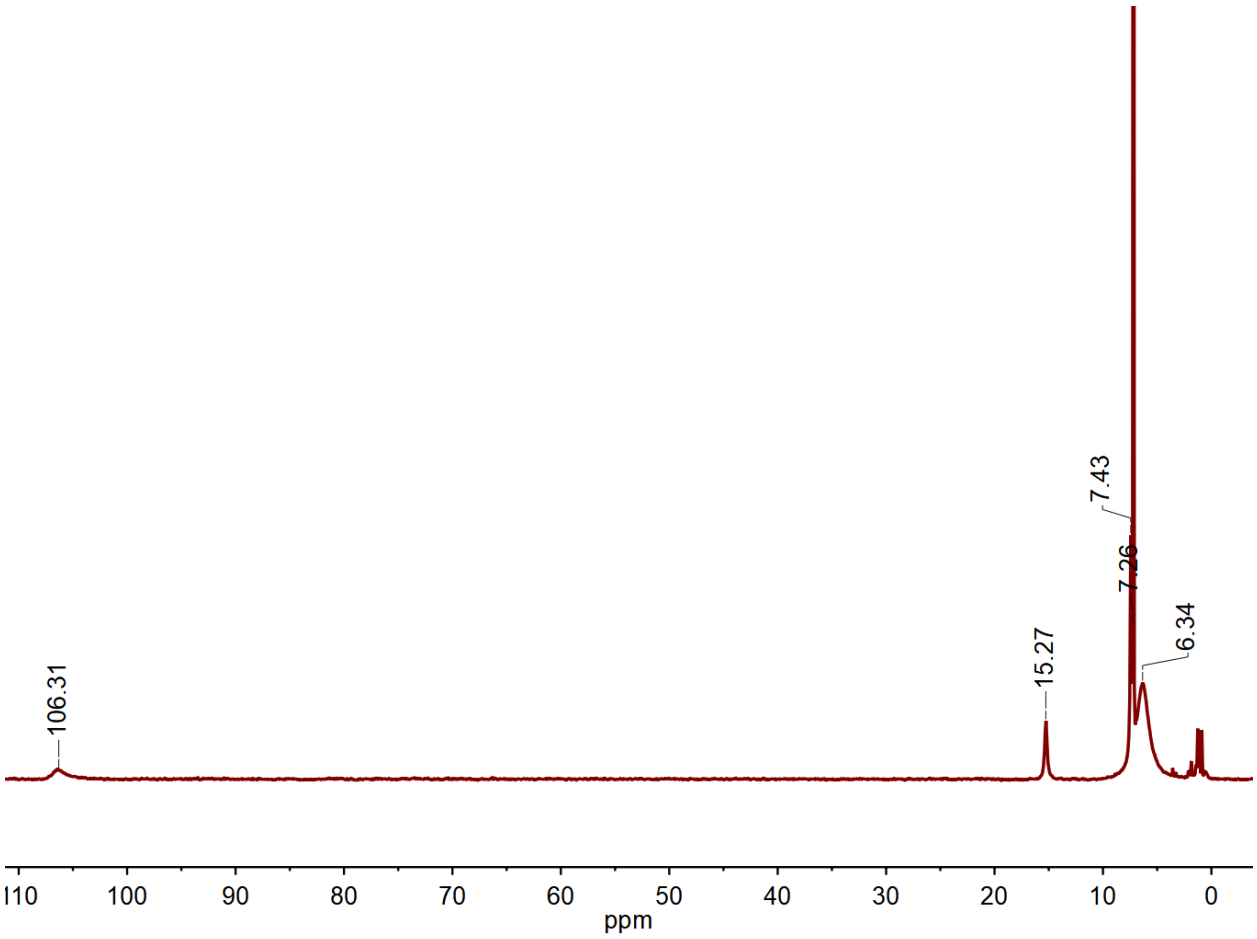

Figure A1.1. The paramagnetic ^{1}H NMR spectrum of 1a in C_6D_6 at 298 K.

Top of the solvent residual peak has been clipped to more clearly see paramagnetic features.

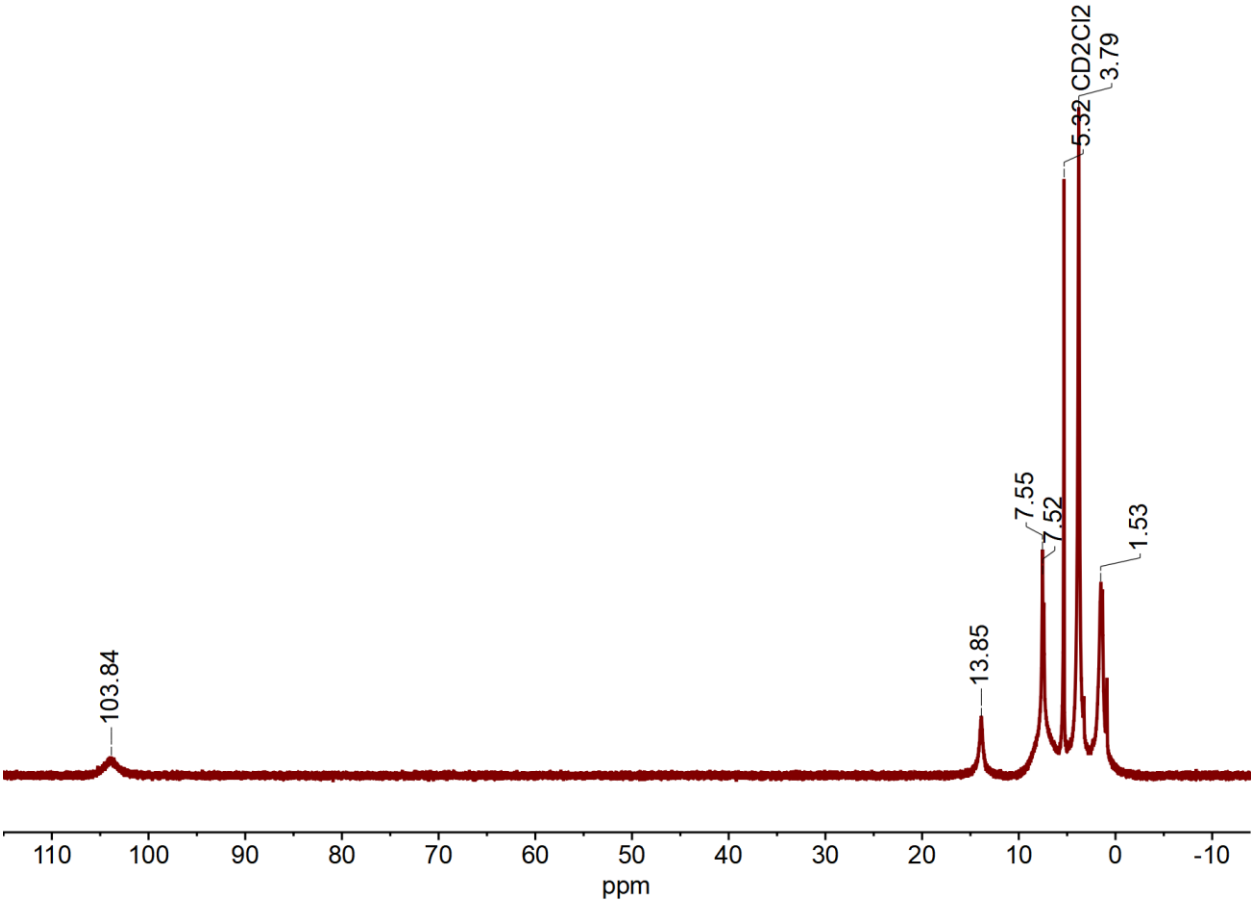

Figure A1.2. The paramagnetic ^{1}H NMR spectrum of 1b in CD_2Cl_2 at 298 K.

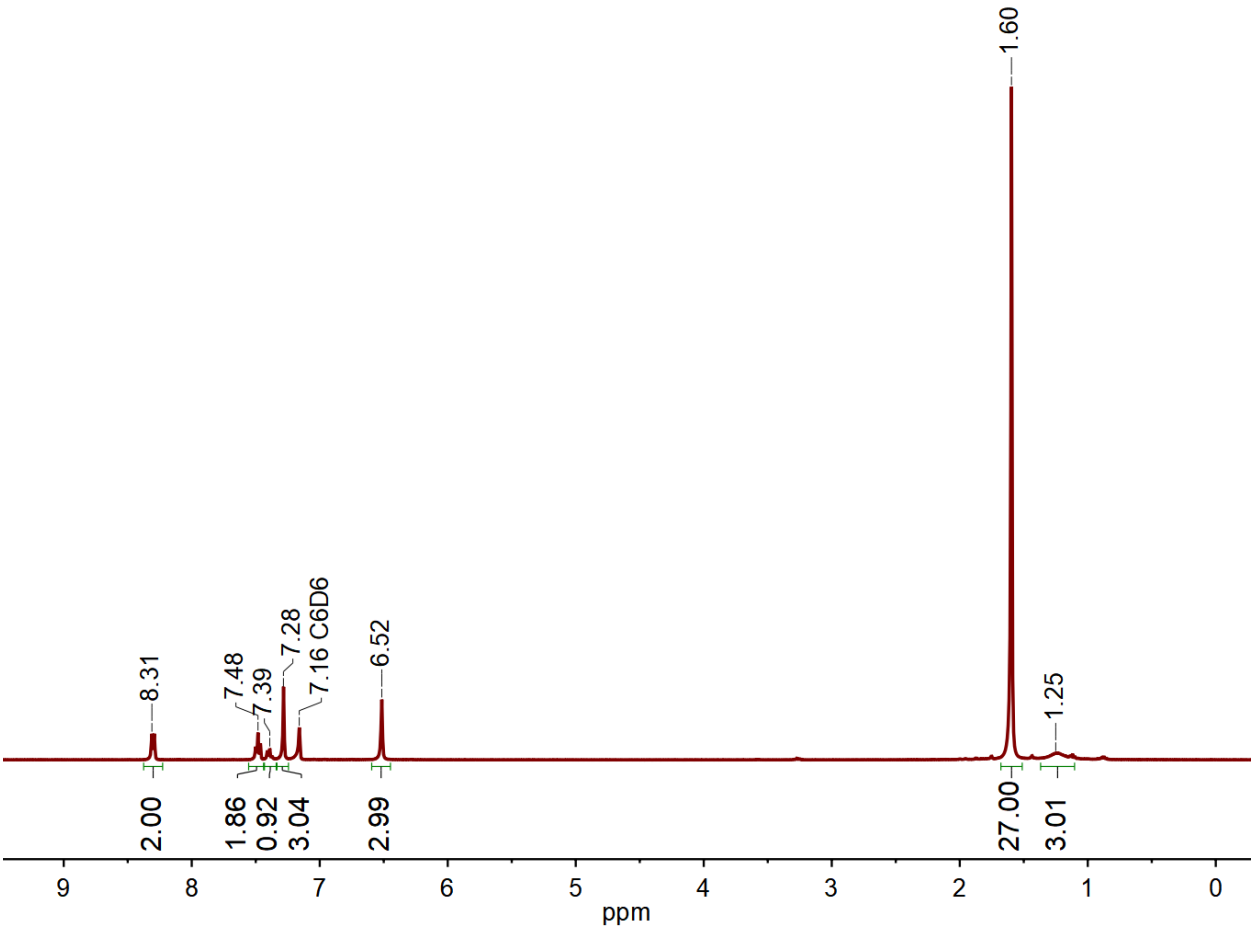

Figure A1.3. ^{1}H NMR spectrum of 2a in C_6D_6 at 298 K.

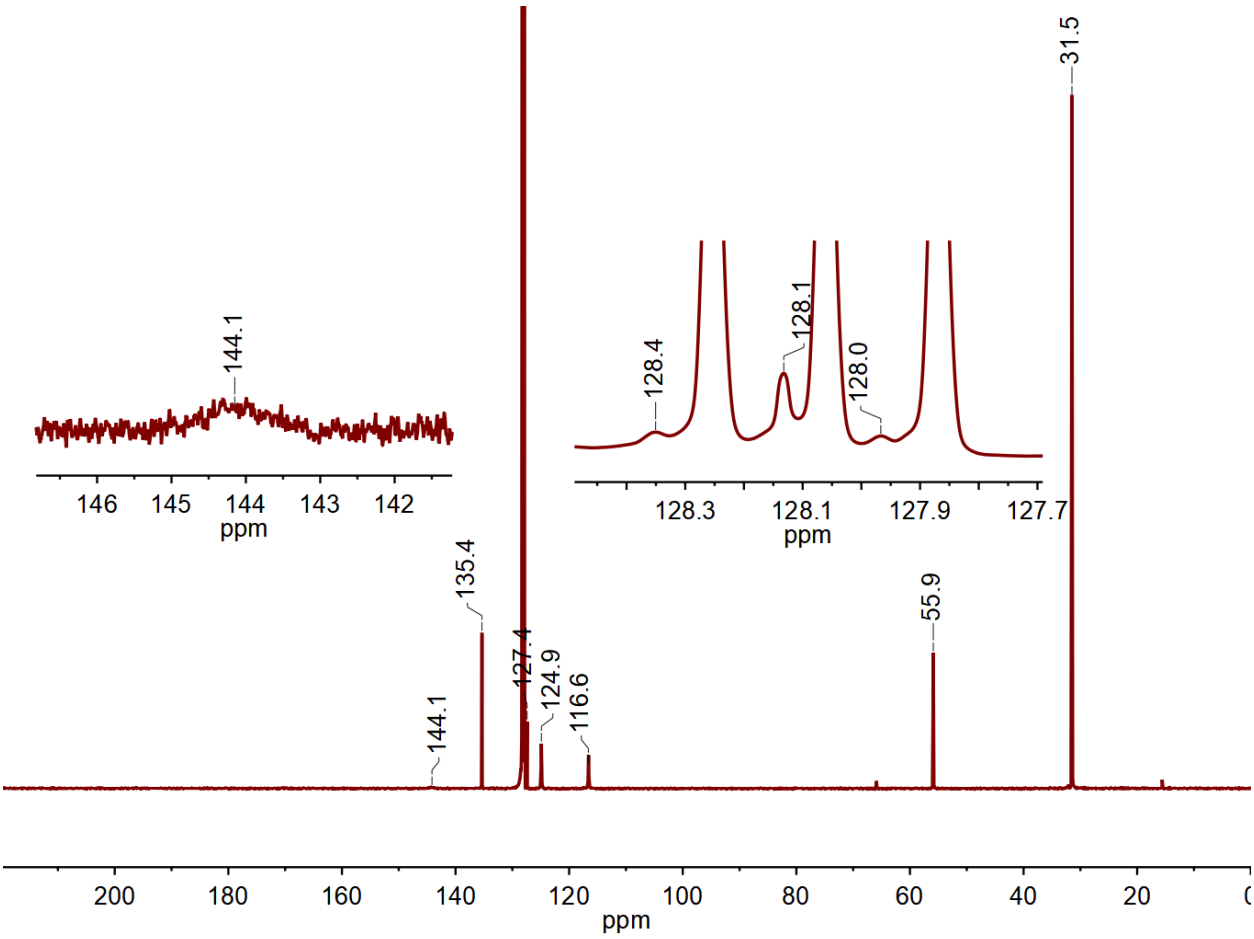

Figure A1.4. ^{13}C NMR spectrum of 2a in C_6D_6 at 298 K.

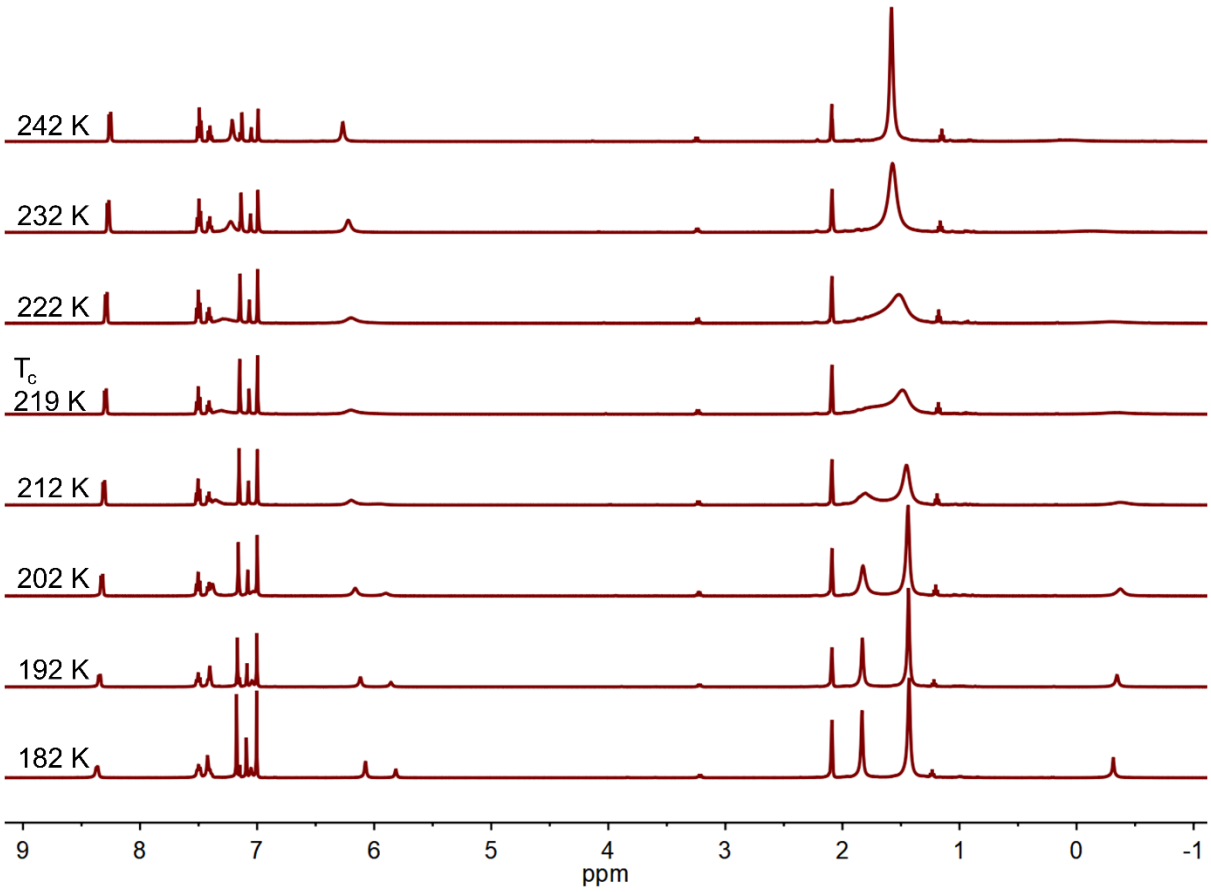

Figure A1.5. Variable temperature ^{1}H NMR spectra of 2a in d_8-toluene.

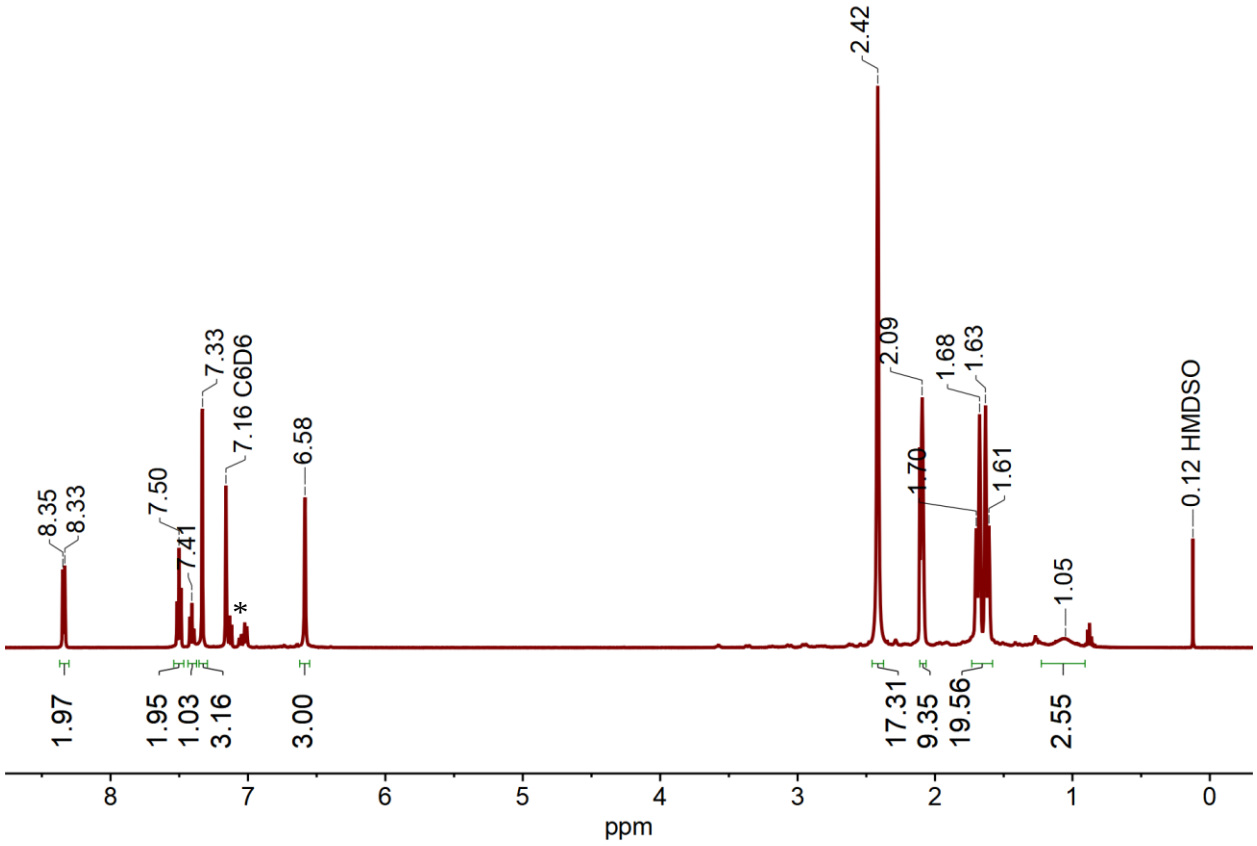

Figure A1.6. The ^{1}H NMR spectrum of 2b in C_6D_6 at 298 K.

Resonances for residual toluene are marked with an asterisk.

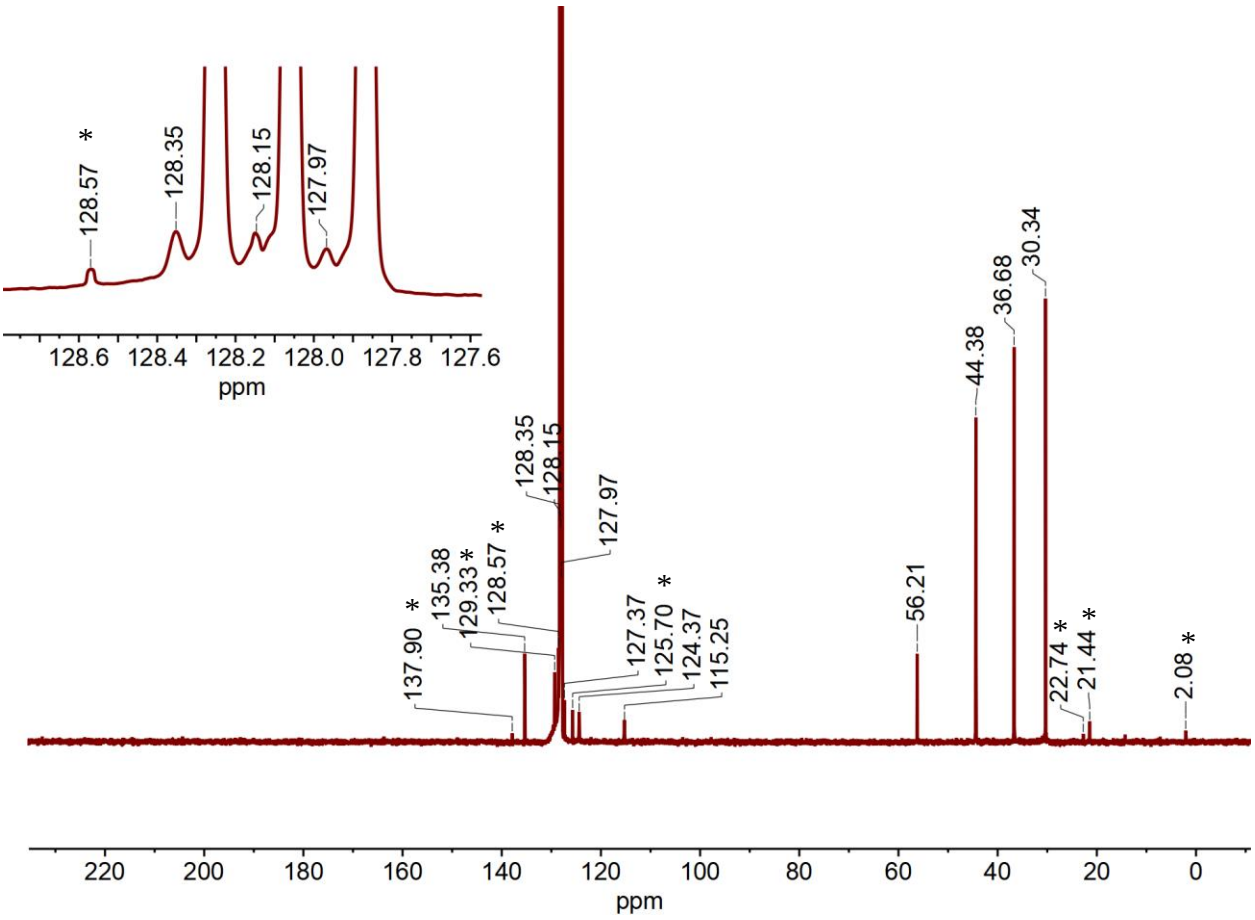

Figure A1.7. The ^{13}C NMR spectrum of 2b in C_6D_6 at 298 K.

Residual solvent peaks for toluene, pentane, and HMDSO marked with asterisks.

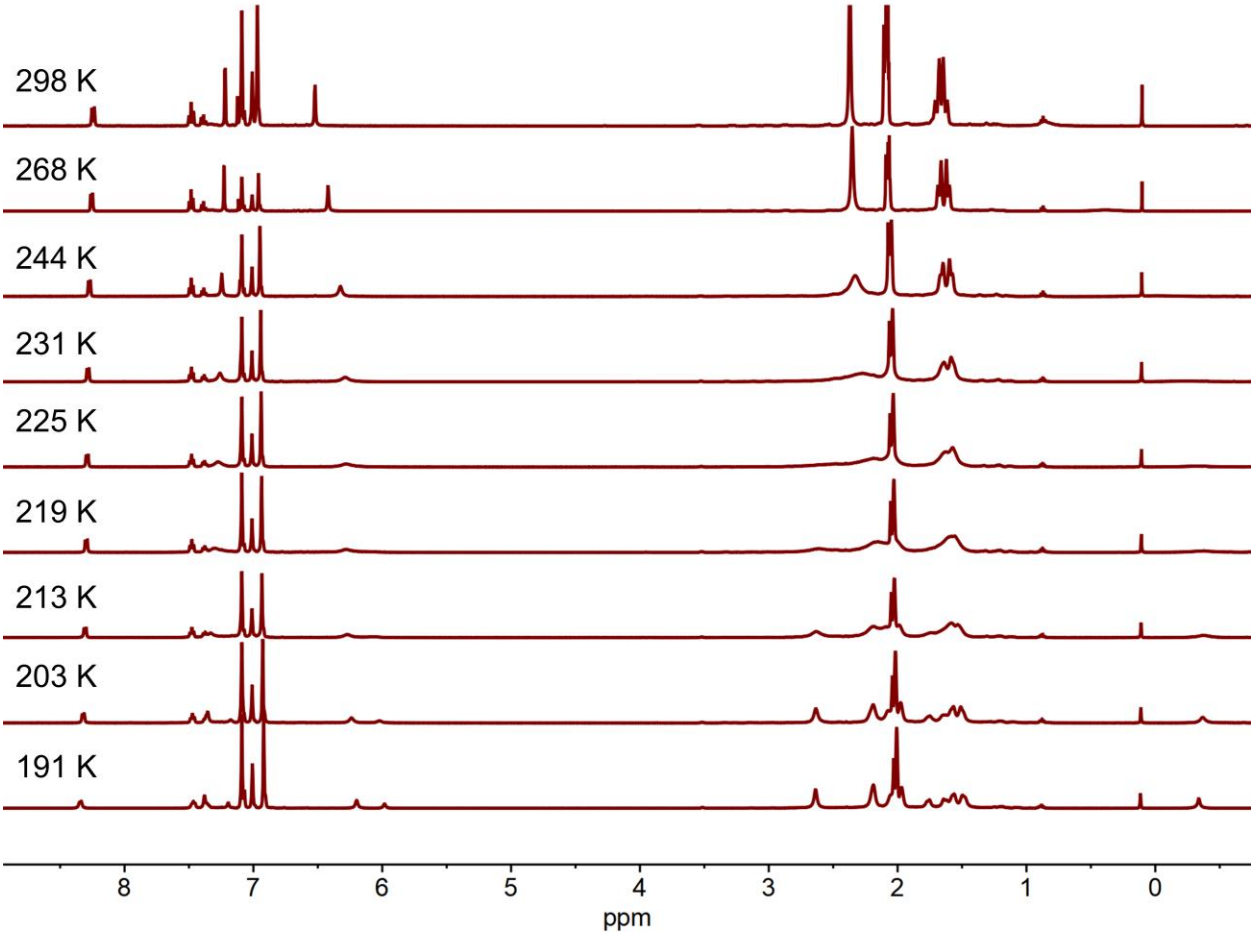

Figure A1.8. The variable temperature ^{1}H NMR spectra of 2b in d_8-toluene.

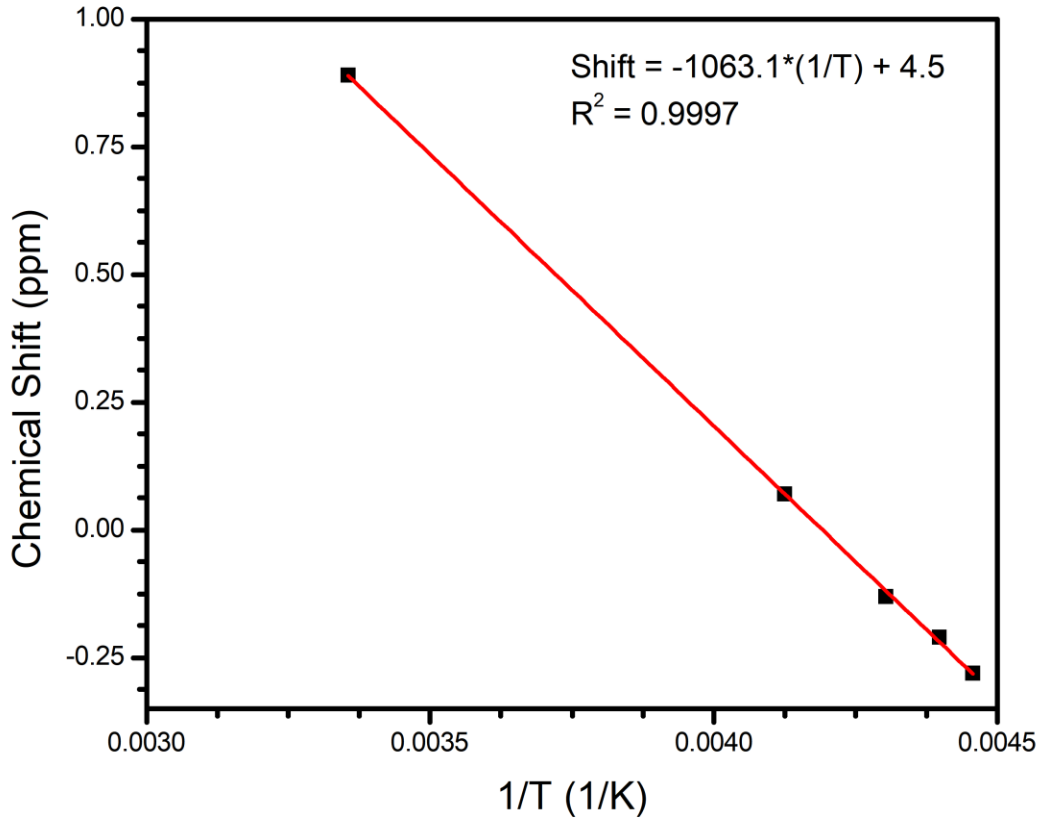

Figure A1.9. Plot of chemical shift versus 1/T for Ni-CH_3 resonance of 2a in the fast exchange regime (T = 224-298 K).

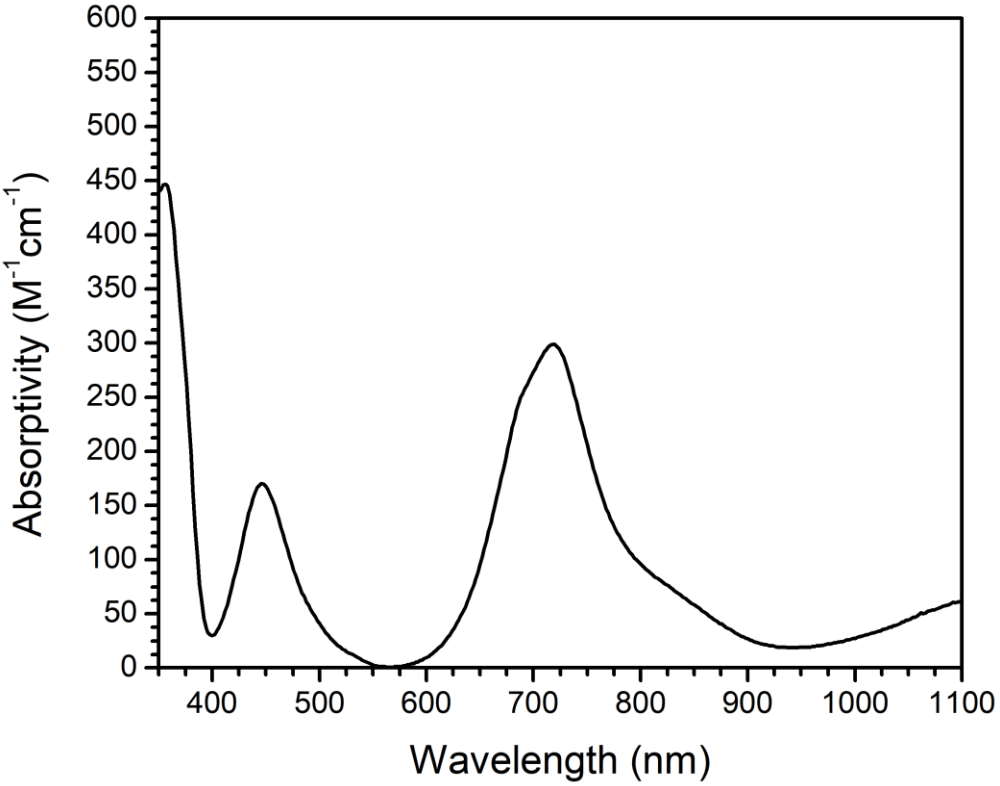

Figure A1.10. UV-vis spectrum of 1a in DCM at 298 K.

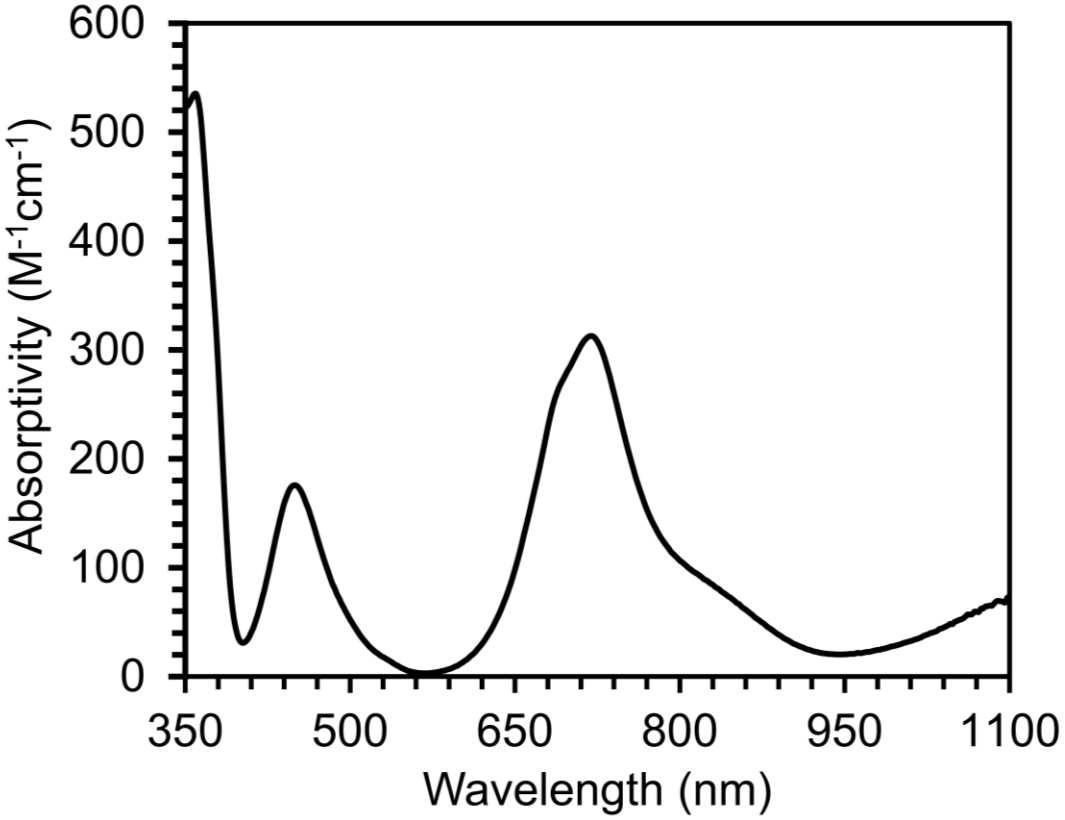

Figure A1.11. UV-vis spectrum of 1b in THF at 298 K.

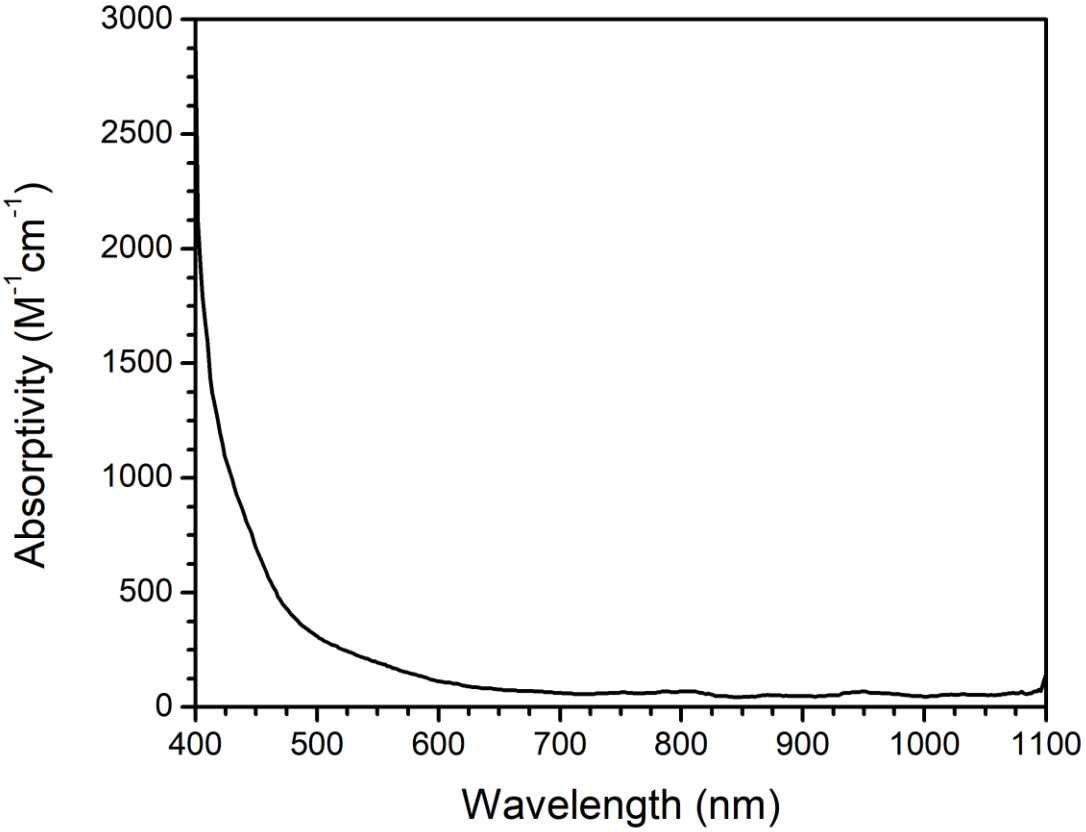

Figure A1.12. UV-vis spectrum of 2a in THF at 298 K.

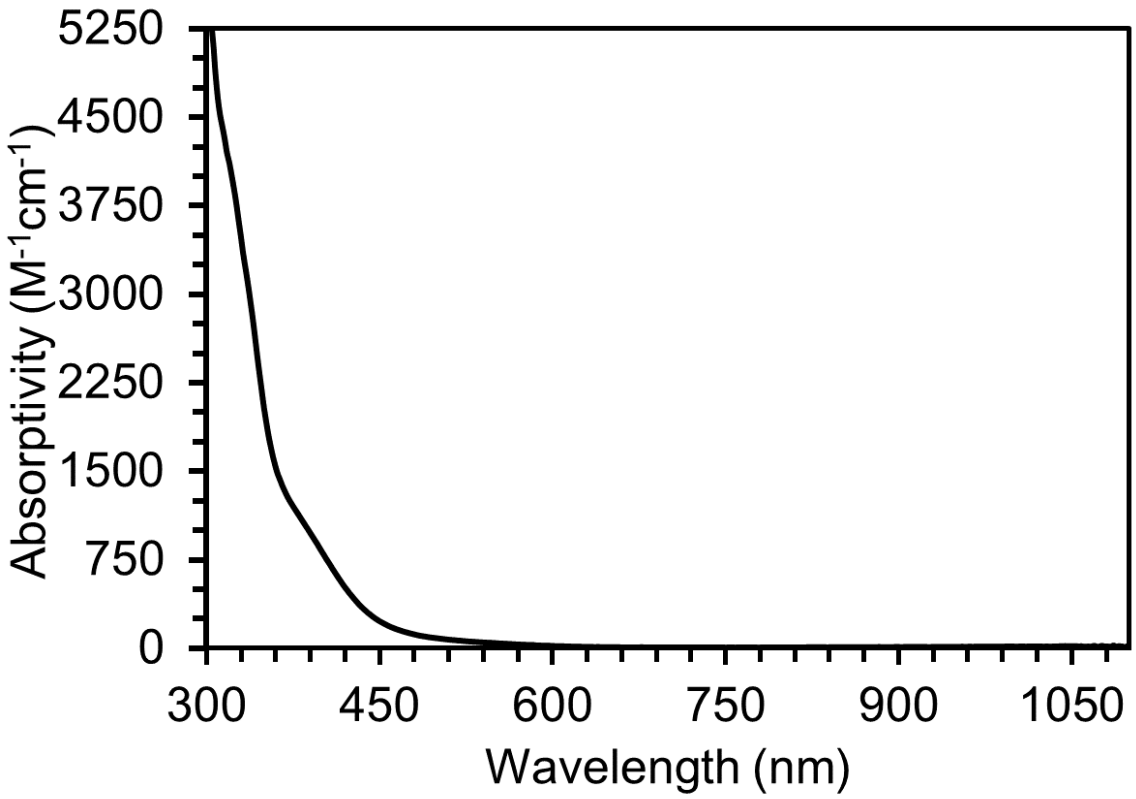

Figure A1.13. UV-vis spectrum of 2b in THF at 298 K.

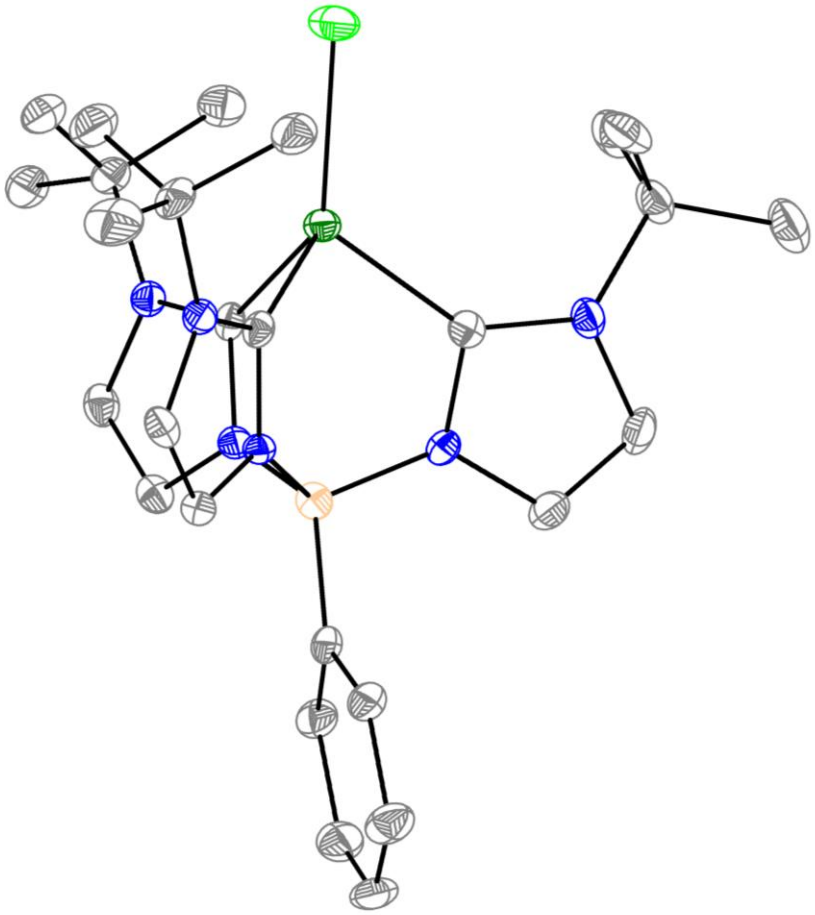

Figure A1.14. Molecular structure of 1a determined by single crystal XRD.

Ellipsoids drawn at 50% probability, H-atoms and solvent molecules omitted for clarity. Only one molecule in the unit cell is shown. Atom colors are dark green = Ni, light green = Cl, blue = N, tan = B, and gray = C.

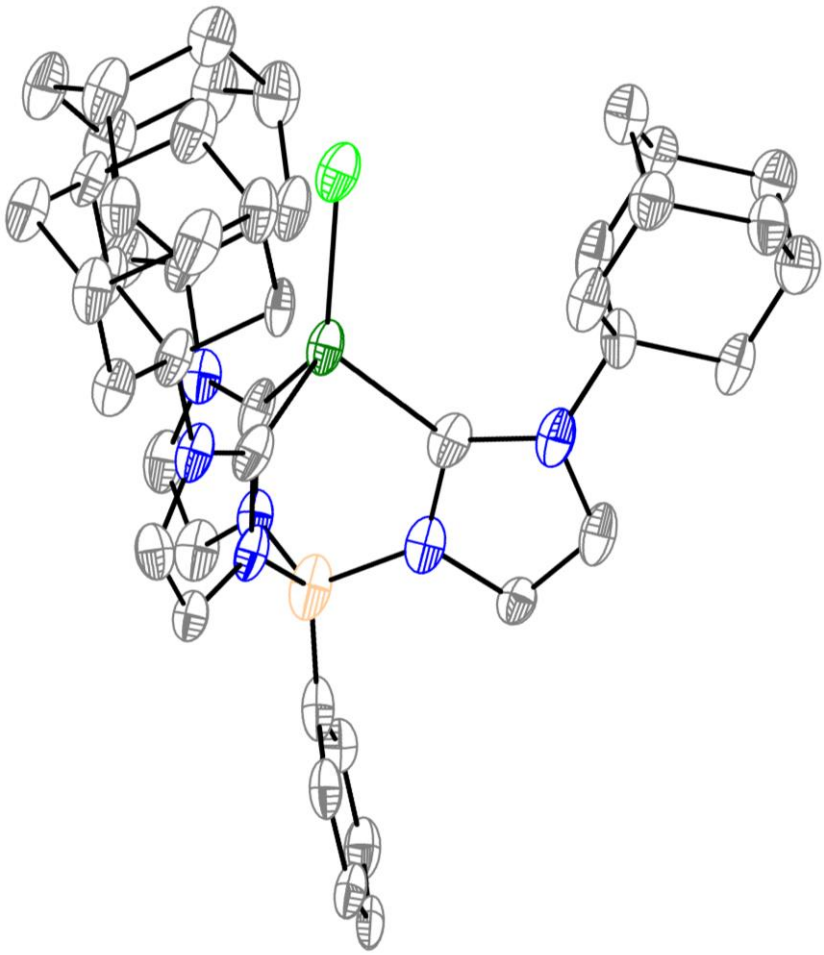

Figure A1.15. The molecular structure of 1b determined by single crystal XRD.

Ellipsoids drawn at 50% probability, H-atoms and solvent molecules omitted for clarity. Atom colors are dark green = Ni, light green = Cl, blue = N, tan = B, and gray = C.

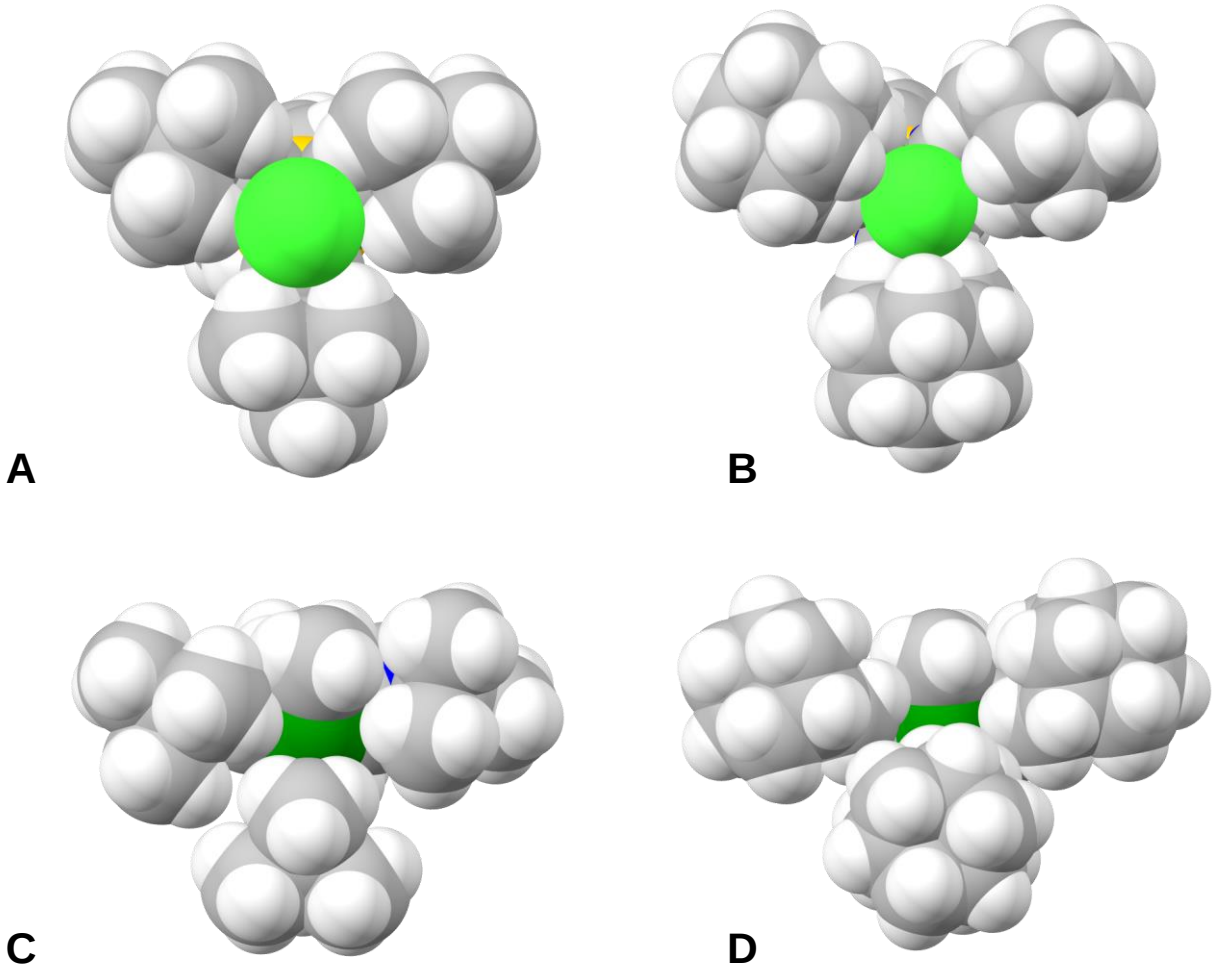

Figure A1.16. Depiction of the space-filling models of 1a (A), 1b (B), 2a (C), and 2b (D) to show the distortion around the nickel center due to the change in geometry.

Color code: dark green = Ni, light green = Cl, gray = C, white = H, blue = N, tan = B

Conformation	Free Energy Difference Relative to Optimized Singlet (kcal/mol)
Optimized Singlet	0
Triplet	+11
Singlet, linearized	+31

Table A1.2. Computed free energies of different conformations of 2a.

Note that "linearized" indicates the energy of a geometry optimization with a constrained B-Ni-C(Me) angle of 168°. Basis sets and functional listed in general procedures above.

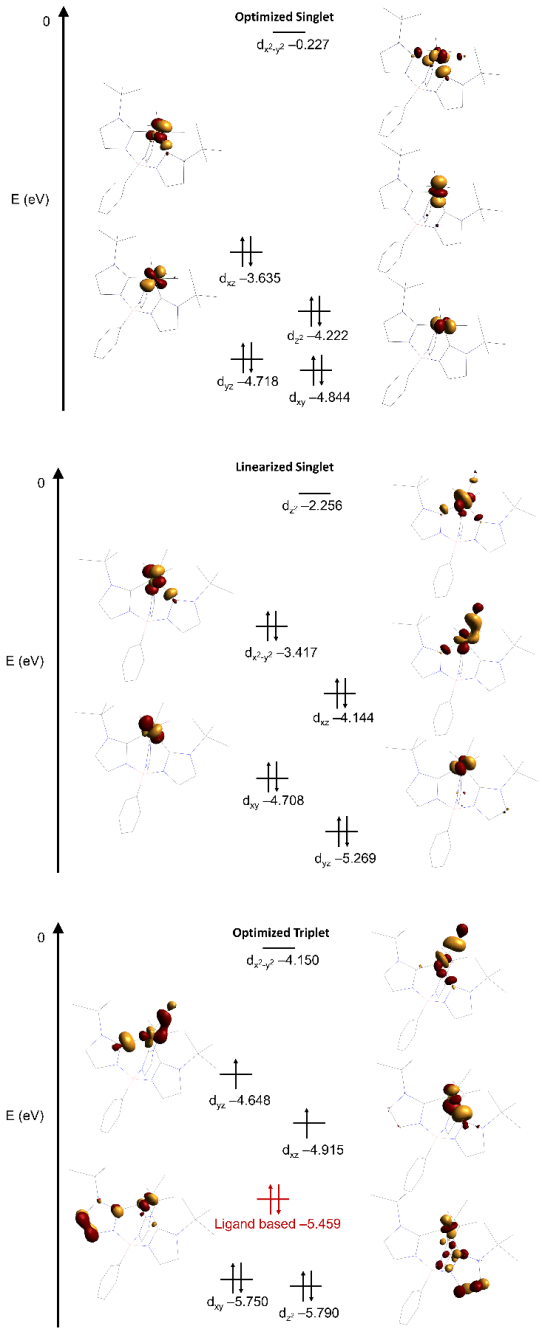

Figure A1.17. Kohn-Sham orbitals of 2a.

Computed both seesaw (optimized singlet, top) and tetrahedral (linearized singlet, middle) geometries in a singlet electronic configuration, and optimized linear geometry in a triplet electronic configuration (bottom). Not to scale.

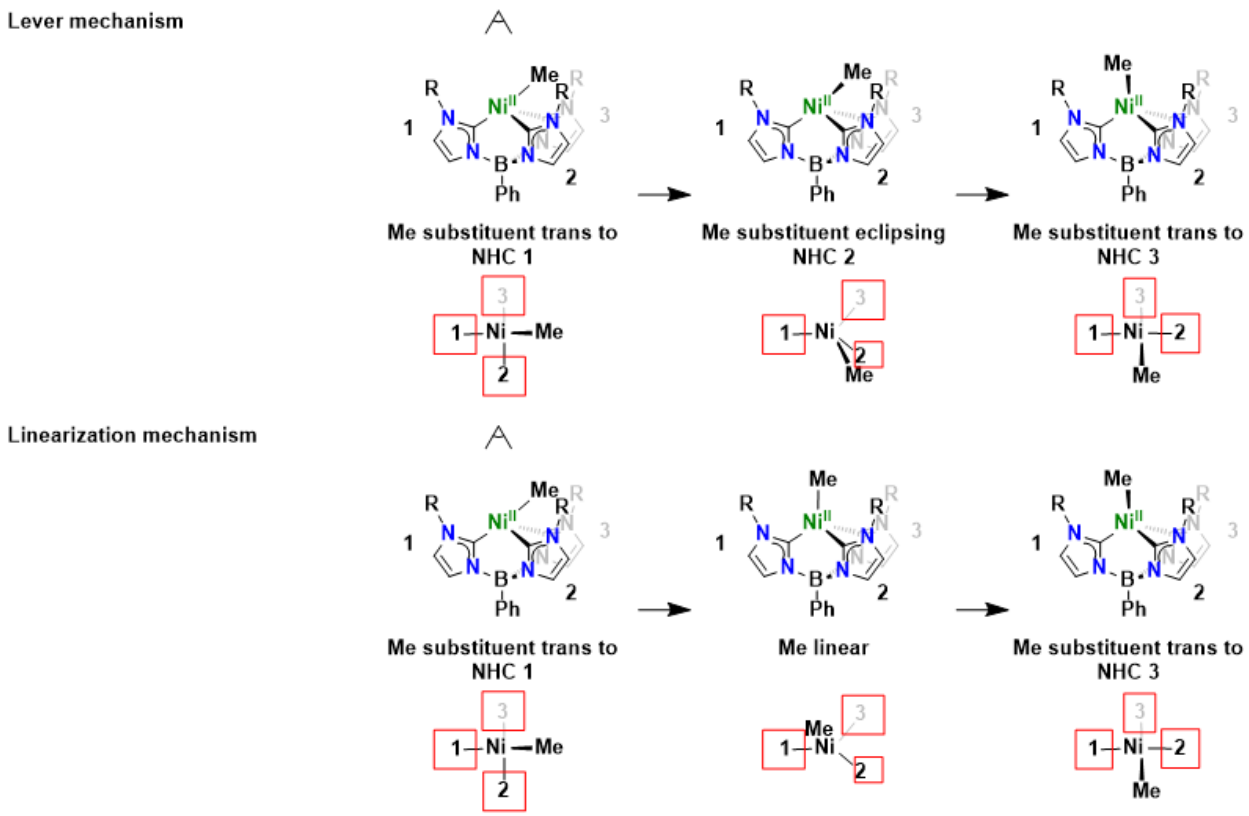

Figure A1.18. Pictorial representation of the lever and linearization mechanisms for isomerization of the Ni-Me complexes.

NHC groups have been abbreviated as numbered boxes for top-down view.

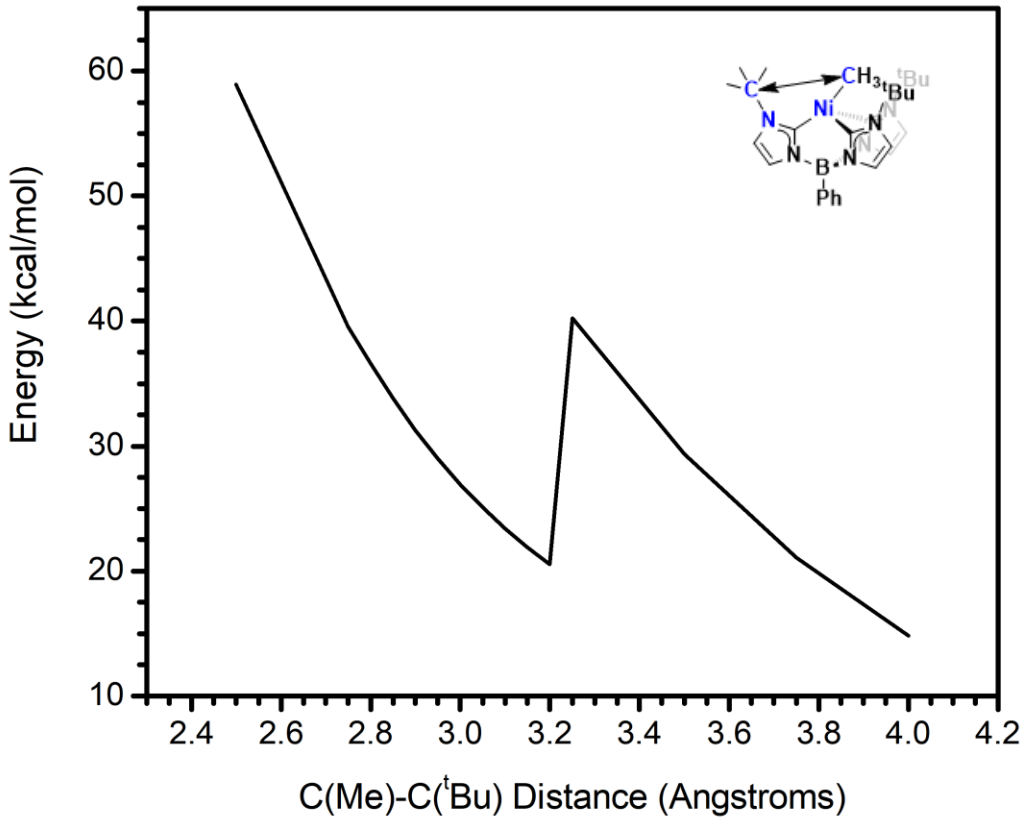

Figure A1.19. Plot of free energy on singlet manifold in 2a scanning C(Me)-C(^{t}Bu) distance.

Constrained dihedral angle of blue atoms to 0º. Geometry scan run using BP86. Energies are relative to optimized singlet (BP86). These data were used to assess the viability of a lever mechanism in the isomerization of **2a**. Note that the discontinuity is associated with a reorganization of the ^{t}Bu and Me groups.

O3LYP	BP86	B3LYP
10.9	13.0	1.2

Table A1.3. Triplet-singlet energy difference (kcal/mol) calculated for 2a using different functionals.

Table A1.4. Crystal structure refinement details for complexes 1a, 1b, 2a, and 2b.

Identification code	**1a**	**1b**	**2a**	**2b**
Empirical formula	$C_{27}H_{38}BClN_6Ni$	$C_{45.7}H_{57.4}BCl_{2.4}N_6Ni$	$C_{28}H_{41b}N_6Ni$	$C_{46}H_{59}BN_6Ni$
Formula weight	551.60	845.37	531.19	765.51
Temperature/K	100(2)	100(2)	100(2)	110(2)
Crystal system	monoclinic	monoclinic	triclinic	tetragonal
Space group	$P2_1/n$	$P2_1/n$	P-1	$I4_1/a$
a/Å	9.6383(16)	19.896(3)	9.8692(5)	34.481(3)
b/Å	17.821(3)	11.9883(15)	12.4359(7)	34.481(3)
c/Å	16.177(3)	21.333(3)	12.6239(7)	13.9826(14)
α/°	90	90	99.808(2)	90
β/°	91.925(6)	107.846(3)	97.233(2)	90
γ/°	90	90	113.118(2)	90
Volume/Å^3	2777.0(8)	4843.3(11)	1371.98(13)	16625(3)
Z	4	4	2	16
ρ_{calc}g/cm^3	1.319	1.159	1.286	1.223
μ/mm^{-1}	0.822	0.568	0.735	0.127

Table A1.5 Continuted

F(000)	1168.0	1790.0	568.0	6560.0
Crystal size/mm^3	0.48 × 0.28 × 0.19	0.35 × 0.31 × 0.21	0.298 × 0.295 × 0.153	0.03 × 0.03 × 0.03
Radiation	MoKα (λ = 0.71073)	MoKα (λ = 0.71073)	MoKα (λ = 0.71073)	synchrotron (λ = 0.41328)
2Θ range for data collection/°	4.572 to 50.148	4.78 to 50.81	4.504 to 55.016	1.374 to 32.464
Index ranges	-11 ≤ h ≤ 11, -21 ≤ k ≤ 20, -19 ≤ l ≤ 19	-24 ≤ h ≤ 23, -14 ≤ k ≤ 14, -25 ≤ l ≤ 25	-12 ≤ h ≤ 12, -16 ≤ k ≤ 16, -16 ≤ l ≤ 16	-46 ≤ h ≤ 46, -46 ≤ k ≤ 46, -18 ≤ l ≤ 18
Reflections collected	25048	59965	37813	252183
Independent reflections	4930 [R_{int} = 0.0560, R_{sigma} = 0.0487]	8900 [R_{int} = 0.0944, R_{sigma} = 0.0736]	6259 [R_{int} = 0.0424, R_{sigma} = 0.0366]	10760 [R_{int} = 0.0435, R_{sigma} = 0.0120]
Data/restraints/parameters	4930/0/334	8900/0/514	6259/0/335	10760/0/488
Goodness-of-fit on F^2	1.014	1.032	1.055	1.087
Final R indexes [I>=2σ (I)]	R_1 = 0.0385, wR_2 = 0.0847	R_1 = 0.1004, wR_2 = 0.2515	R_1 = 0.0345, wR_2 = 0.0691	R_1 = 0.0412, wR_2 = 0.0984

Table A1.6 Continuted

Final R indexes [all data]	R_1 = 0.0633, wR_2 = 0.0939	R_1 = 0.1419, wR_2 = 0.2746	R_1 = 0.0484, wR_2 = 0.0737	R_1 = 0.0434, wR_2 = 0.0997
Largest diff. peak/hole / e $Å^{-3}$	0.56/-0.23	1.31/-1.15	0.56/-0.33	0.49/-0.43

Table A1.7. DFT optimized coordinates of 2a, singlet.

C	-1.883838	1.483102	-0.573295
N	-3.099486	1.859184	-1.042080
C	-3.978341	0.795105	-0.986952
C	-3.276063	-0.266658	-0.524235
N	-1.985106	0.147737	-0.322303
B	-0.744238	-0.704329	0.137471
N	0.444058	-0.217391	-0.732256
C	0.741458	1.087561	-0.688331
N	1.776530	1.270727	-1.538955
C	2.110182	0.061983	-2.128644
C	1.269498	-0.868909	-1.612267
N	-0.397591	-0.292170	1.614323
C	0.136170	0.924645	1.915647
N	0.363659	0.897403	3.252935
C	-0.112670	-0.281065	3.793790
C	-0.595655	-1.013708	2.762382
Ni	-0.394425	2.061303	0.464978
C	-1.561585	3.090002	1.633244
C	-3.476526	3.154730	-1.644169
C	-4.078316	2.883482	-3.025224
C	-4.508890	3.844065	-0.754653
C	-2.250518	4.033389	-1.823504
C	2.383794	2.562421	-1.898200
C	3.896938	2.395862	-2.004879
C	1.809399	3.015660	-3.240041
C	2.065935	3.584809	-0.818812
C	1.074473	1.902232	4.068988
C	1.771690	2.908202	3.168636
C	0.079348	2.599675	4.993796

Table A1.5 Continued

C	2.138191	1.183919	4.900611
H	-4.318423	3.835685	-3.518211
H	-3.367514	2.334654	-3.659014
H	-5.399834	3.215693	-0.616368
H	-4.835101	4.788816	-1.212488
H	-4.091031	4.063216	0.235947
H	-1.516905	3.553200	-2.483733
H	-1.757033	4.243045	-0.869266
H	-2.558351	4.984330	-2.279783
H	4.187469	1.720502	-2.820982
H	4.318284	2.003088	-1.068551
H	4.362753	3.369388	-2.211655
H	1.999810	2.268536	-4.023484
H	2.267790	3.963988	-3.555619
H	2.514360	3.301231	0.141300
H	2.462773	4.565838	-1.114817
H	0.979294	3.677622	-0.662684
H	2.287962	3.649408	3.794645
H	2.515197	2.408989	2.533393
H	0.604161	3.319934	5.638377
H	-0.684283	3.137480	4.417844
H	2.815166	0.606004	4.255257
H	1.704142	0.497811	5.641075
H	2.737160	1.921630	5.454150
H	-5.007925	2.300636	-2.972263
H	-0.433528	1.877994	5.646189
H	0.723882	3.164105	-3.165327
C	-0.894460	-2.297069	-0.111304
C	-1.619896	-2.805435	-1.201314

Table A1.5 Continued

C	-1.622374	-4.159179	-1.529293
C	-0.872838	-5.059957	-0.780425
C	-0.113941	-4.585206	0.284321
C	-0.124089	-3.229000	0.602676
H	-2.185673	-2.122375	-1.837569
H	-2.203575	-4.510260	-2.386271
H	-0.865438	-6.122272	-1.038275
H	0.501214	-5.274243	0.868791
H	0.512677	-2.888368	1.421752
H	-5.015927	0.865660	-1.290056
H	-3.609622	-1.277236	-0.318491
H	2.912714	-0.044054	-2.848709
H	1.202963	-1.934435	-1.804094
H	-0.064650	-0.513749	4.851009
H	-1.063586	-1.990847	2.769897
H	1.065815	3.427991	2.512419
H	-2.125824	3.855369	1.077751
H	-0.971119	3.625673	2.393411
H	-2.298581	2.472445	2.172222

Table A1.8. DFT optimized coordinates for triplet/optimized singlet 2a.

C	-1.88569125509767	1.31575868894759	-0.43811326639217
N	-3.14878526283170	1.66052672609044	-0.80987185296364
C	-3.94040765439654	0.53817616676059	-0.90108192697676
C	-3.14599597204657	-0.52152364579506	-0.62029061451495
N	-1.88909802312851	-0.03379058089814	-0.38456748910611
B	-0.60903224830606	-0.83198993133565	0.00557003480596
N	0.58099083140707	-0.27149129747920	-0.83271162909682
C	0.90777380943085	1.02938935933492	-0.80707721709777
N	1.97312834179302	1.16251631126617	-1.63245098889613
C	2.29995694821602	-0.06055953010583	-2.18088866318950
C	1.42032371699895	-0.95844456947050	-1.67205745532825
N	-0.36843586450341	-0.43236947354582	1.49244461943455
C	-0.10533824350746	0.84820227285494	1.82843366705584
N	0.02261740134565	0.84291570040751	3.18321152202865
C	-0.22023097826837	-0.41772507595790	3.67889590463566
C	-0.47793161906641	-1.21136645578209	2.61185751330369
Ni	-0.21634134244536	2.22182346247562	0.32048308862942
C	-0.34394784346457	4.21078585103639	0.79704147734641
C	-3.64591573532743	3.02874174745787	-1.08787655384876
C	-4.92339356174412	2.95173733071580	-1.91932830642893
C	-3.94045382901606	3.72405757207476	0.23584824375981
C	-2.59307235294179	3.77512114962372	-1.89407119550272
C	2.62977777703495	2.44826959973971	-1.95403282701069
C	3.90073640965399	2.19241724973042	-2.75375811856548
C	1.66161813088817	3.28486156941171	-2.78499761553622
C	2.98739265833306	3.16605494334824	-0.65881066072034
C	0.37277851918442	2.01030408111675	4.02513000073215
C	1.64510549502002	2.63707289344975	3.46735633764218
C	-0.80009949187798	2.98239307544404	4.00780168947619

Table A1.6 Continued

C	0.64266889101337	1.56696546395433	5.45921957389298
H	-5.21600297179344	3.96966258314931	-2.20905498004265
H	-4.77483538139672	2.37195058839875	-2.84158518608729
H	-4.70192302408444	3.16848926704650	0.80170413322900
H	-4.31989971031230	4.74136685954890	0.05973376999149
H	-3.03009909980279	3.79110938650242	0.84167894429443
H	-2.39043153345005	3.25570153156292	-2.84135666891313
H	-1.65812106645400	3.85424467407422	-1.33011623309714
H	-2.94852498820488	4.78893968169072	-2.12469646380177
H	3.69399680593918	1.72896672075373	-3.72866535039449
H	4.60789604917539	1.55695288865215	-2.20166369695313
H	4.39734267406814	3.15177645780343	-2.94973295493965
H	1.37208364888784	2.75054014002131	-3.70124456961360
H	2.12549371185625	4.23873036015142	-3.07341042036880
H	3.65586715875062	2.55080448900828	-0.04059036220796
H	3.49651519664244	4.11397553924886	-0.88305329914110
H	2.08613294515885	3.39678713747206	-0.07657822616097
H	1.92373382864089	3.52210600736703	4.05647836656728
H	2.47543650299482	1.91723804804511	3.50657943155703
H	-0.57145944934482	3.87307972585939	4.60968611547596
H	-1.01744314229579	3.30097893440695	2.98203306983669
H	1.44835055936570	0.82085714842141	5.51828563746324
H	-0.25224679482502	1.16171583159217	5.95138627702716
H	0.96219464561195	2.44370658387497	6.03892175630851
H	-5.76737807001261	2.52157277057606	-1.36262943550942
H	-1.69705648114461	2.50471205252176	4.42856482067915
H	0.75106168820002	3.50533312663273	-2.21252783332477
C	-0.67848552588422	-2.42277801842856	-0.29411299961316
C	-1.37397106180094	-2.93281761939183	-1.40312066318050

Table A1.6 Continued

C	-1.31706870733429	-4.27597537566095	-1.76725055563931
C	-0.53413177577185	-5.16437885729610	-1.03811679492938
C	0.20005203023307	-4.68574699426628	0.04171834071536
C	0.13006038421287	-3.34031831262337	0.39598458795563
H	-1.96020529396477	-2.25878358409135	-2.03025686539491
H	-1.87735065767084	-4.62705649924771	-2.63788073762899
H	-0.47928159742132	-6.21779254316468	-1.32438380876072
H	0.84382746208976	-5.36241272051518	0.60948660431295
H	0.75611429242425	-2.99582335963794	1.22126897797971
H	-4.98834102951826	0.56457244584578	-1.16633260680204
H	-3.39687016065218	-1.57356254922776	-0.56190190759963
H	3.11669580178656	-0.20972105062183	-2.87458595934619
H	1.33639413746554	-2.02451901709759	-1.84794642922798
H	-0.19535956937821	-0.66498041913484	4.73175078062579
H	-0.75011003680776	-2.25892919638108	2.58057951498498
H	1.49929255829484	2.94936774080259	2.42815866711068
H	-0.20077032183951	4.82393582181974	-0.11392781876201
H	0.46806444728223	4.52826774727787	1.47559528470696
H	-1.26779673026511	4.59857317178742	1.25620045505045

Appendix 2: Supporting Data for Chapter 3

Table A2.1. DFT optimized coordinates of 3.

Ni	12.86322693205678	6.16688927020246	5.28198306485283
Ni	16.90588409802913	6.16603576972325	2.99324680723465
O	14.19681476911670	5.90161431631708	4.04029865877887
O	15.57176875260023	5.90066159770645	4.23435065809965
N	11.11161382565552	6.96384788975104	7.36996704410349
N	13.54732790388470	6.77862368975303	7.84798309757723
N	12.52942581291637	8.70591644890413	6.40803804920383
N	14.53953108983692	4.83806319339530	7.56824769231025
N	9.99574241436155	5.57333280165762	6.08856752174053
N	12.37294019687556	9.07047576680663	4.24538172464436
N	18.65843262609937	6.96285303317394	0.90596919344113
N	16.22298714164847	6.77724668439331	0.42679792985542
N	17.23975964669772	8.70489383816642	1.86693331698500
N	15.23104181530957	4.83652262380429	0.70635538912450
N	19.77370829606492	5.57244693966811	2.18802924170378
N	17.39483136651992	9.06998906182067	4.02958028503364
C	11.21779124932483	6.15574643101161	6.28292933146033
C	13.68961238146528	5.73391996688237	6.98628989019677
C	12.56796597104723	8.09920668758263	5.18744438951790
C	11.57811011338135	8.24720394812163	10.23218918864677
C	12.30947327914408	8.69799500829019	9.10359157934029
C	13.12001530231525	9.84750998912667	9.29562547219379
C	13.15130585596359	10.54294695880468	10.51718000491889
C	12.37895227890829	10.09540624355557	11.60173287593215
C	11.60208348795035	8.93426909691100	11.45861900960973
C	14.35839703167022	6.57261503851644	8.95212002215559
C	14.98328159503638	5.36588397404436	8.78132266025526

Table A2.1 Continued

C	14.90827165749032	3.44446868877333	7.12474599459630
C	16.38197708717042	3.45384048676310	6.68142059250640
C	14.69804559428007	2.48766976280292	8.31704773346796
C	13.99510051020760	3.01081891780053	5.97343989197761
C	9.81463239615457	6.92741953667701	7.84607290692093
C	9.11389408215893	6.05071114121717	7.05662994791577
C	9.57544816447879	4.59279425297785	5.02985888756084
C	8.48024099640695	5.25424446722096	4.16983344099564
C	10.78821457990917	4.23397199229168	4.16540370197768
C	9.04035651274645	3.32484044739134	5.72618069790749
C	12.31573051291040	10.06263270727851	6.23588025158127
C	12.23247631777768	10.29861532083423	4.88881511033980
C	12.32517457395731	8.93028441523243	2.74509581540307
C	11.73876315706621	7.56484676056571	2.37049684798571
C	13.75426276738811	9.07193787971910	2.20035505072535
C	11.41924224009618	10.03278424531332	2.16650983061604
C	18.55177735551111	6.15489915588197	1.99306647333769
C	16.08045282203011	5.73265925553469	1.28859215205163
C	17.20075711765773	8.09843030814790	3.08762328114359
C	18.18980300366198	8.24443370758505	-1.95803898471999
C	17.46101883013611	8.69676916843247	-0.82839384562279
C	16.65378116626149	9.84887067846560	-1.01883051029783
C	16.62305184215491	10.54497204849333	-2.24001698301791
C	17.39265396067680	10.09558519362217	-3.32576460575280
C	18.16625460807585	8.93208246970239	-3.18415273045085
C	15.41256617831706	6.57085657848898	-0.67774543099266
C	14.78795097153077	5.36395313059999	-0.50713342211034
C	14.86203901292316	3.44314281335184	1.15032120061492
C	13.38742954975211	3.45221258057385	1.59061894806479

Table A2.1 Continued

C	15.07518974146959	2.48521186058616	-0.04055752161031
C	15.77302888669300	3.01114511325592	2.30399124141017
C	19.95574610890676	6.92667553240902	0.43073182783688
C	20.65609030752459	6.04996713984664	1.22053033053789
C	20.19346473662873	4.59199068833044	3.24703453926735
C	21.28955152375027	5.25283741199093	4.10639537910210
C	18.98066264378177	4.23474686470166	4.11210151802080
C	20.72712208025601	3.32316739116724	2.55118774609571
C	17.45256373555182	10.06176591897914	2.03890236373135
C	17.53484617347017	10.29808894166215	3.38597183074345
C	17.44201392841864	8.93020498687998	5.52991495196292
C	18.03048273366602	7.56584980334781	5.90521720344455
C	16.01236906865281	9.06958790980848	6.07378981970955
C	18.34574032550696	10.03441823648702	6.10868749029164
B	12.37359469723920	7.84928846766226	7.73888567606739
B	17.39651818210823	7.84810447738888	0.53631679566754
H	10.99451097583097	7.31540762307557	10.17725229329034
H	13.76780711366553	10.20624767039442	8.48007755817462
H	13.78432982394684	11.43737841767608	10.62342058222204
H	12.39470082893960	10.63949838111879	12.55840159301235
H	11.01661001717369	8.55510432554446	12.31028766429864
H	14.40713296710576	7.28634977199457	9.77806656578532
H	15.68356354315488	4.83610399472210	9.42925585235820
H	16.69011067864326	2.43644018396905	6.36956630184994
H	16.52029995142032	4.14748200577986	5.82950183275013
H	17.05278765969404	3.76714697090006	7.50642779459747
H	14.88493408100277	1.44705006081217	7.98650006782184
H	15.39097596760241	2.68795535661732	9.15673365513170
H	13.65966172482695	2.54460584661509	8.69965486171594

Table A2.1 Continued

H	14.26415492601993	1.98016398887420	5.67193125944324
H	12.93480214164182	3.00109569349365	6.29374094276914
H	14.10299994881195	3.66785705782853	5.09078311107363
H	9.47831376884292	7.52719932659041	8.69409412904997
H	8.07241819787875	5.72793569251825	7.10879684336726
H	7.58601782599382	5.51277380929151	4.76903960102363
H	8.85370021107916	6.18215332882605	3.69351757347161
H	8.15357727541068	4.56079195940281	3.36998509970301
H	11.58217676856251	3.74572256926055	4.76096055069571
H	10.48070522320258	3.52473373202064	3.37384183464430
H	11.20795051269437	5.12708706498486	3.65907517376256
H	9.80884351975347	2.87561599895439	6.38629449546271
H	8.13908615034777	3.53275556092109	6.33508352156664
H	8.75769197056204	2.57379760347918	4.96311203317317
H	12.20412132466479	10.75114013350068	7.07550102842142
H	12.06958150097497	11.23086234017078	4.34761336722639
H	11.63429877987367	7.50619292714230	1.27847654863588
H	12.40003849681226	6.74337671694580	2.67804010316498
H	10.74063073629457	7.42556279818457	2.81094650928535
H	13.74045099900408	9.05108458681275	1.10102184721293
H	14.20478994832549	10.02429811206091	2.51682926714724
H	14.39131934805397	8.24708413406315	2.54860736996567
H	11.28106960919262	9.84855072654769	1.09224950089913
H	10.42565301028670	10.03319533360121	2.63709775674811
H	11.85704999242446	11.03623712906173	2.26174718631525
H	18.77041273859090	7.31070918615832	-1.90436943848593
H	16.00828775496622	10.20932132465749	-0.20220211406885
H	15.99257588190876	11.44134435474108	-2.34505366010471
H	17.37732939832798	10.64016355723335	-4.28216320793729

Table A2.1 Continued

H	18.74958359995831	8.55160901925880	-4.03670945558249
H	15.36409754027466	7.28444641899721	-1.50383263071998
H	14.08816973041117	4.83389879796058	-1.15537310001364
H	13.07919952784085	2.43498741551448	1.90294928765377
H	13.24698956712550	4.14671453310229	2.44148003057096
H	12.71815302085384	3.76425997127905	0.76388301776805
H	14.88844954978442	1.44481384699928	0.29076994106047
H	14.38366987148523	2.68405812509565	-0.88173264510685
H	16.11423802160436	2.54250332553699	-0.42131125191898
H	15.50405247340989	1.98056469969099	2.60582234641150
H	16.83402697955227	3.00192144168817	1.98601806126331
H	15.66273501137367	3.66887001075361	3.18585420439524
H	20.29253024006320	7.52652227368043	-0.41704887733676
H	21.69762624032964	5.72729541104153	1.16896066780903
H	22.18375086780122	5.51042979409714	3.50674503944745
H	20.91704805647865	6.18120265807818	4.58255790183989
H	21.61597745231947	4.55937498990778	4.90633461404816
H	18.18587831172860	3.74725601901530	3.51702011304238
H	19.28772048694932	3.52533658371466	4.90369018472705
H	18.56218235822386	5.12846465611803	4.61843174232388
H	19.95803841806632	2.87442483894813	1.89143846137689
H	21.62847992474924	3.52987737252821	1.94201109336918
H	21.00916372960361	2.57218291929386	3.31454428984619
H	17.56417165455962	10.75015945032786	1.19917680800839
H	17.69693505777762	11.23053914442421	3.92707725748237
H	18.13432051339531	7.50763792211013	6.99732170052504
H	17.37083273683833	6.74317928479015	5.59742102786355
H	19.02915321099345	7.42818540632153	5.46548585550331
H	16.02558808491974	9.04918231156734	7.17314008150641

Table A2.1 Continued

H	15.56036168700695	10.02103168355502	5.75668418209386
H	15.37695297612553	8.24347654103404	5.72550592545986
H	18.48356695438811	9.85078338219694	7.18309632415202
H	19.33960905985244	10.03634117865188	5.63869399570109
H	17.90630911425197	11.03710209183880	6.01283041286792

Tables and Figures

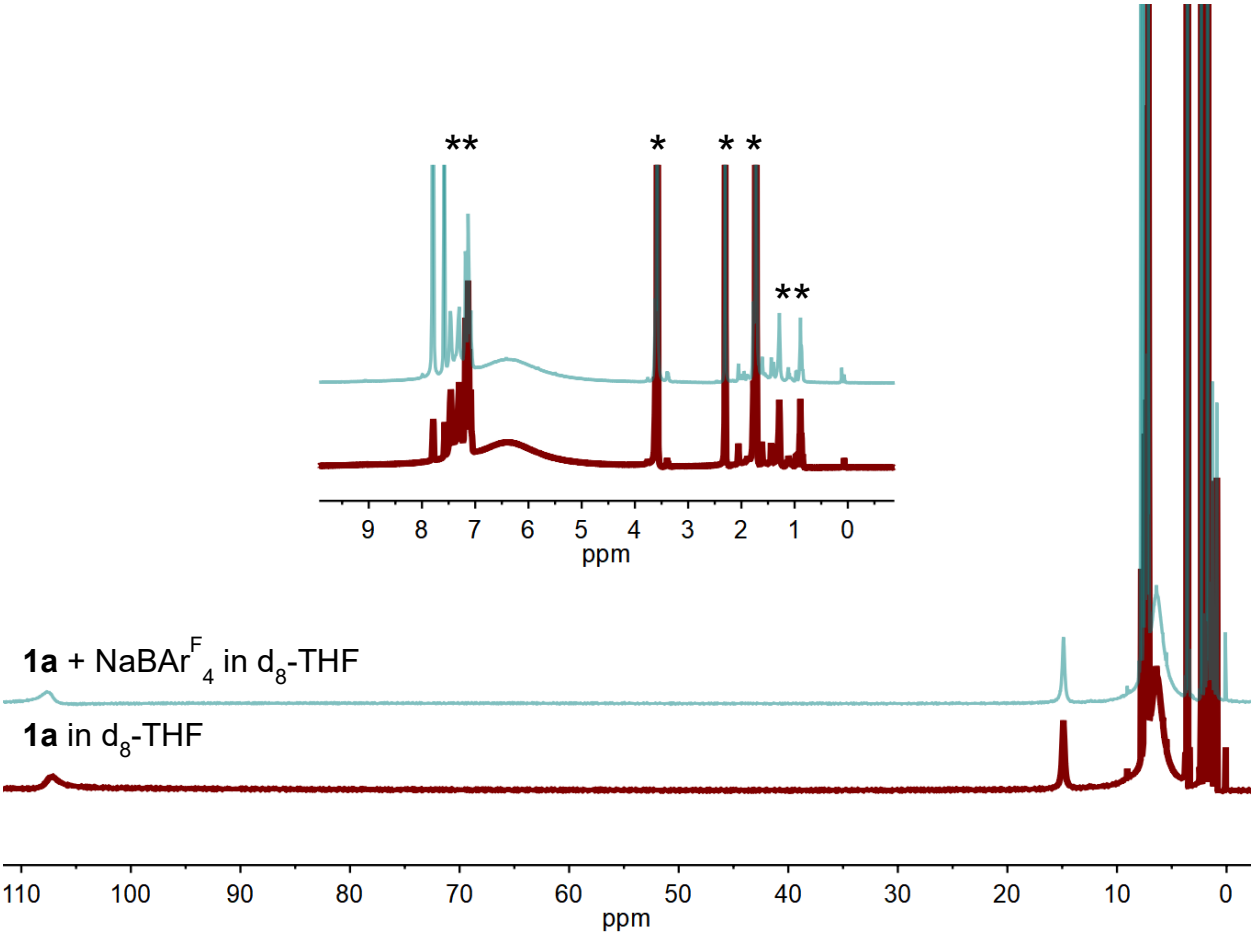

Figure A2.1. ^{1}H NMR spectrum of 1a and 1a + 1 equiv $NaBAr^{F}_{4}$ (298 K, d_8-THF).

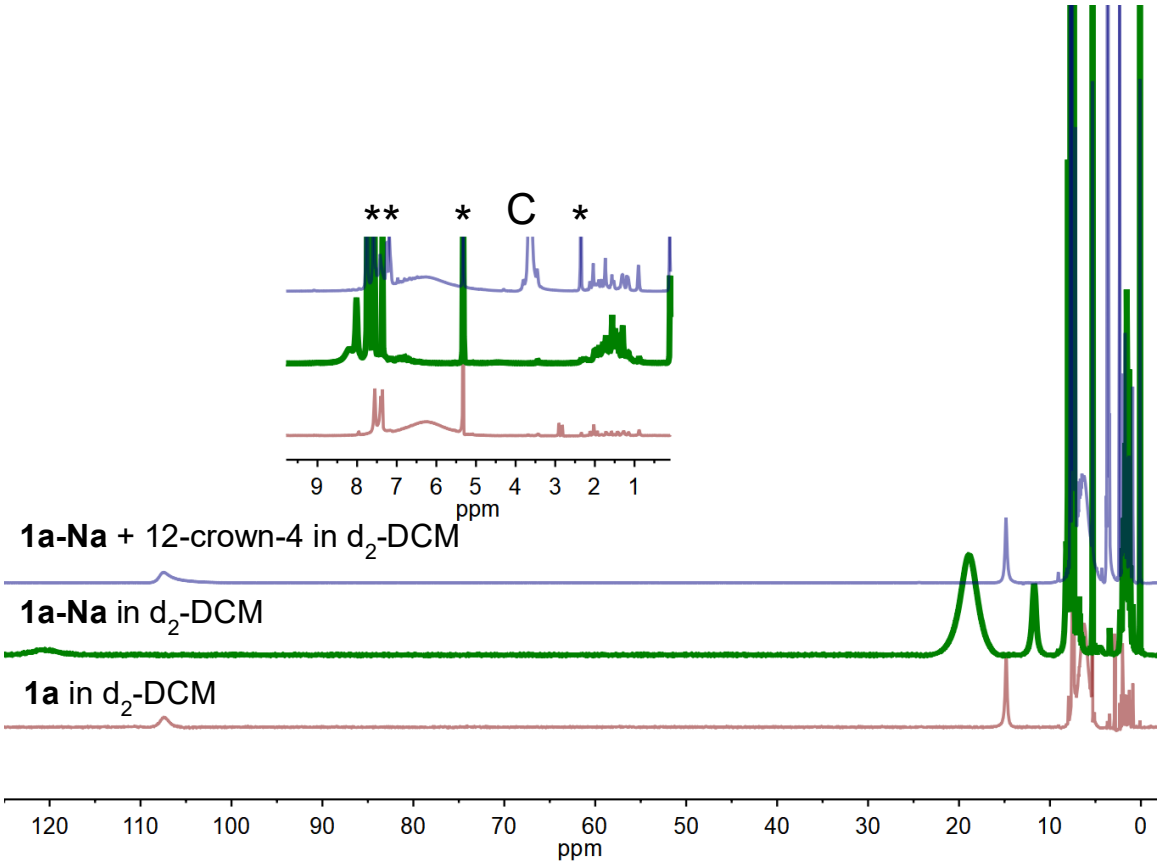

Figure A2.2. ^{1}H NMR spectrum of 1a, 1a-Na and 1a-Na + 1 equiv 12-crown-4 (298 K, CD_2Cl_2). Solvent impurities indicated by asterisks, crown either indicated by "C".

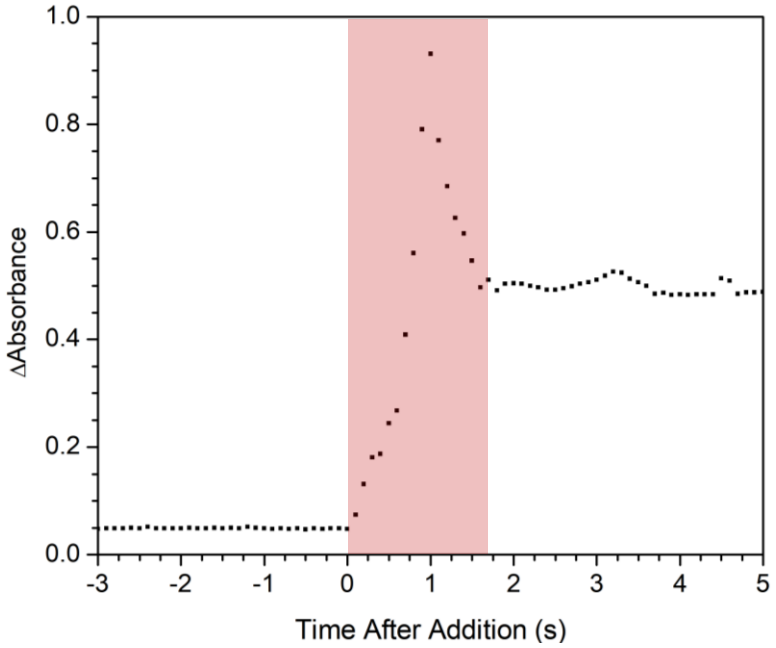

Figure A2.3. Addition of chilled, oxygenated DCM to 1a-Na at –78 °C

Monitoring absorption at 550 nm with 100 ms time points. Red indicates time where oxygenated DCM is being added, precluding accurate reading of reaction mixture absorbance.

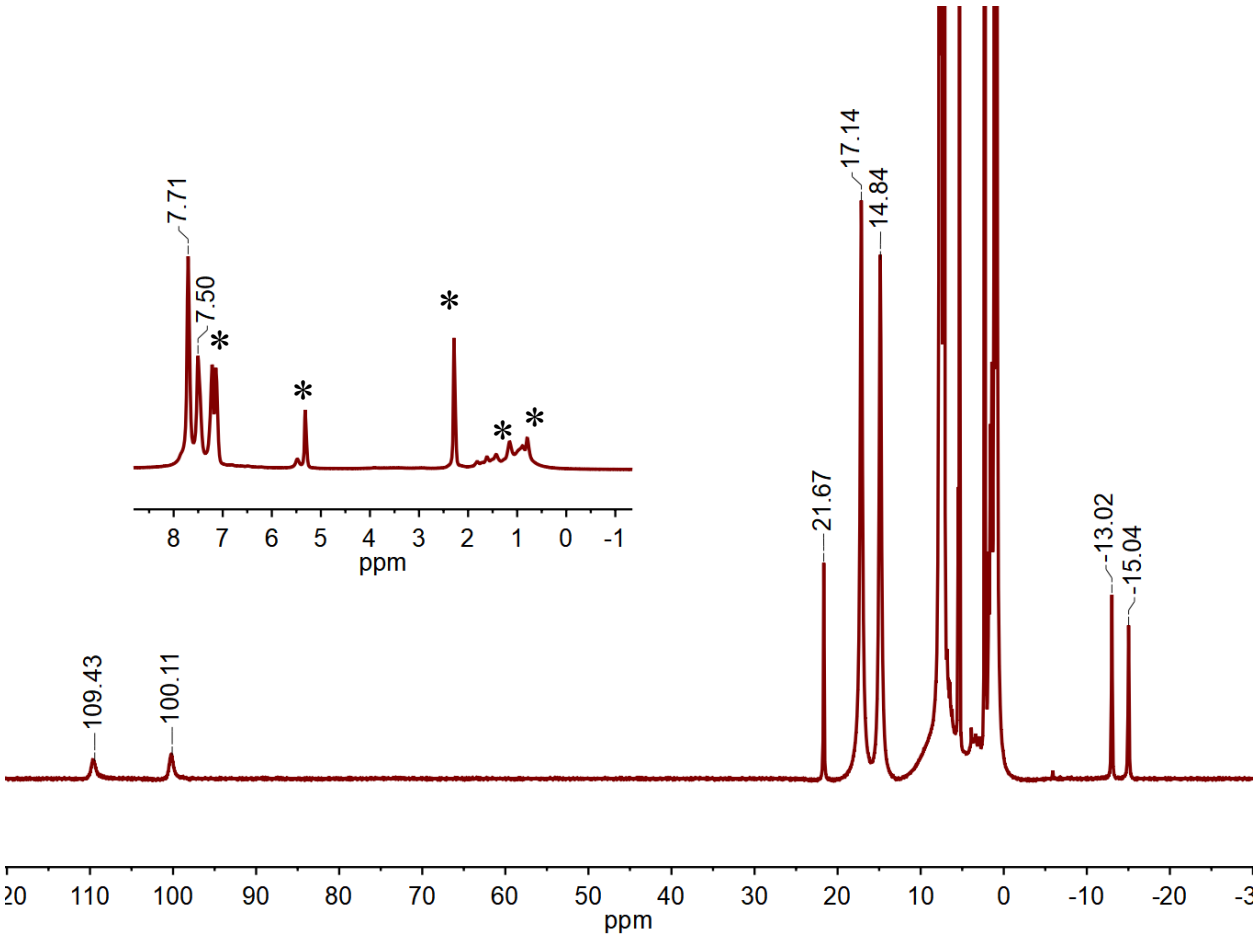

Figure A2.4. ^{1}H NMR spectrum of 3 (195 K, CD_2Cl_2).

Inset of diamagnetic region. Solvent impurities labelled with asterisks.

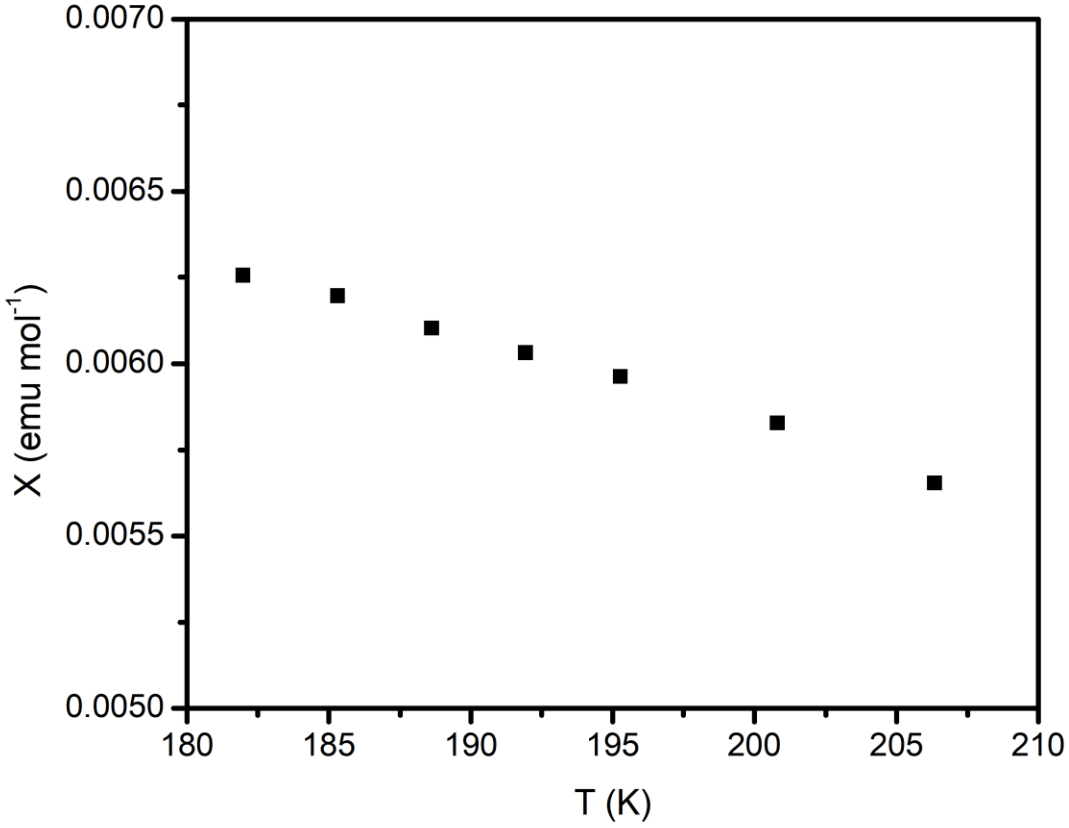

Figure A2.5. Magnetic susceptibility versus T plot obtained by variable temperature Evans' method (500 MHz NMR, CD_2Cl_2).

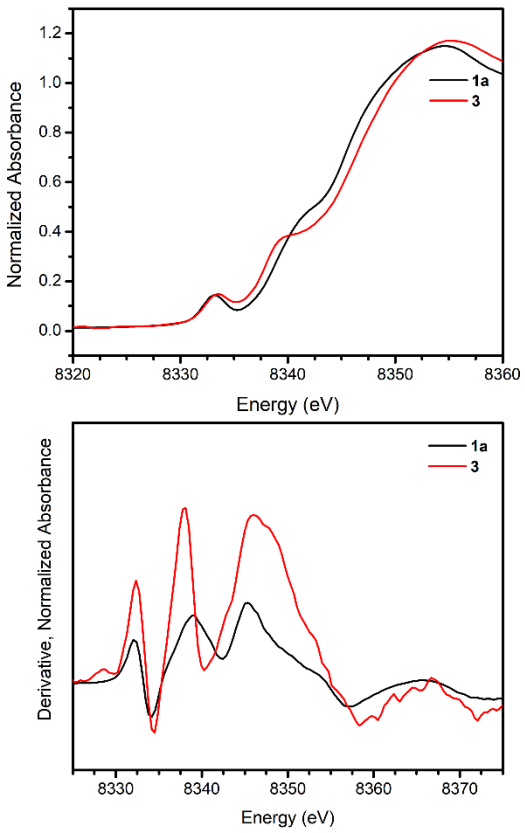

Figure A2.6. XANES spectrum and derivative of XANES spectrum of 1a and 3.

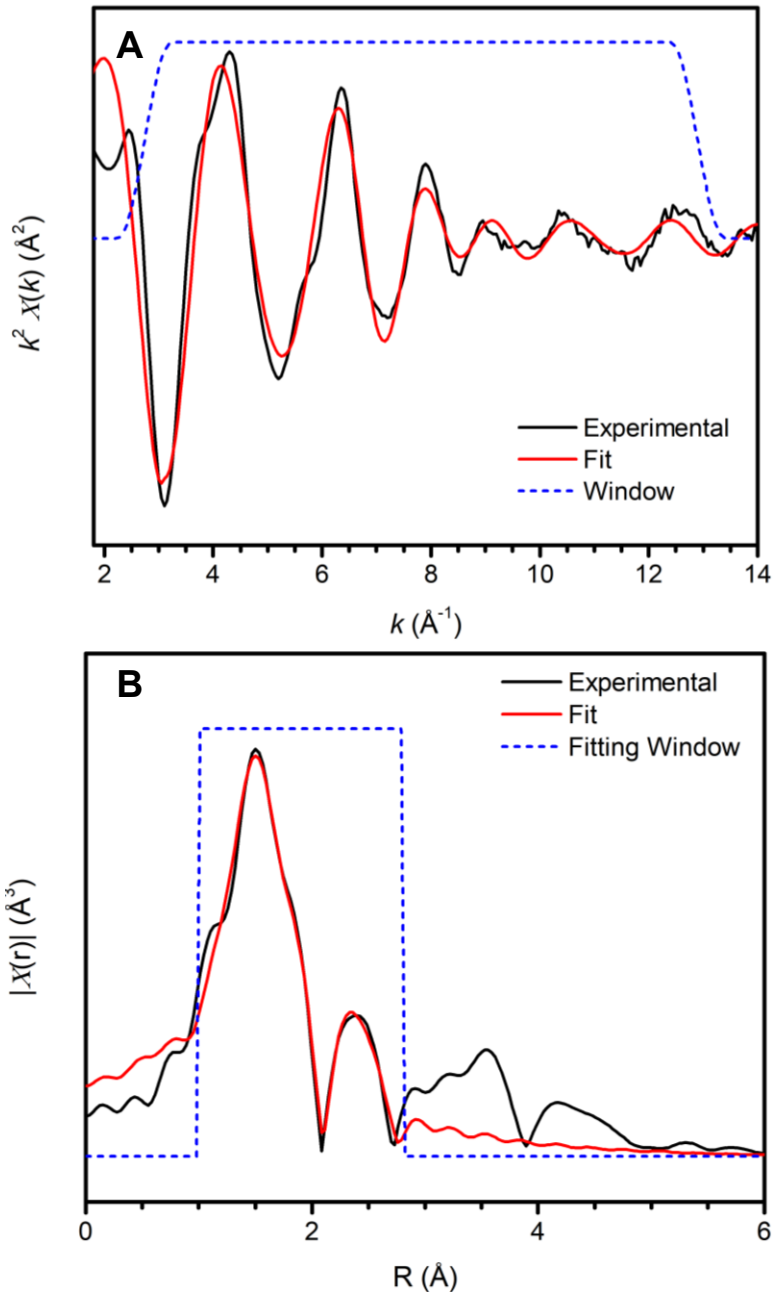

Figure A2.7. EXAFS plot and fits in k-space and R-space at the Ni K-edge absorption of 1a.

For fitting parameters, see Table A2.2.

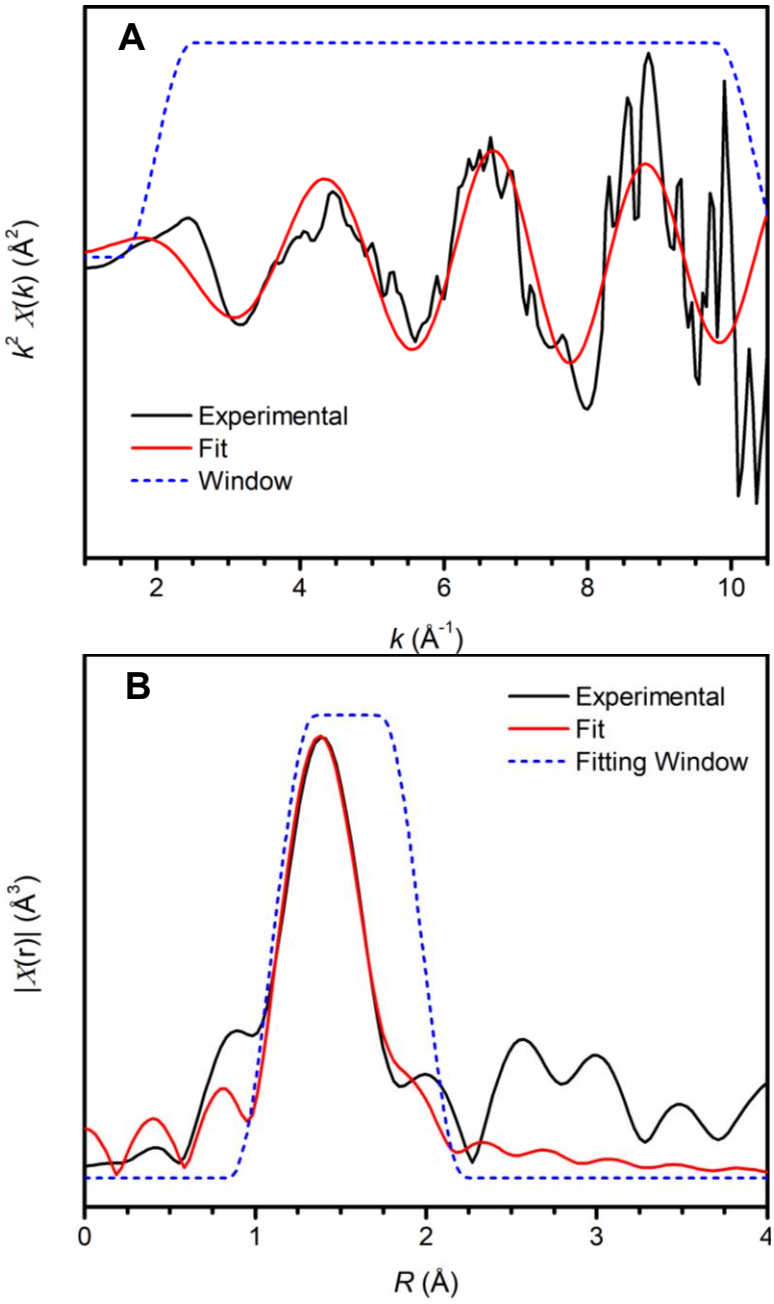

Figure A2.8. EXAFS plot and fits in k-space and R-space at the Ni K-edge absorption of 3.

For fitting parameters, see Table A2.3.

Table A2.2. Tabulated fitting parameters for EXAFS of 1a.

Independent Points: 11.5; Number of variables: 7; Fitting Ranges: *k*: 2.74 – 12.9 Å^{-1}; R: 1 – 2.8 Å. Abbreviations: N, coordination number; R, interatomic distance; σ^2, Debye-Waller factor (the mean-square deviations in interatomic distance). The values in parentheses are the estimated standard deviation; ΔE_0, change in photoelectron energy; S_0^2, amplitude reduction factor. See ORTEP diagram of 1a (below) for atom labels.

Scatterer	N	R (Å)	σ^2 (Å^2)
Ni–Cl	1	2.25(1)	0.005(1)
Ni–C1	3	2.003(8)	0.006(1)
Ni–N4	1	2.833(8)	0.007(2)
Ni–N5	1	2.866(8)	0.007(2)
Ni–N6	1	2.896(8)	0.007(2)
Ni–C1–N4	4	3.10(1)	0.007(1)
Ni–C3–N6	2	3.13(1)	0.007(1)
S_0^2	1.172		
ΔE_0	-2(1)		
R-factor	0.01313		
Reduced X^2	1258.2		

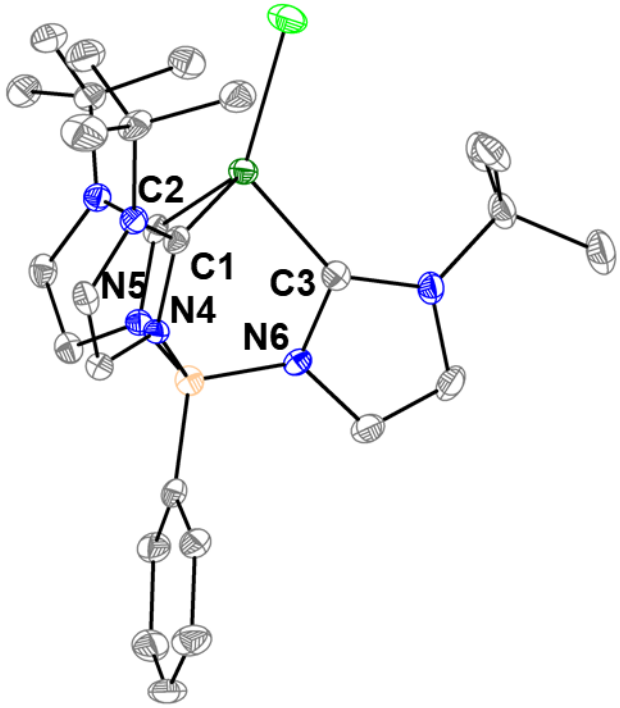

Table A2.3. Tabulated fitting parameters for EXAFS of 3.

Independent Points: 4.51; Number of variables: 2; Fitting Ranges: *k*: 2.0-10.3 Å^{-1}; R: 1.10-1.98 Å. Abbreviations: N, coordination number; R, interatomic distance; σ^2, Debye-Waller factor (the mean-square deviations in interatomic distance). The values in parentheses are the estimated standard deviation; ΔE_0, change in photoelectron energy; S_0^2, amplitude reduction factor.

Scatterer	N	R (Å)	σ^2 (Å^2)
Ni-O	1	1.80(2)	0.001(1)
Ni-C	3	1.90(2)	0.001(1)
S_0^2	0.9 (fixed)		
ΔE_0	–9(4)		
R-factor	0.02887		
Reduced X^2	21.4003		

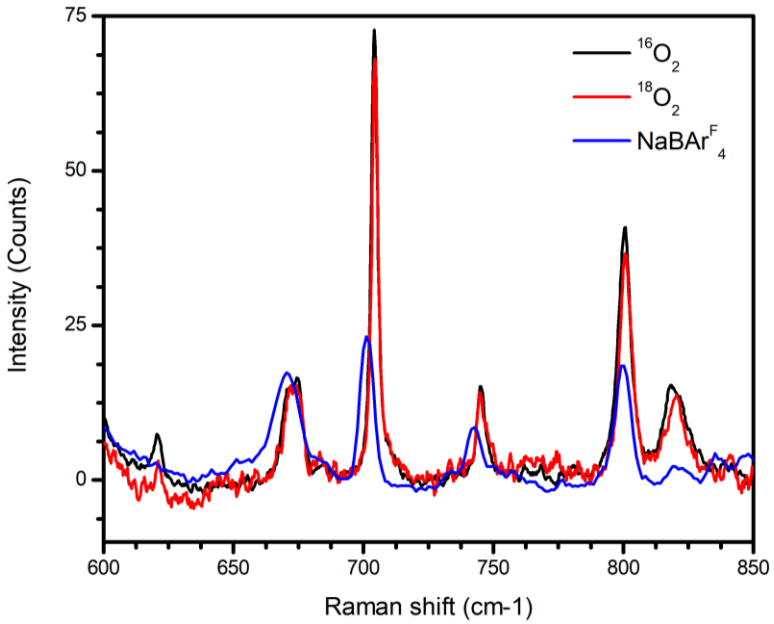

Figure A2.9. Confocal Raman spectrum of $NaBArF_4$ and 3 synthesized with natural abundance O_2, or $^{18}O_2$. Spectra were collected at 100 K. λ_{ex} = 532 nm.

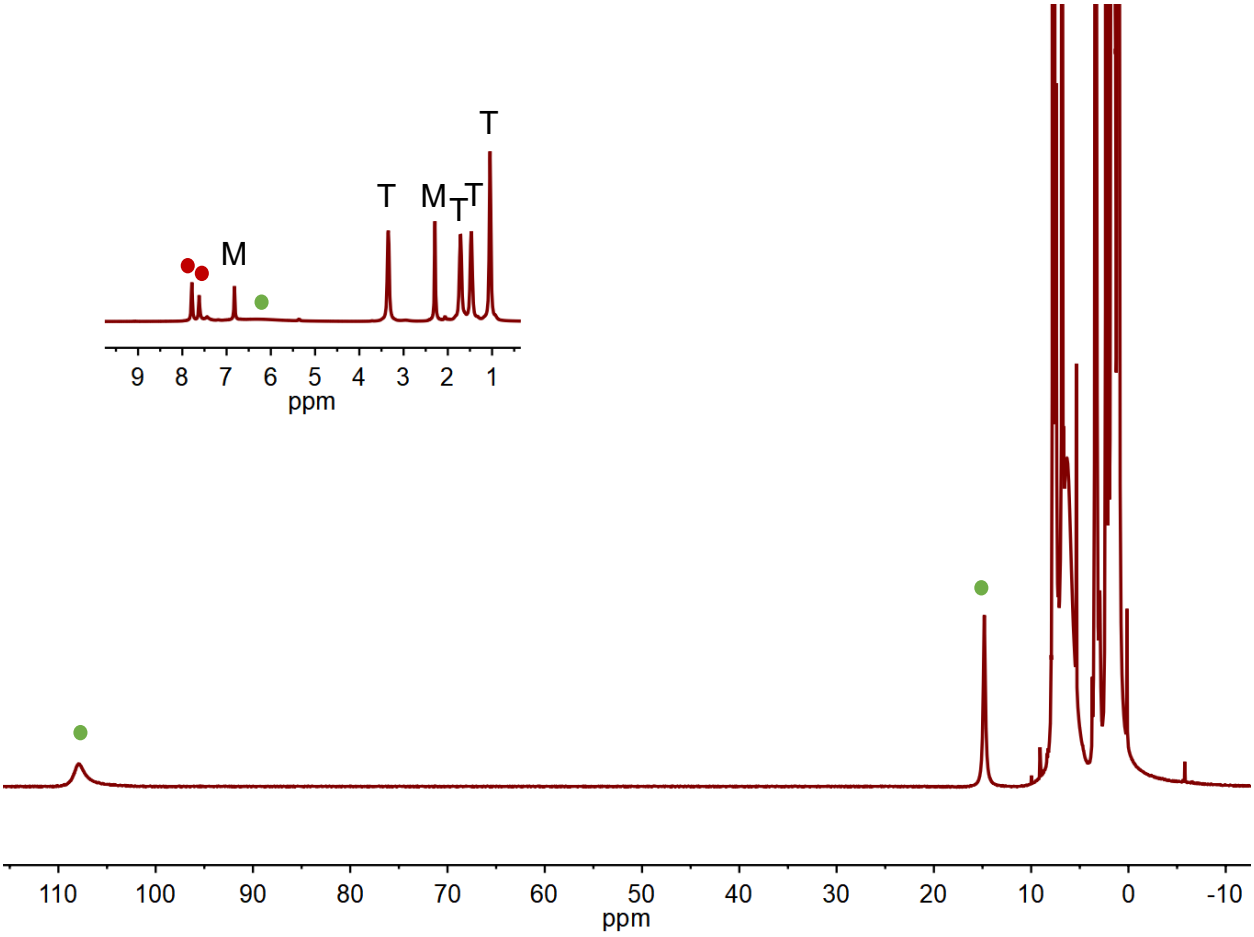

Figure A2.10. ^{1}H NMR spectrum of 3 + 10 equiv. TBACl (CD_2Cl_2).

Inset shows diamagnetic region. Resonances corresponding to 1a indicated by green dot, BAr^{F}_{4} anion by red dot, tetrabutylammonium cation by "T" and mesitylene internal standard by "M".

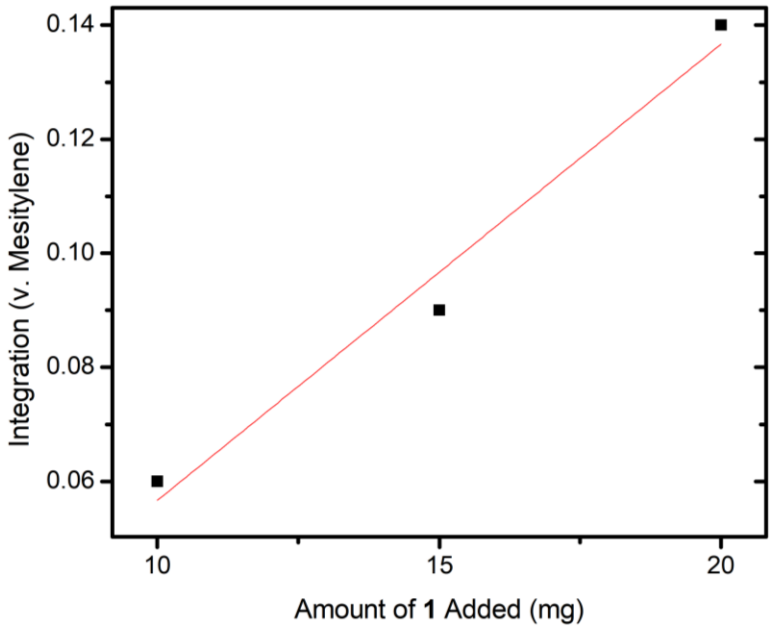

Figure A2.11. ^{1}H NMR calibration curve for 1a.

For calibration, the ^{1}H NMR resonance used for 1a was at 15 ppm, versus 0.01 mmol mesitylene added.

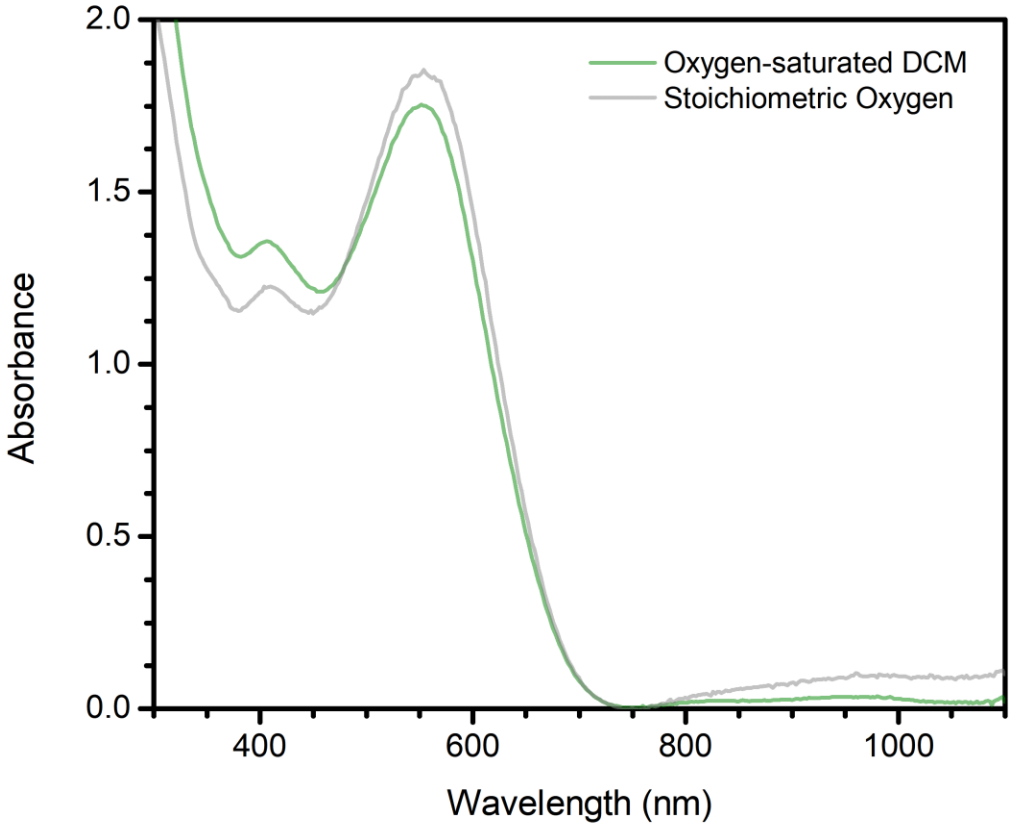

Figure A2.12. Addition of stoichiometric and excess oxygen to 1a-Na.

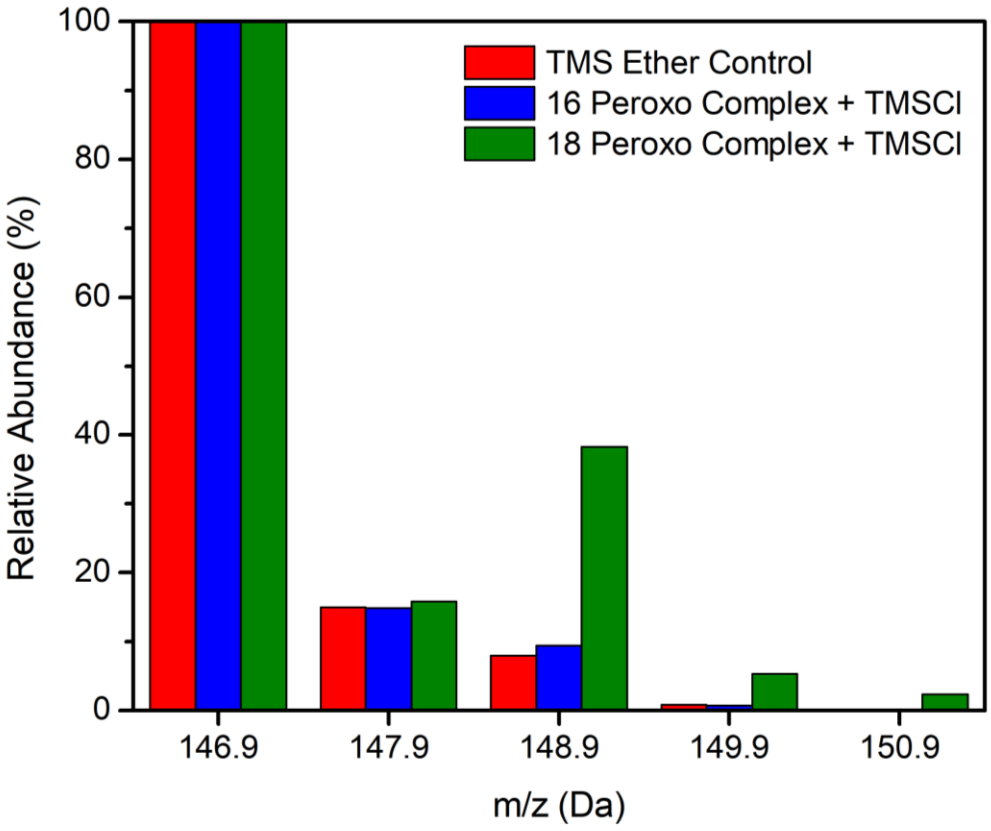

Figure A2.13. Average of mass spectra (three trials) of TMSCl/3 experiments.

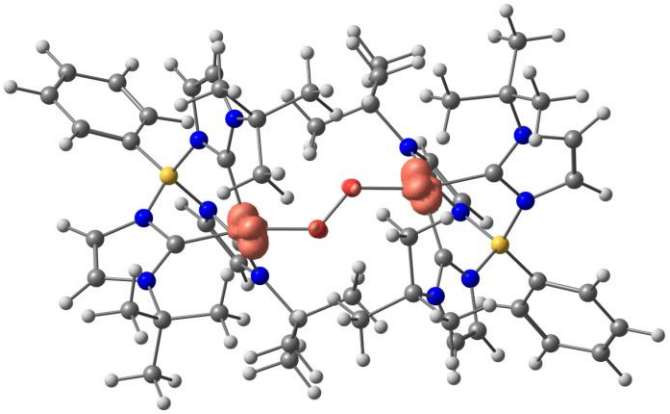

Figure A2.14. DFT calculated spin density distribution on 3.

Isosurface 0.035 a.u. Electronic structure calculations for the target system revealed the triplet as the ground state with closely lying open-shell singlet state (J-coupling constant was calculated to be +35.79 cm-1). Spin density distribution indicates that unpaired electrons are primarily localized on metal centers of the dimer with little density on the oxygen atoms of the bridge. This calculation also indicates that the electronic structure of the of the dioxo bridge-ligand is best described as closed-shell peroxo-species. The influence of the bulky tert-Bu groups of the organic ligands on the spin density distribution was found to be negligible.

Table A2.4. Crystal data and structure refinement for 3.

Empirical formula	$C_{118}H_{100}B_4F_{48}N_{12}Ni_2O_2$
Formula weight	2790.75
Temperature/K	100(2)
Crystal system	monoclinic
Space group	*C*2/*c*
a/Å	34.5565(13)
b/Å	25.3760(9)
c/Å	19.1210(8)
α/°	90
β/°	120.048(2)
γ/°	90
Volume/Å^3	14513.9(10)
Z	4
ρ_{calc}g/cm^3	1.277
μ/mm^{-1}	1.294
F(000)	5664.0
Crystal size/mm^3	0.385 × 0.204 × 0.155
Radiation	CuKα (λ = 1.54178)
2Θ range for data collection/°	4.566 to 101.064
Index ranges	$-29 \leq h \leq 34$, $-22 \leq k \leq 25$, $-18 \leq l \leq 19$
Reflections collected	31629
Independent reflections	7419 [R_{int} = 0.1540, R_{sigma} = 0.1385]
Data/restraints/parameters	7419/1449/778

Table A2.4 Continued

Goodness-of-fit on F^2	1.074
Final R indexes [I>=2σ (I)]	R_1 = 0.1303, wR_2 = 0.2372
Final R indexes [all data]	R_1 = 0.2144, wR_2 = 0.2714
Largest diff. peak/hole / e $Å^{-3}$	0.62/-0.35

$R_{int} = \Sigma \mid F_o^2 - \langle F_o^2 \rangle \mid / \Sigma \mid F_o^2 \mid$

$R_1 = \Sigma \mid \mid F_o \mid - \mid F_c \mid \mid / \Sigma \mid F_o \mid$

$wR_2 = [\Sigma [w (F_o^2 - F_c^2)^2] / \Sigma [w (F_o^2)^2]]^{1/2}$

Goodness-of-fit = $[\Sigma [w (F_o^2 - F_c^2)^2] / (n-p)^{1/2}$

n: number of independent reflections; p: number of refined parameters

Table A2.5. Bond lengths from solid state structure of 3.

Atom	Atom	Length/Å	Atom	Atom	Length/Å
Ni1	O1	1.796(9)	F13	C59	1.3496(9)
Ni1	C16	1.916(16)	F14	C59	1.3494(9)
Ni1	C9	1.820(17)	F15	C59	1.3494(9)
Ni1	C23	1.914(14)	F16	C58	1.3492(9)
O1	$O1^{1}$	1.416(15)	F17	C58	1.3493(9)
C16	N2	1.349(18)	F18	C58	1.3494(9)
C16	N1	1.327(17)	F19	C50	1.3492(9)
N2	C14	1.404(19)	F20	C50	1.3492(9)
N2	B1	1.54(2)	F21	C50	1.3492(9)
C9	N4	1.39(2)	F22	C51	1.3494(9)
C9	N3	1.385(19)	F23	C51	1.3494(9)
N4	C7	1.315(18)	F24	C51	1.3495(9)
N4	B1	1.61(2)	C33	C32	1.3900
C23	N6	1.394(15)	C33	C28	1.3900

Table A2.1 Continued

Table A2.5 Continued

C23	N5	1.353(15)	C32	C31	1.3900
N6	C21	1.361(16)	C32	C35	1.429(5)
N6	B1	1.58(2)	C31	C30	1.3900
C6	C1	1.3900	C30	C29	1.3900
C6	C5	1.3900	C30	C34	1.430(5)
C1	C2	1.3900	C29	C28	1.3900
C1	B1	1.64(2)	C28	B2	1.695(15)
C2	C3	1.3900	C36	C41	1.3900
C3	C4	1.3900	C36	C37	1.3900
C4	C5	1.3900	C36	B2	1.673(16)
C7	C8	1.34(2)	C41	C40	1.3900
C8	N3	1.35(2)	C40	C39	1.3900
N3	C10	1.50(2)	C40	C43	1.427(5)
C10	C11	1.57(3)	C39	C38	1.3900
C10	C12	1.56(2)	C38	C37	1.3900
C10	C13	1.50(2)	C38	C42	1.423(5)

Table A2.5 Continued

C14	C15	1.30(2)	C43	F7A	1.348(4)
C15	N1	1.40(2)	C43	F9A	1.354(4)
N1	C17	1.50(2)	C43	F8A	1.355(4)
C17	C18	1.474(19)	C47	C46	1.3900
C17	C19	1.49(2)	C47	C48	1.3900
C17	C20	1.510(19)	C46	C45	1.3900
C21	C22	1.358(17)	C46	C50	1.418(5)
C22	N5	1.363(15)	C45	C44	1.3900
N5	C24	1.500(15)	C44	C49	1.3900
C24	C25	1.548(16)	C44	B2	1.654(16)
C24	C26	1.489(15)	C49	C48	1.3900
C24	C27	1.495(15)	C48	C51	1.426(5)
F1	C35	1.3497(7)	C53	C54	1.3900
F2	C35	1.3497(7)	C53	C52	1.3900
F3	C35	1.3497(7)	C54	C55	1.3900
F4	C34	1.3498(7)	C54	C58	1.423(5)

Table A2.5 Continued

F5	C34	1.3497(7)	C55	C56	1.3900
F6	C34	1.3496(7)	C56	C57	1.3900
F7	C43	1.3493(9)	C56	C59	1.428(5)
F8	C43	1.3496(9)	C57	C52	1.3900
F9	C43	1.3497(9)	C52	B2	1.655(16)
F10	C42	1.3492(9)	C59	F13A	1.27(3)
F11	C42	1.3494(9)	C59	F14A	1.50(3)
F12	C42	1.3493(9)	C59	F15A	1.36(3)

Table A2.6. Bond angles from solid state structure of 3.

Atom	Atom	Atom	Angle/°	Atom	Atom	Atom	Angle/°
O1	Ni1	C16	165.6(6)	F3	C35	F1	102.7(6)
O1	Ni1	C9	103.9(6)	F3	C35	F2	104.0(5)
O1	Ni1	C23	102.6(5)	F3	C35	C32	114.0(6)
C9	Ni1	C16	84.7(7)	C41	C36	C37	120.0
C9	Ni1	C23	109.3(8)	C41	C36	B2	119.9(7)
C23	Ni1	C16	85.0(6)	C37	C36	B2	119.6(7)
$O1^{1}$	O1	Ni1	122.2(10)	C40	C41	C36	120.0
N2	C16	Ni1	117.5(12)	C41	C40	C43	120.9(7)
N1	C16	Ni1	133.5(15)	C39	C40	C41	120.0
N1	C16	N2	108.9(15)	C39	C40	C43	119.1(7)
C16	N2	C14	109.4(15)	C40	C39	C38	120.0
C16	N2	B1	117.2(14)	C39	C38	C37	120.0
C14	N2	B1	132.8(17)	C39	C38	C42	120.2(7)
N4	C9	Ni1	115.0(13)	C37	C38	C42	119.7(7)
N3	C9	Ni1	145.9(17)	C38	C37	C36	120.0

Table A2.6 Continued

N3	C9	N4	96.8(15)	F10	C42	F11	102.6(8)
C9	N4	B1	116.1(14)	F10	C42	F12	101.9(7)
C7	N4	C9	116.5(18)	F10	C42	C38	117.6(8)
C7	N4	B1	126.2(18)	F11	C42	F12	101.7(7)
N6	C23	Ni1	114.9(10)	F11	C42	C38	116.3(8)
N5	C23	Ni1	139.5(11)	F12	C42	C38	114.5(8)
N5	C23	N6	105.5(12)	F7	C43	F8	110.1(9)
C23	N6	B1	116.7(13)	F7	C43	F9	108.9(9)
C21	N6	C23	108.3(12)	F7	C43	C40	117.1(12)
C21	N6	B1	133.5(14)	F8	C43	C40	109.0(9)
C1	C6	C5	120.0	F9	C43	F8	104.8(9)
C6	C1	B1	118.6(11)	F9	C43	C40	106.2(10)
C2	C1	C6	120.0	F7A	C43	C40	131.0(10)
C2	C1	B1	121.3(11)	F7A	C43	F9A	97.1(12)
C1	C2	C3	120.0	F7A	C43	F8A	103.5(11)
C4	C3	C2	120.0	F9A	C43	C40	113.8(10)

Table A2.6 Continued

C3	C4	C5	120.0	F9A	C43	F8A	89.1(13)
C4	C5	C6	120.0	F8A	C43	C40	113.5(10)
N4	C7	C8	106(2)	C46	C47	C48	120.0
C7	C8	N3	105.9(17)	C47	C46	C50	123.8(7)
C9	N3	C10	124.5(17)	C45	C46	C47	120.0
C8	N3	C9	114.7(19)	C45	C46	C50	116.1(7)
C8	N3	C10	120.3(17)	C46	C45	C44	120.0
N3	C10	C11	106.4(15)	C45	C44	B2	118.1(7)
N3	C10	C12	110(2)	C49	C44	C45	120.0
N3	C10	C13	111.5(16)	C49	C44	B2	121.8(7)
C12	C10	C11	108.9(17)	C44	C49	C48	120.0
C13	C10	C11	110(2)	C47	C48	C51	118.6(6)
C13	C10	C12	109.2(16)	C49	C48	C47	120.0
C15	C14	N2	104.0(19)	C49	C48	C51	121.2(6)
C14	C15	N1	112.3(17)	F19	C50	C46	117.6(8)
C16	N1	C15	105.1(16)	F20	C50	F19	98.3(7)

Table A2.6 Continued

C16	N1	C17	129.5(16)	F20	C50	C46	119.2(8)
C15	N1	C17	125.3(14)	F21	C50	F19	100.5(7)
N1	C17	C20	108.4(15)	F21	C50	F20	97.7(8)
C18	C17	N1	107.4(14)	F21	C50	C46	119.4(9)
C18	C17	C19	109.9(15)	F22	C51	F23	105.8(6)
C18	C17	C20	111.9(14)	F22	C51	F24	104.7(7)
C19	C17	N1	108.0(12)	F22	C51	C48	118.1(7)
C19	C17	C20	111.0(15)	F23	C51	C48	110.9(7)
C22	C21	N6	108.8(14)	F24	C51	F23	104.0(8)
C21	C22	N5	106.6(13)	F24	C51	C48	112.2(7)
C23	N5	C22	110.8(12)	C54	C53	C52	120.0
C23	N5	C24	127.4(11)	C53	C54	C58	120.8(8)
C22	N5	C24	121.8(11)	C55	C54	C53	120.0
N5	C24	C25	107.9(10)	C55	C54	C58	119.1(8)
C26	C24	N5	109.8(11)	C56	C55	C54	120.0
C26	C24	C25	110.4(11)	C55	C56	C57	120.0

Table A2.6 Continued

C26	C24	C27	112.0(11)	C55	C56	C59	122.8(9)
C27	C24	N5	108.2(10)	C57	C56	C59	117.1(9)
C27	C24	C25	108.5(11)	C52	C57	C56	120.0
N2	B1	N4	104.7(15)	C53	C52	B2	118.3(9)
N2	B1	N6	104.3(13)	C57	C52	C53	120.0
N2	B1	C1	118.7(14)	C57	C52	B2	121.6(8)
N4	B1	C1	106.4(13)	F16	C58	F17	101.5(7)
N6	B1	N4	110.4(13)	F16	C58	F18	102.7(8)
N6	B1	C1	112.0(15)	F16	C58	C54	113.8(8)
C32	C33	C28	120.0	F17	C58	F18	100.7(8)
C33	C32	C35	118.3(5)	F17	C58	C54	117.3(9)
C31	C32	C33	120.0	F18	C58	C54	118.4(9)
C31	C32	C35	121.7(5)	F13	C59	C56	121.0(14)
C32	C31	C30	120.0	F14	C59	F13	100.1(10)
C31	C30	C29	120.0	F14	C59	C56	118.4(12)
C31	C30	C34	117.1(5)	F15	C59	F13	99.1(10)

Table A2.6 Continued

C29	C30	C34	122.9(5)	F15	C59	F14	99.1(10)
C30	C29	C28	120.0	F15	C59	C56	115.3(13)
C33	C28	B2	119.3(7)	C56	C59	F14A	102.3(12)
C29	C28	C33	120.0	F13A	C59	C56	123.7(16)
C29	C28	B2	120.6(7)	F13A	C59	F14A	108.2(18)
F4	C34	C30	113.5(6)	F13A	C59	F15A	114.6(18)
F5	C34	F4	105.0(5)	F15A	C59	C56	105.6(13)
F5	C34	C30	114.9(6)	F15A	C59	F14A	99.1(16)
F6	C34	F4	104.2(5)	C36	B2	C28	111.6(9)
F6	C34	F5	103.5(5)	C44	B2	C28	112.9(10)
F6	C34	C30	114.5(6)	C44	B2	C36	101.1(9)
F1	C35	F2	103.4(6)	C44	B2	C52	114.2(9)
F1	C35	C32	114.9(6)	C52	B2	C28	103.6(9)
F2	C35	C32	116.2(6)	C52	B2	C36	113.8(10)

Appendix 3: Supporting Data for Chapter 4

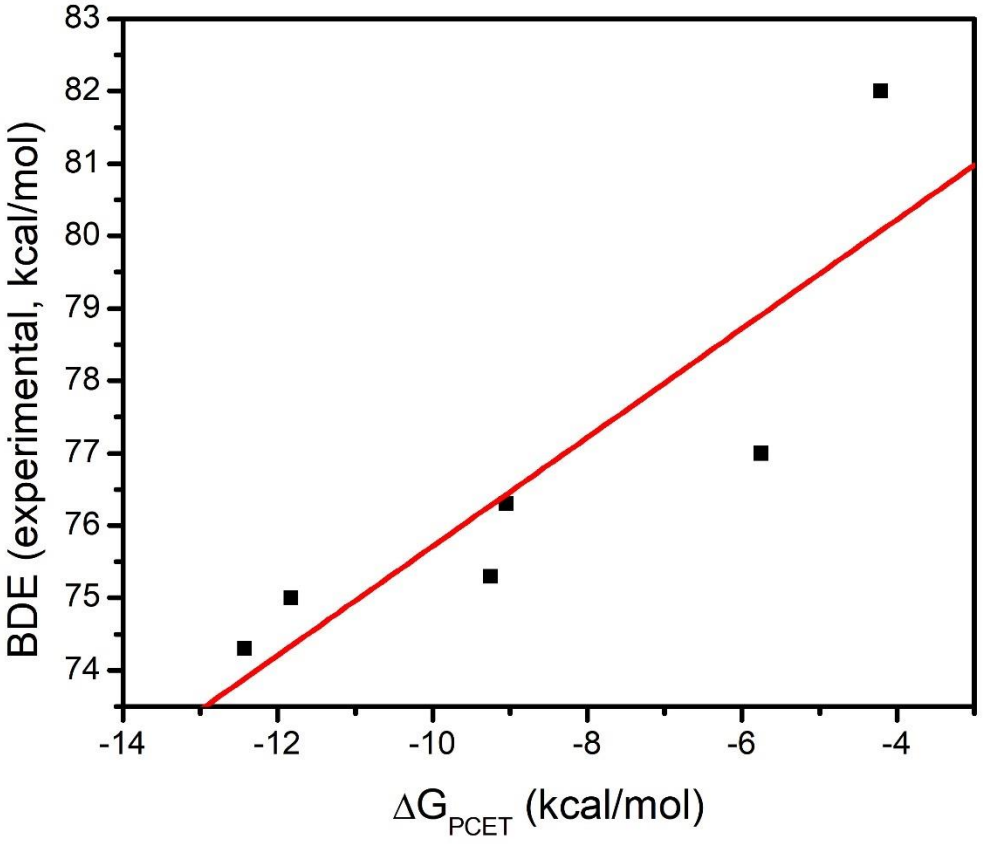

Figure A3.1. Plot of experimental bond dissociation energies versus calculated ΔG_{PCET} for C–H substrates.

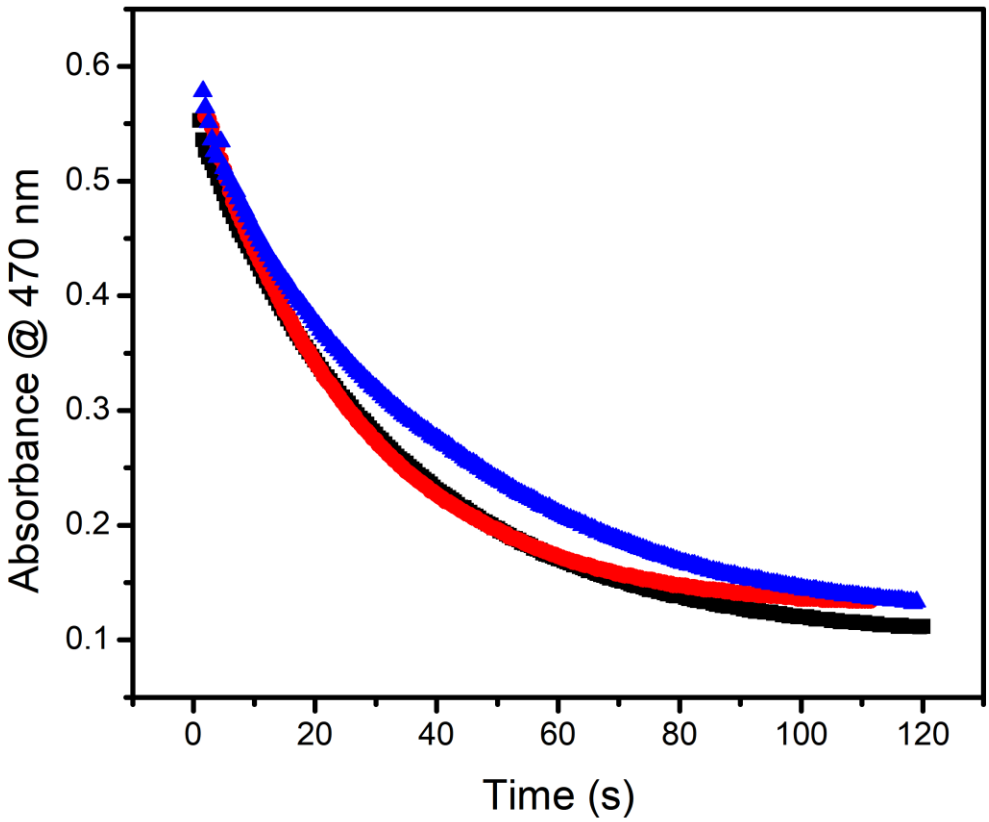

Figure A3.2. Absorbance at 470 nm, monitoring reaction between 4b and 3-phenylindene.

Sample fitting (blue points): Abs = 0.112 + 0.454*exp(–0.02598*t). R^2 = 0.9988.

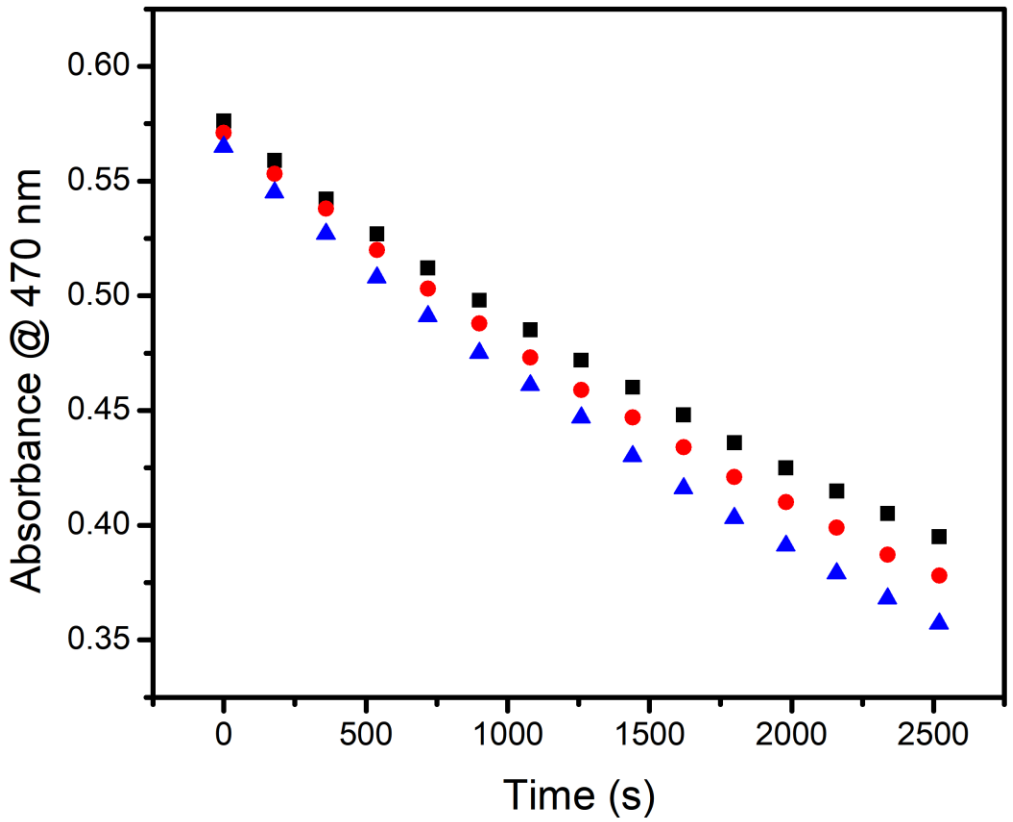

Figure A3.3. Absorbance at 470 nm, monitoring reaction between 4b and fluorene.

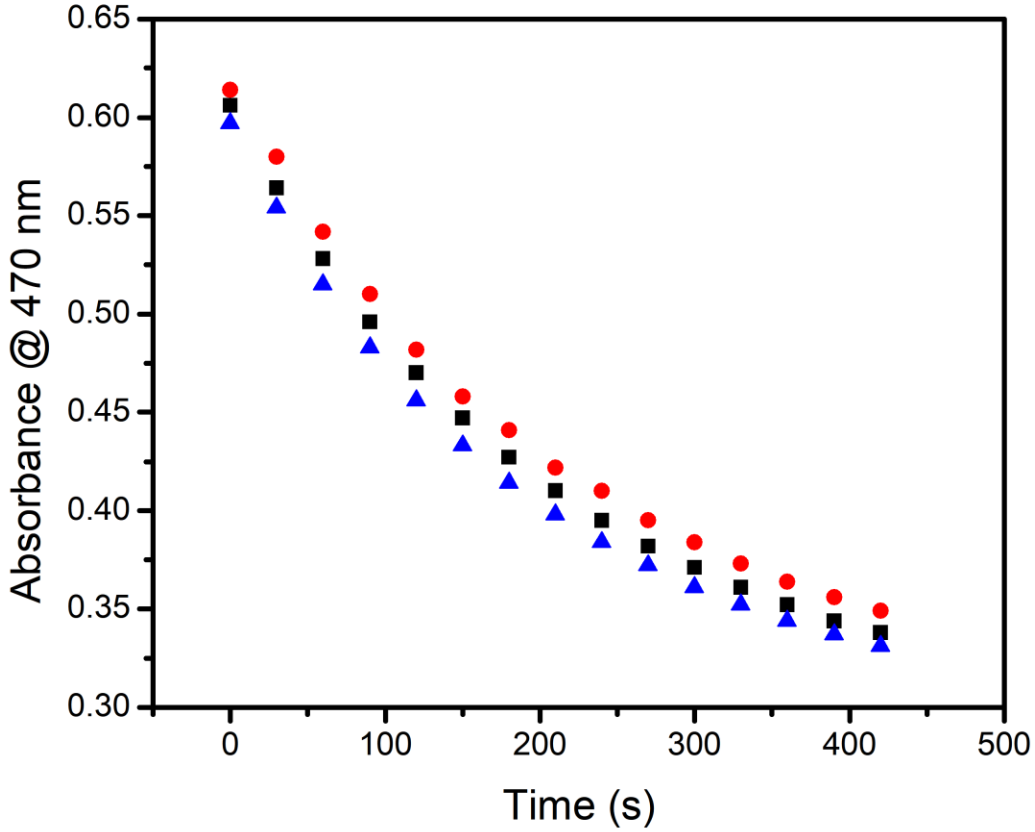

Figure A3.4. Absorbance at 470 nm, monitoring reaction between 4b and indene.

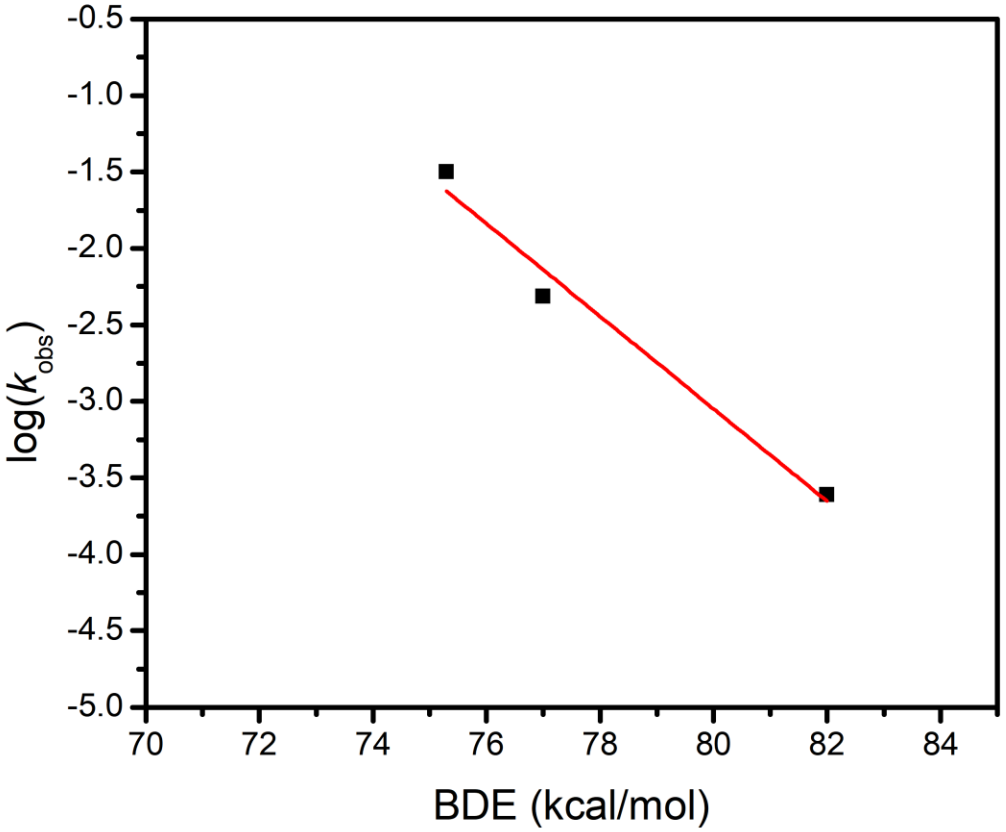

Figure A3.5. Plot of log(k_{obs}) versus substrate BDE. log(k_{obs}) = -0.30(BDE) + 21.1. R^2 = 0.95.

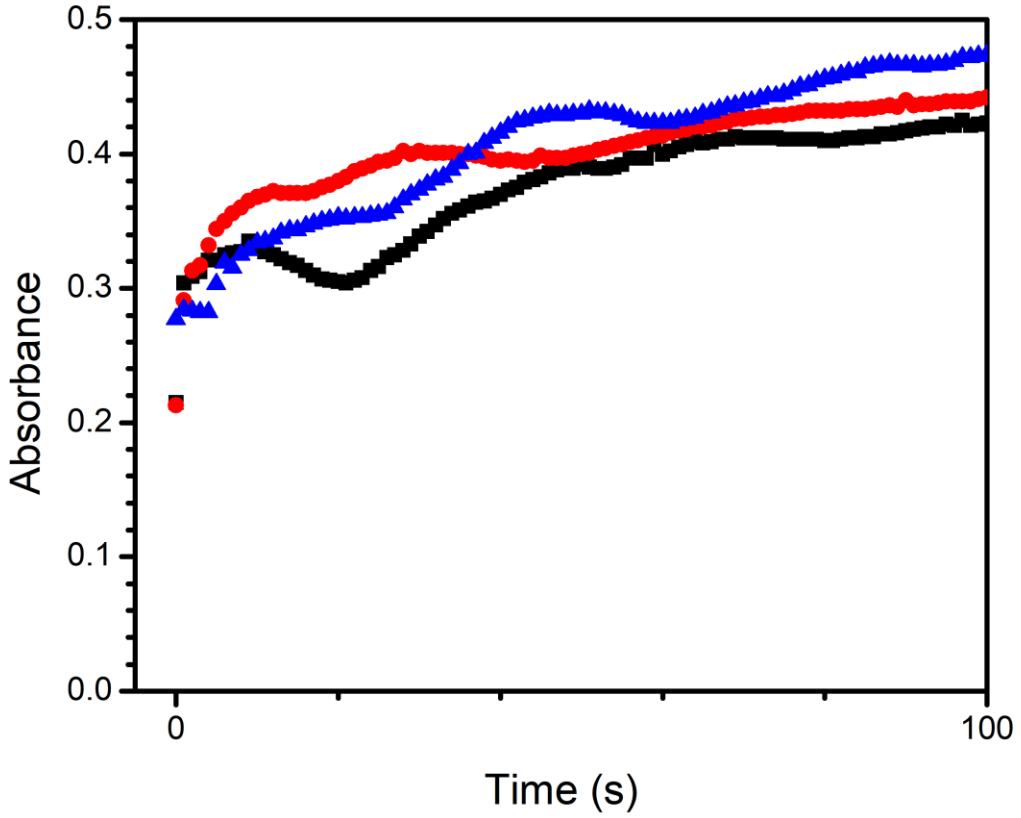

Figure A3.6. Absorbance at 714 nm, monitoring reaction between 4b and 4-OMe-2,6-di-*tert*-butylphenol. Sample fitting (blue points): Abs = 0.515 – 0.232*exp(–0.0178*t). R^2 = 0.9895.

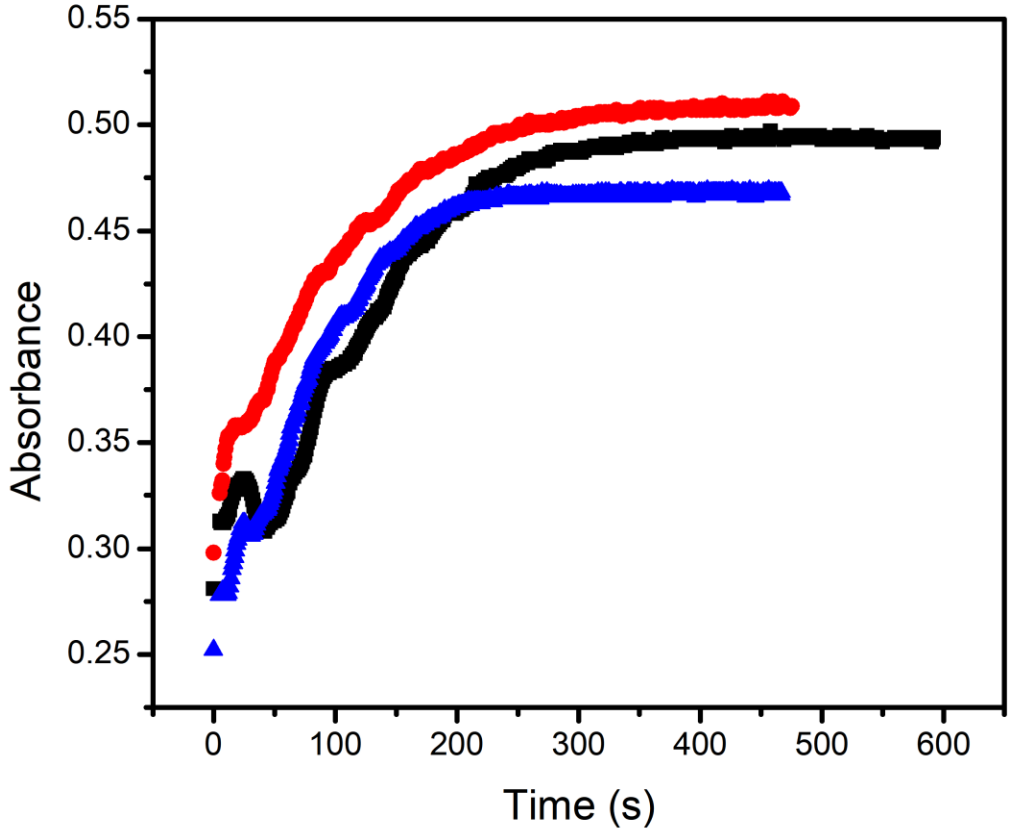

Figure A3.7. Absorbance at 714 nm, monitoring reaction between 4b and (4-H-)2,6-di-*tert*-butylphenol.

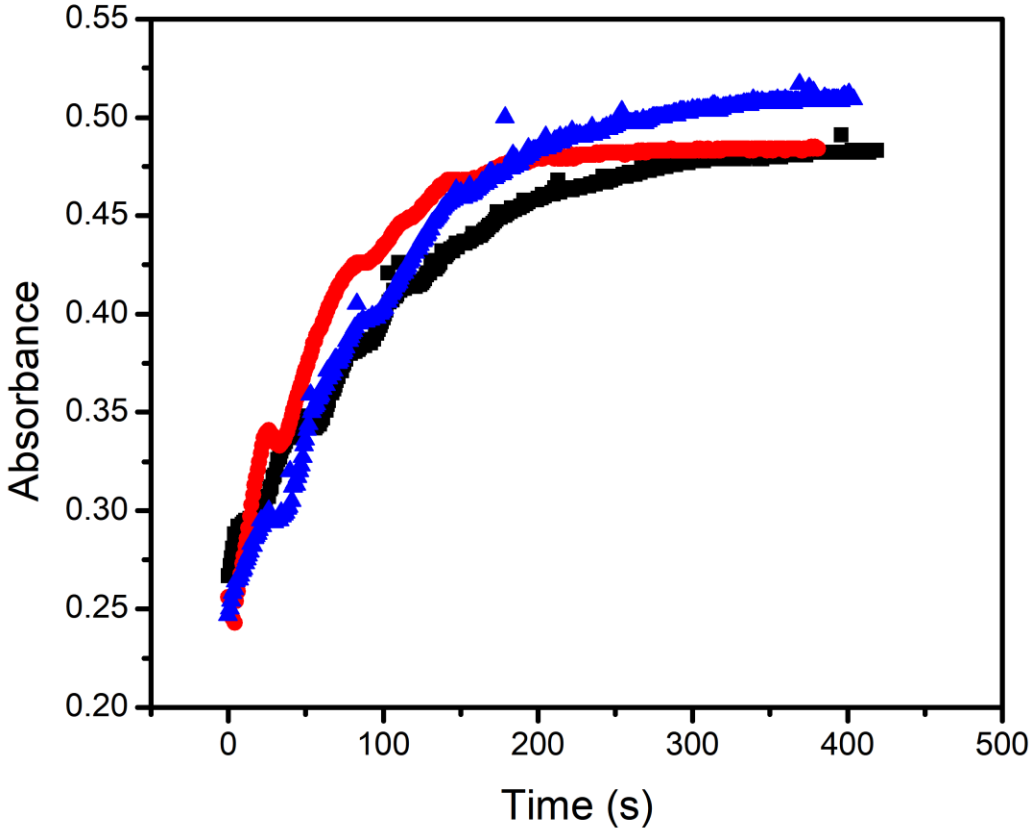

Figure A3.8. Absorbance at 714 nm, monitoring reaction between 4b and 4-Me-2,6-di-*tert*-butylphenol.

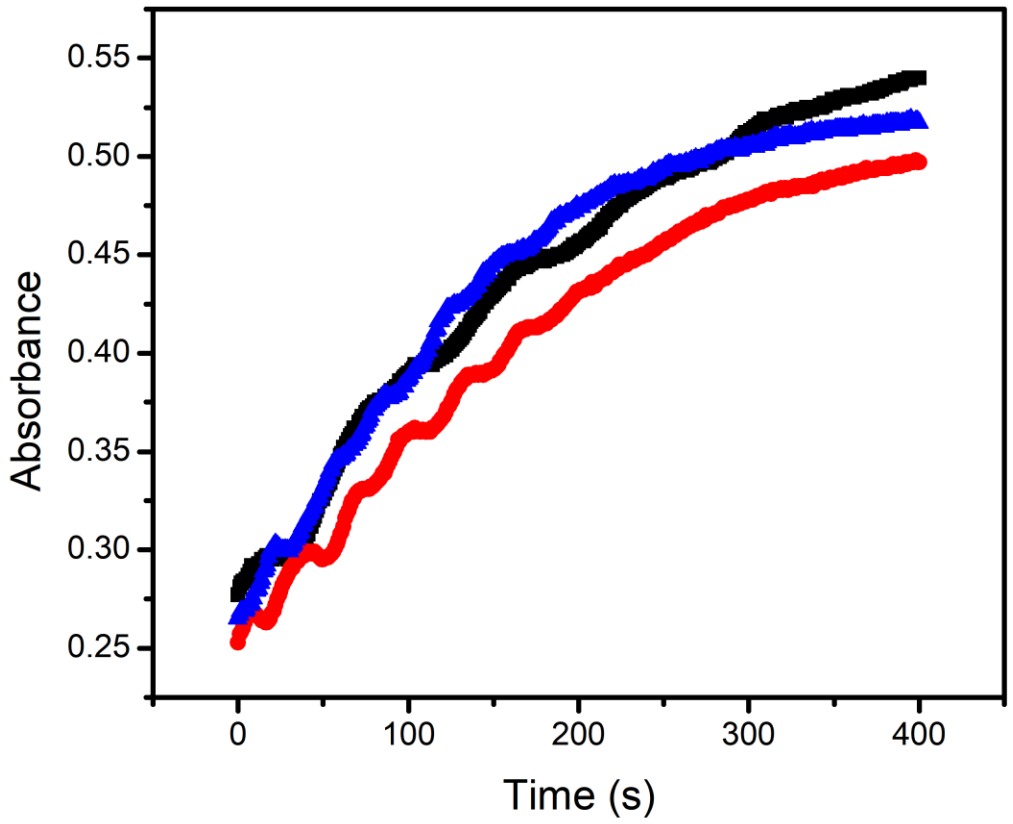

Figure A3.9. Absorbance at 714 nm, monitoring reaction between 4b and 2,4,6-tri-*tert*-butylphenol.

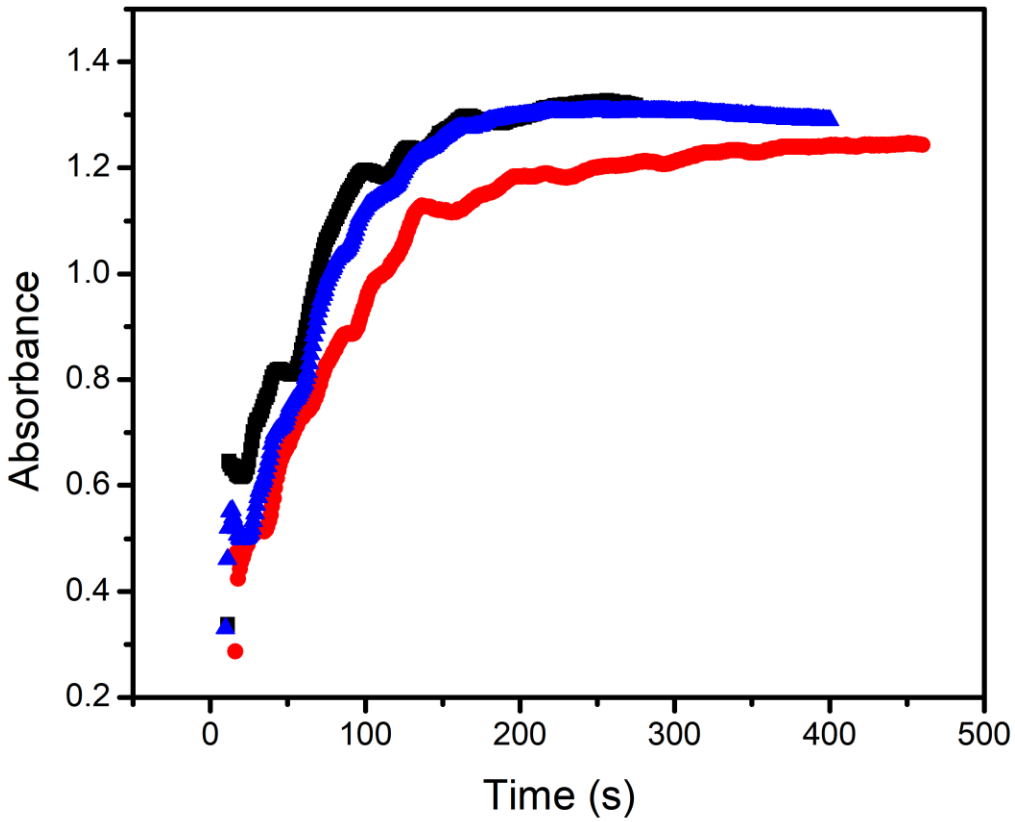

Figure A3.10. Absorbance at 714 nm, monitoring reaction between 4b and 4-bromo-2,6-tri-*tert*-butylphenol.

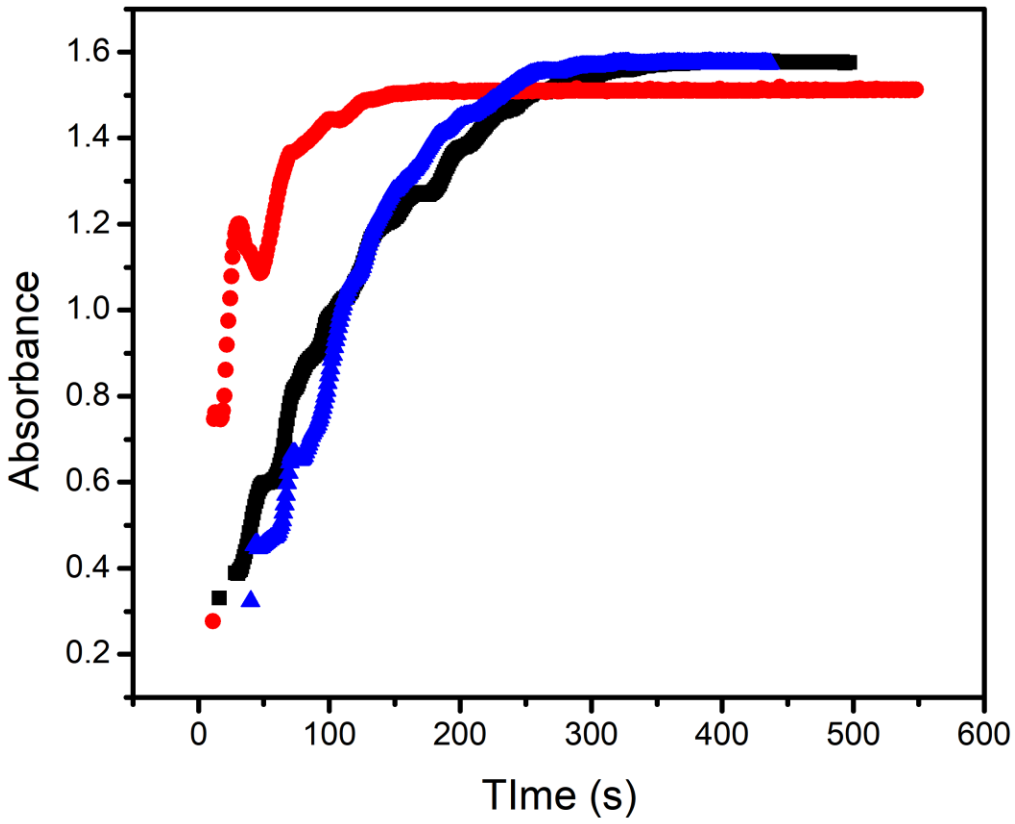

Figure A3.11. Absorbance at 714 nm, monitoring reaction between 4b and 4-COOMe-2,6-tri-*tert*-butylphenol.

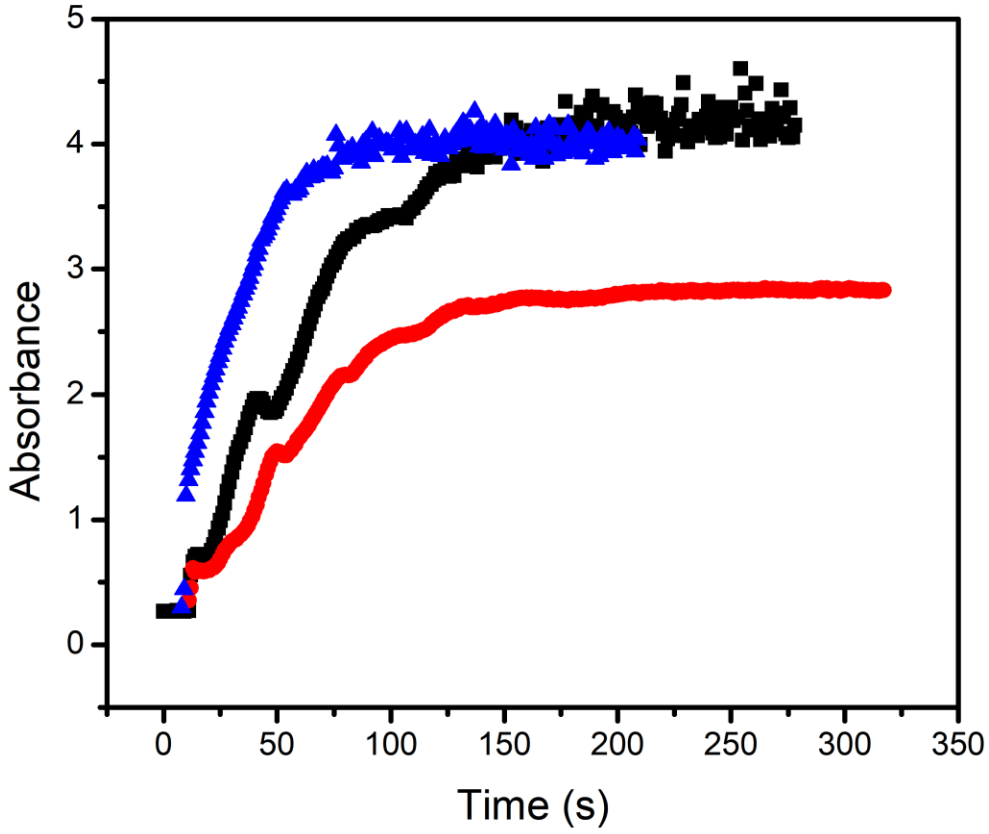

Figure A3.12. Absorbance at 714 nm, monitoring reaction between 4b and 4-NO_2-2,6-tri-*tert*-butylphenol.

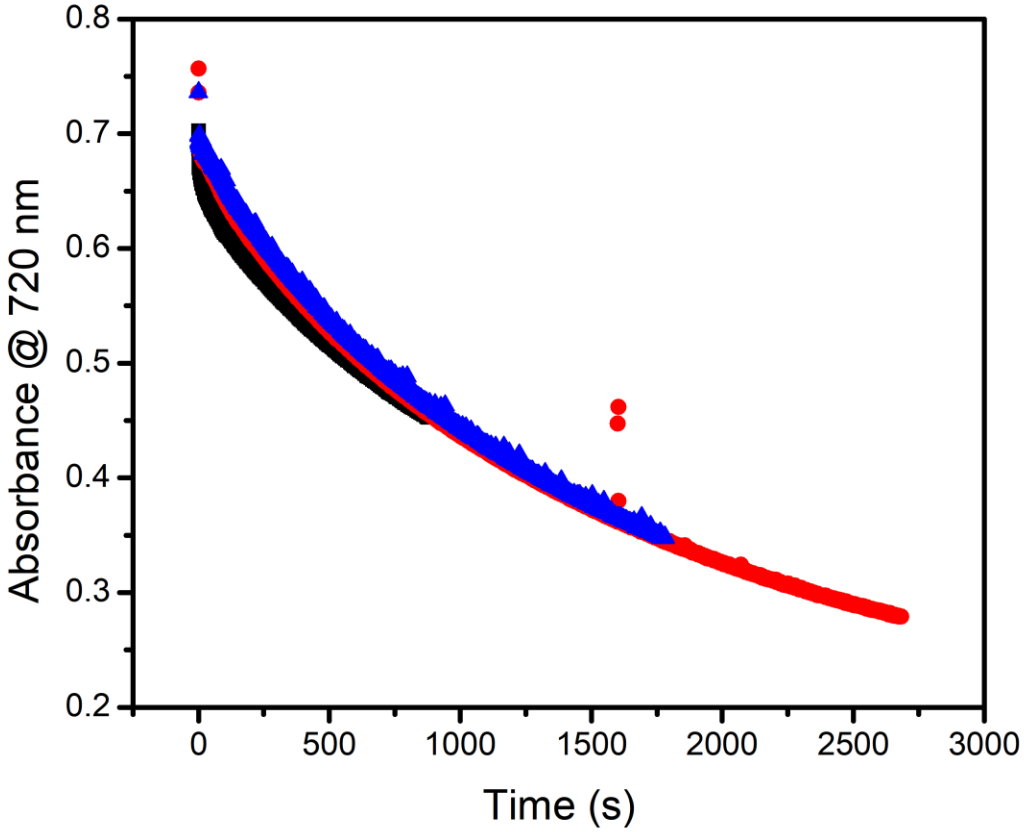

Figure A3.13. Absorbance at 714 nm, monitoring reaction between 5b and tetrabutylammonim 4-COOMe-2,6-tri-*tert*-butylphenolate, triplicate at 5°.

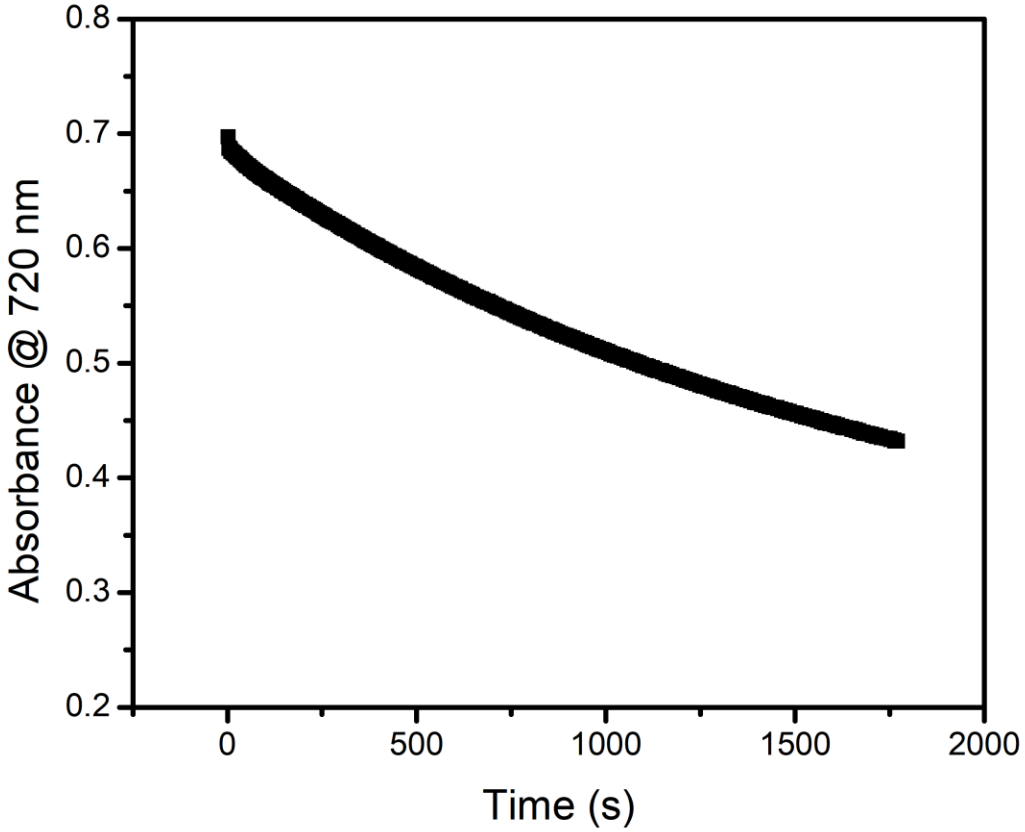

Figure A3.14. Absorbance at 714 nm, monitoring reaction between 5b and tetrabutylammonim 4-COOMe-2,6-tri-*tert*-butylphenolate, single run at 0°.

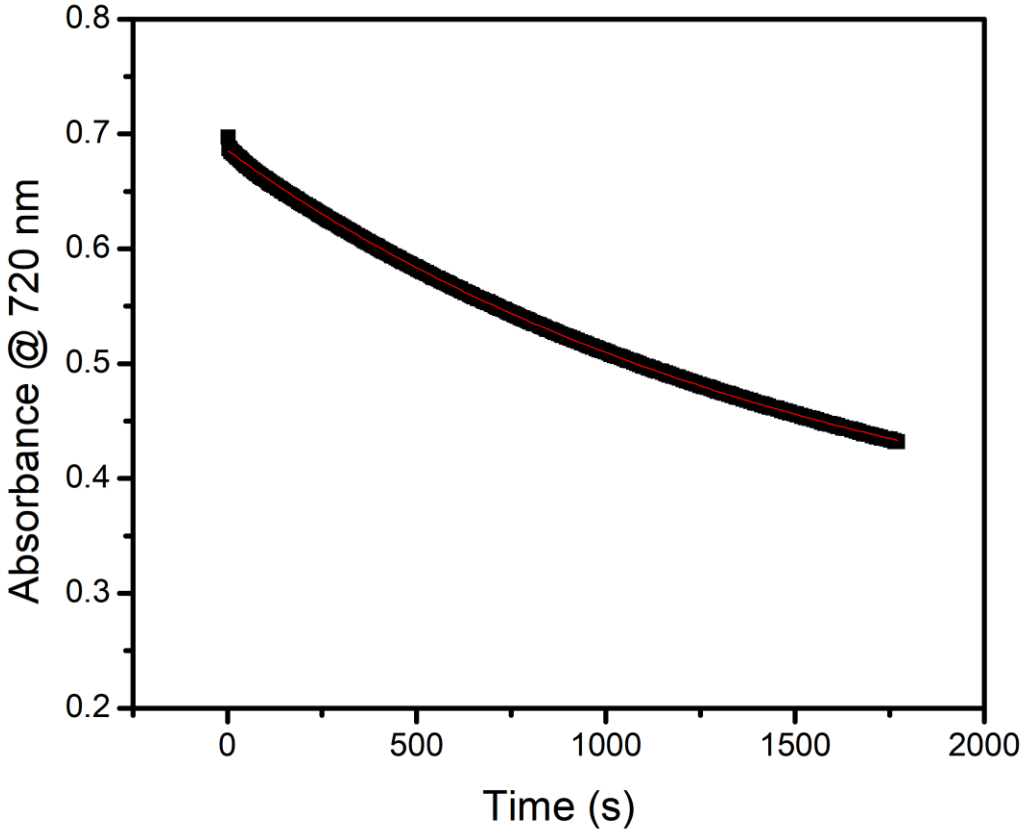

Figure A3.15. Absorbance at 714 nm, monitoring reaction between 5b and tetrabutylammonium 4-COOMe-2,6-tri-*tert*-butylphenolate, single run at 10°.

Sample fitting (red line): Abs = 0.314 + 0.371*exp(–6.41e-4*t). R^2 = 0.9959.

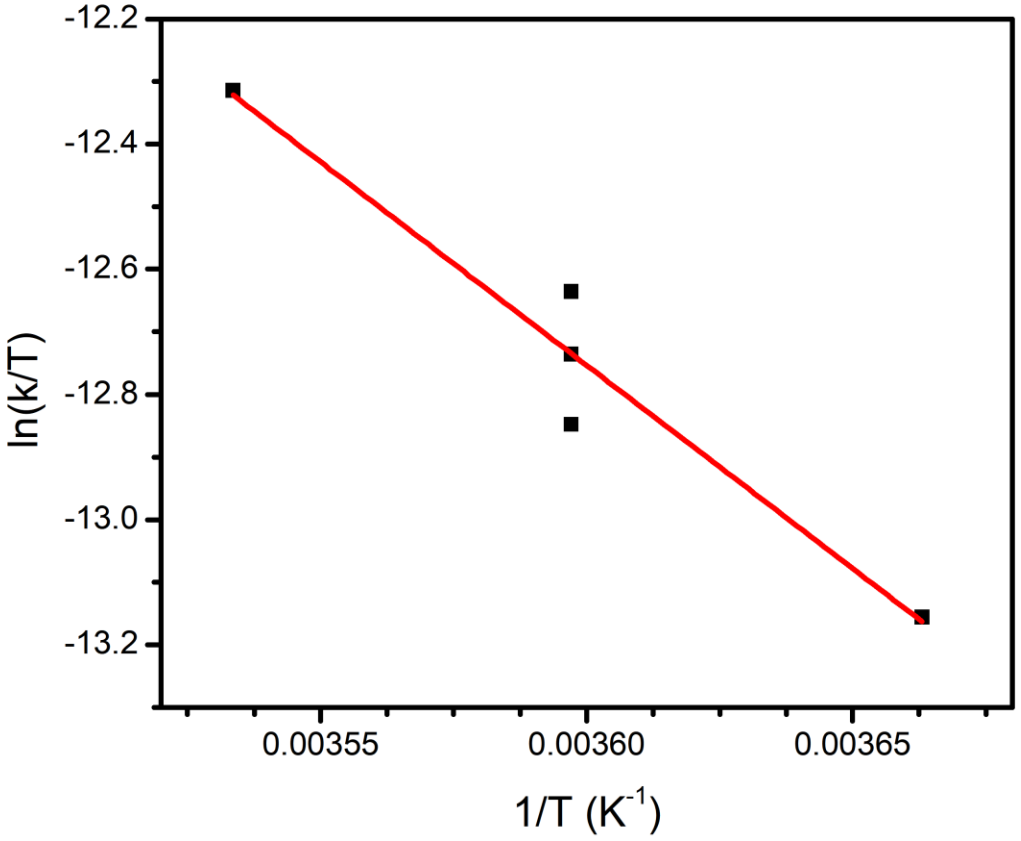

Figure A3.16. Arrhenius plot generated from monitoring reaction between 5b and tetrabutylammonium 4-COOMe-2,6-tri-*tert*-butylphenolate at VT.

Regression: $\ln(k_{obs}/T) = -6497.6(1/T) + 10.641$; $R^2 = 0.9997$.

Extrapolation to T = 173 K: 5.57×10^{10} s^{-1}

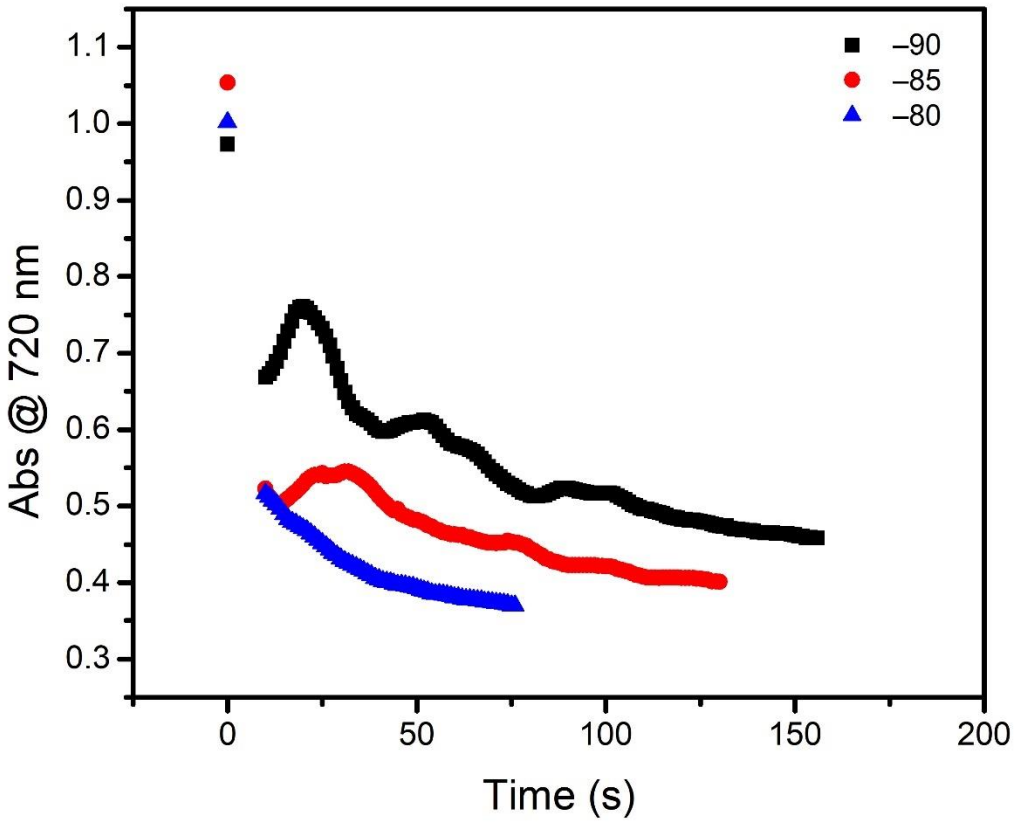

Figure A3.17. Absorbance at 720 nm, monitoring reaction between 4b and tetrabutylammonium 4-Br-2,6-tri-*tert*-butylphenolate, at –80° to –90°.

Observed rate constants, k_{obs}: –90°: 1.8(1) x 10^{-2}, –85°: 3.9(5) x 10^{-2}, –80°: 11(4) x 10^{-2} s^{-1}

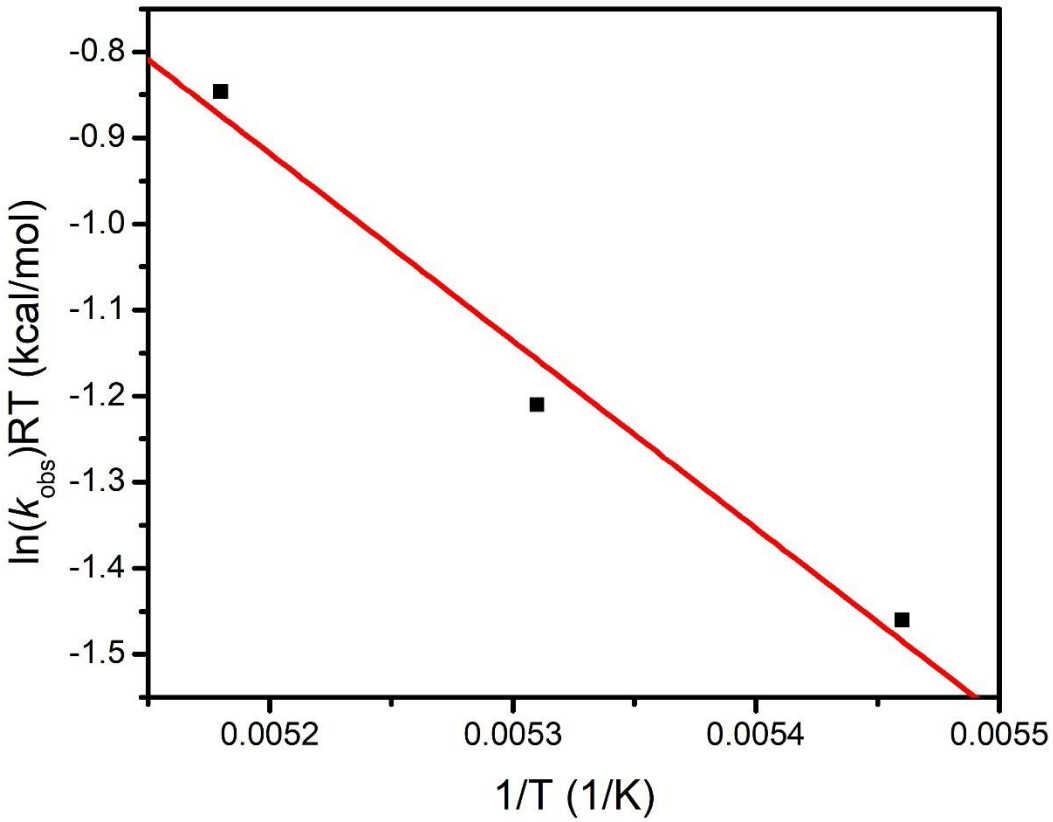

Figure A3.18. Arrhenius plot generated from monitoring reaction between 4b and tetrabutylammonium 4-Br-2,6-tri-*tert*-butylphenolate at VT.

Regression: $\ln(k_{obs})RT = -2179.46*(1/T) + 10.41$; $R^2 = 0.95651$.

Extrapolation to T = 173 K: ln(k)RT = – 2.18 kcal/mol

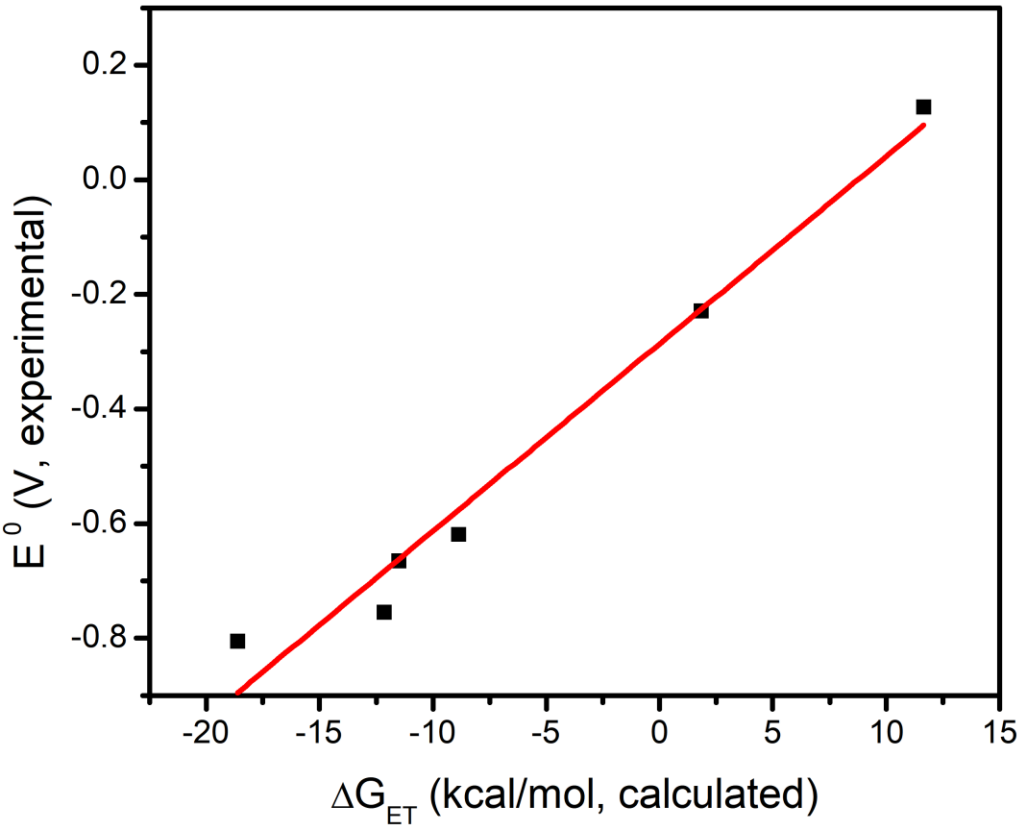

Figure A3.19. Plot of experimental reduction potentials versus calculated ΔG_{ET} for 4-X-2,6-di-tert-butylphenolates.

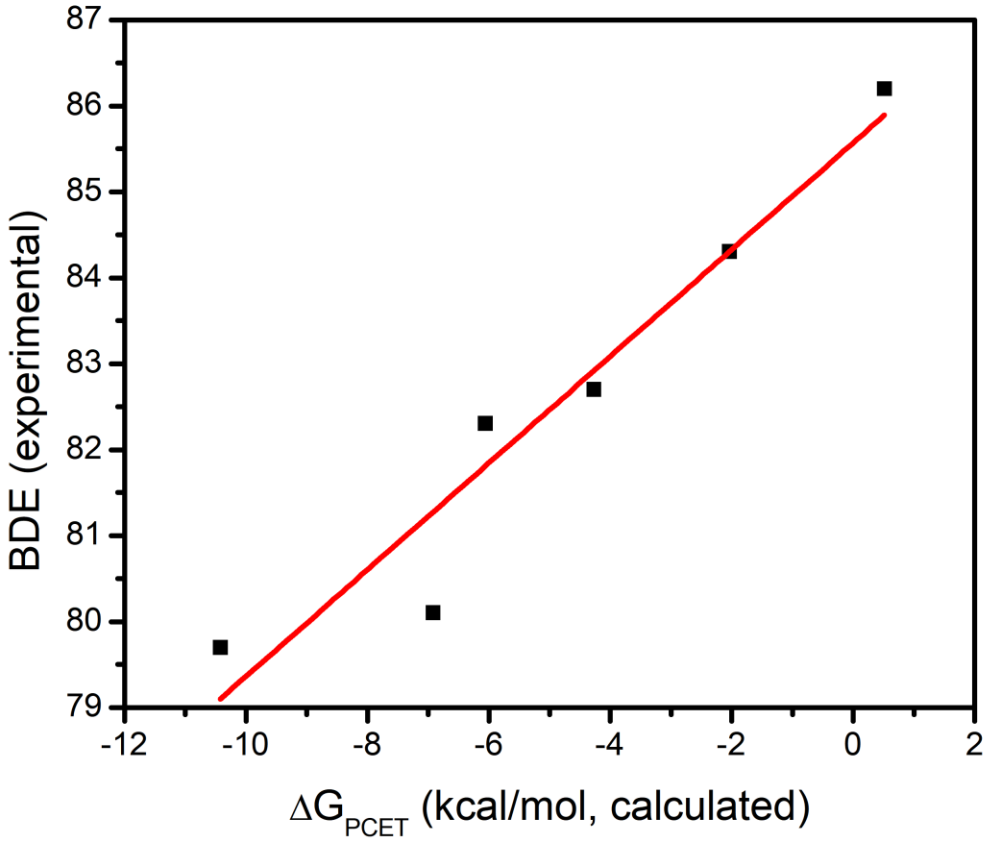

Figure A3.20. Plot of experimental BDE versus ΔG_{PCET} for 4-X-2,6-di-tert-butylphenols.

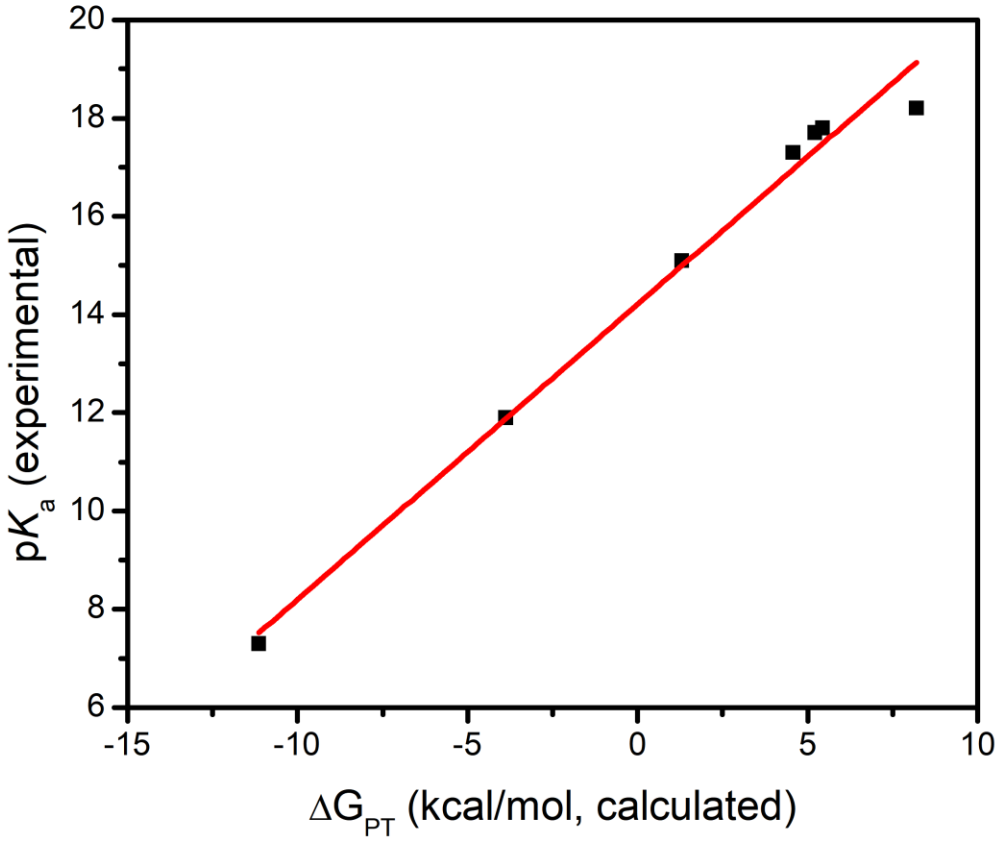

Figure A3.21. Plot of experimental pK_a versus ΔG_{PT} for 4-X-2,6-di-tert-butylphenols.

Arrhenius plot generated from monitoring reaction between 4b and tetrabutylammonium 4-COOMe-2,6-tri-*tert*-butylphenolate at VT.

Regression: ln(k)RT = -2921.13*(1/T) + 6.69; R^2 = 0.95362.

Extrapolation to T = 173 K: ln(k)RT = –10.2 kcal/mol (see Figure A3.22)

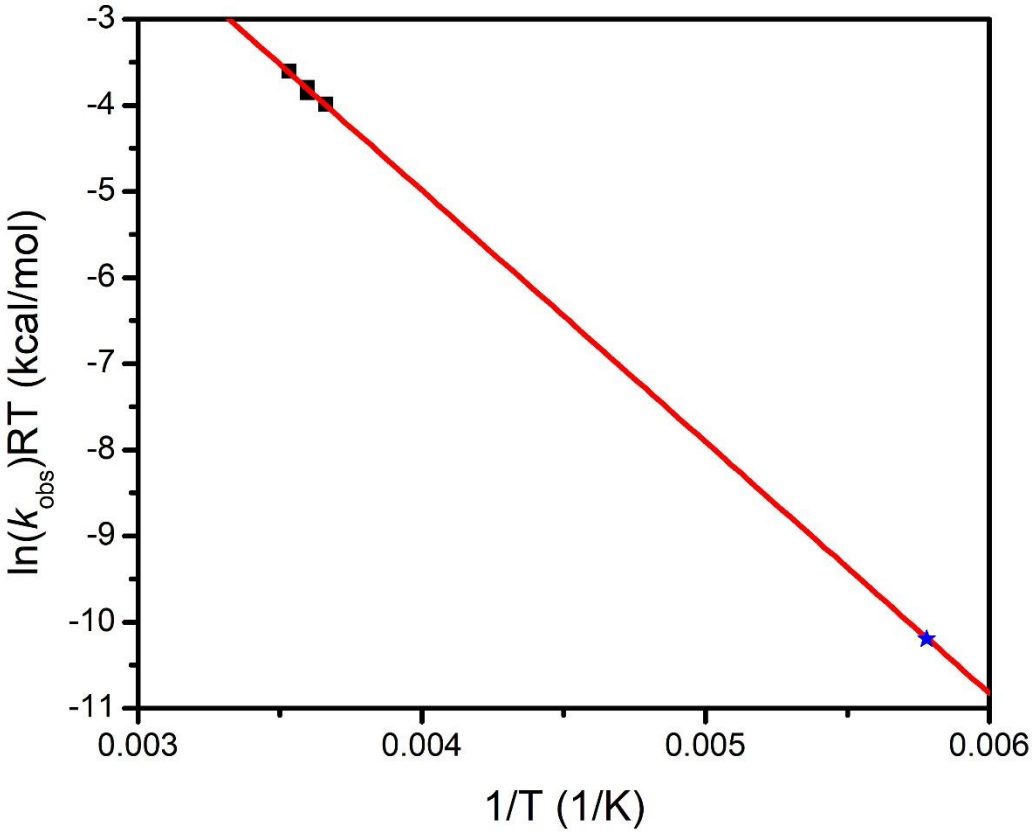

Figure A3.22. Arrhenius plot generated from monitoring reaction between 4b and tetrabutylammonium 4-COOMe-2,6-tri-*tert*-butylphenolate at VT, extrapolated to 173 K.

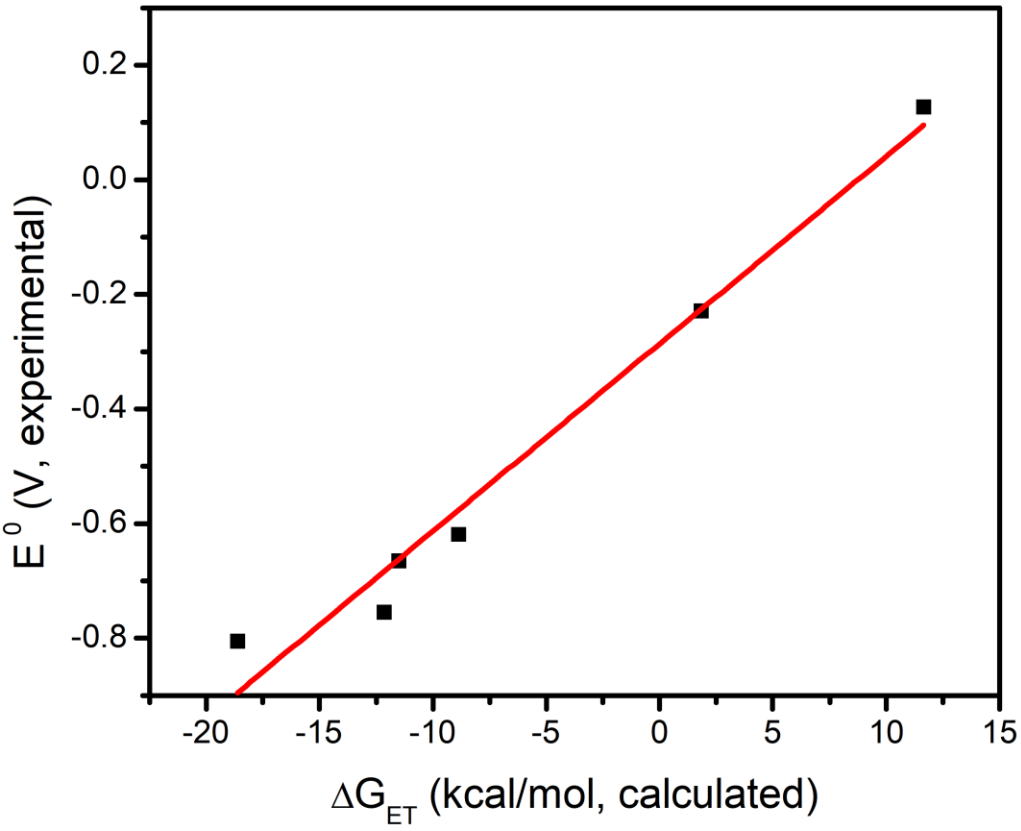

Figure A3.23. Plot of experimental reduction potentials versus calculated ΔG_{ET} for 4-X-2,6-di-tert-butylphenolates.

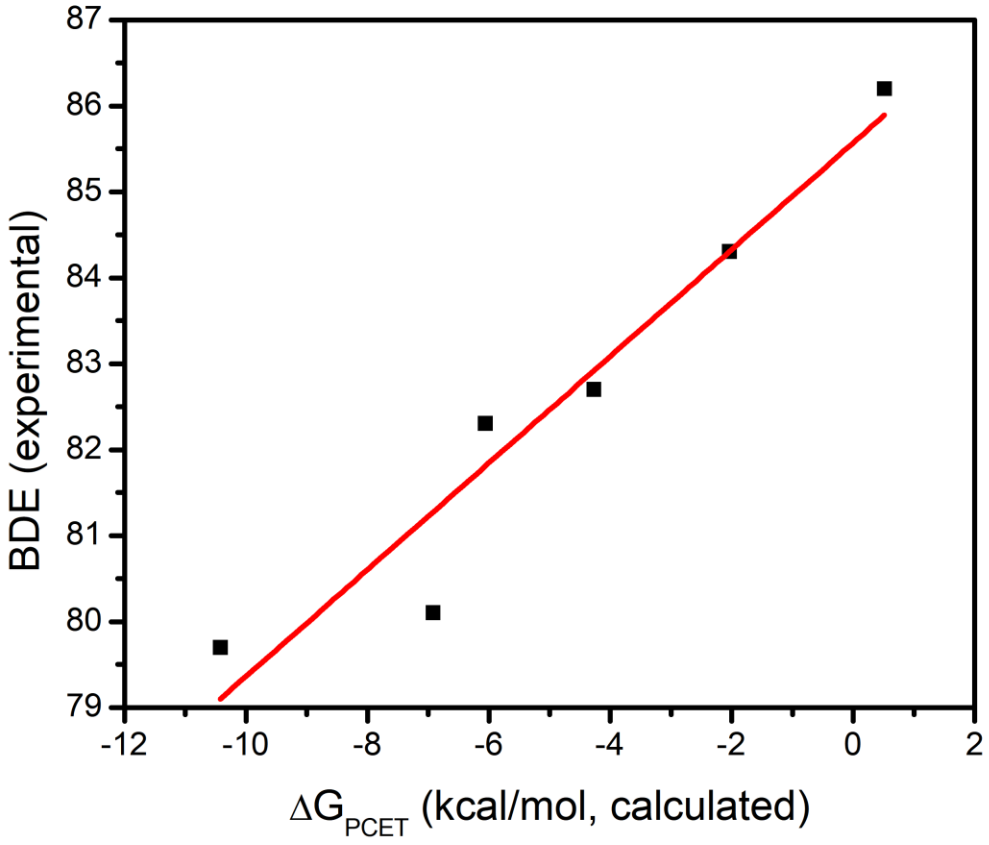

Figure A3.24. Plot of experimental BDE versus ΔG_{PCET} for 4-X-2,6-di-tert-butylphenols.

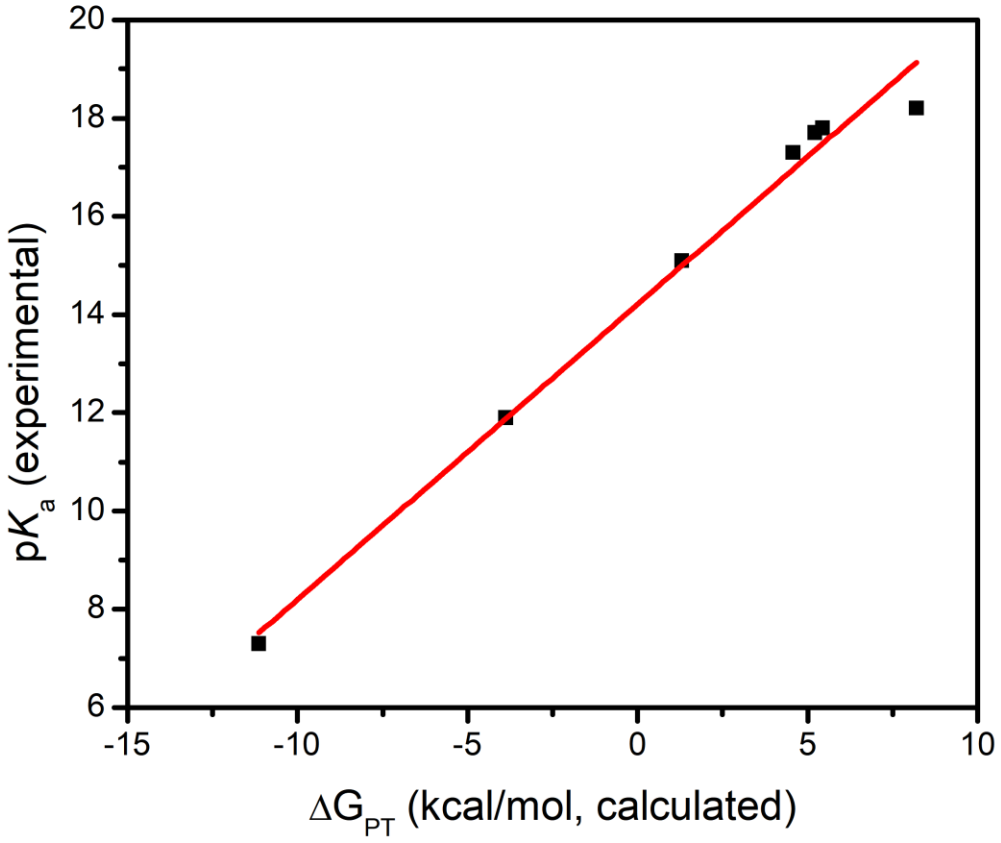

Figure A3.25. Plot of experimental pK_a versus ΔG_{PT} for 4-X-2,6-di-tert-butylphenols.

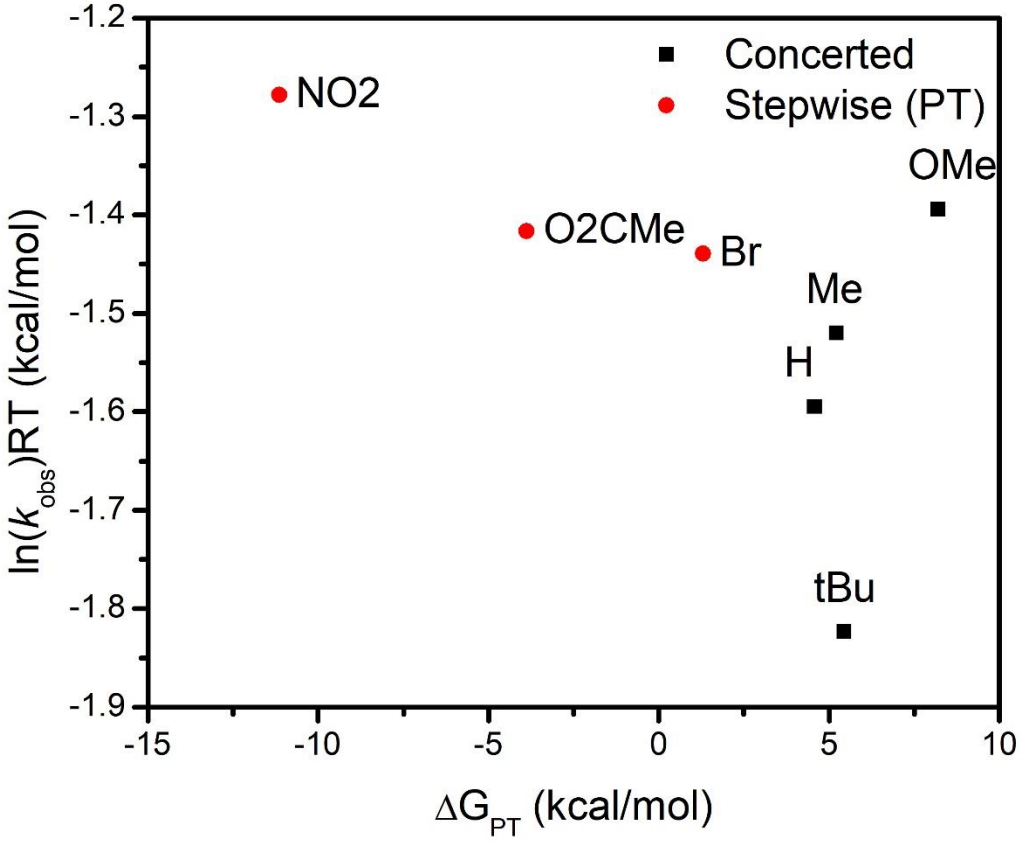

Figure A3.26. Plot of ln(k_{obs})RT v. ΔG_{PT} for 4-X, 2,6-di-*tert*-butylphenols.

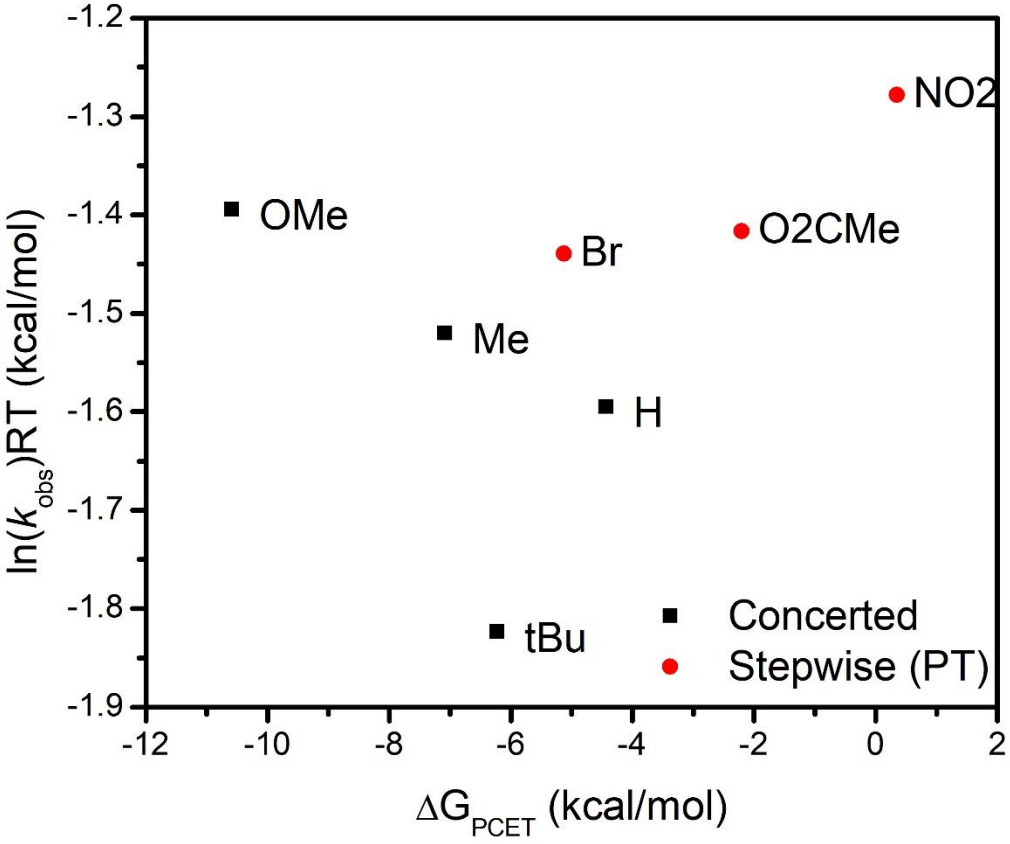

Figure A3.27. Plot of ln(k_{obs})RT v. ΔG_{PCET} for 4-X, 2,6-di-*tert*-butylphenols.

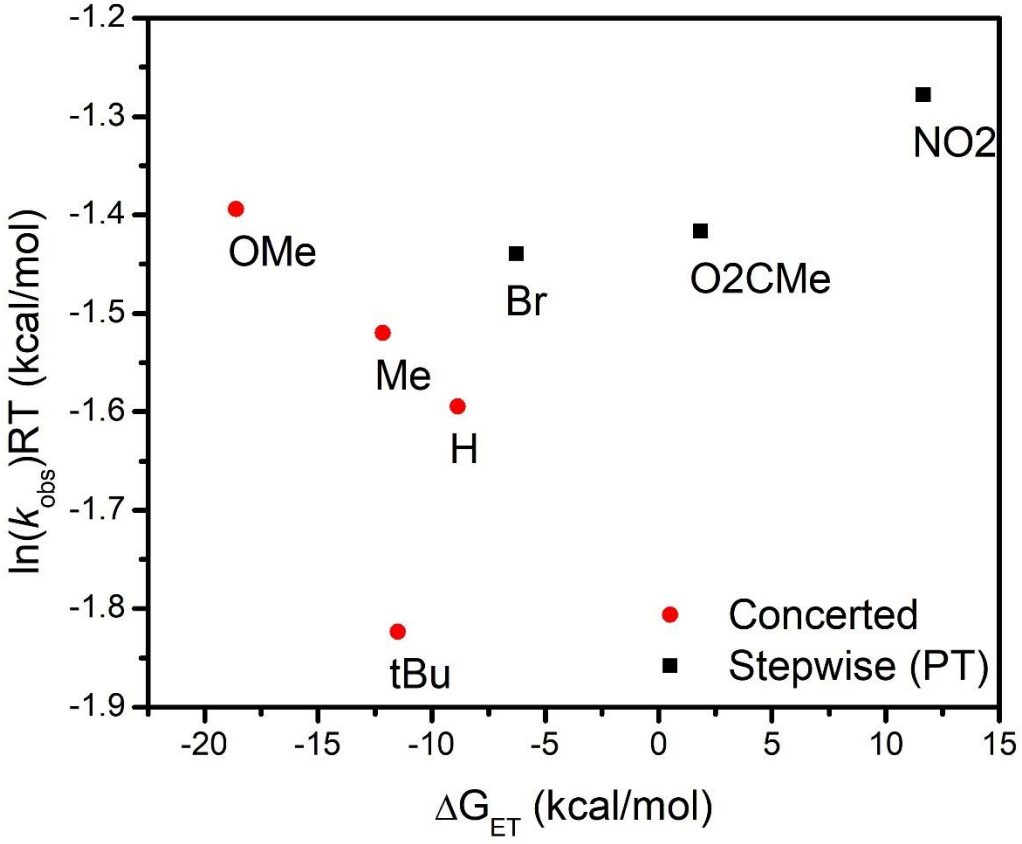

Figure A3.28. Plot of ln(k_{obs})RT v. ΔG_{ET} for 4-X, 2,6-di-*tert*-butylphenols.

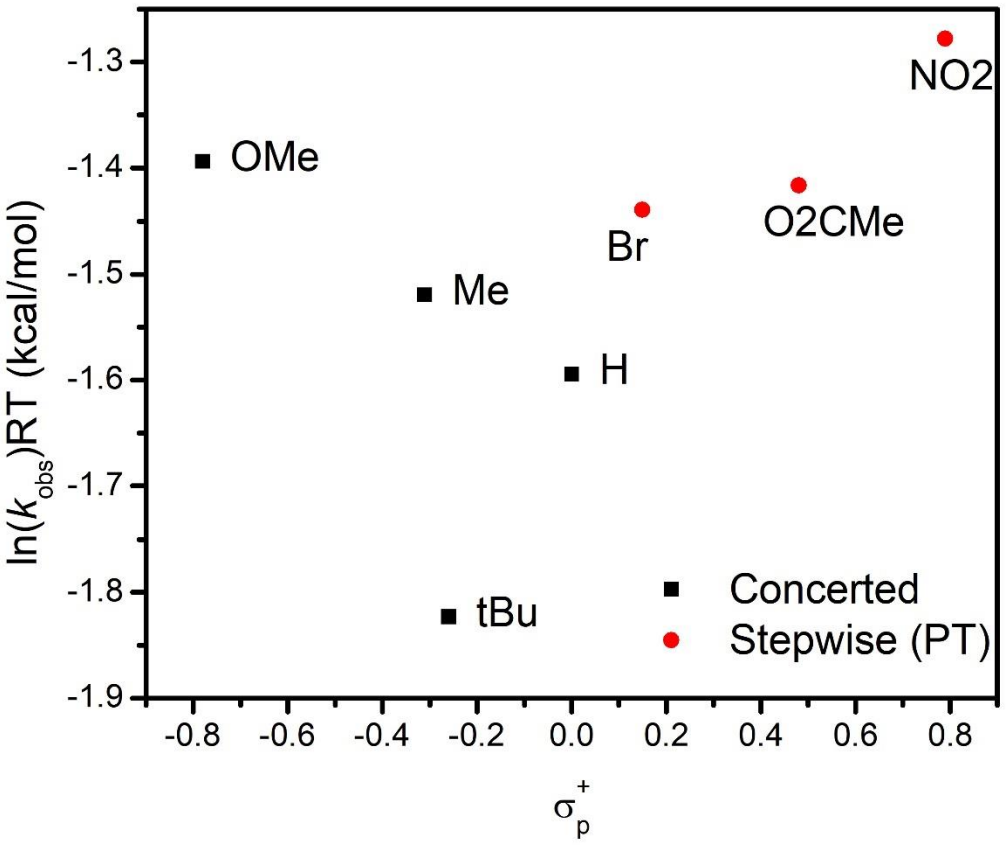

Figure A3.29. Plot of ln(k_{obs})RT v. Hammett parameter σ_p^+ for 4-X, 2,6-di-*tert*-butylphenols.

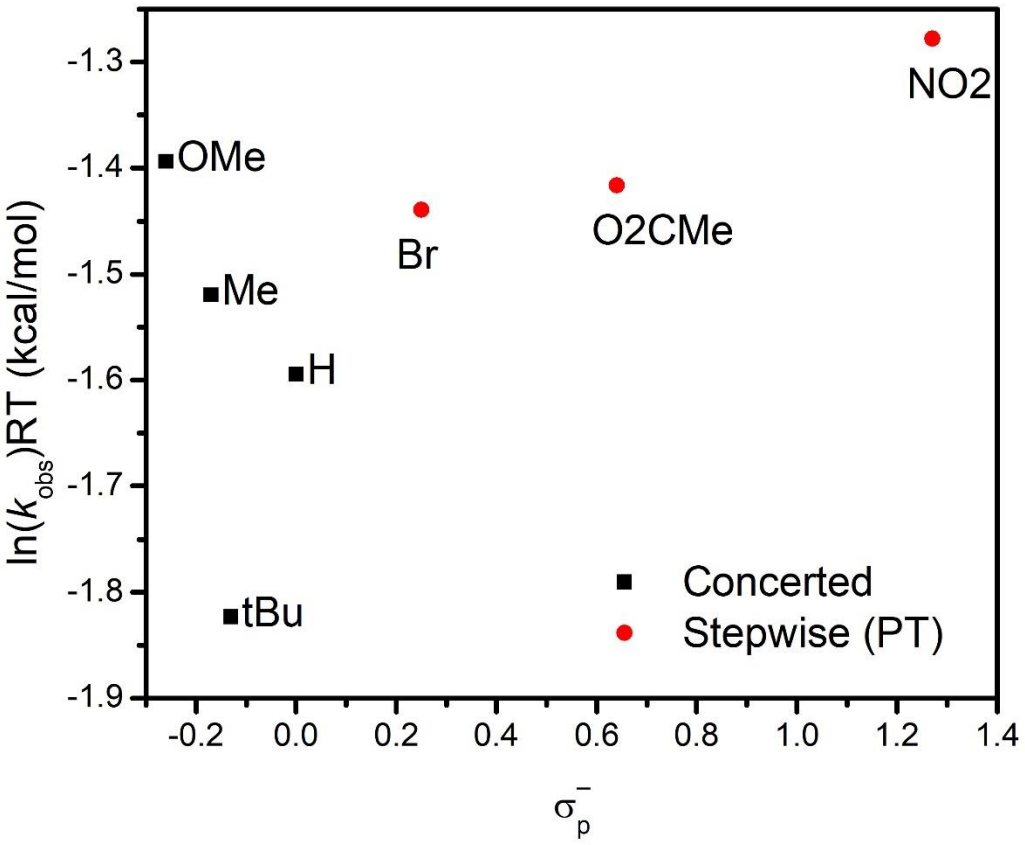

Figure A3.30. Plot of ln(k_{obs})RT v. Hammett parameter σ_p^- for 4-X, 2,6-di-*tert*-butylphenols.

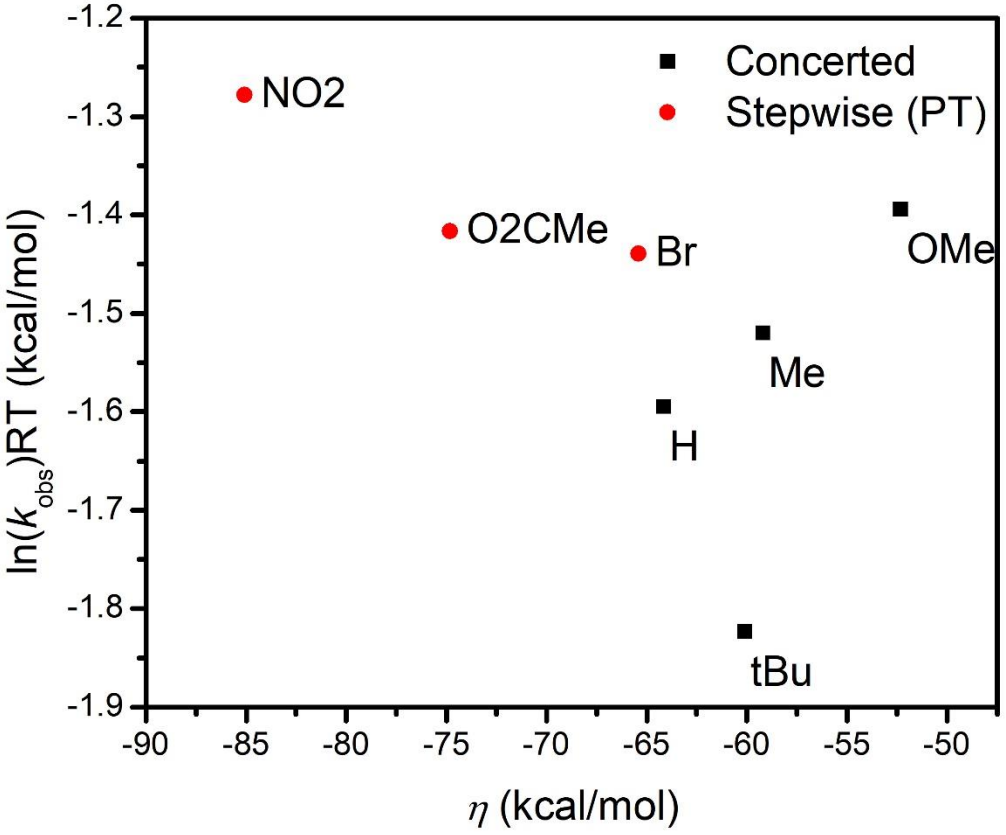

Figure A3.31. Plot of ln(k_{obs})RT v. asynchronicity parameter η for 4-X, 2,6-di-*tert*-butylphenols.

Table A3.1. Tabulated experimental values and calculated values for 4-X-2,6-di-tert-butylphenols.

	Experimental values (literature)			DFT calculated values			
X	**$BDFE_{O-H}$ (kcal/mol)**	**pKa (DMSO)**	**E_{ox} (PhO^-, V vs Fc/Fc^+)**	**ΔG_{PCET} (kcal/mol)**	**ΔG_{PT} (kcal/mol)**	**ΔG_{ET} (kcal/mol)**	**η (kcal/mol)**
				Concerted			
OMe	79.7	18.2	-0.806	-10.4	8.2	-18.6	-52.3
Me	80.1	17.7	-0.755	-6.9	5.2	-12.1	-59.2
^{t}Bu	82.6	17.8	-0.665	-6.1	5.4	-11.5	-60.1
H	82.7	17.3	-0.619	-4.3	4.6	-8.9	-64.1
				Stepwise			
Br	-	15.1	-	-5.0	1.3	-6.2	-65.4
COOMe	84.3	11.9	-0.229	-2.0	-3.9	1.8	-74.8
NO_2	86.2	7.3	+0.127	0.5	-11.1	11.7	-85.1

Table A3.2. Tabulated rates for 4-X-2,6-di-tert-butylphenols. ET rate for X = COOMe extrapolated from Eyring analysis.

X	**k_{obs} (PCET or ET) (x 10^{-2} s^{-1})**	**k_{PT} (x 10^{-2} s^{-1})**
OMe	1.8(2)	-
Me	1.2(3)	-
^{t}Bu	0.6(1)	-
H	1.0(2)	-
Br	1.76 x 10^{-1}	1.5(2)
COOMe	5.57 x 10^{-8}	1.6(9)
NO_2	-	2(1)

Table A3.3. Tabulated rates for C–H substrates.

Substrate	k_{obs} (s^{-1})
Fluorene	3.1(6) x 10^{-2}
3-phenylindene	2.4(1) x 10^{-4}
Indene	4.9(3) x 10^{-3}
Substituted 9-(4-X-phenyl)fluorenes (σ_p^-)	
X = H (0)	6(2) x 10^{-4}
X = Br (0.25)	5.3(9) x 10^{-3}
X = CF_3 (0.65)	2.4(3) x 10^{-2}

Table A3.4. Tabulated experimental and calculated values for C–H substrates. Calculated BDFE calibrated to reported values for DHA.

Substrate	$BDFE_{C–H}$ (kcal/mol)	ΔG_{PCET} (kcal/mol)	Calculated BDFE (kcal/mol)	pKa (DMSO)	ΔG_{PT} (kcal/mol)	η (kcal/mol)
Fluorene	82	-4.21	81.5	22.6	14.48	-58.63
3-phenylindene	75.3	-9.25	76.4	17.3	6.29	-60.94
Indene	77	-5.75	79.9	20.1	11.92	-60.84
Xanthene	75	-11.8	73.9	30.1	22.9	-48.8
9,10-DHA	76.3	-12.4	76.3	30.0	24.0	-54.3
Substituted 9-(4-X-phenyl)fluorenes (σ_p^-)						
X = H (0)	74	-11.68		-	5.61	-64.39
X = Br (0.25)	-	-11.55		-	3.94	-66.46
X = CF_3 (0.65)	-	-11.67		-	1.76	-68.74

A3.2 DFT-optimized coordinates of Co-complexes and substrates

Table A3.5. DFT optimized coordinates for 3-phenylindene cation

C	-3.69834313839348	0.42721329393522	1.07565111222102
C	-3.53677522557995	-0.80534157537792	0.42324261527811
C	-2.64148697245046	1.33787272026971	1.18860570015834
C	-1.42653511950326	1.00708032257287	0.62439141718865
C	-1.25821958071709	-0.22651247890904	-0.06173693499457
C	-2.32280705985044	-1.14760402786593	-0.14235264315785
C	-0.13440072607120	1.75177402278910	0.62411212524160
C	0.77381621277745	0.83323068367117	-0.07606430498262
C	0.10380841504776	-0.32004247723994	-0.51635146738240
H	-4.66511272456602	0.67417541780885	1.52066137988609
H	-4.37480562333695	-1.50369550675494	0.37693594476434
H	-2.78064703213414	2.28218921872918	1.71801425291317
H	-2.19211115617658	-2.12126514047493	-0.61483988855850
C	0.72249273107487	-1.35254203187683	-1.31482044322709
C	-0.00988598272234	-2.07821098375127	-2.27958115564637
C	0.60543984876238	-3.06672063306873	-3.02852779987196
H	-1.05136870539487	-1.82228100909045	-2.47651098593205
C	1.95418776207075	-3.36640230771768	-2.82000243047641
C	2.69487120970057	-2.65299149296102	-1.87471599079736
C	2.09475535540432	-1.64306997433777	-1.14335514474145
H	2.43502383491027	-4.15190607453333	-3.40774806367468
H	0.03611843394043	-3.60676482404933	-3.78766022939454

Table A3.5 Continued

H	2.67658903439217	-1.09736676748286	-0.39833676879052
H	3.74683900108654	-2.89352147473160	-1.70830783186878
H	-0.18351552372705	2.72579897951393	0.10140481753596
H	0.23312696689548	1.99964471112173	1.63760439735446
H	1.82556576456083	1.05228940981180	-0.27128167904458

Table A3.6. DFT optimized coordinates for 3-phenylindene deprotonated anion

C	-3.74436361509288	0.52010883333994	1.05264299372492
C	-3.60874630558914	-0.70902649725841	0.37706940469361
C	-2.66026519481457	1.37901570355716	1.16156847073040
C	-1.42549739520503	1.03278796653191	0.58615257442862
C	-1.28608102171442	-0.21572499071883	-0.13820446823227
C	-2.40111591783409	-1.07467654196560	-0.20438253188365
C	-0.16620342604555	1.68962060092857	0.56559419183665
C	0.72037103804617	0.87396074473749	-0.13120817406038
C	0.07310563220729	-0.30681362706411	-0.59086851609076
H	-4.70404826193335	0.79254210598974	1.50163569057018
H	-4.46466398097479	-1.38775184523040	0.31123603284423
H	-2.76374418026543	2.32629769826736	1.70141484502610
H	-2.32812974279148	-2.04606207972099	-0.69900218395204
C	0.71732680733180	-1.36120320100771	-1.34758668586867
C	0.01223604761701	-2.24895015975537	-2.19489084532565
C	0.65472306364549	-3.25457205158041	-2.90919825476698
H	-1.06348851053890	-2.11958861589055	-2.32159424779620
C	2.03673149392419	-3.42316078346024	-2.82589805787878
C	2.76023709935563	-2.55145366616239	-2.00902339899816
C	2.11980574894850	-1.55156707624092	-1.28982665396043
H	2.54194675478670	-4.21471278694209	-3.38473062010466
H	0.06270260617084	-3.91304818407525	-3.55218818162892
H	2.71240442998009	-0.90418501564883	-0.63909052902597

Table A3.6 Continued

H	3.84525458371517	-2.66467534579160	-1.91725357234672
H	0.05633474590128	2.66439725527122	1.00292788676944
H	1.76322750116946	1.12441155989034	-0.34118516870391

Table A3.7. DFT optimized coordinates for 3-phenylindene

C	-3.67704297877664	0.36456853317432	1.17032132278523
C	-3.48495397131582	-0.85268320233897	0.51443403098503
C	-2.64917414613570	1.30758916540374	1.22796598142353
C	-1.43725407975681	1.01898457693066	0.61715482026433
C	-1.24309181085253	-0.20430999655790	-0.05531613163792
C	-2.26917963169324	-1.14904556458192	-0.10041565458787
C	-0.17572496082051	1.81553192163234	0.54217781407629
C	0.74441906599756	0.92403365681977	-0.21676735658566
C	0.13293712681654	-0.23442237771724	-0.57038994173718
H	-4.63606564095988	0.57973088954147	1.64761334082950
H	-4.29605200015580	-1.58508420226727	0.48472862209807
H	-2.79945799793958	2.25603925994733	1.75010015665266
H	-2.12699463965896	-2.10965181087605	-0.59919505943690
C	0.74246133390034	-1.33347462776899	-1.33285800216736
C	0.06215869535171	-1.95114103678188	-2.39340874344811
C	0.66000100035842	-2.97180617520705	-3.12688473692295
H	-0.93823551953062	-1.60793454476555	-2.66399535387264
C	1.94570229313896	-3.40395158792722	-2.81065382947575
C	2.63199581948069	-2.80193614728886	-1.75803240000229
C	2.03753056988492	-1.77750247351111	-1.02863139093521
H	2.41224965296402	-4.20933080795411	-3.38298565991993
H	0.11536076448764	-3.43249907687884	-3.95465697360869
H	2.57520295904994	-1.31928654236754	-0.19570728260064

Table A3.7 Continued

H	3.63673505394134	-3.14058456156511	-1.49404890753416
H	-0.32102067083734	2.78615885729008	0.03384383940347
H	0.21657109848387	2.07060126157711	1.54356674878214
H	1.76754261457748	1.19643661403878	-0.47952925282700

Table A3.8. DFT optimized coordinates for 3-phenylindene radical

C	-3.72566934009241	0.47672587838892	1.06416308060882
C	-3.57736478041085	-0.75124853566407	0.42380801078554
C	-2.65205101161195	1.37253547208901	1.13804282503481
C	-1.44264724716352	1.02492659624480	0.54986769586339
C	-1.29216913691998	-0.21885012100637	-0.13084162666688
C	-2.36002405630998	-1.11091135848047	-0.16977202456238
C	-0.16993971848545	1.70606147694982	0.49901692635690
C	0.73075644514571	0.90150797699491	-0.17429799334017
C	0.08761764182904	-0.29035608462770	-0.60147751973782
H	-4.68161739150675	0.74050304893097	1.52265310018819
H	-4.41775612367009	-1.44873212057922	0.38561169557852
H	-2.76498453707033	2.32721624474234	1.65779854635785
H	-2.26488035821836	-2.09110846920317	-0.63949738635062
C	0.72173148699459	-1.35109358800831	-1.35587055044879
C	0.00187248165396	-2.17408245921851	-2.24624686144808
C	0.63505963333805	-3.18312522190046	-2.96076973268430
H	-1.05991756155069	-1.98864219748689	-2.41136991631611
C	2.00170708384860	-3.40805511108909	-2.80370455653210
C	2.73379793230809	-2.59942034991640	-1.93356075523786
C	2.10775580445190	-1.58251989414298	-1.22763569749239
H	2.49751026166889	-4.20710938092959	-3.35989947821935
H	0.05499777424910	-3.79908216620759	-3.65229318073443
H	2.69065495671052	-0.96939585921426	-0.53741258000984

Table A3.8 Continued

H	3.80431044844504	-2.77221509998320	-1.79639568946568
H	0.03542413484811	2.69147556159045	0.91874749819790
H	1.76588517751874	1.16096576172707	-0.39455382972512

Table A3.9. DFT optimized coordinates for Indene cation

C	-3.67704	0.36457	1.17032
C	-3.48495	-0.85268	0.51443
C	-2.64917	1.30759	1.22797
C	-1.43725	1.01898	0.61715
C	-1.24309	-0.20431	-0.05532
C	-2.26918	-1.14905	-0.10042
C	-0.17572	1.81553	0.54218
C	0.74442	0.92403	-0.21677
C	0.13294	-0.23442	-0.57039
H	-4.63607	0.57973	1.64761
H	-4.29605	-1.58508	0.48473
H	-2.79946	2.25604	1.75010
H	-2.12699	-2.10965	-0.59920
H	-0.32102	2.78616	0.03384
H	0.21657	2.07060	1.54357
H	1.76754	1.19644	-0.47953
H	0.56057	-1.00424	-1.10848

Table A3.10. DFT optimized coordinates for Indene anion

C	-3.74436	0.52011	1.05264
C	-3.60875	-0.70903	0.37707
C	-2.66027	1.37902	1.16157
C	-1.42550	1.03279	0.58615
C	-1.28608	-0.21572	-0.13820
C	-2.40112	-1.07468	-0.20438
C	-0.16620	1.68962	0.56559
C	0.72037	0.87396	-0.13121
C	0.07311	-0.30681	-0.59087
H	-4.70405	0.79254	1.50164
H	-4.46466	-1.38775	0.31124
H	-2.76374	2.32630	1.70141
H	-2.32813	-2.04606	-0.69900
H	0.05633	2.66440	1.00293
H	0.10645	-0.35704	-1.65917
H	1.71512	1.09605	-0.29302

Table A3.11. DFT optimized coordinates for Indene

C	-3.67704	0.36457	1.17032
C	-3.48495	-0.85268	0.51443
C	-2.64917	1.30759	1.22797
C	-1.43725	1.01898	0.61715
C	-1.24309	-0.20431	-0.05532
C	-2.26918	-1.14905	-0.10042
C	-0.17572	1.81553	0.54218
C	0.74442	0.92403	-0.21677
C	0.13294	-0.23442	-0.57039
H	-4.63607	0.57973	1.64761
H	-4.29605	-1.58508	0.48473
H	-2.79946	2.25604	1.75010
H	-2.12699	-2.10965	-0.59920
H	-0.32102	2.78616	0.03384
H	0.21657	2.07060	1.54357

Table A3.12. DFT optimized coordinates for Indene radical

C	-3.74782250515811	0.49027772103435	1.10086492990947
C	-3.63106052450794	-0.67624508381590	0.34917646408194
C	-2.66065352218269	1.36642607586976	1.24054249875480
C	-1.46138150410336	1.05237603711746	0.61490680562029
C	-1.34188194331322	-0.14214632083567	-0.15585656242716
C	-2.42272987864990	-1.00371722697359	-0.28571459664758
C	-0.18681268628125	1.72890610943844	0.55178271054682
C	0.67917971480078	0.96467580652331	-0.23750661384011
C	0.00449042535057	-0.17890314908172	-0.67908321266828
H	-4.69665181901735	0.73094520439698	1.58600036730726
H	-4.48978809217653	-1.34460934089833	0.24850496052769
H	-2.76416331854584	2.28185703101919	1.82893308238512
H	-2.33979890067986	-1.92214646790480	-0.87266493138685
H	0.05107139946656	2.67601975250296	1.03805026402470
H	0.41501051191906	-0.96904014410708	-1.30995370083148
H	1.71151264307908	1.22302399571464	-0.47359246535665

Table A3.13. DFT optimized coordinates for Fluorene cation

C	-3.65529073235119	0.53252502465854	0.07252781990749
C	-3.28900435170326	-0.83057516892427	0.13687928378974
C	-2.70099729448858	1.55575377545833	0.00128597070488
C	-1.36793382379814	1.20717678006787	-0.00734902985016
C	-0.98991340174211	-0.17288111049247	0.05936818330348
C	-1.96263807345855	-1.19642789657228	0.13176302768235
C	-0.14936839345366	2.06706633590665	-0.07848835903146
C	0.96083635858620	1.06984438833114	-0.04320173075741
C	0.42584462690379	-0.25631588865698	0.03831730750296
C	2.32519475177354	1.25937391454799	-0.07637650393365
C	3.15427553676058	0.13085062439331	-0.03078701728656
C	2.63279577470534	-1.17984924917679	0.04809654285799
C	1.27338993867530	-1.38746809998734	0.08367726263749
H	-4.71649006681089	0.79461143663964	0.07952553064572
H	-4.07009380011695	-1.59090731190460	0.19315756964235
H	-3.01645186915129	2.59951309327589	-0.04743090096869
H	-1.66623314721520	-2.24572054970480	0.18410339530113
H	-0.09421307262846	2.77862131063143	0.76363565959315
H	-0.12748426871370	2.67884241038520	-0.99674749928026
H	2.75983794950108	2.25882286643317	-0.13890767936674
H	4.23872871431334	0.26668475792850	-0.05746316942917
H	3.32027635226884	-2.02678266721860	0.08213111560350
H	0.85792729214396	-2.39474477601953	0.14728022073187

Table A3.14. DFT optimized coordinates for Fluorene anion

C	-3.68484207859336	0.55280370955419	0.12147011581062
C	-3.34361278096712	-0.81708669228529	0.12037643148110
C	-2.71130451769480	1.53735468003262	0.10439935476168
C	-1.34265958579892	1.17986585735721	0.08463143720960
C	-0.99997875543670	-0.22817334197827	0.08466712197813
C	-2.00714817953841	-1.19939716554564	0.10240021574369
C	-0.15440089943329	1.94329193695322	0.06355702164648
C	0.93520441271234	1.04512526721601	0.04977991610497
C	0.42986751893880	-0.31251859415407	0.06311694638152
C	2.33583339923574	1.23984795452415	0.02573291264368
C	3.18752214547473	0.14792990928375	0.01657567127095
C	2.68806436124215	-1.17234511935401	0.03070399117535
C	1.31634347972143	-1.39532650893967	0.05361555526846
H	-4.74094346341759	0.84156682094431	0.13685085207326
H	-4.13202579579913	-1.57442221061702	0.13438346185956
H	-3.00232755845561	2.59299062682200	0.10610558648680
H	-1.74453298227773	-2.26323073067765	0.10195775435560
H	-0.08941041279612	3.03340896636139	0.05720291563646
H	2.74847981376521	2.25415411687914	0.01341684987101
H	4.27019854688460	0.31118946136265	-0.00298789665677
H	3.38166006460116	-2.01730581067802	0.02279140581855
H	0.93101026763263	-2.42072413306100	0.06425237907932

Table A3.15. DFT optimized coordinates for Fluorene

C	-3.69161962788095	0.54539385712426	0.07181406727847
C	-3.32842873256755	-0.80188701128736	0.13644463467633
C	-2.71756653455756	1.54172461157261	0.00126670541536
C	-1.37816310585173	1.17524624744009	-0.00570118082667
C	-1.01135464161037	-0.18302839071980	0.06062249449115
C	-1.98699006009763	-1.17664542891962	0.13189585565638
C	-0.15120563317025	2.03411594872440	-0.07612212846252
C	0.96732909795201	1.03673809480856	-0.04102550927267
C	0.44592179876961	-0.26904613544184	0.03885614330801
C	2.33990180985401	1.24351636083744	-0.07540805033428
C	3.19200754038501	0.13946045213834	-0.03203340373350
C	2.67531439887213	-1.15596964425696	0.04549236809191
C	1.29993879908622	-1.37073476804763	0.08195935326060
H	-4.74903387585012	0.82210525831148	0.07780533341560
H	-4.10465844753989	-1.56888678584891	0.19355928040088
H	-3.00901765473610	2.59405430670709	-0.04901697027753
H	-1.70869875704625	-2.23231792955351	0.18592312290393
H	-0.09619074892713	2.74705331884325	0.76545142659482
H	-0.12879620824163	2.64801733686812	-0.99350995807613
H	2.75131759841001	2.25443727198421	-0.13794378852413
H	4.27437898628946	0.29024021738548	-0.05977668661542
H	3.35705870086266	-2.00914798837181	0.07917590983958
H	0.90157629759605	-2.38644720029790	0.14527898078983

Table A3.16. DFT optimized coordinates for Fluorene radical

C	-3.68914509603750	0.55832923747790	0.12184793540815
C	-3.34572083253541	-0.79770946594037	0.12084578809636
C	-2.70434452549900	1.54176189969929	0.10415896808730
C	-1.35853946938468	1.15315846667058	0.08462598703896
C	-1.01330919320041	-0.23418048392273	0.08425887880215
C	-2.00498740560350	-1.20163985180650	0.10224399403423
C	-0.15587373057333	1.91796087730228	0.06284251907340
C	0.94783438226212	1.01660901602200	0.04900864307615
C	0.44233620449990	-0.32016274355910	0.06235710882791
C	2.32949602688200	1.24511559382130	0.02589572729063
C	3.19240862154666	0.15298886756672	0.01695063101796
C	2.69237569265859	-1.15329199584642	0.03057947950597
C	1.31387018218431	-1.39743161529416	0.05323910823830
H	-4.74271967502467	0.84802693255894	0.13741946716079
H	-4.13478341457361	-1.55331411693961	0.13527136486845
H	-2.97612660643114	2.60027997451758	0.10556511809681
H	-1.75344448145760	-2.26568364230117	0.10206620388666
H	-0.09069968163446	3.00735319612263	0.05701456653343
H	2.72296766691137	2.26462674436385	0.01421161236146
H	4.27278494837846	0.31719172022188	-0.00186350228734
H	3.38688942503339	-1.99656115415777	0.02291109900883
H	0.93973496159849	-2.42442345657711	0.06355030187343

9-(4-X-phenyl)fluorenes

Table A3.17. DFT optimized coordinates for 9-phenylfluorene cation

C	-3.62576274982458	0.57278890915057	0.83611478389640
C	-3.41987907352318	-0.70310787715122	0.26405686188317
C	-2.56952399886924	1.45797034441403	1.06171578830276
C	-1.29406883264323	1.05223615129141	0.72354313347346
C	-1.08060704637539	-0.23269980018657	0.13333976069790
C	-2.15554849358480	-1.11676410486128	-0.09201030702626
C	0.01486051551389	1.77760450217008	0.89065183847783
C	0.98769334098377	0.79908822964873	0.29096857118713
C	0.30777848645442	-0.38489834933430	-0.13508223584546
C	2.35407689897678	0.91081140636487	0.12724647942512
C	3.04019037027364	-0.16087415546260	-0.44890934900537
C	2.37475160539162	-1.33512812278333	-0.86798210322954
C	1.01151417427105	-1.45998924930754	-0.71693190631227
H	-4.63880202295233	0.86947216569776	1.11878752809289
H	-4.27734851960022	-1.35888828829059	0.10234386328788
H	-2.75353017892130	2.43692822495588	1.50698863345311
H	-1.98707751344814	-2.09596308846722	-0.54275786481488
H	2.89160997192142	1.80682115752291	0.44314340618863
H	4.12331075072070	-0.09356508930746	-0.57819582579969
H	2.95413898072681	-2.14449798646447	-1.31653256916024
H	0.48777718231746	-2.35947052277708	-1.04543106943589

Table A3.17 Continued

C	0.02850882824017	3.14449012430001	0.25427997628288
C	0.16733366063041	4.29273124265180	1.03787440819800
C	-0.12238906153767	3.27859975478831	-1.13396520893511
C	-0.12921410088020	4.53724285894430	-1.72266656399915
C	0.00579600241145	5.67727362885781	-0.93340128337088
C	0.15347951241647	5.55226854394957	0.44804225061738
H	0.28834256195732	4.19679322654044	2.12002915177426
H	0.26214394605075	6.44370684914646	1.06964831935183
H	-0.00398652480604	6.66687042901460	-1.39624566111714
H	-0.23751370353184	2.39044492124499	-1.76016054520489
H	-0.24668997615005	4.63073137127028	-2.80481860439137
H	0.23083500739007	1.88794259246884	1.96745634305751

Table A3.18. DFT optimized coordinates for 9-phenylfluorene anion

C	-3.72847352685461	0.30753836436468	0.28748381828695
C	-3.38259370739212	-1.05701018410241	0.29595049371234
C	-2.76371313292543	1.29752439898025	0.18047891542798
C	-1.39734432901230	0.95242647775261	0.06857187396751
C	-1.05593675626445	-0.44625350701496	0.10989680868449
C	-2.04590211882684	-1.42704931686114	0.21568481137320
C	-0.19731359982567	1.73131336179241	-0.01803924556959
C	0.89198780100026	0.79966421602327	-0.02971847102115
C	0.37263072606037	-0.54192657387475	0.03905705242033
C	2.29077501166628	0.95409448521155	-0.16087226236579
C	3.11778801083437	-0.15852082258141	-0.19254841222131
C	2.59796045436904	-1.46336850831943	-0.10143788089978
C	1.22578824004460	-1.64884016866208	0.00691438154865
H	-4.78067065425628	0.59570731321883	0.37514811146977
H	-4.16221457068164	-1.81869964256223	0.37832173580051
H	-3.07469695241113	2.34439233732731	0.19839259090745
H	-1.76716021907449	-2.48564799484002	0.24256851643180
H	2.73512064379250	1.94651666153285	-0.25798015311964
H	4.19781674015678	-0.01648574501135	-0.29971255972707
H	3.27069644187119	-2.32435088020911	-0.12753440316777
H	0.81179573199396	-2.66091303827964	0.05968061295210
C	-0.10369520285061	3.17603507155773	-0.10579003189637
C	0.97988772882366	3.89634860135913	0.45201202207586

Table A3.18 Continued

C	-1.08625776215938	3.95300580211962	-0.76554488216998
C	-0.99092140820482	5.33601896636489	-0.86188767332209
C	0.09477338387161	6.01768999722028	-0.31049681502501
C	1.07747214545711	5.27887867007083	0.34881909261852
H	1.74851776998678	3.35325908995219	1.00354512586087
H	1.93250602713798	5.79081891582599	0.80075202551092
H	0.17539384729831	7.10439451690190	-0.39629105633112
H	-1.92676690098537	3.44782682438281	-1.24349283877069
H	-1.77232986263963	5.89058231035939	-1.39047130344188

Table A3.19. DFT optimized coordinates for 9-phenylfluorene

C	-3.72010261250300	0.47002896611289	0.68582174644489
C	-3.44811771287718	-0.80606111556687	0.18790152706421
C	-2.68661235977837	1.37995009686257	0.91170041417098
C	-1.38197045633289	0.99889493105211	0.63014508667925
C	-1.10822428908535	-0.28205837088957	0.11795934181142
C	-2.14136219448210	-1.19227586665078	-0.10030461904472
C	-0.10220510310758	1.77353284628455	0.82337812849065
C	0.93685455169015	0.81141999116773	0.29031310964382
C	0.33106873063126	-0.39688348103861	-0.09730514895126
C	2.30897108158422	0.98143806104864	0.17436217525175
C	3.07908631451496	-0.06875881745227	-0.32723080708039
C	2.48093138332326	-1.27333665143619	-0.70392601430749
C	1.10330008465005	-1.44724145644762	-0.59282270685317
H	-4.75102494025776	0.75867715510928	0.90587104591140
H	-4.26912151629996	-1.50633708378145	0.01651761736258
H	-2.90484753460008	2.37552543544129	1.30511364768762
H	-1.93329827745486	-2.18902094336273	-0.49645706830147
H	2.78182983355075	1.92181983892296	0.46835581738463
H	4.16015379152146	0.05500874960033	-0.42966122131116
H	3.09925014749449	-2.08565722067866	-1.09343321278468
H	0.63982665215397	-2.38941740607952	-0.89556165544418
C	-0.04962871728787	3.15632608868611	0.22062982088628
C	0.54894024749605	4.20548615806859	0.92295172595163

Table A3.19 Continued

C	-0.55821961570241	3.41272365701752	-1.05704368681346
C	-0.46990432871195	4.68433580438980	-1.61419451768239
C	0.13262051441708	5.72241403582831	-0.90574385533500
C	0.64298750187971	5.47872113391822	0.36563063633208
H	0.94643226469951	4.02124655146002	1.92450790258644
H	1.11413365879290	6.28536274576834	0.93228507001864
H	0.20157504581990	6.72057876052195	-1.34523174177916
H	-1.03362035733868	2.60690978678044	-1.62147983453953
H	-0.87712706036039	4.86805245981028	-2.61131736527648
H	0.06962527196071	1.88556515953234	1.90940864182625

Table A3.20. DFT optimized coordinates for 9-phenylfluorene radical

C	-3.72970173110792	0.33187624259774	0.33343536416580
C	-3.38366985948134	-1.02253830711240	0.33504958320181
C	-2.75470257502009	1.31877998596005	0.21883335334331
C	-1.41082333398693	0.94262291548358	0.08832228102973
C	-1.06620213878986	-0.43988463491680	0.11925188275789
C	-2.04582710452771	-1.41435446605930	0.23628140609442
C	-0.19982083893820	1.72155605489775	-0.01807196627735
C	0.90123044150035	0.78767472521353	-0.04867069884905
C	0.38193656728964	-0.53716989699654	0.02661910020927
C	2.28146768292249	0.97621207423800	-0.20051155555404
C	3.12023745666194	-0.13426453291458	-0.23890493109715
C	2.60269850425530	-1.42913575939427	-0.14317844594712
C	1.22677638724937	-1.63639248350796	-0.01720952874025
H	-4.77829473987006	0.62226769104189	0.43366111075288
H	-4.16446106713663	-1.78093959664567	0.42835483680548
H	-3.04563045554544	2.37033240212734	0.24425648075818
H	-1.77978564508195	-2.47439497358805	0.25915233633096
H	2.70537178583694	1.97596480168240	-0.30472180813034
H	4.19691093654415	0.01037747665993	-0.35754526189972
H	3.27782109160452	-2.28709446610161	-0.18060185378920
H	0.82622572714896	-2.65173382016939	0.03766784019320
C	-0.10613784223092	3.16648242317478	-0.10440210896152
C	0.92842049343018	3.87224820545187	0.54327475652606

Table A3.20 Continued

C	-1.04067250823656	3.91255675735365	-0.85152228181717
C	-0.93648869606242	5.29360078580489	-0.95462826409437
C	0.09662368046881	5.97217609347082	-0.30944413656650
C	1.02392040107250	5.25426996818772	0.44442364238282
H	1.64622397892681	3.32756945266720	1.15816518948445
H	1.82959626747552	5.77871667144105	0.96408281964215
H	0.18081884519445	7.05839754988186	-0.39654970556204
H	-1.83410882732272	3.39288399170339	-1.39036833783391
H	-1.66503288424321	5.84630666836716	-1.55304109855868

Table A3.21. DFT optimized coordinates for 9-(4-trifluoromethylphenyl)fluorene cation

C	-3.64553201038063	0.42663398906357	0.69367968526194
C	-3.51905524354172	-0.78040746623993	-0.03020393867879
C	-2.52972642408936	1.17515629691858	1.08308963099773
C	-1.27836668910208	0.69932199434832	0.75415673046184
C	-1.14262114326413	-0.52324303499318	0.02380110644793
C	-2.27667238760722	-1.26560358890636	-0.37087914220950
C	0.07414577299804	1.28237803060524	1.05945152211384
C	0.99376269216080	0.28093658880290	0.41269268235136
C	0.23935528714006	-0.77848053126623	-0.18365534243314
C	2.37086546562775	0.27466270846004	0.34438017725183
C	2.99514545163523	-0.79435041024054	-0.30775148108687
C	2.25718548440787	-1.84614754011931	-0.89656372579798
C	0.88146522685807	-1.85070578460560	-0.84218583521118
H	-4.64370783584964	0.78258716974151	0.96051066456678
H	-4.41880102607256	-1.32649929445123	-0.31864894649027
H	-2.65567328177916	2.10772094937973	1.63535869970259
H	-2.16718600238749	-2.19580078953729	-0.93037778356816
H	2.96650645622986	1.07514780721020	0.78747443636954
H	4.08658578349104	-0.82101233557708	-0.36302694526407
H	2.79180263404992	-2.65626720212982	-1.39638730602302
H	0.30161516381106	-2.65605679014298	-1.29662274634447
C	0.26915112879512	2.69389811416393	0.56343703826432
C	0.69078128164238	3.70535384501496	1.42206568031970

Table A3.21 Continued

C	0.05113443659063	3.01810723203429	-0.77779399163820
C	0.25668027101891	4.30869177423540	-1.24260861914741
C	0.68796161037613	5.33119638454360	-0.38461547603925
C	0.89868329392027	4.99968587843449	0.95956797973751
H	0.87205203522196	3.48681743805607	2.47683965755739
H	1.23762918111506	5.73544823132212	1.68319001760365
H	-0.28099928444461	2.25572235603702	-1.48586750226404
H	0.08105575593444	4.50058770338497	-2.29738346997768
C	0.97531698789971	6.73225271690602	-0.94689964708709
C	-0.26819679298429	7.27721323012006	-1.72319698512169
C	1.30842495430212	7.76019699685945	0.18135827345233
F	1.48730877482993	8.98688326160111	-0.28133843091278
C	2.20609212991272	6.63127101421148	-1.89842904949967
H	0.23643807389382	1.27048205149995	2.15115039579790
F	-0.56967371360394	6.52264792885609	-2.77392609787382
F	-0.06992475999383	8.50675407539623	-2.17600653153507
F	-1.32885915388421	7.29387835444220	-0.92723227298003
F	2.42404967806337	7.42663662707747	0.82299105684652
F	0.31912930611260	7.80513926154140	1.06646984319635
F	3.23328097822200	6.08377201656501	-1.26179550842032
F	2.58178902915399	7.81877526746278	-2.35091509049828
F	1.93845142356997	5.86814747391333	-2.95072341219829

Table A3.22. DFT optimized coordinates for 9-(4-trifluoromethylphenyl)fluorene anion

C	-3.69123863505679	0.31806713917523	0.29950030568457
C	-3.52313957246137	-1.07358885523838	0.40254383162305
C	-2.60847837877557	1.16633493137605	0.11858670027011
C	-1.30061637426076	0.64146901333138	0.02408845238037
C	-1.14127826497298	-0.77872075268800	0.17013461182320
C	-2.24545314282877	-1.61648009493893	0.34777033232115
C	-0.00579369981890	1.25305200133801	-0.11660415185935
C	0.95683999669569	0.18602536634998	-0.04006701439831
C	0.26501663478263	-1.06433037974858	0.11699637576684
C	2.36378727488611	0.14420148729174	-0.15284547098772
C	3.03525920004235	-1.06888395319713	-0.09304229968011
C	2.34556758222686	-2.28204032808366	0.07340339738493
C	0.95998826793657	-2.27512023169923	0.17246528304235
H	-4.69563983282785	0.74621166419404	0.37137668244971
H	-4.39250162255201	-1.72072857211614	0.54247927742871
H	-2.78539741087784	2.24222147091898	0.06759360491747
H	-2.10175714288628	-2.69635197631310	0.45588535876995
H	2.94037336867556	1.05711004687119	-0.30768458795455
H	4.12546670900415	-1.07986184856513	-0.18650873367550
H	2.89801624938640	-3.22417024285812	0.11850141212524
H	0.41309225505820	-3.21539593307722	0.29034634568467
C	0.25669863741987	2.65400366539098	-0.31799692114903
C	1.45286630762624	3.28943384704966	0.09533224722086

Table A3.22 Continued

C	-0.66852260489495	3.51253917086582	-0.96065994973490
C	-0.45167302354906	4.86962693740716	-1.12257481808588
C	0.71534401838629	5.49376687412535	-0.65234479920821
C	1.67185525180259	4.64671488147200	-0.06389674604645
H	2.22248328886128	2.70824770265627	0.60166245417180
H	2.61457583667993	5.04824969077033	0.30179348851954
H	-1.58128835718806	3.09283470626879	-1.38235273180467
H	-1.22434024434082	5.42969481067938	-1.64359121501692
C	0.98039344811040	6.99582105070858	-0.77533693048493
C	-0.19555781237226	7.74768485691529	-1.46735399182582
C	1.17216868314476	7.62653172595056	0.63941023243894
F	1.52265779979580	8.91070754961703	0.57511260993491
C	2.25557757629442	7.23302482808075	-1.64309704384672
F	-0.31104273338231	7.36574942557013	-2.73667336551905
F	-0.02037671071339	9.06576010705072	-1.46891203584709
F	-1.35623765064262	7.52087023230715	-0.86315448249402
F	2.11080646071268	7.01128857846712	1.34543440397859
F	0.04116967022277	7.54547442130056	1.33167839127650
F	3.36016193542426	6.90001274716129	-0.97896319572160
F	2.39917618044657	8.50416174729934	-2.01318518280883
F	2.20797058078021	6.50055049056274	-2.74678013106380

Table A3.23. DFT optimized coordinates for 9-(4-trifluoromethylphenyl)fluorene

C	-3.69417546563598	0.34333824438884	0.85286056017557
C	-3.56787583241774	-0.86797188632677	0.16945721463876
C	-2.56787597853246	1.11185720789816	1.15040424304699
C	-1.31825916927873	0.65406142398685	0.75582207236221
C	-1.19007889229239	-0.56636955512682	0.06890269363993
C	-2.31633973607801	-1.33302191500049	-0.22666507180732
C	0.03679432800100	1.27519353139528	0.98354087996063
C	0.96192982675288	0.28127736763377	0.31150394476124
C	0.22459760862194	-0.79720612146224	-0.20821294102697
C	2.34328859476006	0.31727579250964	0.18643234168180
C	2.98920505757285	-0.73653708501034	-0.46219984205601
C	2.26010788113158	-1.81124696090011	-0.97572461166535
C	0.87285538415286	-1.85035375500278	-0.85352172170683
H	-4.68245078413355	0.69288427775668	1.16122012822227
H	-4.45919900467204	-1.45741140298557	-0.05808791293274
H	-2.67293022480426	2.05934484066452	1.68391154063707
H	-2.22172780821517	-2.28280089577818	-0.75773107875326
H	2.92068065831733	1.15486267630532	0.58579281591108
H	4.07652650339539	-0.71911897421149	-0.57132238783451
H	2.78357235632784	-2.62818416066012	-1.47870621839615
H	0.30681091547842	-2.69313927483449	-1.25778924278288
C	0.22022317951504	2.69446435630796	0.50362168024345
C	1.05590709408553	3.57237396488240	1.19461978205791

Table A3.23 Continued

C	-0.38784230476905	3.16846011921984	-0.65896132901925
C	-0.15744363110577	4.45737243408876	-1.12533506134917
C	0.70022778626544	5.33180450242434	-0.44657376253410
C	1.29680424255764	4.85879845825612	0.72976909300255
H	1.53645931622054	3.24946025054619	2.12087936429728
H	1.96332084205837	5.49275104311708	1.31010057874125
H	-1.06186949105694	2.52103258754641	-1.22396602458738
H	-0.66631006532285	4.75164576434632	-2.03897894862582
C	1.02865390545155	6.74775270232881	-0.94691449337858
C	0.09318846331990	7.20021723993086	-2.11198887302190
C	0.84554401189462	7.77798638916623	0.21869008997237
F	0.81320655770037	9.03349772337829	-0.20621337566477
C	2.49996044163720	6.77359251007133	-1.45974992129978
H	0.25181157531611	1.26343082817488	2.06751014152508
F	0.16342455582973	6.38631957447226	-3.15992280711770
F	0.39578707961235	8.41028297170621	-2.56184575330755
F	-1.16712337576898	7.22387656538365	-1.69234153445506
F	1.84116071613577	7.70278529869381	1.09858390736815
F	-0.28876864976097	7.54146604701510	0.86293726740410
F	3.35253178133390	6.34748356454997	-0.53689640034159
F	2.87566104639374	7.99756935451519	-1.81661861393510
F	2.62887870400497	5.97837237463833	-2.51366241204995

Table A3.24. DFT optimized coordinates for 9-(4-trifluoromethylphenyl)fluorene radical

C	-3.70082764887656	0.35414779248438	0.38789933533877
C	-3.52442539502726	-1.02721371092332	0.50276011676158
C	-2.61464046702611	1.19777179990896	0.17154346041823
C	-1.33220914954675	0.64510110275119	0.05364641813371
C	-1.15945947862802	-0.76153725881928	0.19897625760765
C	-2.24849986903602	-1.59169730414586	0.41685943849788
C	-0.03611529445230	1.25410918381170	-0.13118847798427
C	0.94197835121394	0.19225941119319	-0.08875854368704
C	0.26384860961272	-1.04666363531660	0.09802061860910
C	2.33313442787604	0.19728325389180	-0.25551265358072
C	3.02832313877666	-1.00813184786559	-0.20713587360086
C	2.35576549396928	-2.21686160123319	-0.01016511643115
C	0.96615145644434	-2.24176084435497	0.13790126032547
H	-4.70223647546936	0.78135892637095	0.47929250739685
H	-4.38954156138977	-1.67070323199463	0.67751494322775
H	-2.77158853014551	2.27592573227758	0.10777826969175
H	-2.11514669479859	-2.67038600965101	0.53284226712469
H	2.87514847006938	1.12607272765725	-0.43772943476477
H	4.11301536158090	-1.00845306014207	-0.33792835114971
H	2.92007516562427	-3.15183448003933	0.01990224895247
H	0.44585398896166	-3.19191124437397	0.27937139707048
C	0.22981019923373	2.66370124088608	-0.32903371698246
C	1.35061963012069	3.29052358865979	0.24379304849545

Table A3.24 Continued

C	-0.62203416511088	3.47594735833145	-1.09793174895840
C	-0.37610087987917	4.82879701643312	-1.27676735228913
C	0.73251549980172	5.45156441238624	-0.68733283375187
C	1.58992562483254	4.64372013492459	0.07501636071790
H	2.03047742451557	2.71703076543357	0.87411444864778
H	2.45947926582076	5.06815723076441	0.57003528710263
H	-1.48541582288358	3.03598557762784	-1.59796525313358
H	-1.08106482235315	5.38089431108742	-1.89243783294145
C	1.01089748613481	6.95626955770093	-0.79978870294043
C	-0.12251642470926	7.70631762786208	-1.56389007751127
C	1.08205306861716	7.56711664434736	0.63867666623771
F	1.05643699935198	8.89296401919899	0.63211479426092
C	2.35584499971673	7.20719695529384	-1.54701758050049
F	-0.29434249892741	7.23227366162715	-2.79288060017447
F	0.13257634093721	9.00054153395077	-1.68812455460530
F	-1.27327901245818	7.57876933163656	-0.90966416511705
F	2.19935250685767	7.20794098128207	1.26438337161025
F	0.05482597698255	7.14399189987635	1.36115806883271
F	3.36151972687767	6.54228798075555	-0.99262333606575
F	2.68561687699352	8.49462658697080	-1.54298715458228
F	2.26117809979442	6.80827588147592	-2.80826722430926

Table A3.25. DFT optimized coordinates for 9-(4-bromo)fluorene cation

C	-3.64660337044764	0.59513698231110	0.80628751625585
C	-3.45927505461091	-0.75703107500074	0.44609437599994
C	-2.57508987987890	1.48539155466056	0.89786681788219
C	-1.30515146081170	1.00814907341392	0.63853233045245
C	-1.11114656529863	-0.35281106453129	0.25202281228493
C	-2.19962508445169	-1.24266265639176	0.16735528795913
C	0.01865733700779	1.72379387037292	0.71532771222902
C	0.96851641041821	0.66960578355088	0.21230333022733
C	0.27450057886481	-0.55973023586028	-0.00711743845085
C	2.32774912473375	0.75301036741575	-0.01901772385238
C	2.99814817824300	-0.39896640563543	-0.43509684386626
C	2.32212415952295	-1.62261820843067	-0.63189246438413
C	0.96279998159890	-1.71629397891496	-0.42355876929041
H	-4.65516896342479	0.94971541202107	1.03214572929127
H	-4.32694844421345	-1.41647154051703	0.38392167004033
H	-2.74316452199027	2.52466980709810	1.18566607872766
H	-2.04909115408106	-2.28240720222418	-0.12811013754626
H	2.87264320821311	1.68686320391184	0.13171891079188
H	4.07613686400851	-0.35702310994218	-0.60860844089264
H	2.88789341269832	-2.49671402401029	-0.95987370728280
H	0.43156015551547	-2.65483274861978	-0.59085014862549
C	0.05511986203696	3.03188807633223	-0.02303262573627
C	0.25737642501330	4.22822163360192	0.67181653269200

Table A3.25 Continued

C	-0.13752407698948	3.07919364859043	-1.41222306994381
C	-0.13060207161901	4.28834320752851	-2.09051188589103
C	0.06606994203324	5.46993738964372	-1.37353341691353
C	0.26274297304469	5.44644706905677	0.00856508778088
H	0.41526716105193	4.20703033637630	1.75269929890577
H	0.42053278909374	6.37501760283064	0.55853144494953
H	-0.30036345762307	2.15795261934152	-1.97675098984864
H	-0.28516359676752	4.31835835400106	-3.17017493886128
H	0.24763569971551	1.91640062938799	1.77816740679544
Br	0.06494343939395	7.11263562863137	-2.26853974187980

Table A3.26. DFT optimized coordinates for 9-(4-bromo)fluorene deprot

C	-3.72778099368403	0.28785823216786	0.27679243269124
C	-3.38299995752135	-1.07602745242179	0.28939273316810
C	-2.76190202766062	1.27711483220979	0.16843516129760
C	-1.39635594979108	0.93041002985991	0.05901200378578
C	-1.05649081591712	-0.46689799456199	0.10643926974304
C	-2.04637968626355	-1.44734189501135	0.21318511913803
C	-0.19296180234270	1.70800892853560	-0.02571404503136
C	0.89631193790494	0.77332388184879	-0.02809144357394
C	0.37310623832180	-0.56526848082978	0.04258273582114
C	2.29556307109142	0.92310794851353	-0.15308777032953
C	3.11923456485542	-0.19276696323256	-0.17675829921634
C	2.59497499384487	-1.49477312031006	-0.08380192292323
C	1.22167018826187	-1.67555432450644	0.01831872736038
H	-4.77955093926474	0.57773466377195	0.36256311197755
H	-4.16329868563299	-1.83684435509285	0.37270381858244
H	-3.07400179407816	2.32343191442019	0.18562552911035
H	-1.76716834669385	-2.50549615899250	0.24496747640110
H	2.74551146007458	1.91246028752929	-0.25336721608379
H	4.20007945396019	-0.05412459180826	-0.27898770298720
H	3.26497334767745	-2.35800496331845	-0.10348864069011
H	0.80289964945094	-2.68541892415027	0.07235829438331
C	-0.10003844979595	3.14835966295710	-0.11374412080973
C	0.99419167246643	3.87221529038515	0.42025754633536

Table A3.26 Continued

C	-1.09749296908927	3.92940181889553	-0.74769502484643
C	-1.01868114687230	5.31224591934519	-0.83857937081578
C	0.07973730769266	5.97808490841587	-0.29842476856138
C	1.08950081294909	5.25457413426827	0.33243521768469
H	1.78020427729142	3.33581555402193	0.95231490682345
H	1.94669037390096	5.77141340324748	0.76911435404161
Br	0.19956741136129	7.86476289213919	-0.42153005598151
H	-1.94656054012500	3.43119347111277	-1.21630752731107
H	-1.80763265637261	5.87197145059092	-1.34546052918377

Table A3.27. DFT optimized coordinates for 9-(4-bromo)fluorene

C	-3.71313039718761	0.51915373251246	0.72478744559582
C	-3.48637209218427	-0.81632406757008	0.38612427055473
C	-2.64940251925237	1.41626947227821	0.82868183711891
C	-1.36111591009693	0.96159843505611	0.58406484332072
C	-1.13220996321635	-0.37973786794685	0.22924841440235
C	-2.19549052267668	-1.27660111786169	0.13657043212227
C	-0.05476422725371	1.71308093452562	0.66822265702176
C	0.94378208287674	0.66934577930056	0.21849667882293
C	0.29849613048465	-0.56216644493370	0.00552266125226
C	2.31574167902223	0.78556615171308	0.04768502948957
C	3.04706027828670	-0.34302814162782	-0.32530619746467
C	2.41126619224741	-1.57105117176230	-0.51939866855699
C	1.03304661531908	-1.69052564632328	-0.35746242898716
H	-4.73187762110294	0.86601702368528	0.91481780885493
H	-4.33095508398620	-1.50525500554016	0.30956613093750
H	-2.83213507007922	2.45900882482859	1.09935120317025
H	-2.02331785787329	-2.32033876115907	-0.13757740466099
H	2.82025998034499	1.74250328087909	0.20403726531074
H	4.12739000434809	-0.26366710067429	-0.46956232338094
H	2.99998557316903	-2.44492618339725	-0.80828016325163
H	0.53914357144491	-2.65173783517644	-0.51924702660379
C	0.00492132980085	3.03412554539591	-0.05472688332967
C	0.53292198842262	4.16040911495484	0.57879278574604

Table A3.27 Continued

C	-0.45329236569698	3.16782886456716	-1.36953889590296
C	-0.40128463797677	4.39027973226000	-2.02837431322877
C	0.12111617265263	5.50001107549109	-1.36692365156947
C	0.59794963724449	5.39253063074376	-0.06573723013468
H	0.89957186523649	4.08019860371044	1.60496403399318
H	1.00964788708717	6.26272382785613	0.44756257171887
H	-0.87132820918093	2.30315583738407	-1.89047480228609
H	-0.77348956659474	4.48186300327162	-3.04974372849232
H	0.14604355379765	1.91937609090935	1.73523975617230
Br	0.16732150257324	7.17051338264957	-2.24125210775501

Table A3.28. DFT optimized coordinates for 9-(4-bromo)fluorene radical

C	-3.72926201597618	0.31270617042199	0.32551563197579
C	-3.38478060272653	-1.04184823427332	0.33011832629779
C	-2.75298257388575	1.29830435035226	0.21039083259984
C	-1.40944998137081	0.92028309662710	0.08168447326481
C	-1.06642937595192	-0.46211575812646	0.11704958654367
C	-2.04720838247052	-1.43536877550372	0.23469792240503
C	-0.19618922699436	1.69684450694851	-0.02377217144493
C	0.90432396466851	0.76139029433006	-0.04713800299547
C	0.38174790081249	-0.56183760318095	0.02950296865111
C	2.28552085014315	0.94611221990777	-0.19438950978613
C	3.12170995516835	-0.16663172505154	-0.22628292014269
C	2.60076126861577	-1.45978049968380	-0.12900263206280
C	1.22387794267316	-1.66334778695763	-0.00806876793310
H	-4.77743924573509	0.60503130969670	0.42404508607580
H	-4.16644017647498	-1.79927099157843	0.42382620288350
H	-3.04419293812871	2.34973549124016	0.23536811649936
H	-1.78207880396160	-2.49548606170868	0.26129208405783
H	2.71372358960101	1.94370525867361	-0.30124607397605
H	4.19910959224445	-0.02452131807220	-0.34102592738329
H	3.27375799011716	-2.31960380237735	-0.16103819028074
H	0.82031123358656	-2.67736849029143	0.04804204201827
C	-0.10294733675186	3.13946270612530	-0.11089091607653
C	0.93940291562527	3.84881670037682	0.51982138572428

Table A3.28 Continued

C	-1.04928289458517	3.88942008807650	-0.83871454646089
C	-0.96139790636595	5.27010056265286	-0.93754608045299
C	0.08262350714286	5.93814272575320	-0.29946298189148
C	1.03343405877612	5.23016847324151	0.43399076479752
H	1.67248964992007	3.31029318144891	1.12143912728797
H	1.84218829991993	5.75738081378314	0.94254825587051
Br	0.20914032050939	7.81203682279512	-0.42891238290549
H	-1.85024394172433	3.37605367154520	-1.37175108399824
H	-1.69887763642050	5.82616260280880	-1.51863061916226

4-X, 2,6-di-tert-butylphenols

Table A3.29. DFT optimized coordinates for 4-H-2,6-di-tert-butylphenol cation

H	-0.08435038519905	2.24394657474436	0.41032839910256
C	-0.09297153687108	3.30963410746594	0.18946727905410
C	0.59320695484184	4.17151292523634	1.05412646930976
C	-0.77157026692757	3.78848784542097	-0.91215960210141
C	-0.72304290565694	5.22930100214466	-1.10326414521343
C	0.00438706575736	6.13693809810139	-0.23847871251263
C	0.63881113480191	5.56069241560514	0.83769794131705
H	1.19732508796797	6.17366277730440	1.54196572752366
C	-1.53441742132953	2.87617990885660	-1.86201934288771
C	0.08066337700741	7.63241911096079	-0.53491512360747
C	-1.32278330206045	8.26978846232720	-0.55562787282651
C	0.88290046294349	8.35618386596552	0.54472730817639
H	0.40514955485798	8.27909559314706	1.53241808541627
H	0.94525622844001	9.42284122672263	0.28967088257779
H	1.91103257847081	7.97597162935384	0.62134502484001
C	0.79743344035474	7.85869131050279	-1.87906864014837
H	0.28464370102501	7.41552097198328	-2.74534846144391
H	1.81444016430990	7.44318311804092	-1.85330644512471
H	0.87426476994529	8.93866683293546	-2.06824764017951
H	-1.89723339953768	8.01062689331427	0.34511742000752
H	-1.94973502414605	8.02212890179771	-1.42901074034174
H	-1.21205442680712	9.36290043552790	-0.58778711775965

Table A3.29 Continued

O	-1.38965912085735	5.68494768914658	-2.12510836731424
H	-1.37773960115055	6.66144538877755	-2.16224170420594
C	-1.42153666088524	1.41809229127410	-1.42499345172159
H	-0.38093368317527	1.06348220047928	-1.42256893668080
H	-1.98102920951356	0.79159537593565	-2.13219802509706
H	-1.85137605695035	1.24849264710601	-0.42708322321454
C	-3.02953865406000	3.24155733240960	-1.86911242939186
H	-3.46119581308750	3.15982309454341	-0.86093483454978
H	-3.56087443097755	2.53194342293473	-2.51867855972908
H	-3.22155604453358	4.25054699568672	-2.25127459903298
C	-0.95300910524461	2.98381341465388	-3.28282410245762
H	0.10931262871315	2.69939379840747	-3.29617961214165
H	-1.05236121107628	3.98846644637511	-3.71058960883275
H	-1.49487056533721	2.28809766643610	-3.93910680618082
H	1.11320167594766	3.75316822837465	1.91936356737267

Table A3.30. DFT optimized coordinates for 4-H-2,6-di-tert-butylphenol anion

H	-0.09913410888146	2.26544740112140	0.40430386360228
C	-0.08038086941777	3.33884866962213	0.20117519609844
C	0.63055795485928	4.15717354234039	1.07705658208190
C	-0.76079442414337	3.84174185434321	-0.90636954008520
C	-0.74003394827269	5.26835184932147	-1.17499401151140
C	0.00438149505858	6.10758258059524	-0.25249861794894
C	0.65818377168782	5.52889404518886	0.83371213895215
H	1.21276591083835	6.16358110236354	1.52787692568440
C	-1.53683334248927	2.91047606430929	-1.84651304817915
C	0.06236012601259	7.61976067591265	-0.49474463922532
C	-1.35567477761187	8.20364808989372	-0.48198321880388
C	0.87679810587124	8.35779356280955	0.56580190441295
H	0.44885255881121	8.23798695619994	1.57355213921435
H	0.88821252845452	9.43592758138269	0.34005210357859
H	1.92274370698121	8.01696725073399	0.60091887825521
C	0.71018801736915	7.89444051802206	-1.85817799706739
H	0.15577942515054	7.36533414005973	-2.64323688369319
H	1.75570687497271	7.54718012148415	-1.86945715884683
H	0.70947465358476	8.97411672184548	-2.08273445800807
H	-1.81531939224730	8.09825152046923	0.51405491643661
H	-1.97802582310910	7.67479674090250	-1.21429615324130
H	-1.33878529819633	9.27747837565260	-0.73521735307799
O	-1.35120592112149	5.76612703326922	-2.18512128245826

Table A3.30 Continued

C	-1.45843150884295	1.44626543729211	-1.42157207303404
H	-0.42455821171010	1.06918297129113	-1.41520614582759
H	-2.03161850817736	0.82510201227310	-2.12699077716924
H	-1.88340786311710	1.28141936331385	-0.41957118291565
C	-3.01833550701742	3.30588410707029	-1.86444845348951
H	-3.46928540206980	3.17889196049529	-0.86725032829449
H	-3.58290109122784	2.67523816446138	-2.57054059702564
H	-3.12145531629400	4.35637521704342	-2.16484639810938
C	-0.97009378939471	3.01042531696703	-3.26836851664869
H	0.07456797257331	2.66205047723890	-3.29718375092086
H	-1.00346901380379	4.05244700452667	-3.61111883216039
H	-1.55201383758931	2.38610632249923	-3.96629266432069
H	1.15028485250979	3.73114524768453	1.93959943374626

Table A3.31. DFT optimized coordinates for 4-H-2,6-di-tert-butylphenol

H	-0.10998030954653	2.26218770473163	0.41012930157079
C	-0.08693153823992	3.33053852666858	0.19780994009582
C	0.61534611242130	4.16136820130524	1.06094463489901
C	-0.75952325706838	3.82657981949961	-0.92121043654919
C	-0.69348233139626	5.22243482503603	-1.14135507795901
C	0.00816155819760	6.09891465411604	-0.28007038088788
C	0.65514177787710	5.52665493513537	0.81943160997630
H	1.20531638495916	6.16267384219104	1.51076323909021
C	-1.53529821674592	2.89257925064623	-1.86248017395408
C	0.07027239470001	7.61485697669546	-0.53244679283959
C	-1.33675847740222	8.23594688161690	-0.50390775220236
C	0.87916504084341	8.33360302406285	0.54800209552463
H	0.43784864811961	8.20406996062499	1.54706424803655
H	0.89695101901747	9.41228977290720	0.33354368383405
H	1.92131765193021	7.98593487378345	0.58389560660212
C	0.77058492883395	7.91118858877722	-1.87001140048231
H	0.28368366410858	7.47124277802483	-2.75243897070616
H	1.80014817856958	7.52498430019433	-1.85476670296202
H	0.81682780416493	8.99756553089854	-2.03855924393771
H	-1.79525073744853	8.10568141351245	0.48789783015503
H	-2.04480781821644	7.81299218175007	-1.23149752347040
H	-1.27400303246565	9.31538583002890	-0.71097919741047
O	-1.34553190979799	5.68849002432857	-2.24027125341025

Table A3.31 Continued

H	-1.23453443139732	6.64382800997037	-2.30292562127489
C	-1.46061509163286	1.43857645602468	-1.39933005442679
H	-0.42857935495713	1.05919948659580	-1.38022819370286
H	-2.03020609818372	0.80741118161788	-2.09641516351805
H	-1.89635406925147	1.29828798195562	-0.39914768273337
C	-3.02027724820209	3.27785446775936	-1.89538412287281
H	-3.46794364849185	3.19650498738357	-0.89319274076178
H	-3.56938474830556	2.59603709862159	-2.56228079824948
H	-3.17501929099991	4.30072968357684	-2.25810223439500
C	-0.94590628159760	2.94568390487507	-3.27882087753758
H	0.10560318054683	2.62041940258315	-3.27540945208573
H	-0.99366608916109	3.95235525525187	-3.71076577097695
H	-1.50331859106364	2.26668121369992	-3.94214726282671
H	1.12919422728234	3.74150697354874	1.92876269234892

Table A3.32 DFT optimized coordinates for.4-H-2,6-di-tert-butylphenol radical

H	-0.08991311100983	2.25430429446614	0.40753031329837
C	-0.08915904398485	3.32136515322090	0.18533498845360
C	0.61345987071789	4.17103244134184	1.04815185096097
C	-0.76809485553836	3.80869820386580	-0.91406234914484
C	-0.72995825066605	5.26055544262550	-1.16128229610635
C	0.01556288647656	6.13705802571822	-0.24057273297229
C	0.65757966619547	5.55346305066894	0.83390664938219
H	1.21554460977783	6.16537001755652	1.54150366674985
C	-1.54654108156816	2.89461207486471	-1.85436127598569
C	0.06629403320271	7.63863496655348	-0.49467944575238
C	-1.35368161404866	8.22452389911014	-0.48862698679418
C	0.87574296617139	8.36585531523859	0.57752978492911
H	0.43851594800555	8.24282565028127	1.58011892958971
H	0.88822808678189	9.44306217256652	0.35563299103728
H	1.92109889905605	8.02549901395957	0.61407160374270
C	0.73173205764040	7.90807632408651	-1.85378608843652
H	0.16796650863184	7.44779156338274	-2.67321780380053
H	1.75976502670839	7.51546598164990	-1.87268282518575
H	0.78217867222728	8.99311556285208	-2.03146676313162
H	-1.83580403207544	8.08451797709890	0.49141155870123
H	-1.98086483607929	7.75809634174070	-1.25647751346291
H	-1.30577145085420	9.30636403224627	-0.68876593853814
O	-1.32385436610770	5.74615354901966	-2.14657861540624

Table A3.32 Continued

C	-1.45816040087318	1.43281813423278	-1.42277924980362
H	-0.42344700150172	1.05994086484590	-1.42469552790232
H	-2.03246082744581	0.81263293970850	-2.12549128982239
H	-1.88142982543340	1.26895163359237	-0.42064107069980
C	-3.03066923135127	3.28984250956220	-1.85602450094746
H	-3.46580283677528	3.19300113409836	-0.84959678467207
H	-3.58954057410979	2.62106353952177	-2.52750202333155
H	-3.17364506344044	4.32086628280196	-2.20010035546154
C	-0.97987667244897	2.99503856100144	-3.27869449418737
H	0.07575295360445	2.68435039415638	-3.30465220293848
H	-1.05419845759009	4.01613280020631	-3.67052947856094
H	-1.54254580805488	2.32650456129918	-3.94752421214571
H	1.13509715575965	3.74485559085797	1.90896948834572

Table A3.33. DFT optimized coordinates for 4-tert-butyl, 2,6-di-tert-butylphenol cation (2,4,6-tri-*tert*-butylphenol)

H	-0.71143561718889	2.26492452218489	0.45354752574800
C	-0.54930621364223	3.31395022676411	0.22082874194928
C	0.05660735141480	4.12869029992320	1.20972372223865
C	-0.93675278165117	3.78418889530955	-1.00931584881347
C	-0.68651262857378	5.18693159279766	-1.25831233897132
C	-0.10316862193755	6.07131646137439	-0.27483006365438
C	0.25485637573283	5.49866665908235	0.92343697536399
H	0.70846399226653	6.12476336437388	1.68480025749252
C	-1.58857920113653	2.88180445116308	-2.05325636286259
C	0.09531297176699	7.56180124293036	-0.54853039389325
C	-1.26185465117493	8.23451225914782	-0.82737385285320
C	0.70602169925155	8.26439683488336	0.66416901330690
H	0.06176570890271	8.18934315338646	1.55168241646542
H	0.82823294374447	9.33168855778663	0.43515661077267
H	1.69899637622232	7.86690974610379	0.91665305281014
C	1.06502550992647	7.77237336620219	-1.72615876617015
H	0.69886457911320	7.42740639454111	-2.70540353952982
H	2.02172536651649	7.26351657398386	-1.54225270661603
H	1.26613577272066	8.84718530483842	-1.83738810527438
H	-1.92876577979015	8.13887073992676	0.04136484779250
H	-1.80737337417833	7.83504580643277	-1.69544767890887
H	-1.10255958812854	9.30539932086019	-1.02029904319838

Table A3.33 Continued

O	-1.01717615860384	5.62548763740460	-2.44402184111263
H	-0.80293324343487	6.56950089053322	-2.55718464693364
C	-1.76264799572776	1.46069757652346	-1.51743508501066
H	-0.80209676081447	0.98756312037623	-1.26806735643920
H	-2.23696033291050	0.84400203416958	-2.29325275253372
H	-2.41051653996229	1.42531085951594	-0.62922517416005
C	-2.98810002004643	3.41200902657340	-2.41117239582862
H	-3.62182002825089	3.47415784286004	-1.51461544032932
H	-3.46652536670961	2.71424152312741	-3.11344866674446
H	-2.96309155761098	4.39795128064606	-2.88979278407684
C	-0.70044537615781	2.79616552602113	-3.30580455502558
H	0.28676404655861	2.37978675661868	-3.05597421267435
H	-0.55444592172707	3.76647019259982	-3.79355712325923
H	-1.17334264766004	2.12163555816384	-4.03456707450351
C	0.46930006019144	3.51272056510081	2.52426157667443
C	1.06286396347212	4.52740445483579	3.49462606996028
H	0.34401051354689	5.31686520200998	3.75620434589908
H	1.97146950856620	4.99939716861062	3.09398279852848
H	1.34431187921151	4.01872367134751	4.42665370965171
C	1.52444598764740	2.42976978467338	2.22667508408060
H	2.41012054698774	2.86243073615813	1.73990684172685
H	1.13349577883599	1.62957544940480	1.58304703251866
H	1.84281881586244	1.97195815100217	3.17503470830972

C	-0.76135522148404	2.85929292622134	3.17822436063642
H	-1.20549726215797	2.07377101726691	2.55168894969317
H	-1.53564105157218	3.60772074749759	3.39824891696560
H	-0.45457580622652	2.39215452674072	4.12507025079255

Table A3.34. DFT optimized coordinates for 4-tert-butyl, 2,6-di-tert-butylphenol anion (2,4,6-tri-*tert*-butylphenol)

H	-0.70714442975472	2.28492398400846	0.43972532124418
C	-0.54712042168269	3.34387932538267	0.22956041477492
C	0.05293921947526	4.12398159648865	1.22611686689286
C	-0.94944215867813	3.83828468265170	-1.00730495396858
C	-0.75238753654418	5.24081324314248	-1.32194175486895
C	-0.15331564070471	6.05549870781510	-0.28703102929806
C	0.22776548546291	5.47693242294777	0.92405287440038
H	0.68914739278144	6.11934270392680	1.67192117172409
C	-1.58653492421084	2.91190800695369	-2.05082249825386
C	0.06145771315982	7.55354230989192	-0.53712108667098
C	-1.28663461342375	8.22439609674641	-0.83360901303214
C	0.68062665390267	8.27441479025711	0.66071346640476
H	0.04562056182517	8.20960270625713	1.55765623407404
H	0.80823571408727	9.34220725681276	0.42319955779280
H	1.67257898309667	7.87578170362312	0.92159983257533
C	1.00226617473051	7.74674779844586	-1.73227963622915
H	0.58519532958626	7.24614366938896	-2.61511383185847
H	1.99363248063260	7.31621982271295	-1.51934002609288
H	1.14025940081683	8.81740902943861	-1.95854284248574
H	-1.94531788866734	8.17983281790232	0.04840086775147
H	-1.77947386590341	7.71011270544087	-1.66848395073766
H	-1.15012874951424	9.28669274694216	-1.09925746581120

Table A3.34 Continued

O	-1.09261986304993	5.73081154628908	-2.45716566533905
C	-1.74021613055286	1.47337926248625	-1.55668539083725
H	-0.77331516547722	1.01248749681619	-1.30513996336473
H	-2.20100532564101	0.85963961379540	-2.34671466944295
H	-2.38675448189080	1.40542553223950	-0.66825166172473
C	-2.98791888921592	3.41980373484055	-2.41703877052755
H	-3.65056819689350	3.39171466120785	-1.53753543618375
H	-3.44052500214668	2.78977748424603	-3.20069023335671
H	-2.92908018409924	4.45366745954624	-2.78079044333991
C	-0.70537500324140	2.87698803656539	-3.30601309153457
H	0.27542330390145	2.43047545590996	-3.07696234128191
H	-0.54837261774896	3.89628040327343	-3.68023999905802
H	-1.17395877623334	2.27071416336803	-4.09939986163174
C	0.47727729024269	3.49106028624077	2.55322750292808
C	1.11318422747521	4.50706508903546	3.49808966542587
H	0.41529288423885	5.31685174077555	3.75636156280337
H	2.01246576805227	4.96558243038326	3.06018100886542
H	1.41427269906919	4.01660127635869	4.43645002135040
C	1.50298837735679	2.37953300068291	2.29494788035002
H	2.39442097769497	2.78101555997572	1.78937019309310
H	1.08894712591191	1.58668205488003	1.65452201568136
H	1.82879779433242	1.91051590999449	3.23841611295287
C	-0.74214137108035	2.88482823062566	3.26101321539066

Table A3.34 Continued

H	-1.23926591838690	2.13034419500443	2.63388225483481
H	-1.48366329728302	3.66288610552353	3.49811080597869
H	-0.44902510580803	2.39383114275813	4.20352676964107

Table A3.35 DFT optimized coordinates for.4-tert-butyl, 2,6-di-tert-butylphenol (2,4,6-tri-*tert*-butylphenol)

H	-0.70692121965858	2.27881927168771	0.43878865386756
C	-0.54199220185405	3.33285194440281	0.22405238321156
C	0.05575853078614	4.12239717046329	1.20922026603893
C	-0.93583636267237	3.82092248448991	-1.02003610643007
C	-0.70983185432329	5.19368295819200	-1.27429310637496
C	-0.13081088338868	6.04394434349777	-0.30918525494039
C	0.24244820582600	5.46869863318358	0.91101887386234
H	0.70090248260385	6.11096255744533	1.65663618682685
C	-1.58173648768049	2.89496784952298	-2.06258922084827
C	0.08537000939544	7.54774942522140	-0.56019864601188
C	-1.25703292382000	8.24756480010542	-0.83354562380017
C	0.69693427624139	8.24460427701347	0.65765705003335
H	0.05271688772785	8.16411323159149	1.54487947239574
H	0.82451845940399	9.31437075726624	0.43726657111281
H	1.68688794306392	7.84159680086577	0.91366884907523
C	1.06510106933404	7.77444234061355	-1.72349022573751
H	0.72185044535870	7.39548649438719	-2.69764187350646
H	2.02799847375488	7.28527829655539	-1.51597829837483
H	1.25239698264043	8.85091055841128	-1.85524153359662
H	-1.91209275360223	8.17593567914341	0.04731520279016
H	-1.82077331513250	7.83019581376055	-1.68017813990790
H	-1.09312422372304	9.31484980489569	-1.04904794660656
O	-1.08356303308022	5.65274149439961	-2.50094788597167

Table A3.35 Continued

H	-0.84140267295303	6.58144689376755	-2.58991584041560
C	-1.73716035017740	1.46686349646991	-1.53659502455330
H	-0.77055731734688	1.00673839656686	-1.28576584208177
H	-2.20339675479253	0.84472581084304	-2.31478940288086
H	-2.38190854075384	1.41702227291110	-0.64671569822515
C	-2.99001706211535	3.39202401699504	-2.42218100277033
H	-3.63204663421935	3.41050882923476	-1.52860895373176
H	-3.45337547009938	2.71326031939705	-3.15474619363558
H	-2.97759247268550	4.39833639825317	-2.85690197294057
C	-0.70238319026024	2.81864180528363	-3.31838520955284
H	0.28436634260146	2.39643038571779	-3.07343079441881
H	-0.55006336422033	3.80248241088323	-3.77666308739194
H	-1.17062649008299	2.16152135243122	-4.06793149259773
C	0.47266393150243	3.49686586119797	2.54182770894501
C	1.08929684878536	4.52110933788741	3.48968687210107
H	0.38286844160953	5.32603628970814	3.73928046453741
H	1.99432206026955	4.98082963920776	3.06551864136803
H	1.37928204712663	4.03279158442073	4.43153972804384
C	1.50900269861246	2.39671992414081	2.28156036491222
H	2.39977652934889	2.80610766301856	1.78175909649389
H	1.10573893747667	1.59728789909985	1.64292127236751
H	1.83206406586535	1.93552401145035	3.22818695720602
C	-0.75434057469837	2.88385003157200	3.22863012787878

Table A3.35 Continued

H	-1.23215640633592	2.11537928314595	2.60390915414770
H	-1.50775472612555	3.65453642308678	3.45026545365183
H	-0.46563838353284	2.40632267619343	4.17771502643571

Table A3.36. DFT optimized coordinates for 4-tert-butyl, 2,6-di-tert-butylphenol radical

H	-0.70816682838930	2.27415294373987	0.45587868878711
C	-0.55594822070986	3.32706594713058	0.22539335779614
C	0.04863079853498	4.13562355555941	1.21310109414585
C	-0.95519495702694	3.80294754495807	-1.00176072746494
C	-0.74062189709065	5.22753909935089	-1.29757392615600
C	-0.13675447236196	6.08010234761296	-0.26450320845848
C	0.23544582319634	5.50016982955568	0.93194551101719
H	0.69601146404872	6.12510895884679	1.69164776009113
C	-1.59633843758705	2.89221035015768	-2.04537023122905
C	0.07139408060840	7.56808005121173	-0.52876995580473
C	-1.27836538969265	8.23837607909621	-0.82922144410311
C	0.68547931832215	8.28059364333123	0.67691082634205
H	0.04421015058238	8.21582334653649	1.56856161862746
H	0.81349673101470	9.34684749532329	0.44052630736356
H	1.67706559967367	7.88260552601124	0.93745977416286
C	1.02471655644694	7.75555194624655	-1.71843549179041
H	0.60924986825922	7.32154297210132	-2.63498309512392
H	1.99895864399422	7.28400110871180	-1.51857478428074
H	1.19991048371698	8.82881177386504	-1.88973539761730
H	-1.95779074305757	8.15700949024362	0.03316116266803
H	-1.76416441833112	7.78349828208812	-1.70019518378951
H	-1.12498308713397	9.30901357321641	-1.03688006551153
O	-1.06378820673975	5.70398074952561	-2.40620915389805

Table A3.36 Continued

C	-1.75039608053026	1.45920508160531	-1.53538101550016
H	-0.78325447745682	0.99821930975208	-1.28764874160066
H	-2.21395020110117	0.84402894684558	-2.32038432710119
H	-2.39732075520044	1.39959482024644	-0.64739942910142
C	-3.00013088661125	3.40698899999169	-2.40154347503646
H	-3.64530769884861	3.42494701142576	-1.51022563719965
H	-3.46536831101786	2.73679977903714	-3.14040256017345
H	-2.96508078123254	4.41667341279895	-2.82727344314486
C	-0.71324837005367	2.84533824096899	-3.30150885483076
H	0.27674033317111	2.42569202824601	-3.06543563928176
H	-0.57507664679477	3.84258936149963	-3.73437678381555
H	-1.17964260468003	2.19795956077486	-4.06016384619010
C	0.47486070503299	3.50624381163636	2.53229501439026
C	1.09281908849011	4.51899751522548	3.49103114807682
H	0.38565439073221	5.31718613012320	3.75859827400926
H	1.99567787828082	4.98590481646295	3.07099544233488
H	1.38715475296464	4.01433403191001	4.42227943673538
C	1.51406961250264	2.41267953812654	2.24375464064710
H	2.39881403423660	2.83138570682932	1.74174148989137
H	1.10942943574907	1.61475076652331	1.60489094492516
H	1.84451469047836	1.94985679216672	3.18631534192659
C	-0.75099985422442	2.87811031896806	3.21182499515894
H	-1.22406071567897	2.10986521723529	2.58416725803014

Table A3.36 Continued

H	-1.50761606300028	3.64165231571860	3.44478650269434
H	-0.44924433548531	2.39696987146112	4.15425982838216

Table A3.37. DFT optimized coordinates for 4-methyl, 2,6-di-tert-butylphenol cation

H	-0.00188236847922	2.24874543361563	0.32266012684586
C	-0.00362285585882	3.31564404955010	0.10654645475906
C	0.71829540254031	4.15886876168312	0.97751435993367
C	-0.70392988848395	3.79472409651800	-0.97666088318833
C	-0.65714575732624	5.22835180904405	-1.17890425332244
C	0.08404299585083	6.12944036454501	-0.32557059584388
C	0.74840865234454	5.55414722677586	0.72878481390197
H	1.31725859020728	6.17608198981186	1.41776526988195
C	-1.50262655004908	2.87777387392241	-1.89715079780042
C	0.09804300836586	7.63735328482555	-0.57410925512472
C	-1.32441429064278	8.20521839484760	-0.41700611840915
C	0.98566070938630	8.35048929541963	0.44367465338407
H	0.61976488615331	8.22045029146372	1.47248510038322
H	0.98318444835484	9.42841373220967	0.22961217537395
H	2.02812432694819	8.00517461643296	0.39589185922450
C	0.66972934298979	7.95872442862517	-1.96753800498470
H	0.08614309544033	7.58489505502398	-2.82244039880303
H	1.68593998514686	7.55402261421950	-2.07707071491533
H	0.72171852673251	9.04971754523471	-2.08797822856683
H	-1.69753348948319	8.03446468048864	0.60309097618496
H	-2.07297219646205	7.78480522378730	-1.10512842605439
H	-1.30270503643231	9.29002560142947	-0.59682615962436
O	-1.34071432847353	5.68094226156126	-2.19617045585529

Table A3.37 Continued

H	-1.26144439414134	6.64826231984694	-2.28581151521174
C	-1.35724550880725	1.41800108132768	-1.47492360927719
H	-0.31347937578169	1.07535487137035	-1.52012444144678
H	-1.93972072881284	0.78971746269017	-2.16175225987488
H	-1.74238178231578	1.23588076755756	-0.46108030500841
C	-2.99600590046513	3.23725980611207	-1.82042061726734
H	-3.37194086481232	3.13604755165938	-0.79176586735892
H	-3.56322108338030	2.54046170599282	-2.45356861488354
H	-3.20816532459482	4.25380694627497	-2.17176152772707
C	-0.99934248824176	2.99001508835289	-3.34594362827755
H	0.06515868643435	2.72104365721494	-3.41622632093632
H	-1.13533622372746	3.99155758480675	-3.76992638674660
H	-1.56425500756884	2.28528627796847	-3.97219574827821
C	1.45319329635763	3.60303441055036	2.12984449087181
H	2.52795895168448	3.53130841931757	1.87208413177419
H	1.11049699822111	2.59649458813869	2.39899985433964
H	1.39712354118221	4.26952282978317	3.00350086792860

Table A3.38. DFT optimized coordinates for 4-methyl, 2,6-di-tert-butylphenol anion

H	0.04521299685753	2.27382261672595	0.28023181224945
C	0.03947960650199	3.35179210711490	0.09743049371645
C	0.77977402631365	4.15542921592059	0.97022030603572
C	-0.69405371940184	3.85635919987550	-0.97337017089415
C	-0.70963916063885	5.28472754505681	-1.22656568820047
C	0.05422762863174	6.11655702619682	-0.31968728051899
C	0.76025584663490	5.53032319095890	0.73064780672204
H	1.33052074625871	6.16679174488462	1.41167028476290
C	-1.49757599944199	2.92187496217454	-1.88686081791019
C	0.06791600723382	7.63517120829071	-0.52558911735892
C	-1.36293877068704	8.17659044153960	-0.42057033113049
C	0.91885141421677	8.36781143625174	0.50917863884576
H	0.54383532218780	8.21788387374539	1.53386816268669
H	0.89813073944643	9.45063850625482	0.30677733781914
H	1.97151333338807	8.04718924195621	0.48597363326820
C	0.63298842113057	7.96092407062983	-1.91388505956082
H	0.05333445304125	7.43011597824919	-2.67925773956036
H	1.68715258835918	7.64846527444140	-1.98968034315414
H	0.58562538361893	9.04481576169391	-2.11255854662767
H	-1.75906501581121	8.03527331245909	0.59798011179873
H	-2.01032586122490	7.64337601059236	-1.12769240353851
H	-1.39482118983682	9.25574632962994	-0.64970151214796
O	-1.37073380143301	5.78526287786792	-2.20593254859812

Table A3.38 Continued

C	-1.37654974011478	1.45392645747240	-1.48583616023030
H	-0.33725592450392	1.09496669032866	-1.53239450234270
H	-1.97117565419154	0.83251129695408	-2.17291856529938
H	-1.75242969176654	1.26849937066772	-0.46788029100196
C	-2.98381689587383	3.29481664191377	-1.82796814531495
H	-3.38188257868695	3.14890291408785	-0.81101896094076
H	-3.57399779960403	2.66360987809718	-2.51229743659057
H	-3.11651949103879	4.34718789678687	-2.11024364128676
C	-1.00136091997006	3.04857868482910	-3.33249590811834
H	0.04664620754067	2.71868771525367	-3.41622962480053
H	-1.06807742192494	4.09456610889279	-3.65758159978940
H	-1.60561887016482	2.42308238410700	-4.00982132769384
C	1.55822365798531	3.55881205761686	2.10562941747894
H	2.34953212025941	2.87048658160396	1.75891330842429
H	0.92098915583776	2.97193181551444	2.79111798132776
H	2.05054885087138	4.33688157336293	2.70935842747425

Table A3.39. DFT optimized coordinates for 4-methyl, 2,6-di-tert-butylphenol

H	-0.00024623500579	2.26828294756809	0.30780521224241
C	0.01070239252375	3.34004084359932	0.10950914490372
C	0.73730287899747	4.15368209396332	0.97683118467205
C	-0.70322098961948	3.83675377910589	-0.98252026500107
C	-0.67054303886949	5.23369438503911	-1.18939312417203
C	0.06313580031053	6.10123364199611	-0.34859191391683
C	0.74951875567331	5.52302618802373	0.72228123880017
H	1.31437701054419	6.16305253997013	1.39932238304321
C	-1.50634799114175	2.89860245801785	-1.89732142770333
C	0.09465801041482	7.62213832925637	-0.57698419576748
C	-1.31499514617668	8.21538079341710	-0.41449517566164
C	0.98476796538788	8.33165332176779	0.44363897235634
H	0.62154845399208	8.19728962266690	1.47297168910899
H	0.98824190196131	9.41206340057507	0.23597584137242
H	2.02553925612755	7.98083047498203	0.39713945880673
C	0.67640359296169	7.95906255472855	-1.96081518534205
H	0.12876110870381	7.53443667682529	-2.81411051916611
H	1.71026291970220	7.59180869576938	-2.04072201375427
H	0.69110538588854	9.04999436775772	-2.10402676253001
H	-1.67341387935023	8.06274352074755	0.61446700008008
H	-2.07649306631469	7.77907711463329	-1.07723777113502
H	-1.29717818152915	9.29848313119318	-0.61204644055395
O	-1.39287487745529	5.70815278685388	-2.24217334959342

Table A3.39 Continued

H	-1.31794069386397	6.66803662210937	-2.28264153883863
C	-1.35703854714891	1.43644947774762	-1.47997653062470
H	-0.31206773722031	1.09684057873882	-1.52666749612401
H	-1.94021161516663	0.80359481754551	-2.16406207596660
H	-1.73361252047570	1.25169284482254	-0.46314117731163
C	-3.00035529300205	3.24028396236529	-1.82301963069535
H	-3.37520863079341	3.12305035860688	-0.79480144488354
H	-3.57594036067010	2.55857120303059	-2.46743191449261
H	-3.20550446087756	4.26665124094320	-2.14985934639809
C	-1.01529268347254	3.00312708149737	-3.34762917574794
H	0.04504341245066	2.71652618486070	-3.42387689957728
H	-1.12718514175697	4.01666930050498	-3.75010911202571
H	-1.59278013898474	2.31949201375443	-3.98819317758075
C	1.49102000706986	3.57453800691925	2.13611700299817
H	2.54916101437135	3.39058377845460	1.88288692691817
H	1.06476774740610	2.61259349938797	2.45373774467234
H	1.48229361440833	4.25134536025322	3.00356386458925

Table A3.40. DFT optimized coordinates for 4-methyl, 2,6-di-tert-butylphenol radical

H	0.00384250126455	2.26305777750526	0.31716548311496
C	-0.00160504955613	3.33309962048742	0.10757296235227
C	0.72187266288339	4.16546947482819	0.98173392947956
C	-0.70775158702784	3.82065081285075	-0.97129656310801
C	-0.70417498357260	5.27247588699630	-1.20535210570267
C	0.07664682448768	6.13918236257517	-0.30790256609688
C	0.74726264649441	5.55378993931248	0.74312374795282
H	1.31914444208106	6.17110226683435	1.43617133781094
C	-1.50507173529192	2.90247305962618	-1.89317878240414
C	0.10090712532389	7.64600135752506	-0.54147700388709
C	-1.32029454349962	8.20757028211203	-0.38595076992578
C	1.00124152408307	8.36283904124014	0.46281407484345
H	0.64880449028373	8.24088202417440	1.49836928874823
H	1.00371082794523	9.44104219297297	0.24417573364621
H	2.04293666946383	8.01298895330880	0.41095519859879
C	0.63131096140567	7.95561160064790	-1.94966809821206
H	-0.00250837223099	7.50832017981626	-2.72308959733940
H	1.65764317328255	7.57780901317606	-2.07660768384662
H	0.65291761456178	9.04535111830403	-2.10279894166889
H	-1.69512408858178	8.04445554707894	0.63638362509935
H	-2.01464014664852	7.73771239476658	-1.09181848060705
H	-1.31480883888428	9.29288880430204	-0.57423219390501
O	-1.36208255370579	5.76404890614458	-2.14647902867011

Table A3.40 Continued

C	-1.34830987412383	1.43363464060468	-1.50729646979987
H	-0.30117538754862	1.10137777793722	-1.56154190416800
H	-1.92792087797963	0.81187510865734	-2.20418222773220
H	-1.72461110479210	1.22531213967512	-0.49471550477576
C	-2.99756836398388	3.25279582167755	-1.80099752386039
H	-3.36821381735940	3.11895082891229	-0.77321082348576
H	-3.57743317156033	2.58427482669192	-2.45488903742912
H	-3.18760196522202	4.28747870418012	-2.11004653922519
C	-1.02375548174396	3.05462270498722	-3.34361681905713
H	0.03754720725669	2.77722775723596	-3.43857269439336
H	-1.15006168092093	4.08287980391222	-3.70134669581257
H	-1.60422594849538	2.38676183308003	-3.99738868914026
C	1.46850732150454	3.58955669053593	2.13360910823180
H	2.53692379518685	3.46844109946832	1.87909284051066
H	1.08655287363478	2.59937082953960	2.41562738097636
H	1.42808691158586	4.25100681631858	3.01182203288793

Table A3.41. DFT optimized coordinates for 4-methoxy, 2,6-di-tert-butylphenol cation

H	0.01484383360705	2.26891912280552	0.31627542392194
C	-0.01290218904893	3.33135891260332	0.08138321331512
C	0.73987408837125	4.18680062760866	0.92224872913909
C	-0.73767057029580	3.81733669633566	-0.97537151202012
C	-0.68439626384973	5.24343682874398	-1.18447190943567
C	0.05408927493782	6.14254301658528	-0.33039872507358
C	0.75302980923290	5.58240974942110	0.71260611625017
H	1.32325863725986	6.21568250254307	1.38513135643599
C	-1.56029392640211	2.89766615903768	-1.87827715700174
C	0.06141438197024	7.65278008316972	-0.57341402620972
C	-1.36663198774536	8.21723474104527	-0.46991348415886
C	0.90296660928401	8.37474803724530	0.47694726094223
H	0.50770551306234	8.22705412813733	1.49267715184724
H	0.88433536429354	9.45439469207987	0.27313768590694
H	1.95452472543383	8.05507722999433	0.45789599593507
C	0.68523238523758	7.96897129619872	-1.94520826123910
H	0.14633222272638	7.56465808639778	-2.81493841169887
H	1.71312948223421	7.58353371827164	-2.00234862139041
H	0.72062353694502	9.05910573876956	-2.08028986749571
H	-1.77783327063014	8.04928502419726	0.53615297202160
H	-2.09169904259997	7.79708146261100	-1.18233994639010
H	-1.33876437518880	9.30154490735327	-0.65134692788508
O	-1.35701326828611	5.69616463003542	-2.21717500701388

Table A3.41 Continued

C	-1.44917484194141	1.44577768095890	-1.42037874508969
H	-0.41599245092156	1.07224455046866	-1.46659137205377
H	-2.05508870461719	0.81497039255771	-2.08445173199182
H	-1.82814174820956	1.30179882610564	-0.39788672635930
C	-3.04411206992254	3.28975313896355	-1.81628066507251
H	-3.42878831688746	3.21452953818296	-0.78850552987423
H	-3.62471861958837	2.59658333573697	-2.44133413427729
H	-3.23252148794712	4.30481590578316	-2.18488101733724
C	-1.04643314746057	2.96668690112091	-3.32443518223220
H	0.01061735362571	2.66686193734260	-3.38149638978188
H	-1.14957183572163	3.96394162605879	-3.76819922502849
H	-1.62564839351238	2.26672368367959	-3.94331188637898
O	1.40013984633396	3.58283755225713	1.88370573937637
C	2.21235432923056	4.31631422548504	2.79866808637695
H	2.98940199281637	4.87705740580108	2.26085856924897
H	2.67587031892087	3.56625230871478	3.44815787628988
H	1.59249443277541	4.99831368423687	3.39774082195942
H	-1.27438162752217	6.66097991535490	-2.30757053647674

Table A3.42. DFT optimized coordinates for 4-methoxy, 2,6-di-tert-butylphenol anion

H	0.01935288717710	2.27707424951557	0.30616677132184
C	0.00666124145374	3.34799425904607	0.09550770219130
C	0.74930524071798	4.16644322506217	0.94257610125567
C	-0.72431410932191	3.85822548982636	-0.97402773969784
C	-0.72488506806089	5.28429437313819	-1.23902966893888
C	0.04577052919807	6.11222369264761	-0.33967181034566
C	0.75690110406205	5.53811410467161	0.72055589348670
H	1.32771716566424	6.18163273217394	1.38659236372120
C	-1.53630333963335	2.92190800147687	-1.87708705023037
C	0.08089662698713	7.62866154479967	-0.55910472776461
C	-1.34337827454856	8.19019118913850	-0.47540789827295
C	0.93132476204471	8.36215537977220	0.47565480798527
H	0.54514136523908	8.22841404546348	1.49855133549727
H	0.92402897323339	9.44276574916657	0.26203570629273
H	1.98121538490337	8.03187856943872	0.46437279287258
C	0.66433374083779	7.92789579712024	-1.94578443563799
H	0.08382430469891	7.39427901052091	-2.70870578974981
H	1.71441781054256	7.59920930043692	-2.00648503876213
H	0.63466920993701	9.00940876580689	-2.15944563147649
H	-1.75261233748564	8.06837262746685	0.54053119625229
H	-1.98898490819388	7.65504193048413	-1.18283298098835
H	-1.35714074656877	9.26624616581566	-0.71963587759879
O	-1.38005377363645	5.78347060406974	-2.22687568762717

Table A3.42 Continued

C	-1.43257311136813	1.45819612842160	-1.45712034646451
H	-0.39804311208526	1.08531177421824	-1.49970794447015
H	-2.03522837504805	0.83517199832193	-2.13560874225662
H	-1.81032028926852	1.29129960381879	-0.43667421910573
C	-3.01739074511816	3.31463177647349	-1.82527519862531
H	-3.42120098075703	3.18148922514482	-0.80887170410332
H	-3.61279193313415	2.68608409384598	-2.50738102669296
H	-3.13361082242693	4.36672107463921	-2.11590979365429
C	-1.03367162807716	3.02852225508607	-3.32190127875261
H	0.01021999761134	2.68458084444031	-3.39878244907394
H	-1.08659590568718	4.07244544588621	-3.65641623283240
H	-1.64375385018834	2.40404491797026	-3.99485171376939
O	1.43433383862281	3.52895857720913	1.96323557075663
C	2.20639734513084	4.32097586028908	2.81974892760924
H	2.99023895295135	4.88154590690952	2.27812086076366
H	2.69129449754841	3.64109459223521	3.53445021255844
H	1.59296833204649	5.04759511803123	3.38341474432748

Table A3.43. DFT optimized coordinates for 4-methoxy, 2,6-di-tert-butylphenol

H	0.00674716687880	2.27499678575383	0.30756580447882
C	-0.00685258903972	3.34243985855950	0.09320551318611
C	0.73721830642554	4.16957526423287	0.93176321352448
C	-0.74097490316821	3.84693387071189	-0.97592518519604
C	-0.70493383755950	5.24623894431417	-1.18797585059798
C	0.03112925786544	6.10935377855351	-0.35174196820111
C	0.74739618151976	5.53975135732945	0.70969670188547
H	1.31947838905748	6.18475283692384	1.36891873333612
C	-1.55786959598788	2.90939739783292	-1.87843314390520
C	0.06449275968127	7.63113773084575	-0.57719139507902
C	-1.34774203032276	8.22727777724236	-0.45336237004396
C	0.92521634819814	8.34287000056185	0.46691840068347
H	0.53862100385636	8.19820473380975	1.48647483356959
H	0.92266651634089	9.42446339334935	0.26628880667725
H	1.97114348936602	8.00575593857404	0.44191309828629
C	0.68173670419799	7.96091808528597	-1.94697167990216
H	0.15477388658250	7.52495440939685	-2.80788962196052
H	1.71784087522132	7.59505109202087	-1.99742357230558
H	0.69773285079842	9.05049439966693	-2.09982991441036
H	-1.73926185980526	8.07269418579742	0.56319459522313
H	-2.09033189379874	7.79980081434965	-1.14233508612496
H	-1.31711439443682	9.31097876331867	-0.64569830849836
O	-1.42289874054279	5.71653579683932	-2.24864363165644

Table A3.43 Continued

C	-1.43852216753349	1.45252642229567	-1.43509395110413
H	-0.40209030029121	1.08767849072970	-1.47910081370735
H	-2.03827360659850	0.82019314595055	-2.10517037345093
H	-1.81529072027502	1.29662154079330	-0.41342589943831
C	-3.04577238839015	3.27903396137859	-1.81905989813012
H	-3.43072795858933	3.18382367430231	-0.79233000803581
H	-3.62735664633345	2.59707272563611	-2.45768004052461
H	-3.23112611680439	4.30330274766279	-2.16308431276792
C	-1.05377205233090	2.98445087755550	-3.32577764062941
H	0.00063033666279	2.67417499537841	-3.38877713402265
H	-1.14075791880994	3.99494902607544	-3.74239990254041
H	-1.64031374528810	2.30431384867161	-3.96186608340490
O	1.41558496832116	3.54570076555287	1.93643507615717
C	2.19426895692963	4.33288591059005	2.80423185183843
H	2.97822413126815	4.88892183633327	2.26234243777446
H	2.67293862139697	3.64088095548343	3.50919691164895
H	1.57703632225355	5.05051093719608	3.37122481731304
H	-1.32243360691605	6.67261092314357	-2.30941300994454

Table A3.44. DFT optimized coordinates for 4-methoxy, 2,6-di-tert-butylphenol radical

H	0.02854176890117	2.27141118273098	0.31078171521764
C	-0.00133802657332	3.33607235380010	0.08038971055867
C	0.74461077536827	4.18296034893764	0.92514729616717
C	-0.72730382995767	3.82681711315348	-0.97565986211040
C	-0.71084821547566	5.27616714402376	-1.22612413464621
C	0.06051873504541	6.14230983527073	-0.32407384562856
C	0.75879762504816	5.57103036206882	0.72019547866326
H	1.33138574583646	6.19912700191238	1.39689104362881
C	-1.54427367515394	2.90597052542602	-1.87924535271000
C	0.08365376145184	7.64987694028620	-0.55781521422182
C	-1.34388926861381	8.21066248383105	-0.48931641372201
C	0.92111742823072	8.37777456279593	0.49183452177544
H	0.52195009169489	8.23864653035033	1.50836213642381
H	0.90989510618940	9.45753899824510	0.28219127869636
H	1.97264093377321	8.05445651946992	0.48673825471090
C	0.69161174234607	7.94590105740898	-1.93728405365752
H	0.10685634116926	7.47804259905515	-2.73728239619050
H	1.72685272135563	7.57645584887153	-1.99850971231643
H	0.71110659841071	9.03320313831498	-2.10772286719999
H	-1.78209187405785	8.05471902767092	0.50888887005548
H	-1.99256929702549	7.73627455483437	-1.23396615000247
H	-1.32516646403276	9.29466141129836	-0.68356344241866
O	-1.34052536764338	5.76345858753023	-2.19070172377479

Table A3.44 Continued

C	-1.43373026220353	1.44568580290950	-1.44884626157446
H	-0.39934863844079	1.07481900644290	-1.49791360262087
H	-2.03838537079464	0.82172978422834	-2.12220388163483
H	-1.80969213489733	1.28392936821009	-0.42750603132125
C	-3.02636380163015	3.29973841549263	-1.81499870832273
H	-3.41656576996982	3.19691327363242	-0.79081654283328
H	-3.61576310362908	2.63588414432935	-2.46512047531346
H	-3.18217541454097	4.33322392378075	-2.14624327475880
C	-1.04085914849015	3.00556160124779	-3.32604939200477
H	0.01316182820674	2.69584637116100	-3.39807336994056
H	-1.13228581684616	4.02725922900039	-3.71284611575787
H	-1.63104545749133	2.33720508904755	-3.97091412401788
O	1.41197219720222	3.56291617593654	1.90585027140866
C	2.20566697645366	4.31727536030573	2.80387034687379
H	2.98851317226386	4.87828103693369	2.27096653204219
H	2.67531952003087	3.59096694952175	3.47790576793902
H	1.58820786848926	5.01379634053264	3.39170372453893

Table A3.45. DFT optimized coordinates for 4-methylester, 2,6-di-tert-butylphenol

H	-0.23986124782607	2.52270451346120	0.65877975686123
C	-0.23506669600757	3.56091285595539	0.33456039752247
C	0.40044994430315	4.49181102200039	1.17029737926258
C	-0.82972009629295	3.93679423891631	-0.84880714343953
C	-0.72236975080866	5.34610699184017	-1.18746157620666
C	-0.15564860151168	6.34386558204589	-0.30194686469280
C	0.40823875537006	5.86853586157820	0.85780990212158
H	0.87742085383384	6.55183635850504	1.56039505132128
C	-1.54429672449796	2.94381900996510	-1.74984945455883
C	-0.15926865299605	7.82752076857445	-0.66031797091093
C	-1.58418568947500	8.31690897794841	-0.98823155649691
C	0.33439147244643	8.66591051514811	0.51745433484177
H	-0.30201623946724	8.53560051813409	1.40442402107363
H	0.30401158124002	9.72749528469261	0.23693874021771
H	1.37158861003681	8.43079914734507	0.79287872280187
C	0.79202998248580	8.07528266171095	-1.84510271621784
H	0.52836252193629	7.53295686858141	-2.76617587597215
H	1.82007129082006	7.78610835226737	-1.58527274072763
H	0.78792206263334	9.14616959703784	-2.09416194509835
H	-2.28689189383668	8.06548717999463	-0.18125081942688
H	-2.01525813190558	7.93607075331992	-1.92714024793327
H	-1.56546126112770	9.41064126342767	-1.09370581774832
O	-1.16136388970929	5.67529276769282	-2.36526170611379

Table A3.45 Continued

C	-1.63875189755494	1.57534449739464	-1.07745629379248
H	-0.65069840732391	1.13505858141444	-0.88378095113794
H	-2.17644161859268	0.88817372512918	-1.74463547934669
H	-2.19330163731027	1.61892850377515	-0.12897169364135
C	-2.98032398633014	3.41880546284895	-2.04249544430783
H	-3.53571151608922	3.59184023939261	-1.10926110715730
H	-3.50322365626202	2.63081052095871	-2.60242823251182
H	-3.01617218831058	4.33356402137115	-2.64462520342972
C	-0.75247757656535	2.77341818907770	-3.05995297916451
H	0.25680824327975	2.38602622094180	-2.85750521866051
H	-0.66180700350437	3.70743361080411	-3.62654285792909
H	-1.27466698035688	2.04191323754836	-3.69350588998891
C	1.04010209889773	3.96280578069679	2.41395762848544
H	-1.07243763629256	6.63199719415237	-2.54022487329217
O	0.96463736019914	2.80180806631183	2.74424343279445
O	1.68376591246474	4.90312769853181	3.08760275388587
C	2.31721427738409	4.49506777196389	4.30207032404211
H	2.76980165643635	5.39910687195500	4.72316805052310
H	3.08639059156813	3.73934451738924	4.09367336762516
H	1.57443576461960	4.07584419819920	4.99445879652397

Table A3.46. DFT optimized coordinates for 4-methylester, 2,6-di-tert-butylphenol anion

H	-0.25817892730637	2.54885080336622	0.65203977472279
C	-0.25520167450823	3.59653257049180	0.35155275742064
C	0.37429269676975	4.50024392924694	1.22759264715848
C	-0.84715120738456	3.98471266235316	-0.83184408074053
C	-0.83466482329483	5.39473736842773	-1.20995717801367
C	-0.17522233432675	6.33010007872095	-0.30176245210045
C	0.39688024374311	5.86073466131712	0.86422508165215
H	0.88855013525366	6.55605460417172	1.54255812610870
C	-1.51333501643409	2.95927128770403	-1.75521001605517
C	-0.12338302852334	7.81810122887751	-0.66607373922321
C	-1.54700111170698	8.37599204069284	-0.80232178704423
C	0.59805367690688	8.65351114998159	0.39057747993428
H	0.09457812283789	8.61009433134029	1.36842257624776
H	0.61454065416477	9.70840406359340	0.07598454983441
H	1.64213201101836	8.33663635233981	0.53415427372815
C	0.62459152890300	7.99900112686983	-1.99357794230077
H	0.13024967581870	7.42874937214564	-2.78945469998045
H	1.66499500734353	7.64850938936579	-1.90634711877662
H	0.64919817523310	9.06253106786590	-2.28246229214906
H	-2.07721929127471	8.32983416440724	0.16161550207845
H	-2.11338797799443	7.79910786535833	-1.54307794056100
H	-1.51961283038878	9.43083598725175	-1.12313622832960
O	-1.37371732297218	5.79016577421311	-2.28439522517899

Table A3.46 Continued

C	-1.43933267781367	1.54024784673634	-1.19549987156055
H	-0.40254928884951	1.19781962418938	-1.06067924458648
H	-1.92935202938212	0.84439507580172	-1.89360416925967
H	-1.95287413893899	1.45206512556658	-0.22669384140758
C	-2.99738380800377	3.30137955810489	-1.93990085733967
H	-3.53164027004056	3.23838282895275	-0.97931254706276
H	-3.47323804828029	2.59373641638113	-2.63780927573295
H	-3.11141225095258	4.31700889167537	-2.33800612804168
C	-0.81033639878991	2.95591258860806	-3.11901027466852
H	0.23780266894996	2.63391133837514	-3.01535782807552
H	-0.82729487484385	3.95874540751703	-3.56353401009442
H	-1.31024985366098	2.25657266160981	-3.80892361643584
C	0.95518395708310	3.99060789250751	2.45263089255737
O	0.94708065240086	2.82141876883015	2.82187897571534
O	1.54292124070729	4.95046820273651	3.21753682556546
C	2.10580369735499	4.51157340955815	4.43926495917705
H	2.51786967438791	5.40498762964404	4.92589329813908
H	2.90851090558100	3.77772719963701	4.27277925565758
H	1.34571446121363	4.05145765346571	5.08869538902171

Table A3.47. DFT optimized coordinates for 4-methylester, 2,6-di-tert-butylphenol

H	-0.25837400580632	2.54595502157981	0.65312632827376
C	-0.24204117826482	3.58888947576791	0.34453477276137
C	0.38495974806548	4.49728743284992	1.19802282763933
C	-0.82556248169185	3.97539507317822	-0.85470435602837
C	-0.74967494031771	5.35077129091002	-1.18872117427928
C	-0.15427688325646	6.31332970333353	-0.33444078821631
C	0.41114279980628	5.84784911589286	0.84988944815713
H	0.88893036032259	6.54681807530174	1.53085128528724
C	-1.51446817123863	2.95034242170693	-1.76568821110148
C	-0.12704845578488	7.81045109123887	-0.68732050693389
C	-1.55676160870672	8.35610310231506	-0.85311598504553
C	0.52381509500553	8.63596956815562	0.42354284380859
H	-0.02062665874054	8.54638954497353	1.37448143070777
H	0.51673145407723	9.69753513715129	0.13724069679989
H	1.57062986929448	8.34881754645629	0.59652729728994
C	0.70197200944404	8.05476349138504	-1.95937697116706
H	0.32340835181050	7.55102818800260	-2.86113752636855
H	1.73658247453238	7.71012640392144	-1.81740302903909
H	0.72906550394574	9.13070382840560	-2.18779085268646
H	-2.11514149526368	8.25793231901800	0.08905620635932
H	-2.15554347452292	7.85540851927571	-1.62745455231744
H	-1.52213456475563	9.42358324452641	-1.11886494468407
O	-1.27989714752864	5.70299285098554	-2.37964242405251

Table A3.47 Continued

C	-1.51726564159286	1.55766917809752	-1.13518937137760
H	-0.50167821903524	1.17189505358243	-0.96686366564014
H	-2.02625285508364	0.85694501193584	-1.81278830287024
H	-2.05515605604525	1.53980120699508	-0.17641123695204
C	-2.98161534164891	3.33955444248735	-1.99900838485883
H	-3.52531557350632	3.39260789292221	-1.04412614326124
H	-3.47357161001583	2.57874226588069	-2.62358333161481
H	-3.08163007721482	4.30580709161183	-2.50621784832391
C	-0.76793929965114	2.84555440114143	-3.10293023995693
H	0.26358654291011	2.49521016473639	-2.94505872275283
H	-0.72937513619002	3.80507278539630	-3.63169238167887
H	-1.27306305628990	2.11720389085433	-3.75580234636828
C	0.98265708469792	3.97907520617931	2.44302379382766
H	-1.16898011186192	6.65003456835991	-2.52760936118716
O	0.94785628010038	2.81474744418630	2.79106578407326
O	1.58203864997500	4.92975400565695	3.17475314675859
C	2.16563237841021	4.50434036468951	4.39976815869004
H	2.58714938249529	5.40366871921481	4.86402900102572
H	2.95938416842793	3.76558506185553	4.22047878733114
H	1.40807189069358	4.05733879788435	5.05919084997214

Table A3.48. 4 DFT optimized coordinates for -methylester, 2,6-di-tert-butylphenol radical

H	-0.24406944372832	2.53981093399565	0.66152421647904
C	-0.25407931362607	3.58114657905649	0.34506330897935
C	0.36453629265018	4.51056713932963	1.19883761359188
C	-0.84959770825905	3.95880537744969	-0.83583826521784
C	-0.82446534003926	5.38933225467426	-1.19600999582611
C	-0.16767411465130	6.35527143264416	-0.29194974154975
C	0.40030020308966	5.87737947377490	0.86881125499507
H	0.89292565562091	6.55631410588162	1.56051510420538
C	-1.51790662245816	2.94733546393040	-1.75742216615693
C	-0.12324518692016	7.83257481144240	-0.66196807216763
C	-1.55057409488701	8.38450939940332	-0.80967922099740
C	0.58792701384779	8.66166101042206	0.40683286736541
H	0.07466104350941	8.61325784486748	1.37866724939423
H	0.60121999610840	9.71609194433824	0.09558193023821
H	1.63259238203161	8.35009309271461	0.55329618940655
C	0.64130525769027	8.00864185607582	-1.98413217581376
H	0.14060639410853	7.48993282301966	-2.80984456572320
H	1.66863089669787	7.62309055380959	-1.90072314723206
H	0.70215870662796	9.07893794832672	-2.23303574083007
H	-2.10043616721260	8.30906152859238	0.14041521456155
H	-2.11129459269976	7.84965457162928	-1.58420334853738
H	-1.50463794067285	9.44844975001254	-1.08938294216839
O	-1.35130524455642	5.77841425775348	-2.25291896895159

Table A3.48 Continued

C	-1.44623291142524	1.53298595315434	-1.18526664754489
H	-0.41081584614579	1.18755523040461	-1.05231150474633
H	-1.93855573355190	0.83795728251078	-1.88021984559457
H	-1.96288531099877	1.45313044967017	-0.21805174438023
C	-3.00256896309220	3.30018870717170	-1.93769226857127
H	-3.52679255803338	3.28866244075331	-0.97070162667780
H	-3.48059855220184	2.55314109413923	-2.58864012661889
H	-3.13260046839810	4.28775250533406	-2.39480814191739
C	-0.80696410511759	2.93884888356615	-3.12007196975890
H	0.24745625752097	2.64316935600282	-3.01031374482141
H	-0.84746912071412	3.92107252960903	-3.60533612597923
H	-1.29381435622016	2.20660833798805	-3.78187485625737
C	0.96082809484270	3.98604550998333	2.45287521806830
O	0.92526932952684	2.81782484842895	2.77999744468628
O	1.53806529797881	4.93586054324199	3.19063738891317
C	2.11067516860600	4.51337399463093	4.42458914707220
H	2.51646272428219	5.41622512260132	4.89481906399147
H	2.91243717981057	3.78250275396868	4.25025118418802
H	1.34573580105937	4.05789030369618	5.06913255790430

Table A3.49. DFT optimized coordinates for 4-bromo, 2,6-di-tert-butylphenol cation

H	-0.47485294168113	2.51991947362808	0.69535351969790
C	-0.42550472948961	3.55830683107159	0.37657212433565
C	0.16194604322963	4.49751309268206	1.24038904242309
C	-0.93133900551733	3.94191884948914	-0.84416081690638
C	-0.80358621172150	5.34362854194553	-1.17936267846595
C	-0.23362021259529	6.32947322533490	-0.28962087679010
C	0.24639825623488	5.86498119075598	0.91215431695404
H	0.69978529101783	6.54401063186505	1.63017704692681
C	-1.58834876551623	2.94005254201190	-1.78677084774108
C	-0.16744623719704	7.81053941009507	-0.66380727631583
C	-1.58464678091258	8.36246371767051	-0.90747454941347
C	0.44729617767849	8.63089830114548	0.46920152425860
H	-0.14293867038884	8.56299770617947	1.39400825823052
H	0.47216578592633	9.68782601800284	0.17124465200745
H	1.48070058632257	8.32756772631784	0.68844126908513
C	0.72256839818469	8.01135109022594	-1.90411507733743
H	0.35094960818346	7.54669645331747	-2.83023214022176
H	1.73314929404483	7.61575364353828	-1.72987708589561
H	0.80655953775208	9.08708630033216	-2.11314724998644
H	-2.20255680859519	8.25917895164483	-0.00440028679647
H	-2.13702248506451	7.88512443031427	-1.73043818213279
H	-1.51612325576141	9.43141808045230	-1.15517718625718
O	-1.24008309970875	5.68348643650049	-2.36289986175510

Table A3.49 Continued

C	-1.65128700208347	1.55264964136328	-1.15019176577163
H	-0.65330178603075	1.14768656790091	-0.93003903257222
H	-2.13427885560848	0.86187117338219	-1.85470456361718
H	-2.24406684228376	1.54608204699978	-0.22413036034150
C	-3.03234989126839	3.37337162052692	-2.09558926872232
H	-3.61571284015891	3.48177981661948	-1.16982625979023
H	-3.51271234968181	2.59575457080853	-2.70628776886417
H	-3.08619533517789	4.31459049257257	-2.65416762077620
C	-0.76478223841989	2.82197452682964	-3.08045851360089
H	0.25180804926255	2.46181959884584	-2.86374026797961
H	-0.69064311743664	3.76910416886209	-3.62669484640684
H	-1.24786381645642	2.08818123348521	-3.74193721857767
H	-1.12120065336923	6.63445255815937	-2.53852976875682
Br	0.83105690428771	3.92319933912300	2.85548961787367

Table A3.50. DFT optimized coordinates for 4-bromo, 2,6-di-tert-butylphenol anion

H	-0.50769088997581	2.54630052351438	0.71790175732188
C	-0.45734229010845	3.59177911658823	0.41485424390543
C	0.11876562060080	4.50826096871021	1.28621337084781
C	-0.96350921744354	3.99139046036586	-0.81869685856096
C	-0.89193213661797	5.38670346856914	-1.21534390326096
C	-0.28294842031576	6.31417756565650	-0.27719804861922
C	0.20508039335531	5.85229589634308	0.94251875586147
H	0.66570979761125	6.54266373049818	1.64839238879348
C	-1.58579361842644	2.96234168124668	-1.76898155521511
C	-0.17296227579350	7.79837975837530	-0.64559191315600
C	-1.57436632808422	8.37746741367688	-0.88498718171515
C	0.49161251438950	8.63109650699368	0.44945714208167
H	-0.07710557135711	8.60937649040301	1.39156705640986
H	0.55241557308806	9.68171097750089	0.12606002148347
H	1.51705489363818	8.29505874321816	0.66575022805882
C	0.66797120363926	7.94943306439378	-1.92003447806579
H	0.22256898691364	7.36367915391048	-2.73372869099441
H	1.69706156263194	7.59397529363643	-1.75294939797026
H	0.72150493561609	9.00665707921790	-2.22848762470562
H	-2.16660628740748	8.35779889671881	0.04312168546140
H	-2.09631962842850	7.78908432775710	-1.64973034832462
H	-1.51095040704653	9.42535241978157	-1.22358981001688
O	-1.34392702171002	5.78154836819416	-2.34209509719245

Table A3.50 Continued

C	-1.59931487147749	1.55074263112385	-1.18564069339848
H	-0.58727996125847	1.17757143796055	-0.96825858990942
H	-2.05530678167939	0.85925587143020	-1.91109472041744
H	-2.18900430922334	1.49173238873662	-0.25852668947355
C	-3.03981283928672	3.34451184157007	-2.07680400492515
H	-3.65062693661515	3.31164639992406	-1.16115286965186
H	-3.48050864166286	2.64233094573733	-2.80325498512926
H	-3.08199268048251	4.35853245586285	-2.49340978082336
C	-0.77573985222903	2.91813427515056	-3.07152160386627
H	0.24746935630529	2.55841316809502	-2.87871112129473
H	-0.71987148056078	3.91997516048151	-3.51523615977983
H	-1.24325861717187	2.23240097299256	-3.79744048520386
Br	0.79582622657360	3.91151054566437	2.96652996144533

Table A3.51. DFT optimized coordinates for 4-bromo, 2,6-di-tert-butylphenol

H	-0.49962305089147	2.54297128703556	0.70492323487913
C	-0.44019284113722	3.58437264166744	0.39785126659121
C	0.13478239402389	4.50493511113653	1.26062400788076
C	-0.93921723862493	3.97839579930473	-0.84371392155184
C	-0.82504425486496	5.34673736770336	-1.18570577358122
C	-0.25723680622250	6.30275349439692	-0.31060264106683
C	0.22323426322419	5.84447467094936	0.91899621361976
H	0.67417205512390	6.53831384408729	1.62393831773346
C	-1.58349668780368	2.95039997250928	-1.78524670217780
C	-0.16484671304819	7.79589175351609	-0.67209514545928
C	-1.56947022696098	8.38082519257265	-0.90067566205916
C	0.46823889382810	8.61081490281303	0.45698758394871
H	-0.11593253916717	8.55212733896384	1.38631360570046
H	0.50915661549048	9.66851758717496	0.15968236858567
H	1.49688066565679	8.29022411360958	0.67444198855619
C	0.72386427549446	8.00354526946974	-1.91013926642191
H	0.35504420685427	7.52474977353055	-2.82917537877962
H	1.73413595951770	7.60796643915485	-1.73063225979945
H	0.81275120984065	9.07784555720793	-2.13000201327476
H	-2.16393855939341	8.31781198852706	0.02217695004994
H	-2.15219742691106	7.87883480469975	-1.68629851938144
H	-1.49452344366072	9.44132011325713	-1.18578843870031
O	-1.29457392568300	5.70025580462190	-2.40906726813090

Table A3.51 Continued

C	-1.62256774676292	1.55664003208658	-1.15774356719326
H	-0.61803402808005	1.16885213898764	-0.93562889001932
H	-2.09342407210827	0.85837924908169	-1.86496487184581
H	-2.21340197716025	1.53415179298036	-0.23059260238741
C	-3.03547991902125	3.34494535750360	-2.09163032757678
H	-3.62712043932402	3.39418349538605	-1.16542417048046
H	-3.49695432173660	2.58999628920070	-2.74612659610359
H	-3.10538040829450	4.31518431633658	-2.59654460567493
C	-0.76952650003238	2.84208023056062	-3.08204508061042
H	0.25082702213051	2.48777762627543	-2.86971003344573
H	-0.69895677819853	3.80100563469494	-3.60823199508496
H	-1.24266714441458	2.11521202946485	-3.76027431671699
H	-1.15948795339420	6.64363996327319	-2.55492431566478
Br	0.80212744171188	3.91857701625824	2.93229882564368

Table A3.52. DFT optimized coordinates for 4-bromo, 2,6-di-tert-butylphenol radical

H	-0.49545309197569	2.53373868385690	0.71622235159396
C	-0.45732981474251	3.57366897044174	0.39776612554075
C	0.12051711655824	4.51276612981784	1.26197672688015
C	-0.96563897363740	3.95937644014815	-0.82328786215900
C	-0.88307924485804	5.38039506193004	-1.19989053514592
C	-0.27057086755597	6.34128119535992	-0.26649290218875
C	0.21247334161458	5.87267934305207	0.93645522456009
H	0.67573842075659	6.54634577423636	1.65442808655018
C	-1.59234058084743	2.94742074155901	-1.77549838590590
C	-0.17161731279604	7.81537423322658	-0.64431078512366
C	-1.57680313717086	8.38927274496382	-0.88726132768396
C	0.48582635261255	8.64040561559956	0.46107512199902
H	-0.08865392443018	8.61143722405120	1.39874058424454
H	0.54141096968238	9.69125415070520	0.14271065432962
H	1.51265701504972	8.30939072582275	0.67541857546696
C	0.68029676679134	7.96598977456964	-1.91458599994139
H	0.23088337774823	7.43956708617100	-2.76441201208134
H	1.69636850752776	7.57339836224989	-1.75691461483631
H	0.76786327609112	9.03194633412085	-2.17433501668444
H	-2.18867323446778	8.32821077461385	0.02532913053332
H	-2.09362169407014	7.85592007347192	-1.69301409092913
H	-1.49788163089318	9.45057253645146	-1.16983575509378
O	-1.32723952238471	5.76719212997770	-2.29808318042567

Table A3.52 Continued

C	-1.60830831791477	1.54097566963887	-1.17968866427862
H	-0.59705691332625	1.16621587484517	-0.96477045080237
H	-2.06620273552465	0.84978811047730	-1.90181042485763
H	-2.19997952820002	1.48979099821780	-0.25409763029463
C	-3.04719398444515	3.33915835350622	-2.07815013101127
H	-3.64433259802621	3.36591562039942	-1.15452787523318
H	-3.49712147632552	2.59256167799828	-2.74968098292653
H	-3.10885464781891	4.31971530451149	-2.56347312724655
C	-0.77465748086487	2.89564845207643	-3.07602193944539
H	0.25434229018882	2.55958048324148	-2.87622967092970
H	-0.73532759856457	3.87471923872936	-3.56715128924100
H	-1.23443665373025	2.17684874655099	-3.77140485984273
Br	0.79286752994978	3.92476736340969	2.90470693261026

Table A3.53 DFT optimized coordinates for 4b (AdLCoO)

Co	0.01391851416718	0.00013979036398	0.00482111587693
O	0.66148355492028	0.01547307999176	1.51886496014820
C	0.76853828817811	-1.32864932296655	-1.09257602366909
N	1.35817292187306	-2.53218619574687	-0.82784808471141
C	1.70941223282540	-3.11806012397480	0.49025931188577
C	2.75551904365815	-2.24109586099126	1.18633541202753
H	3.65008619798443	-2.17531128064058	0.54545980051653
H	2.33814163008445	-1.23174654264841	1.31394459957945
C	0.46189689794304	-3.24375332987601	1.36701930193382
H	0.02355538030311	-2.24886410814894	1.50410396838233
H	-0.27887870868239	-3.87891254724471	0.85482169223558
C	2.30445444836084	-4.52102157741700	0.31057542408328
H	1.58366898067402	-5.17856760391932	-0.20125011365845
H	3.21106157396751	-4.47382872579739	-0.31219547064125
C	3.11438711631526	-2.83920380425770	2.54639642879513
H	3.85332991780546	-2.18397246056105	3.03633466462272
C	0.83120558263294	-3.83266263356774	2.72696786666634
H	-0.08019838924378	-3.89264235237520	3.34437638849141

Table A3.53 Continued

C	2.66928926013590	-5.12125327332929	1.66942453332556
H	3.09237418189752	-6.12484103473823	1.50039435417021
C	3.70320427079540	-4.23445989938557	2.35945378826193
H	4.62414712418130	-4.18377685234705	1.75528353365366
H	3.98372275836291	-4.66852576394237	3.33317911137338
C	1.85504381233028	-2.92476991808707	3.40830980516288
H	1.42986494220905	-1.91867858302932	3.54558370475458
H	2.10316550806970	-3.31927543258699	4.40742289286005
C	1.42087691720398	-5.22669756343017	2.53997497336807
H	0.68101812167177	-5.89392792956560	2.06740665857932
H	1.67575493951531	-5.67131879403961	3.51580933525559
C	1.64398822612930	-3.16367748880102	-2.02036664604030
H	2.10471349901211	-4.13921095858640	-2.07652151837629
C	1.24400982715205	-2.34138182901987	-3.01889557612183
H	1.27714336483493	-2.48946590043823	-4.09171646923227
N	0.73141908205737	-1.21626650766066	-2.43522064455913
C	-1.53287028902828	-0.09045023217550	-1.15689215194175
N	-2.85399759681834	-0.26722903267255	-0.88019757764289

Table A3.53 Continued

C	-3.46262853214967	-0.24591509959306	0.46193718630162
C	-3.14643747940612	1.08806638324156	1.14443520341046
H	-2.05501286273123	1.21398765828041	1.19890265257820
H	-3.54021336469381	1.91327248209011	0.52879114360097
C	-4.98368960854142	-0.39678822895138	0.37706030968522
H	-5.40981807727987	0.41654649223875	-0.23088063996714
H	-5.24375046168145	-1.34859044309117	-0.11206370085628
C	-2.90811443817932	-1.39377615263103	1.30864180633325
H	-3.12786649845843	-2.35265732570489	0.80998142432729
H	-1.81482439375967	-1.29766261854690	1.36808212879575
C	-3.74985804366716	1.12093161089036	2.54663070775973
H	-3.49947209273061	2.08504066883162	3.01981254006430
C	-5.59260319258150	-0.36238574159467	1.77912426586138
H	-6.68449184934919	-0.47297227850187	1.68555644745519
C	-3.51269096408833	-1.35776452528641	2.71052160408127
H	-3.08973620750646	-2.18723589787839	3.30058775801429
C	-3.16994749319889	-0.02504953056907	3.37510772331727
H	-2.07706211157499	0.08453345884825	3.46108445503340

Table A3.53 Continued

H	-3.58000713932279	0.00367880458945	4.39739974769257
C	-5.26513251456478	0.96966627664547	2.44951933105180
H	-5.69512230375497	1.80284869306098	1.86946263702327
H	-5.72043298633723	1.00990208642759	3.45231955153450
C	-5.02783296524632	-1.50984508416642	2.61303099836682
H	-5.28326814825816	-2.47746731131127	2.15024498412499
H	-5.48107579171314	-1.50644326886598	3.61736785700599
C	-3.55257340079738	-0.44744583718399	-2.05531221153460
H	-4.61942339748526	-0.62303435736692	-2.09104425907720
C	-2.65222047853219	-0.36257050255032	-3.06660208163873
H	-2.80462696127211	-0.47844405797717	-4.13335198420433
N	-1.43040447810123	-0.11626954679840	-2.49807445438827
C	0.63045297180007	1.39423284688466	-1.06233684401052
N	1.18160398761995	2.61480964088986	-0.80230535164646
C	1.44812253414587	3.23907112396286	0.51665798687769
C	1.91505148024804	4.68912013247299	0.33562994505228
H	2.83996046959058	4.72125027897605	-0.25988290645372
H	1.15157383946271	5.27086937790791	-0.20536949424145

Table A3.53 Continued

C	0.17222012861263	3.25325065562411	1.36179881407988
H	-0.61158077137505	3.81256633912015	0.82607055621419
H	-0.17412732590413	2.22154948229117	1.49643447930608
C	2.55064970297038	2.46600949618001	1.24729569703605
H	2.22161716686839	1.42403702371732	1.37592093342106
H	3.46428709549871	2.47260676101766	0.63011297182633
C	2.18627379493202	5.33199579581024	1.69702209153424
H	2.51834221141571	6.36942461941493	1.52968945303359
C	0.45027939620028	3.88486317979848	2.72471368125553
H	-0.47805649850361	3.86454638050086	3.31877094017003
C	2.81914076433444	3.10740422327402	2.60841217625032
H	3.60361360568803	2.52878486915866	3.12326101200395
C	3.27999172898090	4.54984416502698	2.42016425882543
H	4.21537005415768	4.57706423067713	1.83724116586161
H	3.49647657948124	5.01512776278471	3.39598476962226
C	0.91217113536949	5.32655833345934	2.53659976383125
H	0.12510509046142	5.91749232729574	2.03970283143514
H	1.10003526118608	5.80229563588682	3.51329658795207

Table A3.53 Continued

C	1.53687726064689	3.08235086455199	3.43990876488099
H	1.20411231648268	2.04190593935680	3.57831353290233
H	1.72358080691045	3.50673394525200	4.44026924408638
C	1.51073779751135	3.21970689446520	-1.99931105599662
H	1.96485854310116	4.19822424927636	-2.05962929545040
C	1.15863147674411	2.36871038827561	-2.99212635359630
H	1.25013128923859	2.47098157516216	-4.06762290016827
N	0.61828196877482	1.26112707032792	-2.39822156957101
B	0.00718134590246	0.00395188104088	-3.07566931782395
C	0.15056623738808	0.14966058934366	-4.67317301425050
C	-0.83201568375225	0.77359268065850	-5.45845574985914
H	-1.75908302704006	1.11916892861210	-4.99839104500920
C	-0.65765095319255	1.00468890363857	-6.82179439643248
H	-1.45305910068818	1.48849475652049	-7.39498869218063
C	0.52721905432085	0.63141750173995	-7.44910752368073
H	0.66924150589436	0.81078871359840	-8.51791565778886
C	1.53729835225683	0.04558391817559	-6.69094264633947
H	2.48516901654358	-0.23133619926161	-7.15996282671587

Table A3.53 Continued

C	1.34836612876601	-0.18082346705966	-5.32937266980402
H	2.17790636443331	-0.60985802876960	-4.76307882760765

Table A3.54. DFT optimized coordinates for 5b ([AdLCoOH]+)

Co	0.42361378346207	-0.01426914106443	0.00045933262991
O	1.67746983099114	-0.24492147732357	1.23997741472855
H	2.57472672657879	-0.44327178265274	0.94825321671126
C	0.74374035598936	-1.48139413432627	-1.07740600166427
N	1.02700808923983	-2.78762826006672	-0.83328685592029
C	1.00208122632460	-3.55588261721702	0.43982026163091
C	2.38224114739018	-3.55396455418389	1.10617463445545
H	3.12154949356611	-3.98965099967163	0.41523829895845
H	2.68891373542660	-2.51971232762312	1.31217145336226
C	-0.03684203814552	-2.97032949303765	1.39346024024778
H	0.23823749531855	-1.93503523340821	1.62768535154389
H	-1.02374445239230	-2.97786566151700	0.90480830984942
C	0.60620474308030	-5.01300085199966	0.15152418533237
H	-0.36858607419053	-5.03706822514805	-0.36014395213637
H	1.34086837568317	-5.49048655999012	-0.51145261376416
C	2.32897113563120	-4.35772992927161	2.40742959161938
H	3.32616136322897	-4.33447785245798	2.87516308874382
C	-0.07851988699131	-3.76973249949691	2.69649048321432

Table A3.54 Continued

H	-0.82050399485297	-3.30611558078434	3.36651979373195
C	0.55252942038417	-5.81675948860177	1.45065310148650
H	0.26965596222855	-6.85199631555489	1.20292868967817
C	1.93215282556171	-5.80078459586316	2.10623530186334
H	2.67550594080154	-6.27106893397807	1.44140625918346
H	1.91590899137868	-6.39116376279593	3.03600118271826
C	1.30177968066398	-3.73528581234410	3.35173634240995
H	1.58397411815166	-2.69733017031381	3.59090375240720
H	1.28107054623417	-4.28867658835577	4.30356660593263
C	-0.47713720206493	-5.20991275654907	2.39634472746591
H	-1.47970226267536	-5.23846160420758	1.93914672521551
H	-0.53087749829952	-5.79495723665825	3.32786015624096
C	1.27960590118106	-3.40080626900374	-2.04454202533762
H	1.55286444741925	-4.44353654616132	-2.12280539939892
C	1.11360488703403	-2.47399717722689	-3.01701681640825
H	1.20691830761333	-2.55906690706765	-4.09387528781975
N	0.76700002370134	-1.30544106105633	-2.39994042926091
C	-1.14984233544238	0.28346278582118	-1.02832233703473

Table A3.54 Continued

N	-2.40976116933803	0.62640982091454	-0.67724479024096
C	-2.98725474570842	0.65495126275860	0.67299067396804
C	-3.54185589041705	2.05063604444191	0.98444683865908
H	-2.73112157147802	2.79314916038381	0.90965673980416
H	-4.30222540371680	2.32683038417524	0.23906476314797
C	-4.12105548210566	-0.37528527996449	0.76701803255736
H	-4.89475676370273	-0.14561823809262	0.02025294684368
H	-3.72580796063810	-1.37615123510630	0.52905042113645
C	-1.92741574039184	0.30647682147304	1.71049261753989
H	-1.52547287015894	-0.69594355871511	1.50025539861728
H	-1.10297277724713	1.03583903089684	1.65845147419595
C	-4.15514827099215	2.06420562891761	2.38518535687110
H	-4.55192409849449	3.07180681882036	2.58612687641381
C	-4.72950848155638	-0.35443734281514	2.16842621407613
H	-5.54172109776047	-1.09682165289682	2.21109664191251
C	-2.52965437741592	0.32502724737880	3.11722733615004
H	-1.73976795804754	0.07141828734530	3.84066221703207
C	-3.08240557706225	1.71707363061344	3.41411741184318

Table A3.54 Continued

H	-2.27246740123664	2.46441695117684	3.39108792286125
H	-3.50794537975468	1.74060133350085	4.42983104589152
C	-5.28498187278033	1.03870476530832	2.45741544911817
H	-6.07381228457552	1.29046181856414	1.73030957020275
H	-5.75178115868138	1.06123046084244	3.45474563578279
C	-3.65549703234284	-0.70359235022346	3.19464480966219
H	-3.26318257346376	-1.71661071846926	3.00640493669659
H	-4.08560384602304	-0.71255063947758	4.20844731283349
C	-3.13941819222355	0.90528291293060	-1.81083672690123
H	-4.17832943961500	1.21150648587490	-1.78009698587016
C	-2.30925699818298	0.71676177017494	-2.86907968996291
H	-2.49950523419569	0.86033624001551	-3.92615420876940
N	-1.10118895242430	0.31128686595547	-2.37175768587701
C	1.22795364625690	1.25948396617152	-1.09782346878903
N	1.83692477017042	2.44506269643276	-0.82574092761763
C	2.07483970509405	3.11953588207043	0.47766621715155
C	2.22593161950399	4.63302967273789	0.26122144137642
H	3.09662308134307	4.84468725334619	-0.37541653063088

Table A3.54 Continued

H	1.33447353774506	5.03020823830410	-0.24851812785012
C	0.88200915783736	2.89733455352100	1.40440047564241
H	-0.03264087472352	3.27132379602648	0.91892320942948
H	0.77139981395596	1.82096484217758	1.58705452115091
C	3.35732836803806	2.60313934472181	1.13851659380218
H	3.27718343875554	1.52031981287508	1.29465997316372
H	4.20993445117282	2.78499318443717	0.46494746202505
C	2.43736948230143	5.34393000845621	1.59816589310612
H	2.53886473138770	6.42229380107671	1.40021806399114
C	1.10665909090937	3.59502713082780	2.74546193636593
H	0.24015162795260	3.39287401576720	3.39489329323009
C	3.57097271702502	3.31224549225752	2.47702703564628
H	4.48913698026905	2.91602235631405	2.93940811510576
C	3.71224232506393	4.81462700016239	2.24944235059785
H	4.58209713856496	5.02105572540099	1.60456879398732
H	3.89337920621395	5.33010405077631	3.20608955153521
C	1.24551431105917	5.09582918383883	2.51613257680447
H	0.32483820694308	5.50070104879625	2.06539651310481

Table A3.54 Continued

H	1.38832199097046	5.61758863692698	3.47570419501995
C	2.37705864302371	3.04568806272962	3.39278582643009
H	2.27184133170021	1.96462476376679	3.57700202514867
H	2.53772985108943	3.52382681197460	4.37217801071036
C	2.17679286674369	3.03784183102891	-2.02349800904827
H	2.68570573819888	3.98893905598843	-2.08227587141516
C	1.75749078682058	2.22160584476708	-3.01810922257060
H	1.81304783386473	2.35318614042806	-4.09193024168359
N	1.18149032138735	1.13097930398756	-2.43059181349300
B	0.28259509488288	0.02011382763137	-3.04627222340901
C	0.30746585911632	-0.12005243782276	-4.64224340094629
C	1.48900817269003	0.09082361771518	-5.37249072072516
H	2.39782543585723	0.41879527383161	-4.86305919585301
C	1.55998553275410	-0.13362205940088	-6.74550635892150
H	2.49770400023191	0.04902857098525	-7.27661580877474
C	0.44399229615840	-0.59705981324404	-7.43645254225025
H	0.49395333695195	-0.77366606682772	-8.51378669122775
C	-0.72980916036468	-0.85304182311890	-6.73394264114741

Table A3.54 Continued

H	-1.60769932865853	-1.24286027021850	-7.25542040894601
C	-0.78814169816281	-0.62463643255110	-5.36085004228830
H	-1.71488764557377	-0.87821900061847	-4.84308516575019

Table A3.55. DFT optimized coordinates for [AdLCo^{II}O]$^{-}$

Co	0.03118273307228	0.01062538992094	0.02933232467182
O	0.85412022142837	0.05721974186413	1.53442588923329
C	0.78587424175974	-1.41721166704363	-1.06612010227455
N	1.39309595418882	-2.62954037948532	-0.86880222581094
C	1.70303212526054	-3.22439981223268	0.44245027058803
C	2.71801007148573	-2.34348022585986	1.17717027490610
H	3.63210497175151	-2.26146081851965	0.56448533383064
H	2.25757463718814	-1.34046906681283	1.29635994983345
C	0.43117647694668	-3.31457926465758	1.28728614474434
H	0.03746450948361	-2.29474454740398	1.39904187661740
H	-0.31940167609231	-3.92410214892416	0.75723340186761
C	2.28711125997012	-4.63136865000100	0.28271450797020
H	1.57662969696699	-5.28329460450392	-0.25219121636499
H	3.21297321250093	-4.59403639294106	-0.31293178459058
C	3.04139224387494	-2.94597650005751	2.54302417442273
H	3.77291251997849	-2.29815801709931	3.05523793549712
C	0.74577076073748	-3.91142074235185	2.65636484406174
H	-0.18488545790740	-3.96179853454970	3.24661580233990

Table A3.55 Continued

C	2.60171626750015	-5.22848424553258	1.65558332819251
H	3.01912832443066	-6.23908944104404	1.51110375857641
C	3.62183244835052	-4.34804583394275	2.37559704612422
H	4.56065596166268	-4.30683884718592	1.79807891230391
H	3.86997178306150	-4.78509280139547	3.35781005997084
C	1.75783252717200	-3.01572831844064	3.36970389736023
H	1.34078271857376	-2.00266007555450	3.47739574802507
H	1.96969054475012	-3.40885028101800	4.37880648717489
C	1.32426164663037	-5.31380281220951	2.48737934802663
H	0.59096584925826	-5.97141166025178	1.99075573049025
H	1.54277308260401	-5.76293646478046	3.47096236244455
C	1.70860354214121	-3.21295442255393	-2.07916048821669
H	2.18202188624715	-4.18140882673009	-2.17292409328150
C	1.30691511244481	-2.34915706365750	-3.04395173162944
H	1.35644719257452	-2.45750668843792	-4.12148053209442
N	0.77163414787040	-1.25251488502811	-2.41631656189581
C	-1.49388293146905	-0.09865605940078	-1.09916142404556
N	-2.83046385150931	-0.28566539586063	-0.84381060545733

Table A3.55 Continued

C	-3.43369552343357	-0.25586134798683	0.49193505535053
C	-3.13767950799174	1.09428092058011	1.15357038893040
H	-2.04546382070417	1.23206118204127	1.18273770667277
H	-3.55474138258127	1.90174157968034	0.52882087311302
C	-4.95150035892719	-0.44065470004390	0.42629399205188
H	-5.40270185854506	0.35240212376583	-0.19112932099759
H	-5.19674994245826	-1.40563733582858	-0.04561534427931
C	-2.84560573235914	-1.37403503114680	1.35688352388869
H	-3.04845393566206	-2.34687987858411	0.87739408065942
H	-1.75269917262361	-1.24581237905618	1.39209044743620
C	-3.72807141525774	1.13993411737056	2.55971234276834
H	-3.49480598799234	2.11696149046123	3.01623097234100
C	-5.54667227580855	-0.39536911664541	1.83452928881874
H	-6.63774472990303	-0.53076355423039	1.75707265127677
C	-3.43616822092289	-1.32900068086481	2.76288727915752
H	-2.98999964509191	-2.13858045605425	3.36417124624712
C	-3.11406597866786	0.02153835123108	3.40099387767438
H	-2.02235564454437	0.15526546595493	3.46157955594368

Table A3.55 Continued

H	-3.50973794444316	0.05985852708852	4.42955388451228
C	-5.24100859276459	0.95416735055563	2.48099295280883
H	-5.69411392701238	1.76814699473818	1.89078357406976
H	-5.68961536388668	1.00064492730231	3.48737827715475
C	-4.94886243896950	-1.51501442294474	2.68394675197653
H	-5.18701383686617	-2.49582128518306	2.23938640505192
H	-5.39453367030323	-1.50367388216900	3.69241111108711
C	-3.51783455610022	-0.48345050638419	-2.02557592804950
H	-4.58226497560835	-0.67513318604384	-2.07151070726556
C	-2.60867121076095	-0.39142803876453	-3.02803684986884
H	-2.75446517268335	-0.51869948877587	-4.09510911646235
N	-1.39061976367085	-0.12236571044322	-2.45302346532021
C	0.61771338353408	1.47281197742336	-1.02270382291775
N	1.21967991128384	2.68761753011385	-0.82387145447266
C	1.45062263330130	3.32875536912879	0.48112449696314
C	1.88405665265455	4.78761566443054	0.30120745337129
H	2.81941058656405	4.84015949459310	-0.27726410466807
H	1.11744951559507	5.34697062400799	-0.26041585088668

Table A3.55 Continued

C	0.16632557121050	3.29839192391061	1.31311166149720
H	-0.63636387544108	3.81948860864423	0.76559253370547
H	-0.12236473025673	2.24377349405712	1.43821143198457
C	2.54650380998858	2.57486988589573	1.24098430726926
H	2.19153423436705	1.53168668170254	1.37146120897957
H	3.47194766287482	2.57857491029520	0.63938453905794
C	2.11552299668591	5.44078354165695	1.66516387660214
H	2.42435385885867	6.48742100050383	1.50564841904754
C	0.40191820765770	3.94962432148195	2.67381050319296
H	-0.53510334617322	3.90877223395936	3.25444640204077
C	2.78805342366214	3.23333115431262	2.59803387027369
H	3.57968939485829	2.67841344905204	3.12973132341684
C	3.21620065766785	4.68653306586756	2.40889534919543
H	4.15851305225442	4.73249682290203	1.83750809579658
H	3.40922132982204	5.16373028529471	3.38496501034364
C	0.82790512791610	5.40301446859956	2.48469017303088
H	0.03359815350739	5.96883181032801	1.96942759953832
H	0.98596822667374	5.89195917643844	3.46118702775549

Table A3.55 Continued

C	1.49631836726366	3.18113227671088	3.41298352555450
H	1.18725448636940	2.13210236799897	3.54020378003426
H	1.65634835718825	3.61400582157880	4.41548354178957
C	1.64200975599436	3.21355456424929	-2.03036297366109
H	2.14772163280304	4.16563862500124	-2.12180838764406
C	1.28781457809606	2.32536792135178	-2.99069385005339
H	1.43636752147246	2.37006811489718	-4.06416331018641
N	0.65980728633205	1.27633504347926	-2.36599509301447
B	0.04745045121651	-0.00198354527460	-3.01649389324075
C	0.17100292641422	0.15983965941659	-4.62538992794975
C	-0.82052207867686	0.79955726455786	-5.38713010285759
H	-1.73850572859809	1.13815044010793	-4.90369451472944
C	-0.67051270763155	1.05407076420853	-6.74953527125200
H	-1.47496070382679	1.55040861218856	-7.29980528527864
C	0.50174270617889	0.68923763110443	-7.40542016357871
H	0.62598162882858	0.88682178769270	-8.47346673736124
C	1.52210837926759	0.08830764199775	-6.67305513690269
H	2.46210592206598	-0.18251635106603	-7.16204219588704

Table A3.55 Continued

C	1.35481886025956	-0.16056489908267	-5.31194830340587
H	2.19339375157135	-0.59905290165535	-4.76668990085316

Table A3.56. DFT optimized coordinates for 6b (AdLCoOH)

Co	0.06972655003861	-0.03043517680415	0.12465484756970
C	0.66297116698286	-1.60213054282411	-0.95006547471738
C	-1.63650825995609	0.21109577704261	-0.94177223857880
C	1.04917203396780	1.33381504460643	-1.01172309577381
O	-0.05361611030934	0.02326524046809	1.98260699281725
H	0.79129926801370	-0.07994247393818	2.43299934710719
N	1.15147682273462	-2.85570656162857	-0.82850157730827
C	1.43510207409757	-3.50982010878572	0.45985399932651
C	2.55675424611877	-2.75951065521684	1.18591898462093
H	3.46102584935491	-2.75611402717431	0.55611373369357
H	2.25649571683328	-1.71048884800134	1.32218361413195
C	0.17498200058407	-3.50449003340386	1.33073176855628
H	-0.15767646586459	-2.46686375617217	1.48097966723506
H	-0.63047319746238	-4.03834384894904	0.80128275337303
C	1.87901770089777	-4.95934164725099	0.24762238523641
H	1.09303423678558	-5.51952895733006	-0.28301802793914
H	2.78608966957918	-4.99217582591457	-0.37586053422410
C	2.84127178565009	-3.41724090542473	2.53501854793357

Table A3.56 Continued

H	3.64326661215098	-2.85756466504854	3.04315101658905
C	0.46447035746020	-4.16523295556679	2.67721101964153
H	-0.45250298898372	-4.14408232315754	3.28802572177612
C	2.16617550379915	-5.62214938010715	1.59535854919341
H	2.48296655636618	-6.66166927509448	1.41335177320009
C	3.28104092799954	-4.86209809131375	2.31052051738677
H	4.20547042435042	-4.88938468383147	1.71051044290457
H	3.51064265326057	-5.34385643846329	3.27494060143077
C	1.57540974530284	-3.39549306264327	3.39047634971740
H	1.25690245273418	-2.35629450999433	3.57256234157982
H	1.77700910064686	-3.84572177893040	4.37625602082845
C	0.90418301873998	-5.60999888235074	2.45433420177874
H	0.10109781287097	-6.17988936180774	1.95890134300091
H	1.09854624397094	-6.10574699894450	3.41960152224688
C	1.34918558332019	-3.41136711157265	-2.07546978556265
H	1.73541186889466	-4.40989023357229	-2.23189298071680
C	0.96855440558197	-2.47414022457307	-2.97899232091046
H	0.96598829671835	-2.51937969683240	-4.06188552622830

Table A3.56 Continued

N	0.54907284407572	-1.36878423390318	-2.27549218036112
N	-2.92530801432174	0.57624782640338	-0.75341143500933
C	-3.58761626117227	0.64601905449395	0.56100466615046
C	-2.96364199310172	1.76120827372528	1.40618268280329
H	-1.89024043195834	1.56157094177898	1.52669641369699
H	-3.07425508969238	2.72211327133210	0.87624143876025
C	-5.08203044562912	0.93369956976228	0.39801691503016
H	-5.22794122460313	1.89542942531511	-0.11846156826862
H	-5.55154587284980	0.15148494041985	-0.21944245477122
C	-3.42161462022862	-0.69230931199945	1.28996354118105
H	-3.86387470874680	-1.49474974654636	0.67687445076497
H	-2.35047627175880	-0.90788195691878	1.40591700339899
C	-3.64137506577152	1.82031324347436	2.77539645929273
H	-3.17416905824153	2.62419656744370	3.36771697389927
C	-5.75953906521196	0.98993524495302	1.76803031485469
H	-6.83156751763124	1.19640572432353	1.61884955592455
C	-4.09659143488008	-0.63005616105060	2.65937279808513
H	-3.95864030375432	-1.59842973369297	3.16843094565678

Table A3.56 Continued

C	-3.45511291632431	0.48158008819776	3.48869162843802
H	-2.38204326520028	0.27558462411623	3.62371254514425
H	-3.91412249054185	0.51974231459507	4.48993971848548
C	-5.13077094879169	2.10351178479160	2.60219409235176
H	-5.27950084931072	3.07871948054766	2.10913621302503
H	-5.62501129428174	2.16354070875362	3.58536714326083
C	-5.58593146866221	-0.34859182389511	2.48200860319125
H	-6.05897345851431	-1.15418662057063	1.89620522401359
H	-6.09232047385207	-0.32390850882055	3.46068234068615
C	-3.51789079641105	0.87058757624524	-1.96275254517163
H	-4.54354586584013	1.20016082331509	-2.06252074326113
C	-2.57406401162524	0.66276329722357	-2.91522148850161
H	-2.63868786514583	0.80853859605275	-3.98689918838593
N	-1.43673272136285	0.22768017688606	-2.28014312970101
N	1.69779754000352	2.51446186587376	-0.88015500138930
C	2.15716432848604	3.07644211862625	0.40177481254571
C	2.98574750278668	4.34172921986116	0.16946340466287
H	3.84992900708257	4.11394525000580	-0.47445687876843

Table A3.56 Continued

H	2.37736456800220	5.10018969177725	-0.34721965502251
C	0.95640156147437	3.42980588003857	1.28595188409348
H	0.32234114242442	4.16129231040969	0.75847108695750
H	0.35530696904618	2.52435258642937	1.45284355358159
C	3.02878237168761	2.04804465395839	1.12909926849966
H	2.43695748007563	1.13442641595603	1.28383221346686
H	3.88416681442861	1.77577216044385	0.48995048103273
C	3.46879484305699	4.90639884776280	1.50520272545111
H	4.06217746116127	5.81360832627246	1.30731036091492
C	1.43815321056784	3.99841907793919	2.62086922943362
H	0.55954193389689	4.24235093286514	3.23989544021500
C	3.50651190741199	2.61222553208226	2.46599056144072
H	4.12437555588977	1.85307525467410	2.97286298652291
C	4.33404802681597	3.87064355606156	2.21822451178456
H	5.22105534450212	3.63055570676559	1.60895231997876
H	4.70463124214539	4.27885401577511	3.17268544430394
C	2.26393636987261	5.25811031903804	2.37374513034781
H	1.64860389437434	6.02511534352813	1.87465539932555

Table A3.56 Continued

H	2.59917931648212	5.68978820677277	3.33066324992472
C	2.29873104863617	2.95729965771936	3.33557724279703
H	1.70407211191843	2.05291901739600	3.54069155234474
H	2.63461061918350	3.34655741482446	4.31012200679640
C	1.85735541115481	3.10939959202745	-2.11305427313264
H	2.33884289411357	4.06689507292640	-2.26039959275353
C	1.30678609360457	2.26590657204500	-3.02186394488108
H	1.20928910764092	2.38364948049962	-4.09464543168788
N	0.84416277033576	1.16855730375925	-2.33845140085766
B	-0.01072707617106	-0.03182974907112	-2.88392837021435
C	0.02712378939581	-0.19970162535009	-4.49346237892694
C	1.19163909915517	0.07032521585016	-5.23173894143077
H	2.07117044695540	0.47862309931407	-4.72945638653050
C	1.28725131426075	-0.19304740578800	-6.59674995170554
H	2.21319676106365	0.03969133895354	-7.12966303002073
C	0.21305607177371	-0.75973047514245	-7.27698406042674
H	0.28152880100886	-0.96793786036711	-8.34780996319049
C	-0.94124969755676	-1.07789378051188	-6.56732452247162

Table A3.56 Continued

H	-1.78623785948413	-1.54904668105449	-7.07677719607455
C	-1.02161872965604	-0.80861175668210	-5.20230165452166
H	-1.92939207389695	-1.11209017951200	-4.67702567199555

Table A3.57. DFT optimized coordinates for 4a (tBuCoO)

C	-1.78924832452360	1.15790330732344	-0.42576490582969
N	-3.02005114234227	1.61701505224234	-0.78178551628331
C	-3.85335687939715	0.54958014932654	-1.04016723516664
C	-3.12092373538417	-0.57747063057100	-0.85691592467082
N	-1.85724170992840	-0.18225991669804	-0.50901410382516
B	-0.58831843198325	-0.96120811010235	-0.06800696734363
N	0.58075857526896	-0.32436960669562	-0.86603074070295
C	0.79687307481139	1.00019836795779	-0.83724575604190
N	1.85502424095273	1.23531589012615	-1.66333387315997
C	2.28498362986869	0.03442838672162	-2.19046757244917
C	1.48591122938196	-0.93682148793274	-1.68812253538366
N	-0.39780021968418	-0.48946108744575	1.40300290432591
C	-0.23543495487144	0.82375029145789	1.66128450204195
N	-0.17390521352325	0.93963904431474	3.02031931744011
C	-0.34607741079466	-0.30633957417128	3.58416061728954
C	-0.49423332181475	-1.19210026081348	2.57102845325702
Co	-0.23778383028357	2.08508615537667	0.26718556749807
O	0.46876996108554	3.50915555645705	0.71151470133002

Table A3.57 Continued

C	-3.43868311381965	3.03970804586042	-0.84042574015526
C	-4.82490927386079	3.14825788365932	-1.46198769735855
C	-3.47592202154468	3.59273592378545	0.57888551696420
C	-2.44732311225111	3.80905165332788	-1.70250256146934
C	2.51012871400851	2.53901413545096	-1.97078055343790
C	3.55175732146996	2.34370479640514	-3.06665110849270
C	1.45893309514498	3.51876100821453	-2.47633512537823
C	3.19889804948087	3.05016765357491	-0.71088147162691
C	0.10441514606670	2.15736638573040	3.83992786761809
C	1.49879414052203	2.66424138161636	3.49044429569707
C	-0.96406312811219	3.20861874764175	3.57229649777699
C	0.06562338837502	1.79986824927242	5.32148377813962
H	-5.08996412973978	4.21123812381405	-1.53417449831900
H	-4.85349618964016	2.72690510557554	-2.47631323989347
H	-4.18714930729658	3.02888738940233	1.19897043708845
H	-3.78616460854450	4.64696504546993	0.56547503018331
H	-2.48455779449771	3.53538684471713	1.04528588428562
H	-2.40870694289087	3.39611011700978	-2.72017367743892

Table A3.57 Continued

H	-1.43897476121444	3.77196327835517	-1.27082931681826
H	-2.74837528447685	4.86379380792497	-1.76556226917798
H	3.11255663580447	1.95014002710090	-3.99402386944885
H	4.37444778397221	1.68638696144409	-2.75302871679973
H	3.98892536415808	3.32381849319765	-3.29870550016902
H	0.96497168422839	3.12685148573900	-3.37716346803816
H	1.93851862545960	4.47251804781990	-2.73543791722273
H	3.95303098868072	2.32786027934111	-0.36419498372428
H	3.71064803037504	3.99862437378101	-0.92931635712868
H	2.45855345932785	3.22539543309988	0.08273724557789
H	1.73903437613980	3.54012363603330	4.11010646943481
H	2.25138762649519	1.88677954925326	3.68902418596811
H	-0.78209048053670	4.08499049949404	4.20958400071800
H	-0.93089927928221	3.53448660191407	2.52660461157999
H	0.83791015130997	1.06875819363489	5.59803330257622
H	-0.91596247170054	1.41906859041552	5.63643370095024
H	0.26078563866993	2.71568929223017	5.89466657707619
H	-5.59701474169561	2.65965213001922	-0.85139746351243

Table A3.57 Continued

H	-1.96440460048784	2.81674165103949	3.80782783271137
H	0.70573394676252	3.71596803321309	-1.70512395536495
C	-0.58940852137700	-2.55203784482587	-0.31796356554010
C	-1.25616915685671	-3.12043861345751	-1.41584326035969
C	-1.17106622081139	-4.47905773349782	-1.71442476799571
C	-0.39595552429318	-5.32199709939156	-0.92345201987602
C	0.30811844498850	-4.78333044407333	0.14958689570324
C	0.21571316978401	-3.42257273168921	0.43531986860159
H	-1.84397247932400	-2.48744093888951	-2.08316856366746
H	-1.70794441974857	-4.87924095140931	-2.57863056470477
H	-0.32735444471328	-6.38878199130949	-1.15203523707151
H	0.94277116188305	-5.42466223329863	0.76694925872268
H	0.81235951814216	-3.03394606924898	1.26326200017530
H	-4.88685061492880	0.66180228312026	-1.33781375971922
H	-3.42115352824537	-1.61496233201102	-0.94311074505997
H	3.11652965655516	-0.04455175368583	-2.87685866726809
H	1.49159865549452	-2.00744701815642	-1.85899037831800
H	-0.35150530539776	-0.47704413526354	4.65175158925127

Table A3.57 Continued

H	-0.67920115826466	-2.25876897086191	2.60698394644704
H	1.53685230541509	2.96355819549667	2.43414929498286

Table A3.58. DFT optimized coordinates for 5a [^{t}BuCoOH]+

C	-1.80217080130649	1.20653989017833	-0.32089906825179
N	-3.05756690416409	1.65271329806514	-0.61296867199950
C	-3.85752876372060	0.56280888207193	-0.86615525933959
C	-3.09068668270709	-0.54662449222223	-0.74340781554634
N	-1.83158520947903	-0.13201047399899	-0.42943884257982
B	-0.57982103528192	-0.98190053506771	-0.05957006583267
N	0.59286979639901	-0.32183483041904	-0.83443268340631
C	0.86688795073794	0.98081490315783	-0.71742941701585
N	1.97520275411933	1.22627754884788	-1.46692796047464
C	2.36530500709301	0.04484060486864	-2.05792801311683
C	1.49729118716196	-0.91782459705589	-1.66268629956176
N	-0.34449246810395	-0.57856575504774	1.42264516332347
C	-0.15722902861318	0.72563963667514	1.65177175064222
N	-0.03513542729741	0.87881739258273	2.99260912177227
C	-0.18778401335810	-0.34687329652627	3.59635308100312
C	-0.39323944990786	-1.25593885196610	2.60760318882930
Co	-0.24714248074877	2.05733590067984	0.31010075626691
O	-0.22844540575804	3.76431572220345	-0.07788108916560

Table A3.58 Continued

C	-3.57143324762877	3.05200736819720	-0.75842374057164
C	-5.07550123991761	3.02638761061554	-1.01224285546917
C	-3.33787886703349	3.82686215379111	0.53129592477445
C	-2.89592966766159	3.67840835717747	-1.97392662157288
C	2.69424127845036	2.51400963357563	-1.71407917189226
C	4.04482152259491	2.22515540146000	-2.36162269149296
C	1.85625144621448	3.35292551214049	-2.67187406572635
C	2.95161759726306	3.22083242343595	-0.39157615336520
C	0.20616555848727	2.15707472413184	3.71100778682228
C	1.43994392602143	2.81791802739806	3.11443867556737
C	-1.02617268214791	3.03748000842406	3.55525009506434
C	0.45255650876745	1.88142489713119	5.18681013481480
H	-5.41623652709188	4.06596502363927	-1.10055493558388
H	-5.34048654225708	2.52090775945849	-1.95045534678532
H	-3.80703883550509	3.30934918570471	1.37945393525300
H	-3.79761843328813	4.82028764833276	0.44478299208556
H	-2.27472045502437	3.97107963196248	0.73950585431169
H	-3.20982078987716	3.16347081926196	-2.89286450100388

Table A3.58 Continued

H	-1.80485494321728	3.61355626588410	-1.91199579641332
H	-3.18192238087484	4.73574883479313	-2.06172457712345
H	3.95300883729672	1.78376078022762	-3.36289762426015
H	4.66974781006151	1.57321853177599	-1.73521255809703
H	4.57351959309059	3.17941902591926	-2.47998334278015
H	1.73116376602076	2.83417000890059	-3.63244917413299
H	2.35393303162642	4.31332938382989	-2.86371813279616
H	3.48667531628095	2.56116593523797	0.30566306001019
H	3.57715670339167	4.10568060641552	-0.57078300824922
H	2.02440791345458	3.57111562848167	0.07061643308316
H	1.65113507072809	3.76072865817127	3.63651154311459
H	2.31914199762671	2.16493987508486	3.20088849907569
H	-0.88902410044773	3.98072869582766	4.10053687598170
H	-1.20848330075329	3.29132761406642	2.50274997247439
H	1.31497855537417	1.21815299748719	5.34158550843326
H	-0.42647707160902	1.44674619219780	5.68136542296938
H	0.67021089518557	2.83503291572275	5.68481998296497
H	-5.63054548657766	2.56685644511262	-0.18270023489651

Table A3.58 Continued

H	-1.92125824893716	2.53589639490230	3.94836343876351
H	0.86421926385031	3.55786618478669	-2.25697689377594
C	-0.65072679026366	-2.54403612892884	-0.41017147472225
C	-1.27638603587843	-2.99550261147333	-1.58486215322454
C	-1.25298745318769	-4.33473051840576	-1.96683217199929
C	-0.58552626096422	-5.27300794053779	-1.18459839569476
C	0.07482848768452	-4.85089036619112	-0.03501721730390
C	0.04712037733720	-3.50780679590572	0.33505863711804
H	-1.78195800604842	-2.28608757413771	-2.24373784721925
H	-1.75235323952482	-4.64520265588322	-2.88797388506537
H	-0.56641108932020	-6.32538956347653	-1.47884443449416
H	0.62470350889267	-5.56976777730981	0.57741394468568
H	0.61406148088477	-3.21414118730315	1.21979647727691
H	-4.90405429506835	0.64901129089982	-1.11944461236973
H	-3.35973072302645	-1.59081615683693	-0.84481311568172
H	3.22472053997693	-0.02703730551350	-2.70959660987772
H	1.45923540301235	-1.97356127860972	-1.90492012035147
H	-0.13739970378589	-0.48783860315850	4.66820368456085

Table A3.58 Continued

H	-0.58296190341736	-2.32009242396767	2.68003873971729
H	1.29816830282845	3.06687539987027	2.05426507833063
H	-0.43077539713308	4.38479408917879	-0.78463710880773

Table A3.59. DFT optimized coordinates for 6a (^{t}BuLCoOH)

C	-1.90443622592826	1.31344150613692	-0.45982325266035
N	-3.18366136068265	1.64649020554190	-0.74319787069454
C	-3.94655183547675	0.51100433633804	-0.90342694028738
C	-3.11052996058179	-0.54308100406061	-0.72429303235009
N	-1.85665366467137	-0.03829521789253	-0.48413968540015
B	-0.55000915727439	-0.80843875018033	-0.06814254576528
N	0.65568643417017	-0.23124283293973	-0.89575775698444
C	1.00464263710971	1.07370333462078	-0.90469129213204
N	2.07957461696332	1.17162086885867	-1.71558177869468
C	2.40735006586486	-0.06878514856486	-2.22054622075307
C	1.51092102751347	-0.94502523682207	-1.70268399531392
N	-0.35276583500689	-0.41518405877754	1.43865439074095
C	-0.11785099680168	0.86824383089814	1.79720145806968
N	-0.11021715010201	0.88228665331088	3.14875472670898
C	-0.39023630904361	-0.37432216474195	3.63885968875872
C	-0.55503751669208	-1.18115000265477	2.56025339500085
Co	-0.20503728302405	2.16358910908849	0.24562509258973
O	0.02336062561187	3.98227344304656	0.59631697180034

Table A3.59 Continued

C	-3.67633810213622	3.04025148252715	-0.85911923593090
C	-5.14617519087321	3.03830695518855	-1.25405697523186
C	-3.51019835247920	3.73367090822520	0.48835494779474
C	-2.86354444501087	3.74802091126600	-1.93767679236304
C	2.76953057962287	2.44508234132761	-2.03013935880574
C	4.00050023366688	2.16894112514808	-2.88144699181622
C	1.80434143970254	3.33568532576092	-2.80638019695254
C	3.19067638383808	3.10728655650915	-0.72346063256686
C	0.14077981727511	2.09093236191108	3.97083982884864
C	1.44992362973793	2.72162332842052	3.51060180290815
C	-1.02352893750113	3.05716226084844	3.78361903884888
C	0.25280539421612	1.70325386495888	5.43851113234659
H	-5.48380231059293	4.07854299953090	-1.35067686549970
H	-5.31395475758282	2.54510828326908	-2.22201052841347
H	-4.05428362884221	3.19132641606589	1.27501739916918
H	-3.91257764965983	4.75501936450910	0.43455008689656
H	-2.44983718986367	3.79785943418514	0.76729557952505
H	-2.97731696401407	3.24365423820216	-2.90807369637003

Table A3.59 Continued

H	-1.79845404039892	3.75815671000338	-1.67463021014956
H	-3.20418969210964	4.78741988989662	-2.04590280042504
H	3.74348430135587	1.71612337489500	-3.84916285169692
H	4.71732967316473	1.51599347852711	-2.36321986529237
H	4.50602330176264	3.12129690047468	-3.08861351111440
H	1.49050833384491	2.85109884581255	-3.74197201610283
H	2.28537883941034	4.29116123223707	-3.05772155610121
H	3.86071936376490	2.44770733437148	-0.15345498579551
H	3.72641452188192	4.04369983300056	-0.93463834515074
H	2.31506889253835	3.34203003709620	-0.10356511419575
H	1.66465318546090	3.61652298289449	4.11157707764730
H	2.28460696327246	2.01581312885175	3.63137521467860
H	-0.87233287299678	3.95272622940690	4.40248798413264
H	-1.09818124559044	3.37482494976846	2.73625836657249
H	1.06206273598821	0.97957279902070	5.61267834525980
H	-0.68477754356946	1.28618409401218	5.83159245935451
H	0.47875110538134	2.60574896653525	6.02195831031090
H	-5.77853278951293	2.55611072973654	-0.49514884764209

Table A3.59 Continued

H	-1.97141290239020	2.58814092965479	4.08608705507669
H	0.90618360644332	3.54934129624446	-2.21194743023341
C	-0.59109682764169	-2.40119463509374	-0.35484504534123
C	-1.23560810955962	-2.92636974300579	-1.48759369329214
C	-1.16437837558690	-4.27616751105977	-1.82664126764056
C	-0.42510809598672	-5.15683617373443	-1.04218005445180
C	0.25744140143474	-4.66257694519070	0.06531591172604
C	0.17892635718418	-3.30952155689979	0.39023738745769
H	-1.79377001327433	-2.26274699230449	-2.15126515899579
H	-1.68236888063555	-4.63964571465239	-2.71817879494001
H	-0.36676170363775	-6.21693766641547	-1.30242629507423
H	0.86560792688058	-5.33242226977830	0.67911040254357
H	0.76205142461364	-2.95605356455677	1.24288391618752
H	-5.00350792533412	0.52603758053209	-1.13427878127336
H	-3.33223586558707	-1.60354629475474	-0.74273830769152
H	3.23514744607615	-0.24104353264649	-2.89647751566089
H	1.42550857762823	-2.01469265310027	-1.85343033664341
H	-0.45078425780719	-0.60707111297655	4.69442329554092

Table A3.59 Continued

H	-0.81241013847890	-2.23264672087207	2.52442449753572
H	1.38750076939093	3.02359191053699	2.45760780093901
H	0.08278449116866	4.52560282447265	-0.19684513507931

Table A3.60. DFT optimized coordinates for [tBuCo^{II}O]$^{-}$

C	-1.77981573526587	1.26363615742814	-0.53492784758709
N	-3.04938726770148	1.65337000147044	-0.87006013163319
C	-3.88376540844630	0.55730168528637	-0.94941533191926
C	-3.11893439262232	-0.53450864641644	-0.70187337557926
N	-1.83759842915776	-0.09601072743898	-0.49301988862374
B	-0.57690616799386	-0.89904183253562	-0.05072152823641
N	0.60431983881901	-0.33834723446772	-0.86800037659593
C	0.84370197610449	0.98922577670319	-0.80084713274310
N	1.92325315060703	1.19836756884134	-1.61893276334448
C	2.33289784167282	0.00111826872345	-2.17731166582596
C	1.49992401606768	-0.95867697511822	-1.70273826224001
N	-0.34046484791276	-0.46412811821916	1.42627283316161
C	-0.03298106770823	0.83435557654233	1.69835842246330
N	0.01953604008650	0.89900230416999	3.06564865082010
C	-0.33382372570698	-0.31552330092913	3.61745535650261
C	-0.56766057992621	-1.16149745077310	2.58422617494380
Co	-0.22845451802552	2.11388227124880	0.26253115946480
O	-0.71176016068697	3.62252190374062	0.93799577748388

Table A3.60 Continued

C	-3.51712636233877	3.04812758714686	-1.04446952488087
C	-4.83375630696395	3.05692346716947	-1.81503181212802
C	-3.70278077486737	3.66793227339809	0.33675182109271
C	-2.47424360415831	3.82607643169294	-1.83494183276163
C	2.54815521352553	2.51396848493423	-1.85363995325193
C	3.70960794064537	2.38056586000921	-2.82865362020174
C	1.49978416963154	3.45335155529906	-2.43971779267154
C	3.06177177328289	3.04895666034406	-0.52051418454773
C	0.32909750682357	2.10027106476212	3.87448482862605
C	1.48495079969981	2.84958826489898	3.22739363234762
C	-0.91337595727772	2.98379301546820	3.92209607957987
C	0.73715305908056	1.68117384411568	5.28366178857025
H	-5.11551012207894	4.09989164347205	-2.01318851538361
H	-4.74768457051808	2.54274052683760	-2.78403139604206
H	-4.43595262870771	3.09191469221207	0.92254332648901
H	-4.07699156442188	4.69954810622927	0.24171297571417
H	-2.71610495886204	3.68023451828512	0.84225435551181
H	-2.29065852603881	3.36182657442623	-2.81527934843000

Table A3.60 Continued

H	-1.53848380948944	3.85773088343533	-1.25986243905145
H	-2.82938513931881	4.85371292396029	-1.99895663764630
H	3.38521373842841	2.00044453228612	-3.80772210295424
H	4.50215660808277	1.72505807475443	-2.43995244717464
H	4.15027733705903	3.37387752928458	-2.98943485917737
H	1.12434358321271	3.06807110127568	-3.39880638592710
H	1.92987547511044	4.45060729144047	-2.60923174592634
H	3.83160464754419	2.38206802289416	-0.10485625261008
H	3.49866836817710	4.04972520260229	-0.64895721727048
H	2.23145338655252	3.11586325033346	0.19786138281157
H	1.74396508119024	3.72699989025872	3.83847655853630
H	2.37535778107501	2.20896794236367	3.14413950108132
H	-0.72581490500791	3.86923009506501	4.54903713062041
H	-1.14647067287683	3.30872407456069	2.88833478895689
H	1.58114179998174	0.97506887676535	5.27222072126586
H	-0.09060631184229	1.23090385917387	5.84952342288087
H	1.05337852994599	2.57755818103157	5.83455431792180
H	-5.65882036941977	2.60260374768405	-1.24821853711003

Table A3.60 Continued

H	-1.76225689266626	2.43306234644023	4.35702350116545
H	0.65076491852710	3.54910782550207	-1.74689067156538
C	-0.65029371852553	-2.49769113987795	-0.30629035097455
C	-1.31417844980581	-3.03262073994532	-1.42298636555830
C	-1.27529723081402	-4.39087258912690	-1.73419264622456
C	-0.55140463902972	-5.27161510076384	-0.93494424717170
C	0.14542803007481	-4.76979645251447	0.16073803443843
C	0.09859760413982	-3.40830429108485	0.45703112674700
H	-1.86903392215034	-2.36792614526506	-2.08889060069049
H	-1.80816864963324	-4.76239578277867	-2.61405133004446
H	-0.51878049464702	-6.33840483567600	-1.17277544816531
H	0.73780383932012	-5.44153894503302	0.78833175519276
H	0.68231208019511	-3.04717234015429	1.30656708753065
H	-4.93870257257485	0.62474442957423	-1.18141609125666
H	-3.40658532202842	-1.57915731163487	-0.65503013608231
H	3.17012497249332	-0.08291026940375	-2.85838489798739
H	1.48123829711994	-2.02507007193205	-1.90263403453896
H	-0.38983292322388	-0.49322124635856	4.68429993969153

Table A3.60 Continued

H	-0.88632487654224	-2.19753689419948	2.60184272242755
H	1.17601917270699	3.18789227610528	2.22856255569573

Appendix 4: Synthesis and Reactivity of Synthons Toward the Synthesis of High-valent Ni-oxo and -imido Complexes

A4.1 Introduction

Transition metal complexes with multiple bonds, such as metal-oxo, -imido and -nitrido complexes, are important intermediates in synthetic and biological processes, such as C–H bond functionalization, alkene epoxidation and aziridination, ammonia production and water oxidation.[1–3] However, metal-ligand multiple bonds become increasingly difficult to stabilize with higher d-electron counts (see Section 1.2). Nevertheless, high-valent (3+, 4+) complexes of Ni, including Ni^{III}-imido complexes have been isolated.[4–6]

Our group and the Smith group have reported the isolation of terminal Co^{III}-oxo (**4a** and **4b**) and imido complexes using tetrahedral geometry enforcer tris(imidazol-2-ylidene) scaffolds (see Chapters 1, 4).[7–9] Unlike Co, the chemistry of Ni complexes supported by these strongly donating ligands is relatively unexplored.[10] This appendix chapter details the synthesis and reactivity of several synthetic approaches to high-valent Ni^{IV}-oxo and -imido complexes, which are isoelectronic to the aforementioned Co complexes. Synthesis of the proposed Ni-compounds with these scaffolds would allow for closer examination of the effects of metal identity, charge, and oxidation state on the properties (pKa, BDFE, oxidation potential, bond lengths, etc) and oxidative reactivity of this family of compounds. While definitive evidence for the formation of such high-valent intermediates has not yet been obtained, the goal of this appendix is to list efforts thus far and promising or unsuccessful routes.

A4.2 Attempts to Synthesize a Ni^{IV}-oxo Complex

High-valent Ni-oxo complexes have been invoked in the functionalization of inert C–H bonds and O–O bond formation in Ni-based water oxidation catalysts.[11–13] However, the lack of literature precedent for such a species has called into question their role in these processes.[14] Several reports have proposed the intermediacy of such a species on oxidation of a Ni-oxo complex *en route* to substrate oxidation or decomposition, but Ni-oxo complexes have not been isolated and

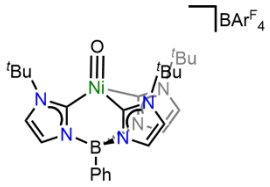

Figure A4.1. Target $Ni^{IV}O$ complex.

characterized to date.[15–17] We hypothesized that the strongly donating tris(imidazol-2-ylidene) scaffold $[PhB(^tBuImH)_3]^-$ would stabilize a terminal Ni^{IV}-oxo complex, which is isoelectronic to its isolable d^6 Co^{III} congener (**Figure A4.1**).

We attempted to synthesize $[PhB(^tBuIm)_3NiO]^+$ from **1a** using a synthetic route analogous to the one used to synthesize **4a**. We attempted to synthesize $PhB(^tBuIm)_3NiOH$ via salt metathesis between **1a** and hydroxide salts (NaOH, KOH, CsOH, NR_4OH, etc). However, in all cases productive reactivity was not observed. Typically, reaction mixtures contained starting material **2a**, as well as a mixture of brown diamagnetic putatively square-planar Ni^{II} complexes. In these square planar complexes, one arm of the tris(imidazol-2-ylidene) scaffolds is protonated, while the other two coordination sites on Ni are occupied by chloride and/or hydroxide ligands.[18,19] Attempts to deprotonate the imidazole arm with lithium diisopropylamide were unsuccessful and resulted in decomposition of these compounds.

2-*tert*-butylsulfonyliodosyl benzene (^{S}PhIO) was screened as an O-atom transfer reagent to install the directly functionalize the Ni^{II}-center in the presence of various salts/halide abstractors for charge balance. The addition of $NaBAr^{F}_{4}$ activates **1a** to labilize the apical chloride ligand and generate **1a-Na** (see Chapter 3). At room temperature, addition of ^{S}PhIO to **1a-Na** results in immediate decomposition. However, a new thermally unstable intermediate is generated at low temperatures, as ascertained by UV-vis spectroscopy. At –90°, this new intermediate decomposes in an isosbestic fashion to a second thermally unstable species (**Error! Reference s ource not found.**, light to dark green trace). Unfortunately, attempts to characterize these intermediates were unsuccessful. We hypothesize that the first intermediate generated is a Ni^{II}-^{S}PhIO adduct, which further decays to a Ni^{IV}-oxo, Ni^{III}-OH or Ni^{II}-OH_2 complex (**Scheme 4.1**). Consistent with this hypothesis, 2,4,6-tri-tert-butylphenol reacts with the second intermediate as it is generated. Additionally, ESI mass spectrometry of this reaction mixture using natural-

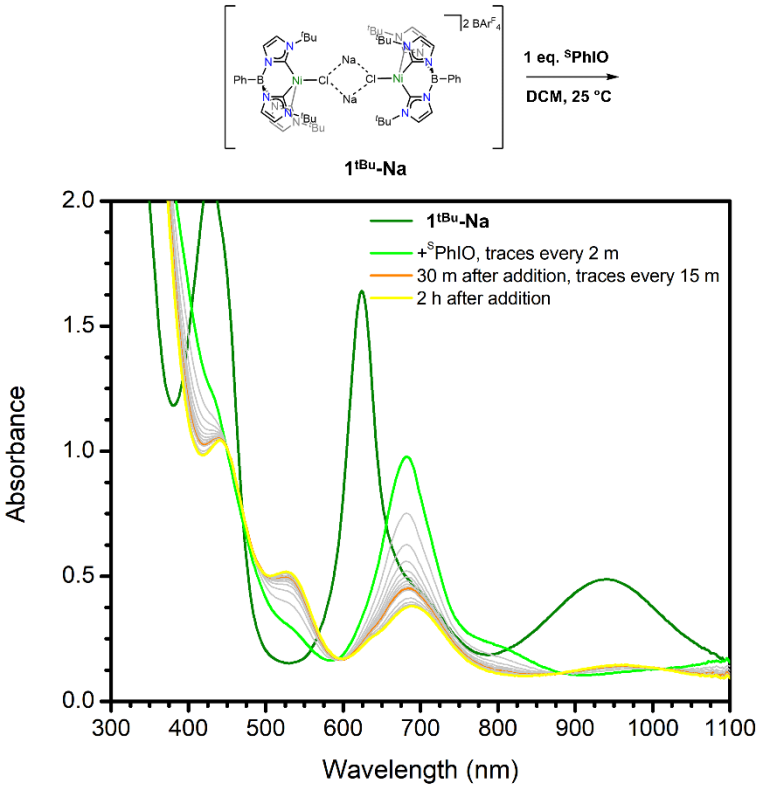

Figure A4.2. UV-vis trace of 1a-Na/^{S}PhIO reaction mixture.

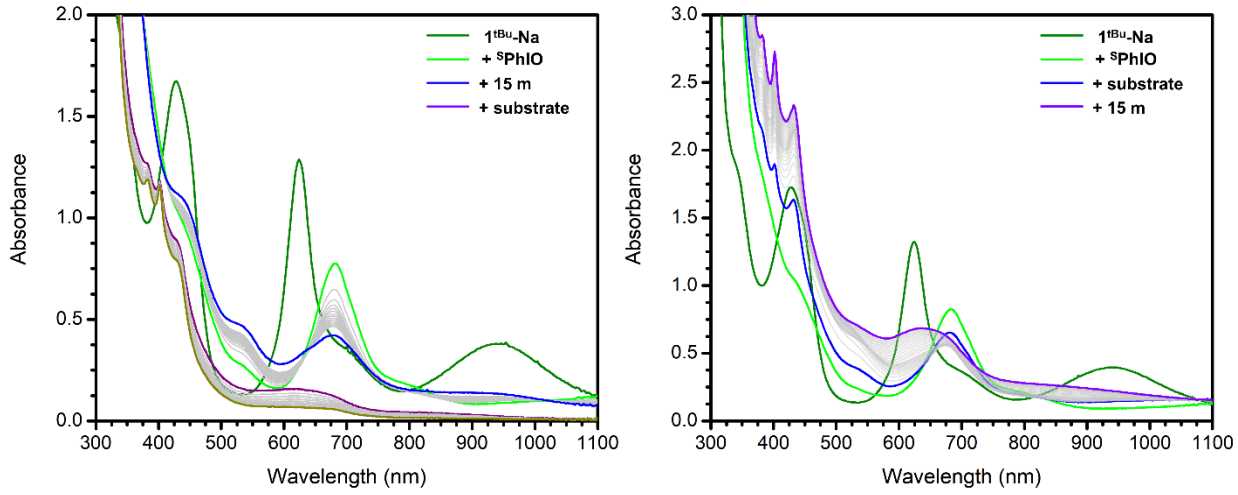

Figure A4.3. UV-vis spectra of 2,4,6-tri-tert-butylphenol added at different stages of reaction between 1a-Na and ^{S}PhIO.

abundance ^{S}PhIO or ^{18}O-enhanced ^{S}PhI^{18}O is consistent with incorporation of the ^{S}PhIO oxygen atom into the ligand framework of **1a**.

Interestingly, the rate of stirring plays a role in this reaction mixture. Layering 1 equivalent of ^{S}PhIO to the top of the **1a-Na** solution and allowing to stand 30 seconds before stirring results in a lower yield of the second thermally unstable intermediate that is generated as ascertained by UV-vis spectroscopy. This suggests that the first intermediate that is generated in this reaction mixture reacts with further equivalents of ^{S}PhIO. While attempts were made to cool and ensure uniform mixing of **1a-Na** and ^{S}PhIO in VT-NMR experiments, we observed a mixture of products in the low-temperature NMR spectra on addition of these reactions conducted in NMR tubes. Attempts to crystallize products obtained in this reaction mixture were unsuccessful. Density functional theory calculations suggest that the target Ni^{IV}-oxo complex is likely not stable in solution;

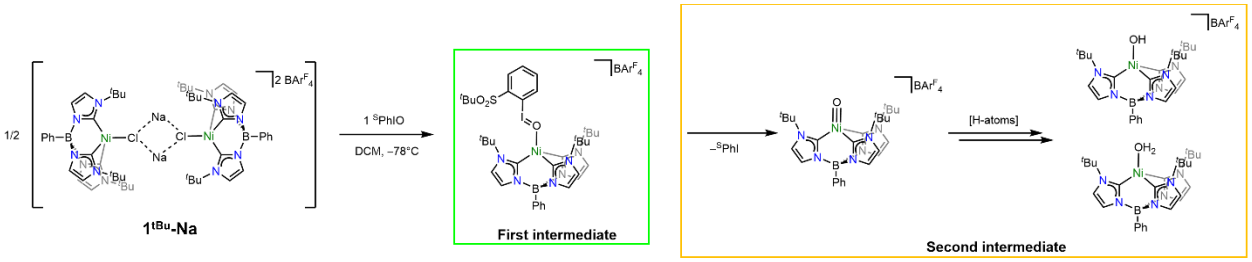

Scheme A4.1. Proposed intermediates for ^{S}PhIO oxidations of 1a-Na.

calculations carried out with O3LYP predict the O–H BDFE of [PhB(^{t}BuIm)$_3$Ni^{III}OH]$^+$ is >105 kcal/mol (~10 kcal/mol higher than solvent, DCM BDFE$_{C–H}$ ~95 kcal/mol). Similarly, activation of the ^{t}Bu groups is likely at these high BDFE's.

A4.3 Attempts to Synthesize a Ni^{IV}-imido Complex

Late transition metal-imido complexes have been implicated in olefin aziridination and other N–group transfer reactions into unreactive C–H bonds.[20–22] As such, a detailed understanding of how structural features affect the stability and reactivity of these imido complexes is critical to informing the design of synthetic catalytic systems. Despite their importance, however, examples of late (Co, Ni, Cu) metal imido complexes are rare due to their often-reactive nature.[6,7,23,24] Recently isolated late metal-imido complexes have demonstrated that the bonding between the metal and imido nitrogen can complicate the assignment of these species.[25,26] In particular, electronic spin density can be localized onto the imido nitrogen, giving rise to iminyl and nitrene isoelectronic analogues. The valence state of the M–NR fragment has been suggested to have profound effects on the stability and reactivity of the overall complex. While Ni^{II} and Ni^{III}-imido

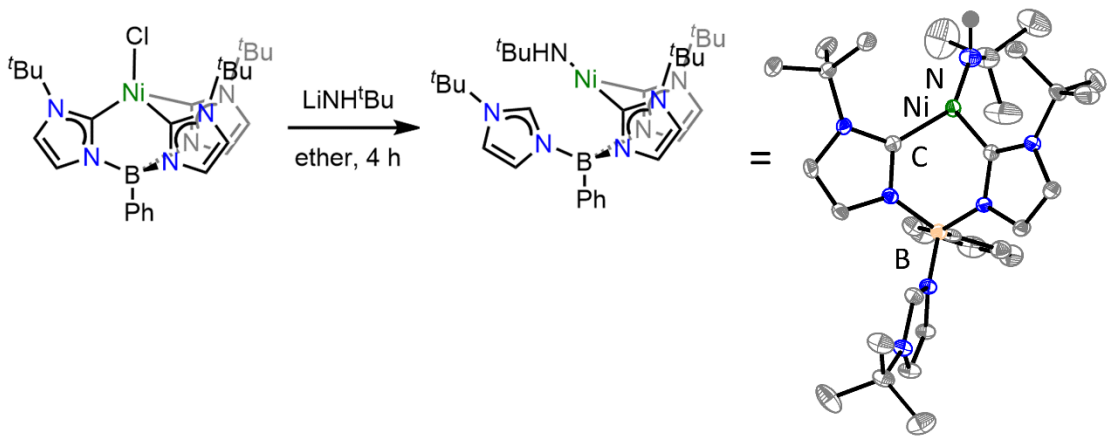

Figure A4.4. Synthesis and solid-state structure of PhB(^{t}BuIm)$_3$NiNH^{t}Bu.

complexes have previously been isolated, Ni^{IV}-imido complexes are unprecedented in the chemical literature. As such the electronic structure and reactivity of such a species is unknown.

While Ni-oxo complex [PhB(^{t}BuIm)$_3$NiO]$^+$ is predicted to react with solvent by DFT, calculations predict that [PhB(^{t}BuIm)$_3$NiN^{t}Bu]$^+$ is significantly more stable (Ni^{III}N(R)–H BDE 81 kcal/mol). We initially attempted to synthesize [PhB(^{t}BuIm)$_3$NiN^{t}Bu]$^+$ through photolysis of PhB(^{t}BuIm)$_3$NiN$_{6a}$. PhB(^{t}BuIm)$_3$NiN$_{6a}$ can be synthesized by addition of ^{t}BuN$_3$ to **1a**–**Na**.

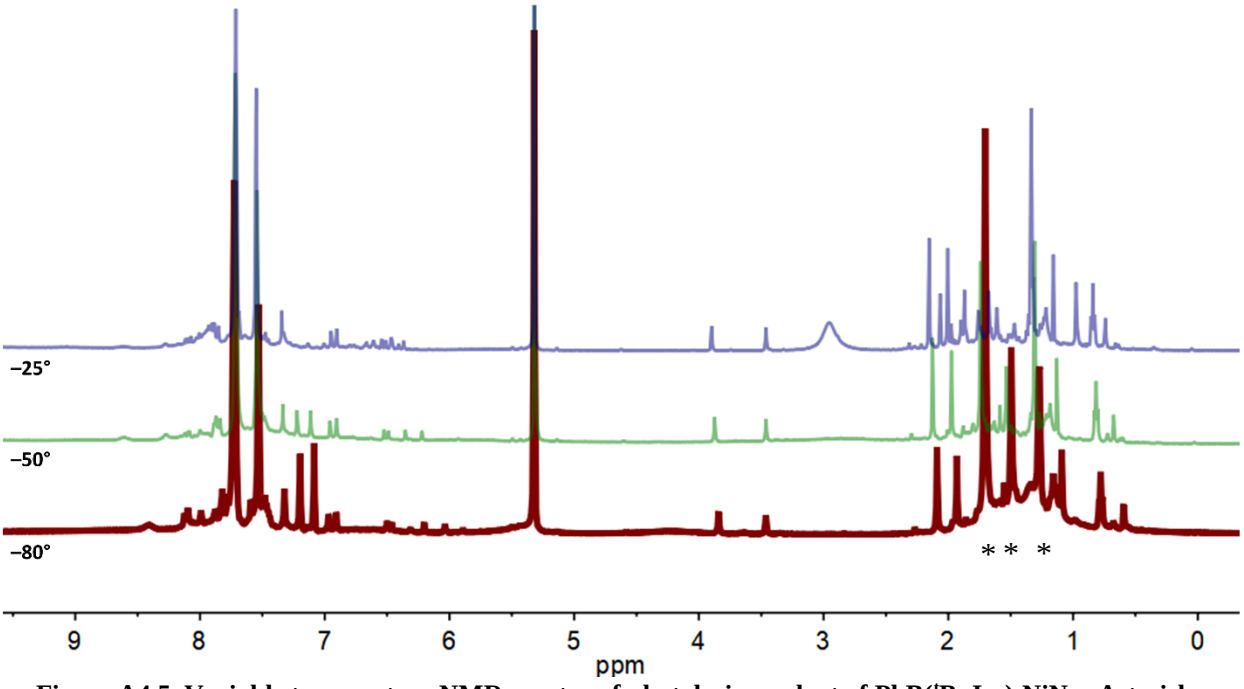

Figure A4.5. Variable temperature NMR spectra of photolysis product of PhB(^{t}BuIm)$_3$NiN$_{6a}$. Asterisks indicate ^{t}Bu groups of interest.

Conversion can be monitored via the ^{1}H NMR signals of PhB(^{t}BuIm)$_3$NiN$_{6a}$, which are shifted relative to that of **1a**. However, Hg lamp photolysis of PhB(^{t}BuIm)$_3$NiN$_{6a}$ and NaBAr$^{F}_4$ in DCM resulted in formation of a diamagnetic product, consistent with a pseudo-tetrahedral Ni^{IV} d^6 complex **(Figure A4.5**). The peaks present at 1.7, 1.5 and 1.3 ppm integrate to a 2:1:1 pattern, consistent with what is expected for the tert-butyl groups an asymmetric NiN^{t}Bu complex. This product is thermally unstable (above –78°), as ascertained by VT-NMR spectroscopy.

We attempted to synthesize [PhB(^{t}BuIm)$_3$NiN^{t}Bu]$^{+}$ through sequential oxidation-deprotonation of the Ni^{II}-amido complex, analogous to the synthesis of **4a** and **4b**. PhB(^{t}BuIm)$_3$NiNH^{t}Bu can be synthesized by treating **1a** with ^{t}BuNHLi (Figure A4.4). Interestingly, this complex is not three-fold symmetric like **1a**. The Ni center adopts a trigonal geometry, with one of the imidazol-2-ylidene arms no longer bound to Ni. Variable-temperature NMR studies are consistent with fluxional behavior, suggesting either a rapid equilibrium between conformers with two of the imidazol-2-ylidene arms of the ligand scaffold bound to Ni or a lever mechanism as proposed in **2a**. This structure has been confirmed by SXRD. While unbound arms

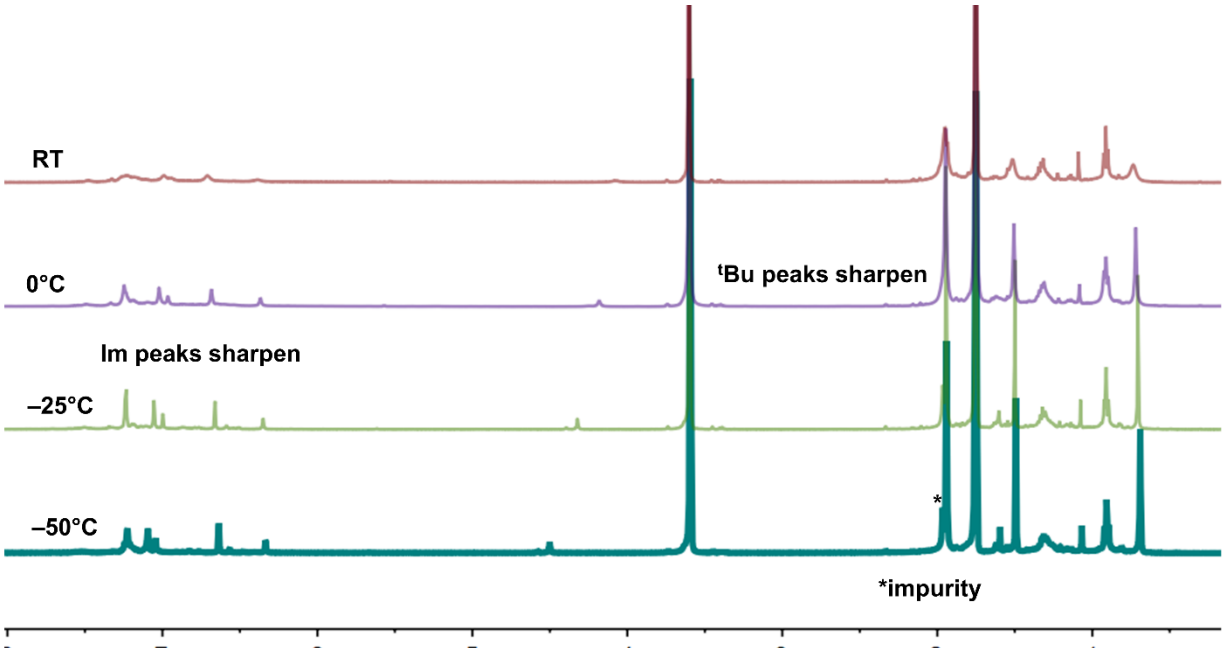

Figure A4.6. Variable temperature NMR of PhB(^{t}BuIm)$_3$NiNH^{t}Bu.

in these tris(imidazol-2-ylidene) phenylborate ligands have been demonstrated in Co and Ni, the imidazol-2-ylidene arm in this complex remains deprotonated, necessary for charge balance in the compound. The trigonal geometry renders the complex susceptible to nucleophilic attack. As such, $PhB(^{t}BuIm)_3NiNH^{t}Bu$ is only stable in hydrocarbon and ethereal solvents. The cyclic voltammetry of this complex shows an irreversible oxidative feature at ~0.3 V v. Fc/Fc^{+} (**Figure A4.7.** Cyclic voltammagram of $PhB(tBuIm)^{3NiNHtBu.}$ We were unable to isolate any oxidation or oxidation/deprotonation generated from the oxidant/base pairs screened.

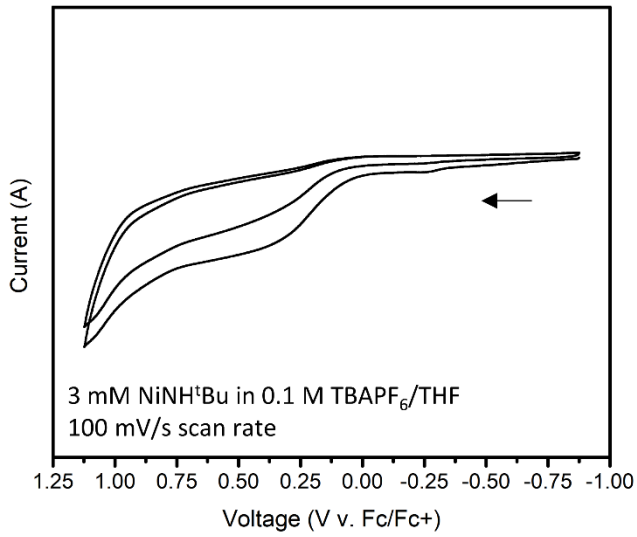

Figure A4.7. Cyclic voltammagram of $PhB(^{t}BuIm)_3NiNH^{t}Bu$.

4.4 Experimental

4.4.1 General procedures

All manipulations were performed under a dry nitrogen atmosphere using either standard Schlenk techniques or in an mBraun Unilab Pro glove box unless otherwise stated. All chemicals were obtained from commercial sources and used as received unless otherwise stated. Solvents were dried on a solvent purification system from Pure Process Technologies and passed through a column of activated alumina before storing over 4 Å molecular sieves under N_2. Diethyl ether and tetrahydrofuran (THF) were stirred over NaK alloy and passed through a column of activated alumina prior to storing over 4 Å sieves under N_2. 2-*tert*-butylsulfonyl iodosylbenzene, and tert-butyl azide were prepared according to literature procedures.[27,28] UV-vis spectra were recorded on a Thermo Scientific Evolution 300 spectrometer with the VISIONpro software suite. A standard 1 cm quartz cuvette with an air-tight screw cap was used for all measurements. A Unisoku CoolSpek cryostat was used for low temperature measurements. ^{1}H NMR spectra were recorded using either Bruker DRX-400 or AVANCE-500 spectrometers and referenced to residual solvent peaks. Electron ionization-mass spectra (EI-MS) were recorded on an Agilent LC/MS 6130 (low resolution) instrument.

4.4.2 Density functional theory (DFT) calculations

Geometry optimizations were performed with help of O3LYP density functional using relativistically re-contracted basis sets of triple-ζ quality for all atoms (ZORA-def2-TZVP). Throughout all calculations the accelerating technique RIJCOSX was applied.[29] All computations were carried out with help of ORCA program package (version 4.2.0).[30]

4.4.3 Preliminary Complex Synthesis and Characterization

[PhB(^{t}BuIm)$_3$]NiN$_{6a}$}{BAr$^F_4$} In a nitrogen-filled glovebox, a vial was charged with equimolar **1a** (10 mg, 0.018 mmol) and NaBAr$^F_4$ (16 mg, 0.018 mmol) to form **1a-Na**. Then, 2 eq. ^{t}BuN$_3$ was added via syringe as a solution in DCM and stirred for 30 minutes, resulting in a dark forest green solution. The chemical shift of the peaks of this compound shift are dependent on the ratio of azide to **1a**. Full conversion is likely only achieved with excess ^{t}BuN$_3$. This complex is unstable as a solid, thus NMR shifts reported may differ from that of the pure compound. ^{1}H NMR (d_2-DCM, 500 MHz, 298 K): δ 104.44 (Im), 12.47 (^{t}Bu), 10.14 (Im), 8.39 (^{t}Bu), 7.73 (BAr$^F_4{}^-$), 7.56 (BAr$^F_4{}^-$), 7.36 (Ph), 2.13 (^{t}BuN$_3$).

PhB(^{t}BuIm)$_3$]NiN^{t}Bu In a nitrogen-filled glovebox, a vial was charged with equimolar PhB(^{t}BuIm)$_3$NiCl (0.1 mmol) and LiNH^{t}Bu (0.1 mmol) in ether over 2h. The ^{1}H NMR peaks are broadened, but better resolved at 248 K than 298 K. In the following, the ^{1}H VT-NMR shifts are calibrated to the H signals closest to the THF oxygen atom (δ3.57 ppm). ^{1}H NMR (d_8-THF, 500 MHz, 248 K): δ 7.22 (Ph, 5H), 7.04 (2H, Im), 6.98 (1H, Im), 6.64 (2H, Im), 6.33 (1H, Im), 4.30 (1H, NH), 1.93 (18H, ^{t}BuIm), 1.48 (9H, ^{t}BuIm), 0.69 (9H, ^{t}BuN). Dark blue crystals suitable for SXRD can be grown from slow diffusion of pentane into a saturated solution of the title compound in ether. The air, moisture and solvent sensitivity of this compound precluded further characterization.

[PhB(^{t}BuIm)$_3$NiNH(p-OMePh) In a nitrogen-filled glovebox, a vial was charged with equimolar PhB(^{t}BuIm)$_3$NiCl (0.1 mmol), then dissolved in ether. The solution was treated with equimolar MeLi and filtered through celite to generate **2a**. Then, 1 equivalent p-anisidine was added to the solution. After 30 minutes, the reaction mixture was concentrated. ^{1}H NMR (C$_6$D$_6$, 500 MHz, 298

K): δ 8.94 (NH, 1H), 7.31 (5H, BPh), 6.71-3.37 (Ar), 1.84 (18H, ^{t}BuN), 0.90 (9H, ^{t}Bu), –0.59 (3H, OMe)

4.4.3 Other Experimental Procedures

Photolysis of [PhB(^{t}BuIm)$_3$]NiN$_{6a}$}{BAr$^{F}_4$}. To a quartz J. Young tube was added a solution of [PhB(^{t}BuIm)$_3$]NiN$_{6a}$}{BAr$^{F}_4$}, generated from 10 mg **1a** and 2 eq. ^{t}BuN$_3$ in 0.7 mL d_2-DCM. The tube was then sealed and brought out of the glovebox. Under positive nitrogen pressure, the reaction mixture was frozen in LN_2, and then warmed to –80°. The reaction mixture was irradiated using a Hanovia Hg lamp for 5 minutes in a dry ice/isopropanol bath. ^{1}H NMR of the reaction mixture was taken using a pre-cooled NMR spectrometer.

General procedure for oxidation reactions of 1a-Na using ^{S}PhIO. A 2 mM solution of **1a-Na** and a 80 mM solution of ^{S}PhIO in DCM were prepared in the glovebox. 2 mL of the **1a-Na** stock solution was then transferred to a screw-top cuvette equipped with a stirbar which was then sealed. This cuvette was then brought out of the box and cooled to –90° in a Unisoku cryostat, with positive argon flow. Added ^{S}PhIO via syringe, then monitored reaction.

Crystallographic Details The diffraction data were measured at 100 K on a Bruker D8 VENTURE diffractometer equipped with a microfocus Mo-target X-ray tube (λ = 0.71073 Å) and PHOTON 100 CMOS detector. Data were collected using ϕ and ω scans to survey a hemisphere of reciprocal space. Data reduction and integration were performed with the Bruker APEX3 software package (Bruker AXS, version 2017.3-0, 2018). Data were scaled and corrected for absorption effects using the multi-scan procedure as implemented in SADABS.[31] The structure was solved by SHELXT and refined by a full-matrix least-squares procedure using OLEX2.[32,33]Crystallographic data and details of the data collection and structure refinement are listed in Table A4.3, Table A4.4**Table A4.5**.

4.5 Supplementary data

Table A4.1. DFT-optimized coordinates for $[PhB(^{t}BuIm)_3NiO]^+$.

B	-2.90506285379324	1.28756524866029	-0.08249394018351
C	-4.27933258965938	-0.36816229775168	-1.40901089392030
C	-4.18918554847744	2.44861196084648	-1.94420026787427
C	-5.36825258418107	1.41243349229543	0.16387288354489
C	-1.48028994049855	1.49578529791083	0.60745041000701
C	-1.29254702037664	2.37620670039765	1.68437451748645
H	-2.14623048269922	2.88381662565290	2.13651196140604
C	-0.02617697026812	2.66823921894205	2.18484301114378
H	0.08079302797131	3.35691641803999	3.02628187794462
C	1.10185322497373	2.09321063962918	1.60982222877722
H	2.09558120446298	2.32308662659236	2.00083936432645
C	0.95113397815613	1.23988739991023	0.52129172896040
H	1.82857421615350	0.79865854033281	0.04328366674652
C	-0.31944687435485	0.95690608168739	0.02746883887686
H	-0.39412895218155	0.32144011774993	-0.85828717381664
N	-4.18738163418982	1.45736534439544	0.79521089345913
N	-3.15277640971511	-0.11762964987442	-0.73766313323990

Table A4.1 Continued

C	-2.49002095809344	-1.29788272215108	-0.54435595853145
C	-3.22621871062826	-2.27499726842693	-1.12867045411833
N	-4.35058037760421	-1.68815580517581	-1.66801260204628
H	-1.56069185076967	-1.36125521333959	0.00802081910557
H	-3.02913233413093	-3.33591478594874	-1.19842301473489
N	-3.07728728999977	2.34303318413817	-1.22287311836259
N	-4.09459760357431	3.52811000428776	-2.74093788309693
C	-2.86575953549016	4.10793647008261	-2.50353460148913
C	-2.23475308680047	3.36627720136734	-1.55947855476278
H	-2.53609614506853	5.00105633739921	-3.01493896314636
H	-1.26477739534947	3.49251419432448	-1.09300818940521
Ni	-5.42686641645014	1.07425482683483	-1.74414882685337
O	-5.84078954487789	0.75622078549829	-3.28628916834229
C	-5.39833605366651	-2.46444178299944	-2.41572575410149
C	-5.07873634557188	4.05696859658215	-3.74103061896251
C	-6.78378220435992	-2.05977581031187	-1.92841794106474
C	-5.21465433551672	-3.95051101117837	-2.13011066771507
C	-5.22597042516678	-2.20437551556668	-3.90603667823354

Table A4.1 Continued

C	-4.99087418885501	3.20813978269746	-5.00377615584579
C	-4.72410405930611	5.50387746802652	-4.06372634933652
C	-6.47632472994062	4.02531833665917	-3.13748687528854
H	-5.95386518667974	-2.80415205861900	-4.46861008665983
H	-4.21974988567808	-2.49679586780502	-4.23949831845613
H	-5.38846950190044	-1.14458051331751	-4.14471296639751
H	-7.53077822093128	-2.70579590206924	-2.40620447765222
H	-7.02901716951030	-1.03022628822766	-2.20752995554913
H	-6.87428435515331	-2.18577745192994	-0.83987991461736
H	-6.02375525852779	-4.49622656943578	-2.63136570311325
H	-5.27613278191049	-4.18307140282536	-1.05730751493855
H	-4.27586838954849	-4.35111515522238	-2.53530421164803
H	-5.49453369196345	5.90478583036164	-4.73427946651053
H	-3.76923719372989	5.59683740110332	-4.59817738641817
H	-4.69918162980389	6.13771731230088	-3.16609837142022
H	-5.68370409566969	3.60147179764094	-5.76023811920730
H	-5.25780007504531	2.16344608532624	-4.79415692228775
H	-3.97654630925482	3.23880816678123	-5.42714824247189

Table A4.1 Continued

N	-6.32792859495756	1.47455214073986	1.10631067792894
C	-5.73425890260118	1.52747602010762	2.34750829340309
C	-4.39108161399308	1.50472674748879	2.14623393435184
H	-3.58188838482209	1.51057689095036	2.86673955216194
H	-6.30311629989919	1.58388377643466	3.26800588709316
C	-7.79828138298112	1.46322403477567	0.91669831600052
C	-8.38417016507288	2.67845303545012	1.62979167969819
C	-8.34339147428351	0.16126355789937	1.49666764852247
C	-8.12791065637201	1.54718405154637	-0.56075929364650
H	-7.74577338879015	2.47044917295920	-1.01286435775202
H	-9.21830180789578	1.54196355267162	-0.69158340137544
H	-7.74643552108674	0.68190399838575	-1.12023242670886
H	-8.21371615469486	2.65038565343919	2.71463922880786
H	-9.47073130514242	2.71397129562734	1.46990083862413
H	-7.95114812874033	3.60963026955450	1.23766453905034
H	-8.13951669855362	0.07312506958566	2.57281867467143
H	-7.89665560219746	-0.70726592383156	0.99241655642391
H	-9.43240951692017	0.11374957857935	1.35682957115560

Table A4.1 Continued

H	-7.17832534557495	4.49963629149730	-3.83563146067208
H	-6.51321729664103	4.58229648412182	-2.19101182939688
H	-6.82716821357474	3.00063387973825	-2.97735538830625

Table A4.2. DFT-optimized coordinates for [PhB(^{t}BuIm)$_3$NiN^{t}Bu]$^+$.

B	-3.00130418699327	1.32119947381061	0.06745407746368
C	-1.66626279018884	1.63330684352951	0.90019375423941
C	-1.60661685798318	2.64790978082099	1.86894431022695
H	-2.50747579931551	3.19861241960983	2.14519283556742
C	-0.41021081845990	3.02340260006211	2.47463399398625
H	-0.40867377578903	3.81696890233358	3.22591746467234
C	0.78118377115071	2.40383381017261	2.11329973204787
H	1.72063332143250	2.69919512142731	2.58554539127681
C	0.76259546365152	1.42234706668148	1.12764841528066
H	1.69183790479580	0.94467087374122	0.80864549973917
C	-0.44038812550761	1.05416396688347	0.53165358424817
H	-0.40579167225418	0.31233540698602	-0.26982337958600
N	-4.35959085195831	1.53160242144746	0.79077363119173
N	-3.14966734471028	-0.12749862783020	-0.46833199174766
C	-2.48474069604747	-1.25016649765403	-0.07063350157936
C	-3.04370087081654	-2.29380303713973	-0.72736234627630
N	-4.05997120039265	-1.79071638211702	-1.50570063975693

Table A4.1 Continued

C	-4.13542167276594	-0.44498537061044	-1.31787618062795
H	-1.67574580663178	-1.22983892740642	0.64954684836592
H	-2.78246576842826	-3.34206423794497	-0.70041359139278
N	-3.03855108843197	2.24511048701921	-1.17391179827382
C	-4.03530236293934	2.24145975037932	-2.06184141985107
N	-3.74243875836696	3.20889950254803	-2.97128888109641
C	-2.55022705351053	3.80135783884470	-2.62370759278779
C	-2.11196312269776	3.19411650679878	-1.49732708565502
H	-2.10290915425918	4.60189365236002	-3.19461808647532
H	-1.22001572507659	3.36248331895642	-0.90603262810709
Ni	-5.46538431902311	0.94083329664497	-1.80716229879404
C	-4.84518580046296	-2.64258386963143	-2.44484152559608
C	-4.55215420798289	3.67091511790711	-4.13026346130716
C	-6.30781278558295	-2.60723242603647	-2.02866742018451
C	-4.36415475018771	-4.08708876054426	-2.37893253680238
C	-4.60463832487709	-2.12380158271624	-3.85692251061710
C	-4.74458446611097	2.49895132452746	-5.08216413455893
C	-3.82030190748300	4.77410192235429	-4.88551000260702

Table A4.1 Continued

C	-5.84747236739162	4.25005198855966	-3.57554916355578
H	-6.91539100553122	-3.20123495409104	-2.72454741205249
H	-6.69292218047938	-1.58452564692764	-2.02120714880509
H	-6.43345749756673	-3.03312117584351	-1.02289554578816
H	-4.96483943818680	-4.67579730805591	-3.08396353305002
H	-4.50437227173271	-4.53692506868816	-1.38633326084340
H	-3.31358758334223	-4.19779314083262	-2.68118780357130
H	-4.44230138606067	5.07206590339646	-5.73987564986069
H	-2.85628950487031	4.43705002682249	-5.28964671195463
H	-3.66420846590100	5.67258052216107	-4.27383313757940
H	-5.36193420856948	2.80295513969259	-5.93805486123194
H	-5.22386918499587	1.65062984266579	-4.58574916177045
H	-3.77328032367476	2.16247554599210	-5.47208443926646
C	-5.50821435807818	1.39637972149957	0.11368700025664
N	-6.50699163489673	1.49921945560037	1.02898586477268
C	-5.95520750085964	1.66519301044824	2.27750238734131
C	-4.61006659540006	1.67121149295143	2.12381800288056
C	-7.97688477708761	1.40218026427958	0.81342690826417

Table A4.1 Continued

C	-8.71896389143835	1.70962899391165	2.10834815922482
C	-8.29024269503761	-0.03178141724653	0.40547054413000
C	-8.38367420859659	2.43971440201296	-0.22427559801158
H	-8.14551574040985	3.45030554091267	0.13697960762334
H	-9.46640424005010	2.39122865501592	-0.40271897891536
H	-7.86706969439818	2.28452077439486	-1.17542042040031
H	-8.50458567570728	0.98355042071040	2.90376393851853
H	-9.79639850254276	1.65241967160230	1.90525794027721
H	-8.50779479838543	2.72264216622628	2.47844081648578
H	-7.98937729843209	-0.72796588338316	1.20111421564083
H	-7.76291540564258	-0.31139158229718	-0.51031226063329
H	-9.36835624206091	-0.15756804786071	0.23604739110412
H	-6.48984516415138	4.60677790437010	-4.39166130677946
H	-5.62373931483877	5.10506942782683	-2.92233740336765
H	-6.40262728171652	3.51028643912182	-2.99045250283859
N	-6.75154543574238	0.76818617927531	-2.83142208004261
C	-7.84343131203020	0.63657521851981	-3.73835953769991
C	-8.30257757941215	2.00703345404967	-4.26384674894478

Table A4.1 Continued

C	-9.04014292601509	-0.02029122394499	-3.02830493825684
C	-7.43982070369780	-0.23774665180707	-4.93679454570026
H	-7.22875053338254	-1.26749491593654	-4.62881411565331
H	-6.55623156440790	0.16397703325186	-5.44828389981414
H	-8.26895897963486	-0.26074983616583	-5.65911502404691
H	-8.55301126084714	2.69264119527952	-3.44434057824497
H	-9.20688431348277	1.86287813189946	-4.87167771501501
H	-7.54289514852065	2.47378797824964	-4.89857446253548
H	-8.78068612525292	-1.00387738342693	-2.61895931876813
H	-9.84943209572030	-0.15942826897665	-3.75884407551527
H	-9.41864745928392	0.61302006205669	-2.21845312802021
H	-3.54333733656632	-2.22544952078604	-4.12339359996327
H	-4.88384372109312	-1.07003383517003	-3.95438380336865
H	-5.19101928359066	-2.70556568664798	-4.58006807317664
H	-3.82552223706137	1.75262508571119	2.86522127634266
H	-6.54770994201922	1.77205821340496	3.17459136755416

Table A4.3. Preliminary crystal data and structure refinement for $[PhB(^tBuIm)_3NiN^tBu]^+$.

Empirical formula	$C_{37.25}H_{63.5}BN_7Ni$
Formula weight	678.97 g/mol
Temperature/K	100(2)
Crystal system	monoclinic
Space group	$P2_1/c$
a/Å	26.2422(12)
b/Å	12.6989(6)
c/Å	24.8019(11)
β/°	95.146(2)°
Volume/Å^3	8231.8(7)
Z	8
ρ_{calc}g/cm^3	1.096
μ/mm^{-1}	0.504
Radiation	MoKα
2Θ range for data collection/°	4.33- 50.238
Reflections collected	215427

Table A4.3 Continued

Independent reflections	14659 unique [R_{int} = 0.0526, R_{sigma} = 0.0188]
Final R indexes [I>=2σ (I)]	R_1 = 0.0464
Final R indexes [all data]	wR_2 = 0.1232

$R_{int} = \Sigma \mid F_o^2 - \langle F_o^2 \rangle \mid / \Sigma \mid F_o^2 \mid$

$R_1 = \Sigma \mid \mid F_o \mid - \mid F_c \mid \mid / \Sigma \mid F_o \mid$

$wR_2 = [\Sigma [w (F_o^2 - F_c^2)^2] / \Sigma [w (F_o^2)^2]]^{1/2}$

Goodness-of-fit = $[\Sigma [w (F_o^2 - F_c^2)^2] / (n-p)^{1/2}$

n: number of independent reflections; p: number of refined parameters

Table A4.4. Bond lengths from solid-state structure of [PhB(^{t}BuIm)$_3$NiN^{t}Bu]$^+$.

Atom	Atom	Length/Å	Atom	Atom	Length/Å
Ni1	N1	1.781(2)	N9	C41	1.389(3)
Ni1	C9	1.867(2)	N10	C40	1.350(3)
Ni1	C16	1.873(2)	N10	C42	1.383(3)
N1	C1	1.462(3)	N10	B2	1.558(3)
N2	C8	1.497(3)	N11	C46	1.493(3)
N2	C9	1.361(3)	N11	C47	1.363(3)
N2	C10	1.387(3)	N11	C48	1.391(3)
N3	C9	1.354(3)	N12	C47	1.351(3)
N3	C11	1.374(3)	N12	C49	1.374(3)
N3	B1	1.561(3)	N12	B2	1.565(3)
N4	C15	1.489(3)	N13	C50	1.376(3)
N4	C16	1.364(3)	N13	C51	1.384(3)
N4	C17	1.386(3)	N13	B2	1.546(3)
N5	C16	1.349(3)	N14	C50	1.366(3)
N5	C18	1.378(3)	N14	C52	1.387(3)
N5	B1	1.558(3)	N14	C53	1.491(3)
N6	C23	1.377(3)	C32	C35	1.524(4)
N6	C25	1.384(3)	C33	C35	1.496(4)
N6	B1	1.547(3)	C34	C35	1.527(4)

Table A4.4 Continued

N7	C22	1.484(3)	C36	C39	1.520(3)
N7	C23	1.361(3)	C37	C39	1.521(3)
N7	C24	1.388(3)	C38	C39	1.525(3)
C1	C2	1.525(4)	C41	C42	1.341(3)
C1	C3	1.518(4)	C43	C46	1.521(3)
C1	C4	1.534(4)	C44	C46	1.524(3)
C5	C8	1.515(4)	C45	C46	1.522(3)
C6	C8	1.520(4)	C48	C49	1.339(3)
C7	C8	1.524(4)	C51	C52	1.341(3)
C10	C11	1.342(4)	C53	C54	1.514(3)
C12	C15	1.524(4)	C53	C55	1.528(4)
C13	C15	1.525(3)	C53	C56	1.528(4)
C14	C15	1.527(3)	C57	C58	1.396(3)
C17	C18	1.341(3)	C57	C62	1.394(3)
C22	C19B	1.467(8)	C57	B2	1.619(3)
C22	C20B	1.570(9)	C58	C59	1.389(3)
C22	C21A	1.447(12)	C59	C60	1.379(4)
C22	C19A	1.591(9)	C60	C61	1.381(4)
C22	C20A	1.467(9)	C61	C62	1.389(3)
C22	C21B	1.577(11)	C63	C64	1.464(6)

Table A4.4 Continued

C24	C25	1.338(3)	C64	C65	1.477(5)
C26	C27	1.396(3)	C65	C66	1.447(6)
C26	C31	1.390(4)	C66	C67	1.517(6)
C26	B1	1.613(3)	C68	C69	1.508(5)
C27	C28	1.385(4)	C69	C70	1.510(5)
C28	C29	1.371(5)	C70	C71	1.508(4)
C29	C30	1.383(5)	C71	C72	1.489(5)
C30	C31	1.391(4)	C73	C76[1]	1.575(10)
Ni2	N8	1.783(2)	C73	C74	1.315(8)
Ni2	C40	1.871(2)	C75	C76	1.391(8)
Ni2	C47	1.870(2)	C75	C76[1]	1.392(8)
N8	C35	1.469(3)	C75	C74[1]	1.645(7)
N9	C39	1.487(3)	C75	C74	1.645(7)
N9	C40	1.364(3)			

[1]1-X,1-Y,-Z

Table A4.5. Bond angles for solid state structure of [PhB(^{t}BuIm)$_3$NiN^{t}Bu]$^+$.

Atom	Atom	Atom	Angle/°	Atom	Atom	Atom	Angle/°
N1	Ni1	C9	135.33(10)	C35	N8	Ni2	132.59(18)
N1	Ni1	C16	136.51(10)	C40	N9	C39	126.71(18)
C9	Ni1	C16	88.02(9)	C40	N9	C41	109.34(18)
C1	N1	Ni1	133.65(18)	C41	N9	C39	123.69(18)
C9	N2	C8	126.3(2)	C40	N10	C42	109.35(18)
C9	N2	C10	109.4(2)	C40	N10	B2	123.05(18)
C10	N2	C8	124.4(2)	C42	N10	B2	127.60(19)
C9	N3	C11	109.6(2)	C47	N11	C46	125.65(19)
C9	N3	B1	122.71(18)	C47	N11	C48	109.33(19)
C11	N3	B1	127.7(2)	C48	N11	C46	125.02(19)
C16	N4	C15	126.94(19)	C47	N12	C49	109.91(18)
C16	N4	C17	109.47(18)	C47	N12	B2	122.21(18)
C17	N4	C15	123.37(18)	C49	N12	B2	127.88(19)
C16	N5	C18	109.70(18)	C50	N13	C51	110.83(18)
C16	N5	B1	123.23(19)	C50	N13	B2	124.36(18)
C18	N5	B1	126.94(19)	C51	N13	B2	124.44(18)
C23	N6	C25	110.78(19)	C50	N14	C52	111.93(19)
C23	N6	B1	124.42(19)	C50	N14	C53	125.38(19)
C25	N6	B1	124.63(18)	C52	N14	C53	122.66(19)

Table A4.5 Continued

C23	N7	C22	125.1(2)	N8	C35	C32	109.3(2)
C23	N7	C24	111.90(19)	N8	C35	C33	111.1(3)
C24	N7	C22	122.9(2)	N8	C35	C34	107.6(2)
N1	C1	C2	109.5(2)	C32	C35	C34	106.8(3)
N1	C1	C3	110.4(2)	C33	C35	C32	110.8(3)
N1	C1	C4	108.0(2)	C33	C35	C34	111.1(3)
C2	C1	C4	109.8(3)	N9	C39	C36	110.28(18)
C3	C1	C2	110.3(2)	N9	C39	C37	108.17(19)
C3	C1	C4	108.7(2)	N9	C39	C38	109.00(19)
N2	C8	C5	109.1(2)	C36	C39	C37	110.5(2)
N2	C8	C6	109.1(2)	C36	C39	C38	108.4(2)
N2	C8	C7	108.3(2)	C37	C39	C38	110.5(2)
C5	C8	C6	109.0(3)	N9	C40	Ni2	131.30(16)
C5	C8	C7	111.3(2)	N10	C40	Ni2	122.04(15)
C6	C8	C7	110.1(3)	N10	C40	N9	106.36(18)
N2	C9	Ni1	131.15(18)	C42	C41	N9	106.83(19)
N3	C9	Ni1	122.57(17)	C41	C42	N10	108.1(2)
N3	C9	N2	106.11(19)	N11	C46	C43	108.53(19)
C11	C10	N2	106.9(2)	N11	C46	C44	108.75(19)
C10	C11	N3	108.0(2)	N11	C46	C45	109.48(19)

Table A4.5 Continued

N4	C15	C12	110.18(19)	C43	C46	C44	111.6(2)
N4	C15	C13	108.96(19)	C43	C46	C45	108.9(2)
N4	C15	C14	108.08(19)	C45	C46	C44	109.6(2)
C12	C15	C13	108.4(2)	N11	C47	Ni2	131.14(17)
C12	C15	C14	110.5(2)	N12	C47	Ni2	122.83(16)
C13	C15	C14	110.7(2)	N12	C47	N11	105.90(18)
N4	C16	Ni1	131.87(17)	C49	C48	N11	106.9(2)
N5	C16	Ni1	121.93(16)	C48	C49	N12	107.9(2)
N5	C16	N4	106.03(19)	N14	C50	N13	103.29(18)
C18	C17	N4	106.9(2)	C52	C51	N13	107.73(19)
C17	C18	N5	107.9(2)	C51	C52	N14	106.2(2)
N7	C22	C20B	107.6(3)	N14	C53	C54	109.97(19)
N7	C22	C19A	107.2(3)	N14	C53	C55	108.5(2)
N7	C22	C21B	106.1(4)	N14	C53	C56	108.26(19)
C19B	C22	N7	110.1(3)	C54	C53	C55	110.2(2)
C19B	C22	C20B	106.3(4)	C54	C53	C56	109.2(2)
C21A	C22	N7	112.5(4)	C56	C53	C55	110.6(2)
C21A	C22	C19B	115.1(5)	C58	C57	B2	121.7(2)
C21A	C22	C20B	104.7(6)	C62	C57	C58	116.8(2)
C20A	C22	N7	112.2(3)	C62	C57	B2	121.4(2)

Table A4.5 Continued

C20A	C22	C19A	109.8(4)	C59	C58	C57	121.6(2)
C20A	C22	C21B	114.1(6)	C60	C59	C58	120.2(3)
C21B	C22	C19A	107.0(5)	C59	C60	C61	119.6(2)
N7	C23	N6	103.34(19)	C60	C61	C62	119.9(2)
C25	C24	N7	106.3(2)	C61	C62	C57	121.9(2)
C24	C25	N6	107.7(2)	N10	B2	N12	104.39(17)
C27	C26	B1	121.6(2)	N10	B2	C57	111.57(18)
C31	C26	C27	116.6(2)	N12	B2	C57	110.49(18)
C31	C26	B1	121.7(2)	N13	B2	N10	110.48(18)
C28	C27	C26	122.1(3)	N13	B2	N12	109.03(18)
C29	C28	C27	119.9(3)	N13	B2	C57	110.68(18)
C28	C29	C30	119.8(3)	C63	C64	C65	112.9(4)
C29	C30	C31	119.8(3)	C66	C65	C64	115.2(3)
C26	C31	C30	121.8(3)	C65	C66	C67	113.0(4)
N3	B1	C26	110.51(19)	C68	C69	C70	113.7(3)
N5	B1	N3	104.89(18)	C71	C70	C69	115.3(3)
N5	B1	C26	112.42(19)	C72	C71	C70	114.7(3)
N6	B1	N3	109.08(18)	C76	C75	C76[1]	180.0(7)
N6	B1	N5	109.75(18)	C76[1]	C75	C74[1]	116.9(4)
N6	B1	C26	110.04(19)	C76	C75	C74[1]	63.1(4)

Table A4.5 Continued

N8	Ni2	C40	134.28(9)	C74[1]	C75	C74	180.0
N8	Ni2	C47	137.75(9)	C75	C76	C73[1]	114.9(6)
C47	Ni2	C40	87.86(9)	C73	C74	C75	115.0(6)

A4.6 References

(1) Larson, V. A.; Battistella, B.; Ray, K.; Lehnert, N.; Nam, W. *Nat. Rev. Chem.* **2020**, *4*, 404–419.

(2) Saouma, C. T.; Peters, J. C. *Coord. Chem. Rev.* **2011**, *255*, 920–937.

(3) Carsch, K. M.; DiMucci, I. M.; Iovan, D. A.; Li, A.; Zheng, S.-L.; Titus, C. J.; Lee, S. J.; Irwin, K. D.; Nordlund, D.; Lancaster, K. M.; Betley, T. A. *Science* **2019**, *365*, 1138–1143.

(4) Kogut, E.; Wiencko, H. L.; Zhang, L.; Cordeau, D. E.; Warren, T. H. *J. Am. Chem. Soc.* **2005**, *127*, 11248–11249.

(5) Mindiola, D. J.; Hillhouse, G. L. *J. Am. Chem. Soc.* 2001, pp 4623–4624.

(6) Ray, K.; Heims, F.; Pfaff, F. F. *Eur. J. Inorg. Chem.* **2013**, *2013*, 3784–3807.

(7) Cowley, R. E.; Bontchev, R. P.; Sorrell, J.; Sarracino, O.; Feng, Y.; Wang, H.; Smith, J. M. *J. Am. Chem. Soc.* **2007**, *129*, 2424–2425.

(8) Goetz, M. K.; Hill, E. A.; Filatov, A. S.; Anderson, J. S. *J. Am. Chem. Soc.* **2018**, *140*, 13176–13180.

(9) Goetz, M. K.; Schneider, J. E.; Filatov, A. S.; Jesse, K. A.; Anderson, J. S. *J. Am. Chem. Soc.* **2021**, *143*, 20849–20862.

(10) Nieto, I.; Bontchev, R. P.; Ozarowski, A.; Smirnov, D.; Krzystek, J.; Telser, J.; Smith, J. M. *Inorganica Chim. Acta* **2009**, *362*, 4449–4460.

(11) Stevens, M. B.; Trang, C. D. M.; Enman, L. J.; Deng, J.; Boettcher, S. W. *J. Am. Chem. Soc.* **2017**, *139*, 11361–11364.

(12) Li, N.; Bediako, D. K.; Hadt, R. G.; Hayes, D.; Kempa, T. J.; von Cube, F.; Bell, D. C.; Chen, L. X.; Nocera, D. G. *Proc. Natl. Acad. Sci. U.S.A.* **2017**, *114*, 1486–1491.

(13) Nagataki, T.; Tachi, Y.; Itoh, S. *Chem. Commun.* **2006**, *0*, 4016–4018.

(14) Qiu, Y.; Hartwig, J. F. *J. Am. Chem. Soc.* **2020**, *142*, 19239–19248.

(15) Corona, T.; Pfaff, F. F.; Acuña-Parés, F.; Draksharapu, A.; Whiteoak, C. J.; Martin-Diaconescu, V.; Lloret-Fillol, J.; Browne, W. R.; Ray, K.; Company, A. *Chem. Eur. J.* **2015**, *21*, 15029–15038.

(16) Pfaff, F. F.; Heims, F.; Kundu, S.; Mebs, S.; Ray, K. *Chem. Commun.* **2012**, *48*, 3730.

(17) Corona, T.; Company, A. *Chem. – A Eur. J.* **2016**, *22*, 13422–13429.

(18) Cowley, R. E.; Bontchev, R. P.; Duesler, E. N.; Smith, J. M. *Inorg. Chem.* **2006**, *45*, 9771–9779.

(19) Sherbow, T. J.; Zakharov, L.; Pluth, M. D. *Inorg. Chem.* **2021**, *60*, 8135–8142.

(20) Laskowski, C. A.; M Miller, A. J.; Hillhouse, G. L.; Cundari, T. R.; Beckman, M. A *J. Am. Chem. Soc* **2011**, *133*, 771–773.

(21) Müller, P.; Fruit, C. *Chem. Rev.* **2003**, *103*, 2905–2919.

(22) Lu, X.; Li, X.-X.; Lee, Y.-M.; Jang, Y.; Seo, M. S.; Hong, S.; Cho, K.-B.; Fukuzumi, S.; Nam, W. *J. Am. Chem. Soc.* **2020**, *142*, 3891–3904.

(23) Liu, Y.; Du, J.; Deng, L. *Inorg. Chem.* **2017**, *56*, 8278–8286.

(24) Zhang, L.; Liu, Y.; Deng, L. *J. Am. Chem. Soc.* **2014**, *136*, 15525–15528.

(25) Baek, Y.; Betley, T. A. *Angew. Chem. Int. Ed.* **2022**, *61*, e202115437.

(26) Dong, Y.; Lund, C. J.; Porter, G. J.; Clarke, R. M.; Zheng, S.-L.; Cundari, T. R.; Betley, T. A. *J. Am. Chem. Soc.* **2021**, *143*, 817–829.

(27) Song, F.; Wang, C.; Falkowski, J. M.; Ma, L.; Lin, W. *J. Am. Chem. Soc.* **2010**, *132*, 15390–15398.

(28) Bottaro, J. C.; Penwell, P. E.; Schmitt, R. J. *Synth. Commun.* **1997**, *27*, 1465–1467.

(29) Neese, F.; Wennmohs, F.; Hansen, A.; Becker, U. *Chem. Phys.* **2009**, *356*, 98–109.

(30) Neese, F. The ORCA Program System. *Wiley Interdiscip. Rev. Comput. Mol. Sci.* **2012**, *2*, 73–78.

(31) Krause, L.; Herbst-Irmer, R.; Sheldrick, G. M.; Stalke, D. *J. Appl. Crystallogr.* **2015**, *48*, 3–10.

(32) Dolomanov, O. V; Bourhis, L. J.; Gildea, R. J.; Howard, J. A. K.; Puschmann, H. *J. Appl. Crystallogr.* **2009**, *42*, 339–341.

(33) Sheldrick, G. *Acta Crystallogr. Sect. A* **2015**, *71*, 3–8.